

**The Synthesis and Coordination
Chemistry of Methylene Bridge-Substituted
Calix[4]arenes**

Angela Fong

Submitted for the degree of Doctor of Philosophy

Heriot-Watt University

School of Engineering and Physical Sciences

June 2019

The copyright in this thesis is owned by the author. Any quotation from the thesis or use of any of the information contained in it must acknowledge this thesis as the source of the quotation or information.

Abstract

Chapter 1 presents an overview of the history of calix[*n*]arenes. There is particular focus on calix[4]arene and its conformational properties, as well as modification at the upper-, lower-rim and methylene bridge positions. Molecular magnetism is then discussed with important literature examples described. Finally, the coordination chemistry of metal clusters formed from calix[4]arenes are discussed.

Chapter 2 covers the synthesis and characterisation of a calix[4]arene derivative that has been mono-substituted at all methylene bridge positions with 2-methylfuran groups. The coordination chemistry with *3d*, *4f*, and *3d-4f* ions was then investigated. The clusters isolated from these reactions were analysed by X-ray diffraction studies and their structures compared with those previously obtained within this research group.

Chapter 3 focusses on the further derivatisation of a furan-substituted calix[4]arene in order to synthesise other heterocyclic-containing calix[4]arenes. This work was carried out with a particular emphasis on expanding the library of methylene bridge-substituted calix[4]arenes. The synthesis and characterisation of these compounds are described.

Chapter 4 presents work that was carried out by the candidate on placement at the University of Edinburgh in collaboration with the Lusby group. In this section the pyridyl-substituted calix[4]arene synthesised in Chapter 3 was utilised in cage-forming reactions with a view to forming metal-organic assemblies. The results of which are described in detail with supporting evidence in the form of Diffusion Ordered NMR Spectroscopy studies.

Chapter 5 describes the post-synthetic modification of a $[\text{Mn}^{\text{III}}_2\text{Mn}^{\text{II}}_2]$ cluster through the addition of chelating co-ligands. The results are that the ligated solvent molecules of the cluster have been displaced by various co-ligands, resulting in a new family of clusters. X-ray diffraction studies were carried out on the resultant clusters in order to determine the stability of the crystalline material upon removal from the mother liquor.

Chapter 6 presents a summary of the work described in this thesis and future work to be carried out in relation to this project.

Acknowledgements

Firstly, I would like to thank my supervisor, Dr Scott J. Dalgarno, for giving me the opportunity to do a PhD in his group. His guidance and support throughout this project has been extremely valuable, especially through particularly tough areas of the project, and I cannot thank him enough. He has been a pleasure to work with and I have thoroughly enjoyed my time in the group.

I would also like to thank Dr Ruairaidh D. McIntosh for his advice over the years. He always has the time to answer my many questions, no matter how small, and has provided many useful hints and tips which have been a great help.

Thanks also to previous and current members of WP 3.23 for putting up with me over the years, especially with all of my complaining. Life in the lab would definitely have been far less enjoyable without you guys. Special thanks go to Dr Marco Coletta for being such a great help and reminding me how to do basic lab techniques when I first started. I would also like to thank the other PhD students at Heriot Watt, especially those in WP 2.14 for always being up for trips to the shop for snacks!

I would also like to thank Dr Simon J. Teat and Dr Laura McCormick at the Advanced Light Source in Berkeley, California for their work on collecting X-ray data. Thanks to Dr David Ellis for his expertise in NMR and help with both the 2D and VT NMR studies. I must also thank Dr Gary Nichol and Alan Taylor at The University of Edinburgh for X-ray data collection and mass spectrometry services, respectively.

Thanks to the Lusby group at The University of Edinburgh for hosting me for 3 weeks and making me feel very welcome in their group. I must also thank Prof. Euan K. Brechin without whom I may never have ended up doing my PhD with Scott and for this I am extremely grateful.

Finally, I would like to thank my family for their support during my time as a PhD student.

ACADEMIC REGISTRY
Research Thesis Submission

Please note this form should be bound into the submitted thesis.

Name:	Angela Fong		
School:	Engineering and Physical Sciences		
Version: <i>(i.e. First, Resubmission, Final)</i>	Final	Degree Sought:	PhD

Declaration

In accordance with the appropriate regulations I hereby submit my thesis and I declare that:

1. The thesis embodies the results of my own work and has been composed by myself
2. Where appropriate, I have made acknowledgement of the work of others
3. Where the thesis contains published outputs under Regulation 6 (9.1.2) these are accompanied by a critical review which accurately describes my contribution to the research and, for multi-author outputs, a signed declaration indicating the contribution of each author (complete Inclusion of Published Works Form – see below)
4. The thesis is the correct version for submission and is the same version as any electronic versions submitted*.
5. My thesis for the award referred to, deposited in the Heriot-Watt University Library, should be made available for loan or photocopying and be available via the Institutional Repository, subject to such conditions as the Librarian may require
6. I understand that as a student of the University I am required to abide by the Regulations of the University and to conform to its discipline.
7. Inclusion of published outputs under Regulation 6 (9.1.2) shall not constitute plagiarism.
8. I confirm that the thesis has been verified against plagiarism via an approved plagiarism detection application e.g. Turnitin.

* Please note that it is the responsibility of the candidate to ensure that the correct version of the thesis is submitted.

Signature of Candidate:		Date:	
-------------------------	--	-------	--

Submission

Submitted By <i>(name in capitals)</i> :	ANGELA FONG
Signature of Individual Submitting:	
Date Submitted:	

For Completion in the Student Service Centre (SSC)

Received in the SSC by <i>(name in capitals)</i> :			
<i>Method of Submission</i> <i>(Handed in to SSC; posted through internal/external mail):</i>			
<i>E-thesis Submitted (mandatory for final theses)</i>			
Signature:		Date:	

Inclusion of Published Works

Declaration

This thesis contains one or more multi-author published works. In accordance with Regulation 6 (9.1.2) I hereby declare that the contributions of each author to these publications is as follows:

Citation details	A. Fong, L. McCormick, S. J. Teat, E. K. Brechin and S. J. Dalgarno, <i>Supramol. Chem.</i> , 2018, 30 , 504-509.
Author 1	Synthesis and characterisation
Authors 2 and 3	Crystallography
Authors 4 and 5	Supervisor
Signature:	
Date:	

Table of Contents

Symbols and Abbreviations	i
Chapter 1: Introduction	1
1.1 History of Calixarenes	1
1.2 Upper and Lower-rim Functionalisation of Calixarenes	7
1.2.1 Upper-rim Functionalisation	7
1.2.2 Lower-rim Functionalisation	9
1.3 Methylene Bridge-Substituted Calixarenes	10
1.4 Molecular Magnetism	18
1.5 Calixarene-Supported Polynuclear Metal Clusters	22
1.6 Aims	36
1.7 References	37
Chapter 2: Synthesis of a Methylene Bridge-Substituted Calix[4]arene and its Use in Polynuclear Metal Cluster Formation	41
2.1 Introduction	41
2.2 Furan Derivatisation at the Methylene Bridge of Calix[4]arenes	42
2.3 Deprotection at the Lower-rim of 4	45
2.4 Exploration of Metal Cluster Formation with H45	47
2.4.1 Reaction of H45 with Mn ^{II} ions	48
2.4.2 Reaction of H45 with a 1:1 mixture of Mn ^{II} :Ln ^{III} ions	50
2.4.3 Reaction of H45 with a 1:4 mixture of Mn ^{II} :Ln ^{III} ions	53
2.5 Conclusions	56
2.6 Experimental	57
2.7 References	63
Chapter 3: Exploration of Furan Derivatisation at the Methylene Bridge of a Calix[4]arene	64
3.1 Introduction	64
3.2 Examples of Derivation of Furan Moiety	64
3.3 Hydrolysis of 4 and Subsequent Synthesis of <i>N</i> -substituted Pyrrole derivatives	65
3.3.1 Synthesis and Characterisation of 13	70
3.3.2 Synthesis and Characterisation of 14	73
3.3.3 Synthesis and Characterisation of 15	75
3.3.4 Reaction of 11 with 2- or 4-aminopyrriine	84
3.3.5 Synthesis and Characterisation of 16	86
3.3.6 Synthesis and Characterisation of 17	87
3.4 Oxidation of 4 and Subsequent Synthesis of Pyridazine TBC[4] derivatives	89
3.4.1 Synthesis and Characterisation of 19	92

3.4.2	Deprotection of 19	93
3.5	Conclusions	97
3.6	Experimental	98
3.7	References	105
Chapter 4: Metal-Organic Cage Chemistry		106
4.1	Introduction	106
4.2	Ligand Design for Cage Assembly	106
4.3	Cage Formation using Compound 15	114
4.3.1	Reaction of 15 with $[\text{Pd}(\text{CH}_3\text{CN})_4][\text{BF}_4]_2$	116
4.3.2	Reaction of 15 with ZnBr_2	117
4.3.3	Reaction of 15 with CoBr_2	120
4.3.4	Reaction of 15 with $[\text{Pd}(\text{dppp})][\text{OTf}]_2$	121
4.4	Conclusions	124
4.5	Experimental	125
4.6	References	127
Chapter 5: The Effects of Co-Ligands on the Magnetic Properties of a Mn_4 Cluster		128
5.1	Introduction	128
5.2	Examples of Mn_4 Clusters as Building Blocks for Extended Systems	128
5.3	$[\text{Mn}^{\text{III}}_2\text{Mn}^{\text{II}}_2]$ Cluster Formation Using $\text{H}_4\text{TBC}[4]$ (1)	135
5.4	Structural Alteration of the $[\text{Mn}^{\text{III}}_2\text{Mn}^{\text{II}}_2]$ Cluster Motif through the Addition of Chelating Co-Ligands	137
5.4.1	Reaction of I with 1,10-Phenanthroline	137
5.4.2	Reaction of I with 2-Methylphenanthroline	139
5.4.3	Reaction of I with 3-Methylphenanthroline	140
5.5	Structural Comparison of Chelating Systems 27 – 29	141
5.6	Powder X-ray Diffraction Studies of Co-Ligand Appended $[\text{Mn}^{\text{III}}_2\text{Mn}^{\text{II}}_2]$ clusters	142
5.6.1	Powder X-ray Diffraction Studies of 27	143
5.6.2	Powder X-ray Diffraction Studies of 28	143
5.6.3	Powder X-ray Diffraction Studies of 29	144
5.7	Conclusions	146
5.8	Experimental	147
5.9	References	149
Chapter 6: Conclusions		150

Appendix: Publications

End of thesis

Symbols and Abbreviations

°C	Degrees Celsius
1,10-Phen	1,10-Phenanthroline
1-D CP	One-dimensional coordination polymer
2,2'-bpy	2,2'-Bipyridine
2-MePhen	2-Methylphenanthroline
3-MePhen	3-Methylphenanthroline
4,4'-bpy	4,4'-Bipyridine
Å	Angstrom (0.1 nm)
AcOH	Acetic acid
AIBN	Azobisisobutyronitrile
AlCl ₃	Aluminium chloride
ASU	Asymmetric unit
<i>B</i>	Applied magnetic field
BF ₄ ⁻	Tetrafluoroborate anion
bpe	<i>trans</i> -1,2-Bis(4-pyridyl)ethane
BPhen	Bathophenanthroline
br. s	Broad singlet
CD ₂ Cl ₂	Deuterated dichloromethane
CD ₃ CN	Deuterated acetonitrile
CDCl ₃	Deuterated chloroform
CH ₃ CN	Acetonitrile
CHCl ₃	Chloroform
COSY	Correlated SpectroscopY
CrO ₃	Chromium trioxide
Cs ₂ CO ₃	Caesium carbonate
d	Doublet
D	Diffusion coefficient
<i>D</i>	Axial zero-field splitting parameter
dbmH	Dibenzoylmethane
dc	Direct current
DCM	Dichloromethane

DMF	<i>N,N</i> -Dimethylformamide
DMSO	Dimethylsulfoxide
DOSY	Diffusion Ordered Spectroscopy
dppp	1,3-Bis(diphenylphosphino)propane
ESI-MS	Electrospray ionisation mass spectrometry
Et	Ethyl
Et ₂ O	Diethyl ether
Et ₃ N	Triethylamine
EtOAc	Ethyl acetate
<i>H</i>	Magnetic field
H ₂ SO ₄	Sulfuric acid
H ₄ C[4]	Calix[4]arene
H ₄ TBC[4]	<i>p-tert</i> -Butylcalix[4]arene
H ₈ C[8]	Calix[8]arene
HFEPN	High-frequency electron paramagnetic resonance
HFIP	Hexafluoroisopropanol
HMBC	Heteronuclear Multiple Bond Correlation
hmp	2-Hydroxymethylpyridine
HSQC	Heteronuclear Single Quantum Correlation
Hz	Hertz
IR	Infrared spectroscopy
<i>J</i>	Coupling constant
<i>k</i>	Boltzmann constant
K	Kelvin
KOH	Potassium hydroxide
LiAlH ₄	Lithium aluminium hydride
Ln	Lanthanide metal
<i>m</i>	Multiplet
<i>M</i>	Magnetisation
MALDI-TOF	Matrix assisted laser desorption ionisation-time of flight
MCE	Magnetocaloric Effect
mCPBA	meta-Chloroperbenzoic acid
Me	Methyl
MeOH	Methanol

mmol	Millimoles
MQT	Macroscopic Quantum Tunnelling
MRs	Magnetic Refrigerants
m_s	Spin quantum number
MS	Mass spectrometry
NaH	Sodium hydride
NaOH	Sodium hydroxide
NBS	<i>N</i> -bromosuccinimide
<i>n</i> -BuLi	<i>n</i> -Butyllithium
Neo	Neocuproine
NMR	Nuclear Magnetic Resonance
OBu	Butoxy
OH	Hydroxy
OMe	Methoxy
OPr	Propoxy
OTf	Triflate anion
PET	Petroleum ether (40-60°)
Ph	Phenyl
PhOH	Toluene
ppm	Parts per million
PPTS	Pyridinium <i>p</i> -toluenesulfonate
<i>p</i> -TsOH·H ₂ O	<i>p</i> -Toluenesulfonic acid monohydrate
py	Pyridine
r	Hydrodynamic radius
<i>S</i>	Ground spin state
s	Singlet
SMMs	Single Molecule Magnets
T	Temperature
t	Triplet
^t Bu	<i>tert</i> -Butyl
TetraMePhen	Tetramethylphenanthroline
TFE	Trifluoroethanol
THF	Tetrahydrofuran
TLC	Thin Layer Chromatography

TM	Transition metal
U_{eff}	Potential energy barrier
VT	Variable temperature
η	Viscosity
π	Pi

Chapter 1

Introduction

1.1 History of Calixarenes

Calixarenes are cyclic polyphenols formed through the base-induced condensation reaction of phenols with formaldehyde. The phenol and formaldehyde reaction was first studied in 1872 by Adolph von Baeyer where he reported the product as a hard resin-like substance.¹ However, he was unable to fully characterise this product and so the chemistry was left relatively unexplored until the 1900's. It was then that Leo Hendrik Baekeland began investigating the reaction of phenol and formaldehyde along with small amounts of base which gave the same resin-like material as obtained by Baeyer which he named Bakelite[®], and from this began the start of the industrial production of synthetic plastics.^{2,3}

Zinke and Ziegler then began investigating the reaction between *para*-substituted phenols and aqueous formaldehyde instead of phenol itself, as the latter can react at both the *ortho*- and *para*-positions which would result in cross-linking between the phenolic units. By restricting the reactivity of the phenol, only the *ortho*-positions are available to react with formaldehyde which reduces the possibility of cross-linking leading to much more linear products. Zinke *et al.* reacted various *p*-substituted phenols, e.g. *p*-methyl, *p*-*tert*-butyl, *p*-cyclohexyl etc. with formaldehyde in the presence of sodium hydroxide (NaOH).⁴ The compounds isolated from these one-pot base-catalysed condensation reactions were high melting insoluble materials, e.g. the reaction using *p*-*tert*-butylphenol resulted in a solid with a melting point of greater than 300 °C, and from this Zinke assumed that only one product was formed, the cyclic tetramer.⁴ Other researchers tried to rationalise the synthesis of the cyclic tetramer and one group who managed to do this were Hayes and Hunter. They formed a cyclic tetramer through a stepwise synthesis with *p*-cresol, and found that it was a high melting point (>300 °C), crystalline material which gave further evidence that the compound Zinke and co-workers had synthesised was in fact the cyclic tetramer.⁵ However, Cornforth *et al.* discovered that the reactions carried out by Zinke actually resulted in the formation of two products with different melting points and then went on to postulate that perhaps the products obtained were conformational isomers of the cyclic tetramers.⁶ Examination of molecular models

indicated that the tetramers could adopt four different structures from which Cornforth assumed that they could not readily interconvert and therefore can exist independently of one another. Kammerer *et al.* carried out dynamic nuclear magnetic resonance spectroscopy (NMR) studies which showed that these molecules could indeed interconvert even at room temperature.⁷

An important step in calixarene chemistry was made by Gutsche and co-workers who were interested in investigating the synthesis of compounds that mimicked the catalytic activity of enzymes. At this time, there were few examples of macrocycles containing cavities that were readily-accessible through facile synthesis that could also be used for this purpose. One of these examples is the cyclodextrins which are naturally occurring basket-shape like products that are required to be isolated by enzymatic treatment of starch. Another example is the crown ethers which are annular in shape and can be synthesised in the laboratory. However, they are more disc-like, and as such lack the cavity required for them to act as enzyme mimics. The tetramers formed by Zinke and co-workers seemed to be ideal candidates as they were cyclic cavity-containing compounds that were readily synthesised, and it was from this that they began their investigation into the condensation products from the phenol-formaldehyde reaction.

Work carried out by Gutsche and co-workers revealed that, although the Zinke procedure was the most reliable at the time, it was not the most reproducible as these reactions generally yielded mixtures of cyclic oligomers of varying sizes. For example, this largely afforded the cyclic tetramer, hexamer and octamer, with small amounts of the pentamer and heptamer also being obtained.⁸ Following these studies they discovered that slight alterations in the reaction conditions, namely the choice of solvent, base and temperature employed, can greatly influence the final product obtained, and so they used this to maximise the yields of several of the condensation products from these reactions.⁹ They found that the reaction is extremely base-sensitive, as any deviations from the ideal equivalents of NaOH can result in the yield tending to 0% when lower amounts of base are used, whilst higher concentrations give increasing amounts of hexamer over the tetramer. They also investigated the base used for the reaction and found that varying this can also influence the calixarene that is formed,¹⁰ as the cyclic tetramer and / or the cyclic octamer is formed when NaOH is used, while the cyclic hexamer is primarily formed when potassium hydroxide (KOH) is employed. This therefore suggests that the nature of the cation of the base influences the product formed from these reactions. The reason for this may be due to the template effect of the cation during the reaction in which the polymer formed is broken down and the fragments are recombined to form the cyclic

products. Another result from their study showed that the reactions are dependent on the temperature, and therefore the solvent, when the cation of the base is kept the same, as formation of the thermodynamic product (e.g. calix[4]arene, H₄C[4]) can be favoured over the kinetic product (e.g. calix[8]arene, H₈C[8]) and vice-versa. It is largely due to Gutsche and co-workers that researchers now have optimised procedures for the synthesis of these macrocycles of varying sizes.

The second general method of forming a calixarene is the lengthy multi-step process developed by Hayes and Hunter which involved the bromination of *p*-cresol to give 2-bromo-4-methylphenol. This was followed by base-catalysed hydroxymethylation to add the methylene groups and then acid-catalysed arylation with additional *p*-cresol to add the aryl groups. Repetition of these steps first produced the dimer, followed by the trimer and then finally the tetramer. This tetramer was then cyclised to give the final target product.⁵ Through the use of new analytical techniques such as infrared spectroscopy (IR) and elemental analysis, they determined that the final product was indeed the cyclic tetramer which was ultimately used as proof that the compounds from Zinke and co-workers reactions that had been assigned as tetramers was at least feasibly possible.

The nomenclature adopted over the years for these cyclic tetramers has changed considerably, and one system that was invented by Cram and Steinberg in 1951 means that these compounds can also be known as [1_n]meta-cyclophanes.¹¹ The term calixarene, however, was introduced by Gutsche in which *calix* is derived from the Greek word for chalice (as the cyclic tetramer resembled the shape of an ancient Greek vase) and *arene* which refers to the aromatic rings upon which these macrocycles are built.¹² Initially, the Gutsche nomenclature was not accepted by IUPAC, but eventually it gained its official status and is now used to include any compounds with a general similarity to the phenol-derived calixarenes. As calixarene chemistry was further explored, it led to much more complex products being formed and this resulted in the requirement for a systematic nomenclature. Normally these are written as calix[*n*]arenes where the [*n*] denotes the number of phenolic units that form the macrocycle, e.g. calix[4]arenes contain four phenyl units, calix[6]arenes six units and so on. A systematic nomenclature has developed in which the term “calixarene” refers to only the basic structure of the macrocycle without any substituents and each of the atoms are numbered in order to be able to add the positions of any substituents. For example, a calix[4]arene where each phenolic ring has a *tert*-butyl group in the *para*-position and hydroxyl groups at the lower-rim is named 5,11,17,23-tetra-*tert*-butyl-calix[4]arene-25,26,27,28-tetrol (Figure 1.1).

This nomenclature system can lead to long and difficult to understand names, so they are commonly simplified to shorter forms. The commonly adopted abbreviation is thus *p*-R-calix[*n*]arene where R is the group *para* to the phenolic hydroxyl group and *n* is as before. The work presented in this thesis will focus solely on *p*-*tert*-butylcalix[4]arenes and its derivatives, and so, when not otherwise stated, the name will be shortened to H₄TBC[4] (**1**, Figure 1.1) hereafter to represent the level of protonation of the macrocycle relative to the lower-rim hydroxyl groups. The same nomenclature will be applied to any other ligands presented throughout this thesis.

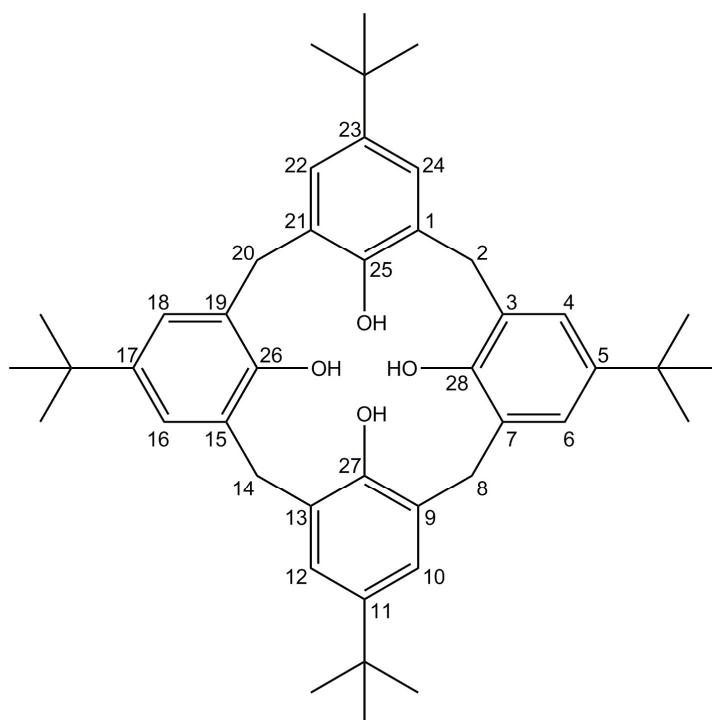


Figure 1.1. Numbering scheme of 5,11,17,23-tetra-*tert*-butyl-calix[4]arene-25,26,27,28-tetrol (H₄TBC[4], **1**).

Calix[*n*]arenes can be split into two groups, the first of which are the “major” calixarenes where *n* = 4,6,8 and the second of which are the “minor” calixarenes where *n* = 5,7. Both the “major” and “minor” calixarenes can be synthesised using a base-induced process, however the routes to the “minor” compounds are much more synthetically demanding and usually result in low yields. The synthesis of calix[5]arene was first reported in 1982 by Ninagawa *et al.* who carried out the base-catalysed reaction (potassium *tert*-butoxide) of *p*-*tert*-butylphenol with paraformaldehyde in tetralin.¹³ From this reaction, they were able to isolate calix[4,5 and 8]arenes. The calix[4 and 8]arenes (1.9 and 0.9 g, respectively) were afforded as the major products, whilst calix[5]arene was isolated in a

much smaller yield (0.5g). Nakamoto *et al.* also reported the synthesis of calix[7]arene in the same year using similar reaction conditions, however they used 1,4-dioxane and KOH in place of tetralin and potassium *tert*-butoxide.¹⁴ The reaction afforded calix[7]arene (12%) as the major product as well as side products of calix[6 and 8]arenes (2 and 5%, respectively). Gutsche and co-workers were also able to isolate and characterise calix[9-20]arenes using acid-catalysed reaction conditions.¹⁵ From the work carried out by the Gutsche research group, optimised reaction conditions were found in order to synthesise these larger calixarenes in which the acid catalysed process led to higher yields of these particular cyclic oligomers compared to the base-catalysed reaction. The crude obtained from the acid-catalysed reaction contained a mixture of different calix[*n*]arenes which required separation *via* tedious and time-consuming methods such as fractional crystallisation and column chromatography.

Calixarenes are said to adopt a vase-like shape due to the way in which they are normally orientated, with the *para*-substituents pointing up (*exo*) and the hydroxyl groups pointing down (*endo*). The *exo* and *endo* faces are more commonly referred to as the upper-rim and the lower-rim, respectively (Figure 1.2).

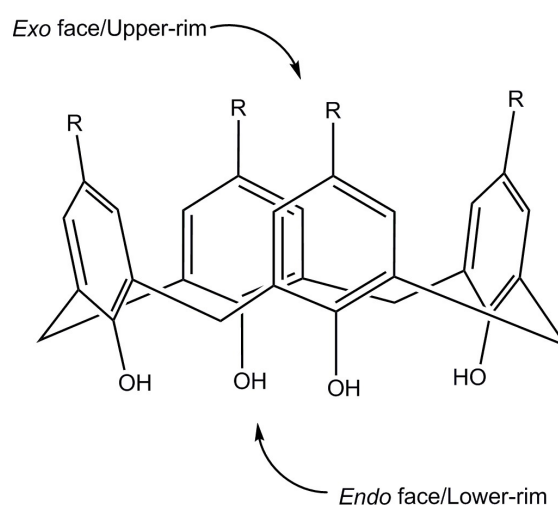


Figure 1.2. Representation of the *exo* and *endo* faces of calix[4]arenes (where R = alkyl, halogen etc).

As proposed by Cornforth *et al.*, calix[4]arenes can adopt four different conformations. The most common is the cone conformation which gives the macrocycles their name as the *para*-substituents all point up whereas the hydroxyl groups point down. These four possible conformations were named by Gutsche to be the cone, partial-cone, 1,2-alternate and 1,3-alternate as shown in Figure 1.3. The names of these conformations are described

by a phenol group which is pointing (up or down) relative to the others and an average plane defined by the methylene bridges. This therefore means that as the size of the calixarene increases the number of conformations that exist also increases (calix[6]arenes and calix[8]arenes have eight and sixteen conformations, respectively).

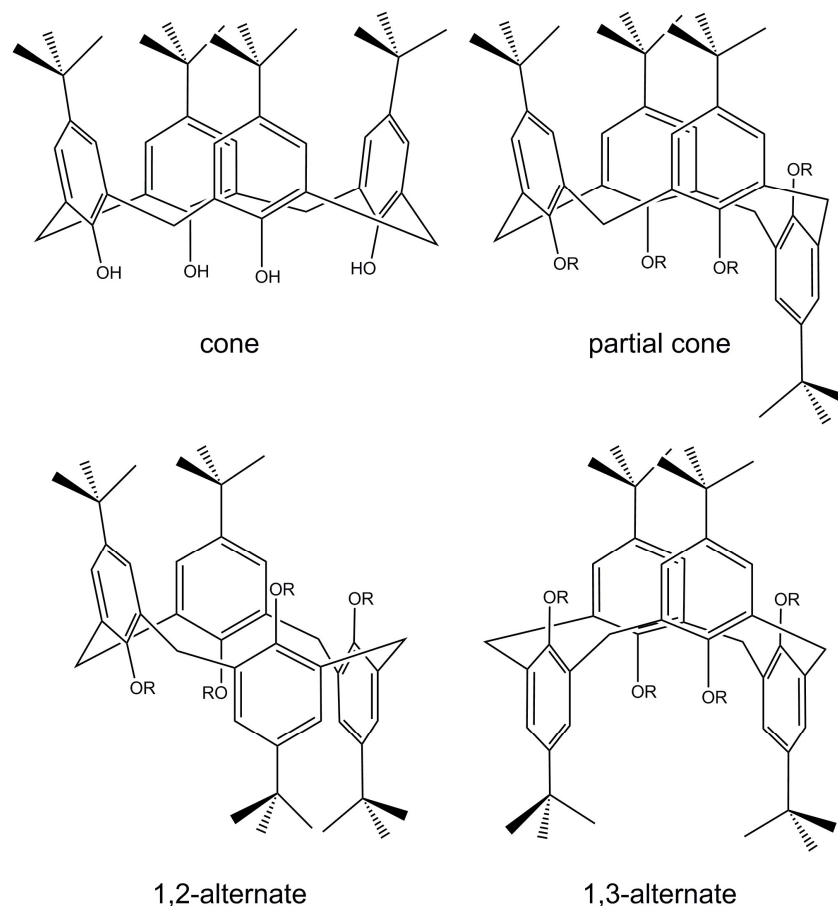


Figure 1.3. The four possible conformations of calix[4]arenes (where R = Me, Et, Pr).

The cone conformation is favoured due to strong intramolecular hydrogen bonding between the hydroxyl groups located at the lower-rim of the calixarene. However, at higher temperatures or in solution, they are conformationally mobile and all the conformers exist in equilibrium due to ring flipping of the phenolic units through the annulus of the calixarene. Ring-flipping is also dependent on the size of the substituent at the lower-rim position. For example, it occurs at room temperature with small substituents such as $-OMe$, however, the tetra-ethers containing groups larger than *n*-propyl are conformationally inflexible even at elevated temperatures.

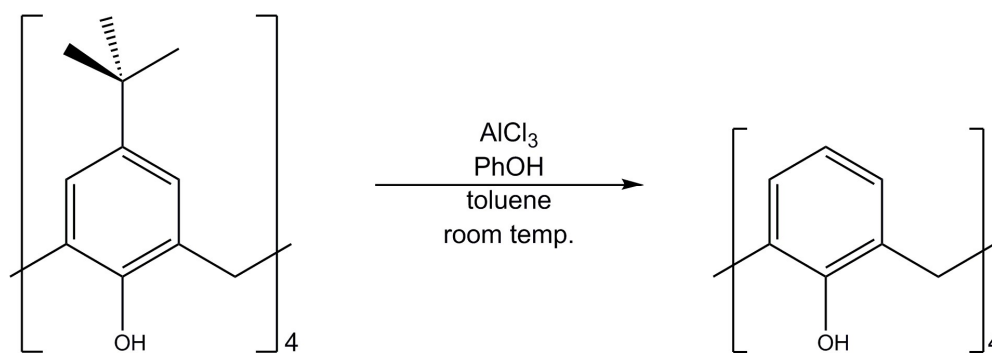
1.2 Upper and Lower-rim Functionalisation of Calixarenes

Calixarenes are versatile ligands as they can be functionalised at various regions of the macrocyclic framework. They have the ability to be functionalised at both the upper- and lower-rims to give an almost infinite number of derivatives, as well as at the methylene bridge position. An extensive amount of research has gone into functionalisation at both the upper- and lower-rims, however there are far fewer examples in the literature that document methylene bridge substitution. For brevity, only a few examples of upper- and lower-rim substitution shall be described in this work as the main focus is on methylene bridge functionalisation.

1.2.1 Upper-rim Functionalisation

The fragment condensation reaction was developed by Böhmer *et al.* and is well-adapted to synthesise calixarenes that are functionalised at the upper-rim. They developed what is referred to as a “3+1” stepwise procedure in which they reacted a linear trimer with a 2,5-bis-halomethyl phenol to give the final cyclic tetramer. Functionality at the upper-rim can be introduced by reacting different *p*-substituted phenols. However, these procedures take considerably longer than the one-pot method developed by Zinke and co-workers due to the need for protection and deprotection. As a result, most functionalisation at the upper-rim has focused on reactions that employ Zinke products as a starting point.

The de-*tert*-butylated calix[4]arene (H₄C[4] for short) has been shown to be an attractive starting material for the synthesis of various *p*-substituted calix[4]arenes and this has been synthesised by the aluminium chloride-catalysed de-*tert*-butylation reaction (Scheme 1.1).¹⁶



Scheme 1.1. Synthetic scheme for the de-*tert*-butylation of $\text{H}_4\text{TBC}[4]$.

With the *para*-positions now available for further functionalisation, a wide variety of procedures have been developed to introduce a diverse range of functional groups at the upper-rim. Halocalixarenes are useful synthetic intermediates for the synthesis of other *p*-substituted calix[4]arenes through cross coupling reactions. One way to introduce a halogen at the upper-rim is through the bromination reaction of the tetramethyl ether of calix[4]arene with *N*-bromosuccinimide (NBS) to give the tetra-brominated derivative.¹⁷ This compound can then be cross coupled with arylboronic acids in the presence of a Pd catalyst to afford other *p*-substituted calix[4]arenes.¹⁸

An alternative method of functionalisation at the upper-rim was through the *p*-quinonemethide route which involves the reaction of $\text{H}_4\text{C}[4]$ with formaldehyde and a secondary amine to produce a Mannich base. This is then treated with iodomethane to yield the quaternary salt which is then reacted with 2 equivalents of a nucleophile (1 equivalent acts as a base) to produce the *para*-substituted calix[4]arene derivative.¹⁹

Another valuable intermediate can be produced through the *p*-Claisen rearrangement route. The tetraallyl ether can be prepared through reaction of sodium hydride and allyl bromide in a DMF/THF mixture. This was then thermally rearranged to the *p*-allylcalix[4]arene by heating a solution of the tetraallyl ether in dimethylaniline. The benzyl tosylate ether of this compound could then be used as an intermediate in the synthesis of more *p*-substituted calixarene derivatives such as the aldehyde, the alcohol, the bromide, the azide and the amine compounds.²⁰

1.2.2 Lower-rim Functionalisation

Functionalisation at the lower-rim can be carried out due to the presence of the phenolic hydroxyl groups and reactions at this position are often used as protecting steps. Calixarenes have been found to be much stronger acids as compared to their monomeric acyclic counterparts, however their poor solubility in solvents commonly used in photo- and potentiometric titrations led to difficulty in determining accurate pK_a values. Shinkai and workers synthesised “neutral”, water-soluble calix[4]arenes that had $SO_2N(CH_2CH_2OH)_2$ or NO_2 groups in the *para*-positions and used these compounds in their pK_a value determinations. From their investigation they found that the first deprotonation of calixarenes occurs at an unusually low pK_a (pK_{a1} 1.8-2.9) with the pK_a values increasing to around 10-14 for subsequent deprotonations. This low pK_a value suggests that the calix[4]arenes possess a relatively acidic proton that can be easily removed due to stabilisation of the mono-anion through strong hydrogen bonding to the $-OH$ groups next to it. The removal of subsequent protons is more difficult compared to the first and this is due to unfavourable electrostatic repulsions generated upon further deprotonation.²¹

Given the ease in which a calixarene can be deprotonated, one of the simplest ways to functionalise the lower rim is to introduce an ether group through a Williamson-ether reaction with an alkyl halide in the presence of a base.^{22, 23} The huge gap in pK_a values between the first and second deprotonation suggests that the mono-alkylated product is favoured over the di-, tri- and tetra-alkylated species, and a strong base is required to isolate the latter. Tetra-alkylation can be carried out in the presence of a base such as NaH with an excess of alkylating agent, surprisingly however, it can also be performed in the presence of a weaker base such as CS_2CO_3 using longer reaction times.²² Alkylation at the lower-rim has been studied extensively to the point that it is now possible to obtain the mono-, di-, tri- and tetraethers through both one-pot or multi-step reactions.²⁴ Different alkyl functional groups can be introduced at the lower-rim through further reaction of the mono-ether with a disparate haloalkane.

The esters of calixarenes are the earliest examples of substitution at the lower-rim. These derivatives are generally synthesised by reaction with acid halides and NaH,²⁵ acid halides and $AlCl_3$,²⁶ or acid anhydrides and H_2SO_4 ⁹ to give the tetra-substituted calixarene. As with etherification, partial esterification can also occur if the reaction is carried out under milder reaction conditions with different solvents and base and smaller amounts of acylating agent.²⁷

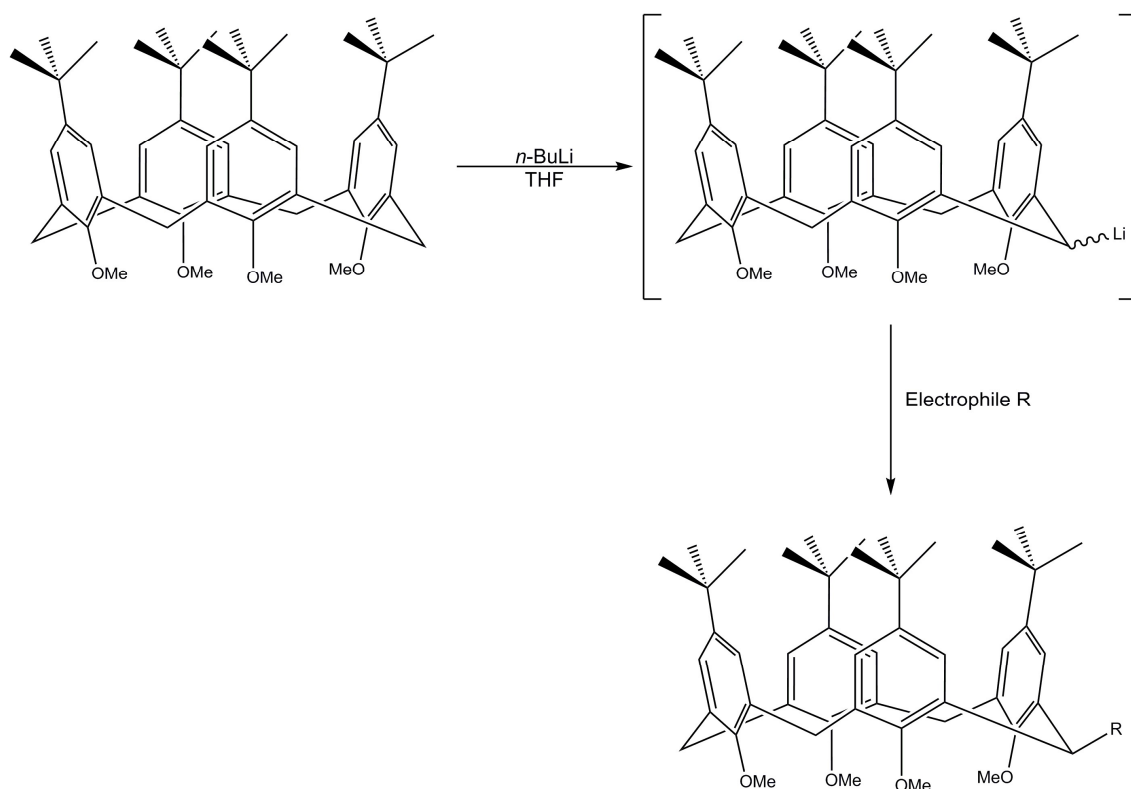
Typically, reactions at the lower-rim are carried out as a protection step from reagents used in subsequent reactions, however it is possible to introduce functionality through reaction with an alkylating agent that has a second functional group attached to it. The simplest examples of these agents are those containing C=C and C≡C functionality and the use of these reagents results in the synthesis of allyl-²⁴ and propargyl-like²⁸ calix[4]arene derivatives, respectively.

1.3 Methylene Bridge-Substituted Calixarenes

This thesis will mainly focus on the synthesis and characterisation of methylene bridge-substituted calix[4]arene derivatives, followed by the investigation into their metal cluster formation. It is therefore worthwhile dedicating a section to this particular type of functionalisation. As mentioned above, functionalisation at the methylene bridge position has been much less explored than that undertaken at the upper- and lower-rims, and significantly fewer papers published regarding mono-substitution at all four bridge positions. Functionalisation at the methylene bridge position is of particular interest, as it allows one to tune the calix[*n*]arene framework, introducing features such as additional binding sites for metal ions in close proximity to the lower-rim or internal cavity.

When the ¹H NMR spectrum of H₄TBC[4] is obtained it can be seen that the spectrum is rather simplistic as the aromatic protons, the *t*-butyl protons and the hydroxyl protons all appear as singlets, with the methylene bridge protons appearing as a pair of doublets. Kammerer *et al.* discovered that this pair of doublets coalesced to a singlet at higher temperatures due to the conformational flexibility of the compound.⁷ The protons on the methylene bridge are in equatorial or axial positions, and so geminal coupling is observed, leading to the pair of doublets in the NMR spectrum. Arduini *et al.* were able to assign each of the protons with the lower field doublet being the proton in the axial position that is closer to the hydroxyl groups and the higher field doublet as the equatorial proton closer to the aromatic rings; this was achieved through Nuclear Overhauser Effect experiments and pyridine-induced shift experiments.²⁹

Substitution at one or two methylene bridge positions has been achieved through various ways, such as the fragment condensation method,³⁰ through a spirodienone route,^{31, 32} by a homologous anionic ortho-Fries rearrangement,³³ and through alkylation of a mono-lithiated tetra-methoxycalix[4]arene as an intermediate.³⁴



Scheme 1.2. Synthetic scheme for the preparation of TBC[4]OMe derivatives substituted at one methylene bridge position through alkylation of the lithiated derivative.

Scheme 1.2 shows the general reaction scheme for the alkylation of a lithiated calix[4]arene, in which R can be groups such as methyl, ethyl and benzyl.³⁴ This is achieved through lithiation of tetra-methoxy-*p*-*tert*-butylcalix[4]arene (TBC[4]OMe) with *n*-butyllithium (*n*-BuLi) followed by the addition of electrophile, R. The alkylation of a lithiated calix[4]arene is of interest as it a method by which it is possible to prepare a biscalixarene linked directly *via* the methylene bridge. Fantini and co-workers reported the synthesis of 2,2'-bis(calix[4]arene) (H₈BisTBC[4], Figure 1.4) using this procedure.³⁵

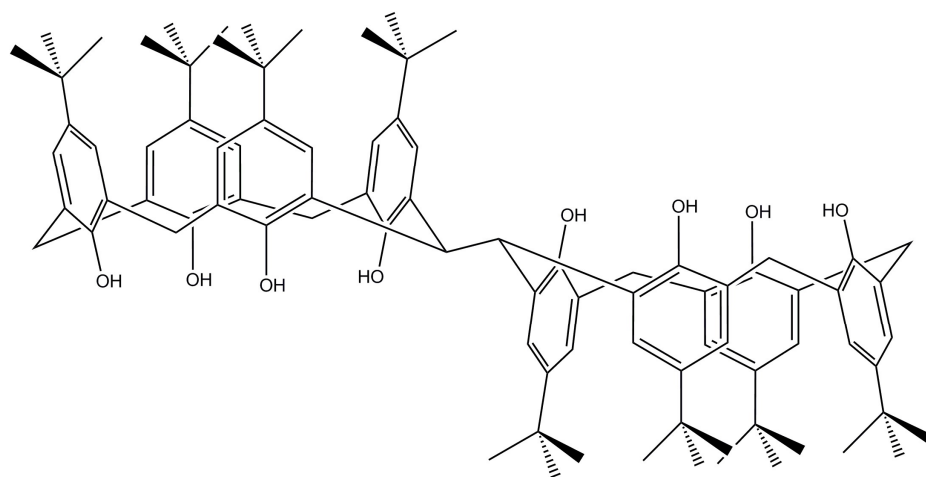


Figure 1.4. Schematic of 2,2'-biscalixarene isolated by Fantini *et al.*³⁵

Investigations into this chemistry were carried out by the Dalgarno group, and they were able to synthesise a series of biscalix[4]arenes with a variety of tethers such as alkyl chains³⁶ and xylyl linkers.³⁷ The coordination chemistry of these biscalix[4]arenes is discussed in Section 1.5.

When a calix[4]arene is mono-substituted at all four methylene bridge positions with identical substituents, four isomers (*rccc*, *rcct*, *rcct* and *rtct*) can exist and these are shown in Figure 1.5. These are configurational isomers and are determined by taking one of the substituents as a reference (*r*) with the other substituents being assigned as either *cis* (*c*) or *trans* (*t*) relative to the reference (e.g. *rc* etc). When a calixarene adopts the cone conformation then the *rccc* isomer is the only one in which the substituents at the bridge are equatorial and positioned away from any steric hindrance.

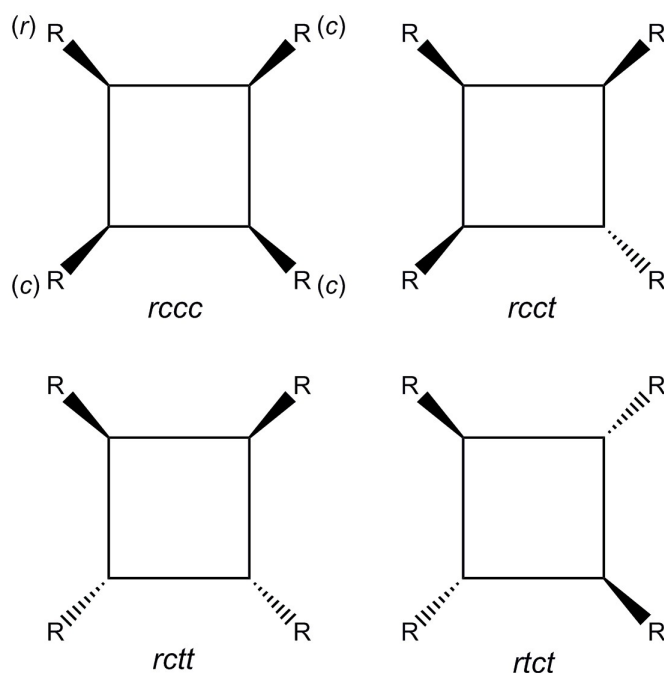
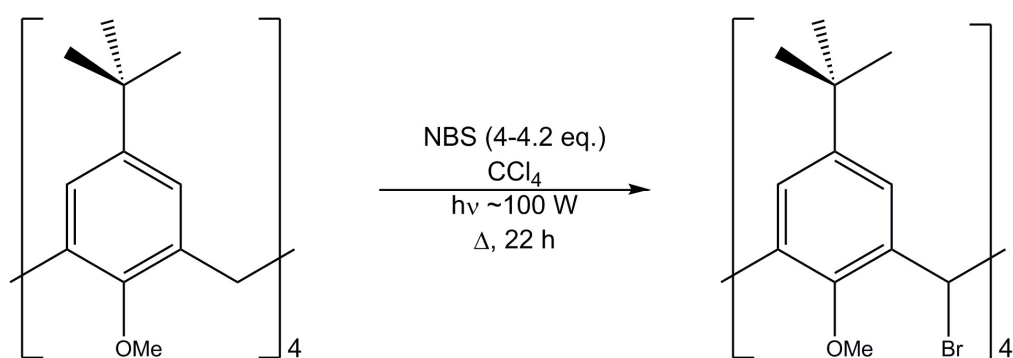


Figure 1.5. Representations of the isomers of calix[4]arenes that have been mono-substituted at each of the methylene bridge positions and assigned configuration.

The preparation of calix[4]arene derivatives with all four methylene bridges functionalised is particularly challenging, but Biali and co-workers have pioneered this work and it is now possible to synthesise a relatively small number of calixarenes substituted at one or all of the bridge positions. One of the first examples where all four bridge positions had been mono-substituted was reported by Gormar *et al.*, the product in this case being a ketocalix[4]arene derivative isolated through CrO_3 oxidation of the methylene groups which, upon further reaction, yielded the octahydroxy calix[4]arene derivative.³⁸ Itzhak and Biali repeated the experimental procedure reported by Gormar and found that it did not yield the octahydroxy calix[4]arene derivative, but instead produced the derivative where the methylene bridge was substituted with methoxy groups and the phenolic hydroxyl groups were still intact.³⁹

Calix[4]arenes in which the methylene bridge has been functionalised with bromine atoms have been shown to be useful synthetic intermediates for the preparation of analogues in which all four bridges are mono-substituted, provided that the bromine atoms can be replaced with another group. The first reported synthesis of the tetra-bromo calix[4]arene derivative was carried out by Klenke *et al.* in 1998 when they reacted the tetra-methoxy calix[4]arene derivative with an excess of NBS in carbon tetrachloride in the presence of azobisisobutyronitrile (AIBN). AIBN has been added to the reaction

mixture to act as an initiator in this case. A single crystal of the major product obtained from this reaction was found to adopt the cone conformation with the bromine groups located in equatorial positions.⁴⁰ Kumar *et al.* then modified this procedure slightly to remove the need for AIBN, and instead carried the reaction out in the presence of light with a large excess of NBS (14 equivalents).⁴¹ Biali and co-workers repeated the photochemical bromination as described by Kumar *et al.* and found that the NMR of the crude product indicated the formation of a mixture of products. Upon recrystallisation from hexane they isolated a product that, on the basis of its ¹H NMR spectrum, they characterised as a hexabromo derivative. Following this, they carried out the same reaction using nearly stoichiometric equivalents (4-4.2 eq., Scheme 1.3) of NBS to attempt to prevent formation of the hexabromo derivative.

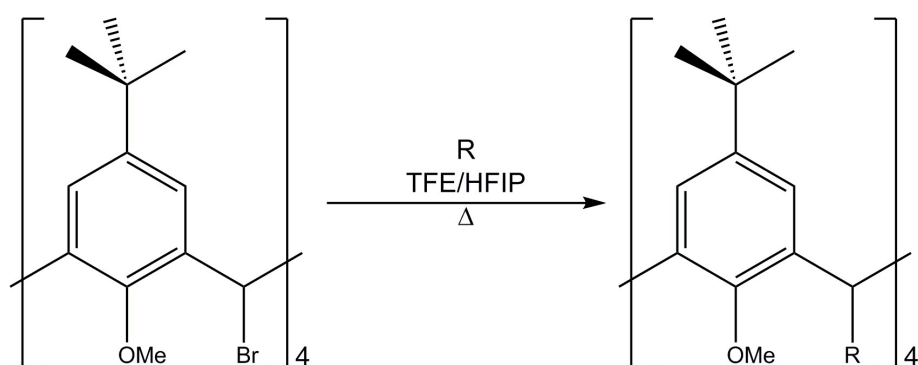


Scheme 1.3. Synthetic scheme for the tetra-bromination of TBC[4]OMe as reported by Biali and co-workers.⁴²

The compound obtained from this reaction had a very different ¹H NMR spectrum as compared to that in the literature so the authors grew a single crystal from chloroform/hexane. The structure obtained from the diffraction studies showed that the calix[4]arene derivative existed in the cone conformation, with the methylene bridge positions mono-substituted with bromine atoms which were located in the equatorial positions.⁴² It was thought that the literature ¹H NMR spectrum reported by Kumar and co-workers was in fact that of a mixture of products, such as the tetra- and hexa-substituted derivatives.

Biali and co-workers thought that they could replace the bridge bromine atoms through lithiation followed by reaction with an electrophile, or through reaction with strong nucleophiles under S_N2 conditions. However, preliminary experiments resulted in decomposition and so they decided to concentrate on solvolysis under S_N1 conditions.

They then reacted the tetra-brominated derivative under solvolytic conditions to form new compounds with C-O, C-N and even C-C bonds at the four methylene bridges. These compounds were formed through reaction in a mixture of a nucleophile and a solvent of high ionising power such as trifluoroethanol (TFE) or hexafluoroisopropanol (HFIP). The ionising solvent is generally present in a much larger concentration than the nucleophile and so ideally the ionising solvent would have a low nucleophilicity to ensure tetra-substitution by the nucleophile since there is a competition between the solvent and the nucleophile with the carbocation that is formed by dissociation of the C-Br bond (Scheme 1.4).

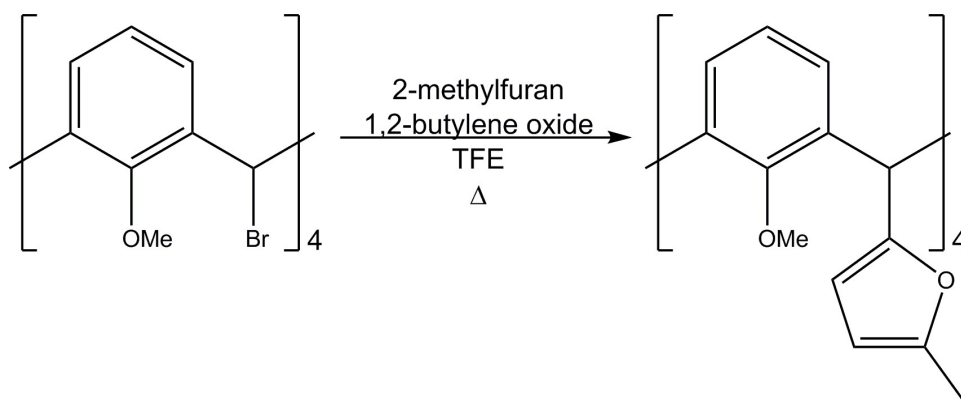


Scheme 1.4. Synthetic scheme for the solvolysis of the tetra-brominated C[4] derivative (where R = OMe, OEt, O-*n*-Pr, O-*i*-Pr, O-*t*-Bu or N₃).

Initially, they carried out a control reaction in TFE alone without the addition of a nucleophile and obtained the tetra-substituted product. The next set of reactions were conducted in TFE and an alcohol which were successful in forming the tetra-alkoxy calix[4]arene derivatives. They successfully carried out the reactions with methanol, ethanol, 1-propanol, 2-propanol and *t*-butanol with the major product being the *rccc* isomer. C-N bonds are also readily formed at the bridge position and this is achieved through reaction of the tetra-bromo species with sodium azide yielding the tetra-azido calix[4]arene derivative. Unlike the reactions with alcohols which formed the *rccc* isomer preferentially, the reaction with the azide formed a mixture of the *rcct* (major product), *rcctt* and *rccc* isomers.

One reaction of particular interest is where a new C-C bond is formed at the bridge. This was achieved by reaction of the tetra-bromo derivative of C[4] with 2-methylfuran under solvolytic Friedel-Crafts conditions as shown in Scheme 1.5.⁴³ These conditions were based on a report by Mayr and co-workers in which Friedel-Crafts

alkylations can be carried out in the absence of Lewis acid catalysts, if the nucleophilicity of the solvent is lower than that of the nucleophile.⁴⁴ The authors formed the tetrakis(2-methylfuranyl) calix[4]arene derivative using 1,2-butylene oxide as a HBr scavenger and in the absence of the epoxide a mixture of products are obtained which could not be separated.



Scheme 1.5. Synthetic scheme for the preparation of tetrakis(2-methylfuranyl) calix[4]arene derivative.

A single crystal of the furanyl derivative was grown from chloroform/methanol and X-ray analysis showed that the calixarene adopts a pinched-cone conformation with the furan groups in the equatorial positions (*rccc* isomer). The pinched-cone conformation is one in which the calixarene adopts a cone conformation where two phenyl rings opposite to one another are almost parallel while the other two are spread outward. It is possible to see from inspection of the crystal structure that the furan groups are oriented in such a way that the O-atoms are pointing down towards the lower-rim (Figure 1.6).

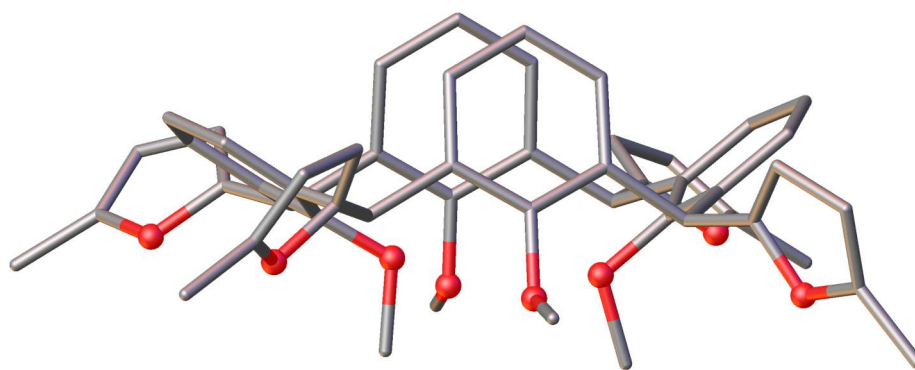
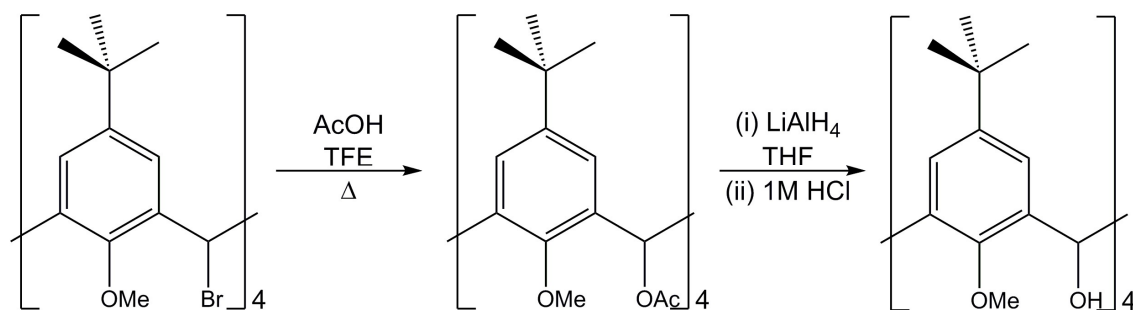


Figure 1.6. Single crystal structure of tetrakis(2-methylfuran-2-yl) calix[4]arene shown in ball and stick representation.⁴³ Colour code: C – grey; O – red. H atoms are omitted for clarity.

Biali and co-workers were able to repeat this reaction using TBC[4]OMe in place of C[4]OMe under the same reaction conditions as previously described.⁴² Interestingly, this is one of the only compounds that has been further functionalised by the same group, as furan groups are attractive for Diels-Alder reactions. The tetra-furan TBC[4] derivative was reacted with benzyne which was followed by deoxygenation to give the corresponding arene derivatives.

Given that the literature procedure reported by Gormar did not yield the octahydroxy calix[4]arene derivative when repeated by Biali and co-workers, another method of introducing hydroxyl groups at the methylene bridge was devised. This was achieved through a two-step synthesis by solvolysis of the tetra-brominated derivative in acetic acid to afford the tetra-acetoxy compound which was then reduced to the tetra-hydroxy derivative by LiAlH_4 (Scheme 1.6).



Scheme 1.6. Synthetic scheme for the tetra-acetylation at the bridge of tetra-methoxy TBC[4] and subsequent reduction of the acetoxy groups to hydroxyl groups.

Mono-substitution at all of the methylene bridge positions is not only limited to calix[4]arenes but also expands to substitution at the methylene bridge position of calix[5, 6 or 8]arenes again through the brominated derivatives of these calixarenes.^{40, 41} From these brominated derivatives, Biali and co-workers were able to prepare derivatives that were again mono-substituted at all bridge positions^{45, 46} or compounds that possessed a single monofunctionalised methylene bridge.⁴⁷

1.4 Molecular Magnetism

The main aim of the work in this thesis was to synthesise new mono-substituted calix[4]arene derivatives and subsequently isolate *3d*, *4f* or *3d-4f* polymetallic clusters to test whether they exhibit any interesting magnetic properties for their use as Single Molecule Magnets (SMMs) or Magnetic Refrigerants (MRs). It is therefore worth discussing this topic with particular detail into important literature examples of SMMs or MRs. Magnetic materials play a prominent part in our daily life and they can now be found in a wide range of applications such as medical equipment. One of the most important uses of these materials is in information storage technology and the miniaturisation of such devices is what drives the search for new magnetic materials. Due to fluctuations in magnetisation, information cannot be stored permanently at room temperature below a certain size of magnet, typically between 10-100 nm. However, smaller particles can be used as magnetic materials by working at lower temperatures or by taking advantage of quantum size effects, thus making nanomagnets appropriate candidates for quantum computers. Molecules containing several transition metal ions have been shown to exhibit similar magnetic behaviour compared to nanoscale magnetic materials. This has led to the study of these polynuclear metal clusters which display superparamagnetic-like properties and these materials have collectively become known as single molecule magnets, or SMMs for short.⁴⁸

SMMs are complexes that are able to retain their magnetisation in the absence of an applied magnetic field.⁴⁹ This means that the relaxation of magnetisation of these complexes occurs over long periods of time. It was discovered that molecules that possess an isolated high spin ground state with strong easy type axis magnetic anisotropy can behave as SMMs. The easy axis is the preferential direction of magnetisation.⁵⁰ This results in the formation of a potential energy barrier, which leads to magnetic bi-stability where the magnetisation exists in one of two potential wells, and this barrier must be

overcome in order to reverse the direction of magnetisation.⁵¹ In transition metal SMMs, the potential energy barrier can be expressed as $U_{\text{eff}} = |D|S^2$ for integer spins and $U_{\text{eff}} = |D|(S^2 - 0.25)$ for non-integer spins, where D is the axial zero-field splitting parameter and S is the spin ground state. Therefore it is desirable to prepare new SMMs with large S values and large and negative D values to make the energy barrier as large as possible.⁴⁹

The study of polynuclear clusters as magnetic materials was first reported by Bencini *et al.* when they synthesised two complexes in which a gadolinium(III) ion is bound to tetradentate copper salicylaldiminates. The results after testing the magnetic properties of these clusters are that the Gd^{III} and Cu^{II} ions interact ferromagnetically through a superexchange interaction mediated by the bridging oxygen ligands.⁵² The first SMM in the literature contains a $[\text{Mn}^{\text{IV}}_4\text{Mn}^{\text{III}}_8]$ metal core (Figure 1.7) and was reported by Sessoli and co-workers in 1993.^{53, 54} Using the published procedure by Lis,⁵⁵ they synthesised the complex with formula $[\text{Mn}_{12}\text{O}_{12}(\text{OOCCH}_3)_{16}(\text{H}_2\text{O})_4] \cdot 2\text{AcOH} \cdot 4\text{H}_2\text{O}$ which they found had a spin ground state of $S = 10$ through variable-field magnetisation and high-frequency electron paramagnetic resonance (HFEP).⁵⁶

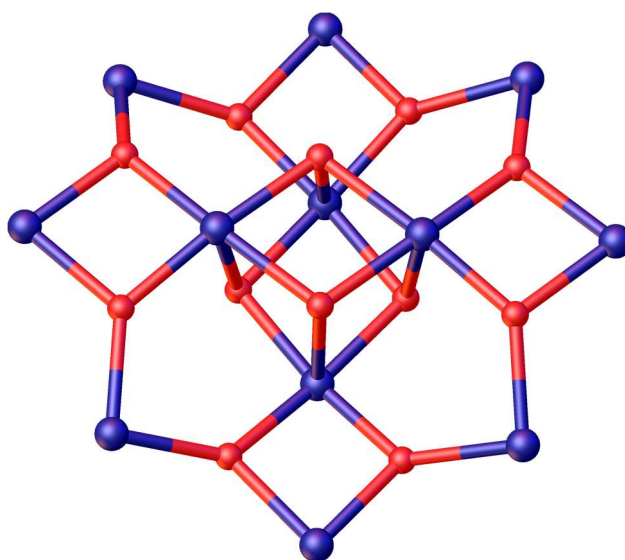


Figure 1.7. Partial single crystal X-ray structure showing the $[\text{Mn}^{\text{IV}}_4\text{Mn}^{\text{III}}_8\text{O}_{12}]$ core shown in ball and stick representation. Colour code: O – red; Mn – purple. Acetic acid and water of crystallisation and ligated acetate and water are omitted for clarity.

The large spin ground state is a result of antiferromagnetic interactions between the “spin-down” Mn^{IV} ($S = 3/2$) and “spin-up” Mn^{III} ($S = 2$) ions.⁵⁶ The presence of an axial zero-field splitting results in the splitting of the $S = 10$ states into 21 different levels, with each

level characterised by an energy and a spin quantum number, m_s , where $-S \leq m_s \leq S$. This Mn_{12} cluster has an axial zero-field splitting parameter D which is negative meaning that the states with large m_s are lowest in energy. The negative value of D leads to a potential energy barrier between the “spin-up” ($m_s = -10$) and “spin-down” ($m_s = 10$) orientations of the magnetic moment of each molecule with the $m_s = \pm 10$ levels being the lowest in energy. Therefore, in order to flip the moment from one orientation to the opposite orientation *via* the perpendicular $m_s = 0$ state then energy is required for this to occur due to the potential energy barrier. If this energy barrier is large, then the spin of the SMM can be magnetised in one direction with an exponential dependency on the height of the energy barrier for the magnetisation to reorient. The magnitude of the barrier is one way to compare the success of different SMMS as generally the larger the barrier, the more prominent the SMM properties are at higher temperatures. The size of the barrier was calculated to be around 70 K for the Mn_{12} cluster and due to this barrier, after magnetisation at 2 K and subsequent removal of the field, the relaxation of the magnetisation is so slow that after two months around 40% of magnetisation is still retained. The same measurements were carried out at 1.5 K and it was found that the relaxation was so slow it couldn't be measured. These results show that slow relaxation is due to individual molecules rather than long-range ordering as observed in bulk nanomagnets. When a magnetic field is applied to the Mn_{12} cluster all the spins will align with this field and this is the point where magnetic saturation is reached. If the external field is removed the magnetisation of the material is blocked by the presence of the energy barrier meaning that the spins cannot reorient and so some magnetisation of the cluster remains making it useful as a magnetic memory device. If a negative field is applied to this material then the height of the energy barrier is reduced and the spins can be magnetised in the opposite direction. A hysteresis loop is therefore observed in a plot of magnetisation (M) vs magnetic field (H) and these can vary between different magnetic materials.

As discussed previously, SMMs should have large S values and negative D values in order to maximise the height of the potential energy barrier and minimise relaxation. However, relaxation of the magnetisation of a nano-sized particle can also occur through macroscopic quantum tunnelling (MQT). It is rare for macrocycles to display MQT behaviour as these systems are generally large enough that they behave in a classical manner for the time they are observed. MQT of the magnetisation of the $\text{Mn}^{\text{IV}}_4\text{Mn}^{\text{III}}_8$ cluster has been observed as the hysteresis loops of this cluster are not smooth as “steps” can be seen at regular intervals that correspond to an increase in the magnetisation rate

when there are spin state energies of similar values on opposite sides of the potential energy well. At these critical field values, quantum tunnelling is allowed and therefore the relaxation rate from one spin state to another is enhanced.⁵⁷

Another important application of molecular nanomagnets is in the field of magnetic refrigeration in low temperature regions. A refrigeration system using magnets for a cooling effect is of interest as this means of cooling has greener advantages over traditional techniques that use vapour / gas compression. Cryocoolers capable of reaching temperature ranges of 1.8-20 K are of particular interest, not just for everyday applications, but for more advanced applications such as H₂ and He liquefiers, superconducting magnets and medical instrumentation, etc.⁵⁸ Normally these devices are cooled by liquid He which can generally reach around 1.8 K. However, the use of liquid He is not convenient as it is a difficult procedure to replace the liquid He that has been lost through evaporation, and also it is not economical due to the loss of expensive liquid He. Examples of low temperature (2-20 K) paramagnetic garnets that have been used as refrigerants are Gd₃Ga₅O₁₂ garnet (GGG) and Dy₃Al₅O₁₂ garnet (DAG).⁵⁹ Magnetic refrigeration is based on compounds displaying an enhanced magnetocaloric effect (MCE) at low temperatures. The MCE is the heating or cooling of a material due to variation of a magnetic field.⁶⁰ This is due to the coupling of the magnetic moment of a system to its temperature, through entropy changes of the material which result from varying the magnetic field. As entropy is a measure of disorder, the magnetic entropy of a material is related to the ordering of the magnetic moments of these materials. In these magnetic materials, the alignment of randomly oriented magnetic moments due to the application of a magnetic field (decreased entropy) results in the temperature of the material increasing, and if the applied magnetic field is then removed, the ordering is decreased (magnetic entropy increases) and the temperature of the material is decreased to balance the entropy increase.⁶¹ It is this concept that scientists are hoping to exploit in their search for low temperature magnetic refrigerants.

The first magnetic materials investigated for the MCE effect were the [Mn^{IV}₄Mn^{III}₈] cluster as previously described for its SMM properties⁵³ and the [Fe₈] cluster.⁶² Both these clusters have $S = 10$ and slow magnetisation relaxation times which make them suitable candidates for SMMs, but poor magnetic refrigerants (MRs). Some examples of clusters that display a large MCE with high spin ground states are the [Fe₁₄] cluster with $S = 25$,⁶³ the [Mn₁₀] supertetrahedron with $S = 22$,⁶⁴ and the [Mn₁₄] planar disk with $S = 7$ and the large MCE of these clusters is caused by the large spin ground state.

1.5 Calixarene-Supported Polynuclear Metal Clusters

Methylene-bridged calix[4]arenes possess a polyphenolic pocket at the lower-rim which is an attractive feature for metal complexation. In the cone conformation the metal cations can bind either in an *exo* or *endo* fashion shown in Figure 1.8.

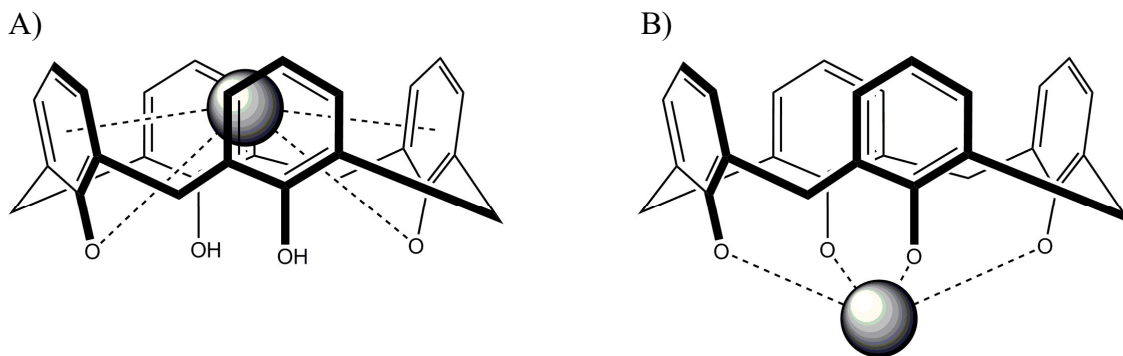


Figure 1.8. Representations of A) *endo*-H₂C[4] metal ion binding and B) *exo*-C[4] metal ion binding at the lower-rim position.

In the *exo* case the metal ion only interacts with the lower-rim phenolic oxygens and resides outside the calixarene cavity, whereas in the *endo* case the metal ion resides in the cavity and can interact with the phenolic oxygens as well as the π -faces of the aromatic groups. There are few metal cations that are large enough to participate in multiple cation- π -arene interactions in the aromatic cavity of the calixarene and so this makes *endo* metal coordination less favourable over *exo* coordination, particularly when there are alternative methods of coordination available through solvent interactions and / or O-phenolate complexation. Generally, the alkali and alkaline earth metals have a greater tendency to bind in an *endo* fashion to the phenolic oxygen atoms and also to the aromatic rings through cation- π interactions.⁶⁵

The first transition metal complexes utilising calixarenes as ligands were reported by Power *et al.* in 1985 where they reacted metal amides with H₄TBC[4] to obtain Ti^{IV}, Fe^{III} and Co^{II} complexes.⁶⁶ However, the first high-nuclearity calix[4]arene-based transition metal cluster was reported in 2008 by Luneau and co-workers.⁶⁷ They reacted H₄TBC[4] with VOSO₄ under anaerobic and solvothermal conditions in the presence of different bases to give compounds that all contained a mixed valence V^{III}V^{IV}₅O₁₉ core (Figure 1.9). The series of compounds are of the general formula [cat][V₆O₆(OCH₃)₈(TBC[4])(CH₃OH)] where cat is the conjugate acid of the base (e.g.

NH₄⁺). This was the first polyoxovanadate cluster with a Lindqvist-type structure and magnetic studies showed that the interaction between the V^{III} and V^{IV} metal centres was weakly ferromagnetic whereas the interaction between V^{IV} metal centres was antiferromagnetic.

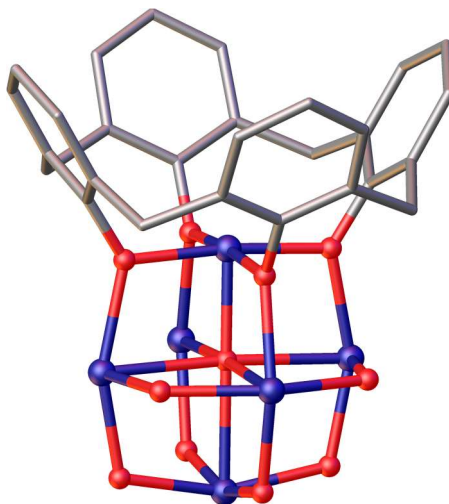


Figure 1.9. Single crystal X-ray structure of the polyoxovanadate cluster shown in ball and stick representation.⁶⁷ Colour code: C – grey; O – red; V – purple. H atoms, ^tBu groups, cations and ligated methanol and methoxide molecules are omitted for clarity.

Initial work carried out by Dalgarno and co-workers led to the synthesis of the first manganese cluster and the first SMM using a methylene-bridged calix[4]arene as a ligand. The cluster was of the formula [Mn^{III}₂Mn^{II}₂(μ₃-OH)₂(TBC[4])₂(DMF)₆] (**I**) in which the metallic core is in a planar diamond or butterfly-like shape with the wing-tip manganese ions in the +3 oxidation state and the body manganese ions in the +2 oxidation state.⁶⁸ This is a common structure type in manganese SMM chemistry, however the oxidation state distribution of compound **I** is the reverse of what is generally observed with other ligands.⁶⁹ The body Mn^{II} ions are a distorted octahedral geometry. The wing-tip Mn^{III} ions are also in a distorted octahedron with a Jahn-Teller axis.

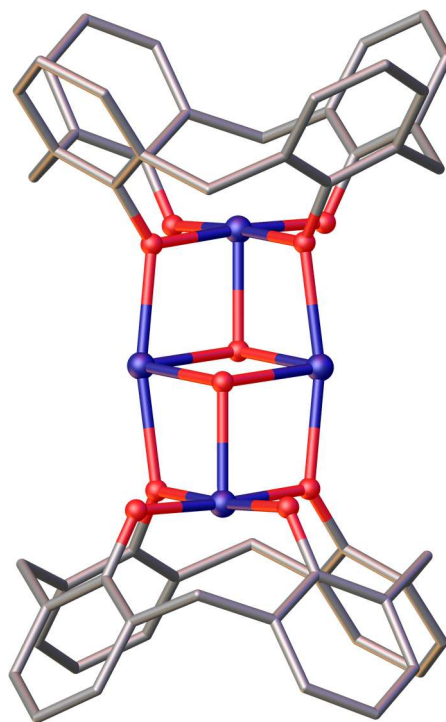


Figure 1.10. Single crystal X-ray structure of **I** showing formation of the mixed-valence $[\text{Mn}^{\text{III}}_2\text{Mn}^{\text{II}}_2]$ core that is supported by two tetra-anions of **1** shown in ball and stick representation.⁶⁸ Colour code: C – grey; O – red; Mn – purple. H atoms, ^tBu groups and ligated DMF molecules are omitted for clarity.

The magnetic properties of compound **I** were studied and it was found that the cluster displayed dominant but weak intramolecular ferromagnetic exchange. The spin ground state of the cluster is $S = 7$ which has several excited states with very little energy difference between them, thus defining a quasi-continuum of states. The magnetisation vs field experiments carried out in the ranges 0.5-7.0 T and 2-7 K showed that M increases slowly with H and does not reach saturation as quickly as it would for an isolated spin ground state. Hysteresis loop measurements carried out on single crystals of **I** confirm SMM behaviour. The loops indicate a well isolated SMM, with no intercluster interactions, even one in which there are many excited states mixed with the ground state. The formation of the $[\text{Mn}^{\text{III}}_2\text{Mn}^{\text{II}}_2]$ cluster core was further investigated by Taylor *et al.* through a number of solvent systems in the presence of an appropriate base (and in some cases co-ligand). From this resulted a family of calix[4]arene-supported $[\text{Mn}^{\text{III}}_2\text{Mn}^{\text{II}}_2]$ clusters with different solvent composition around the cluster periphery.⁷⁰

Another cluster type was isolated through the reaction of $\text{H}_4\text{TBC}[4]$ with Cu^{II} salts to yield calixarene-supported enneanuclear Cu^{II} clusters of formula

$[\text{Cu}^{\text{II}}_9(\text{TBC}[4])_3(\mu_3\text{-OH})_3(\text{NO}_3)_2(\text{DMSO})_6][\text{NO}_3] \cdot 6\text{DMSO} \cdot \text{MeOH}$ (**II**) shown in Figure 1.11.⁷¹

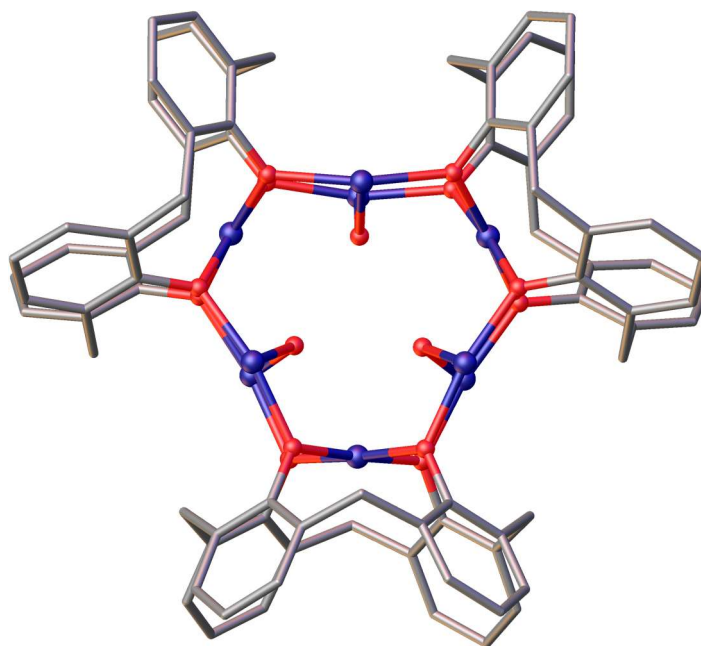


Figure 1.11. Single crystal X-ray structure of **II** showing the $[\text{Cu}^{\text{II}}_9(\text{TBC}[4])_3(\mu_3\text{-OH})_3]$ core shown in ball and stick representation. Colour code: C – grey; O – red; Cu – purple. DMSO and methanol of crystallisation, ^tBu groups, H atoms, nitrate anions and ligated solvent molecules are omitted for clarity.

The metallic core has been described as a tri-capped trigonal prism (Figure 1.11), which has three hydroxides positioned in the core that bridge Cu^{II} ions located at the vertices of the prism. The Cu^{II} ions that cap each of the rectangular faces of the prism are themselves capped by a TBC[4] moiety. The magnetic properties of this complex were explored and the measurements suggested relatively strong antiferromagnetic exchange between the Cu^{II} ions. The cluster has a spin ground state of $S = 3/2$ which was confirmed by magnetisation measurements carried out at various magnetic fields. The spin ground state can then be rationalised as the Cu^{II} ions of the trigonal prism being “spin-up” and the face-capping Cu^{II} ions being “spin-down”.

The group then went on to synthesise a series of calixarene-supported Ln^{III}_6 clusters (in which Ln = Gd, Tb or Dy, **III**).⁷² The structure of these clusters differ significantly from those formed with TMs, as the Ln^{III} ions are arranged at the vertices of an octahedron with formula $[\text{Ln}^{\text{III}}_6(\text{TBC}[4])_2(\mu_4\text{-O})_2(\mu\text{-OH})_{3.32}(\mu\text{-Cl})_{0.68}(\text{HCO})_2(\text{DMF})_8]$

(Figure 1.12). There are integer values for the bridging OH⁻ and Cl⁻ ligands due to disorder.

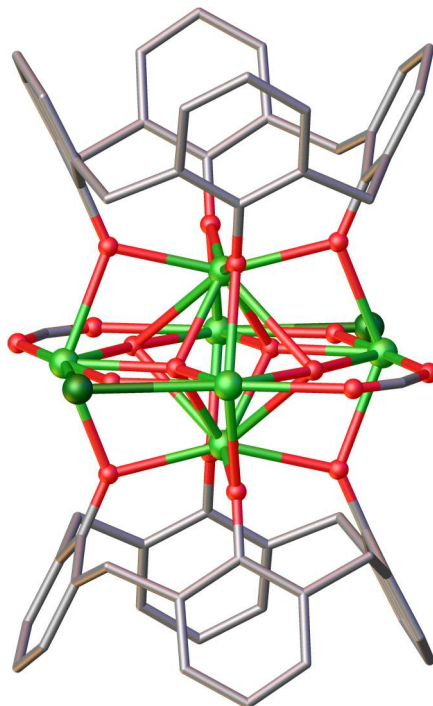


Figure 1.12. Single crystal X-ray structure of **III** showing Ln^{III}₆ octahedra and disordered Cl⁻/OH⁻ shown in ball and stick representation. Colour code: C – grey; O – red; Ln – green; Cl – dark green. H atoms, ^tBu groups and ligated solvent molecules are omitted for clarity.

The fully deprotonated TBC[4] ligands coordinate one Ln^{III} ion each within their lower-rim tetra-phenolic pocket. The remaining four Ln^{III} ions form the central metal square of the octahedron. The magnetic properties of this compound were investigated, through direct current (dc) magnetic susceptibility measurements, and these were indicative of weak antiferromagnetic exchange.

Research in the same group then moved on to the synthesis of the first calixarene-based mixed *3d-4f* metal clusters by reacting H₄C[4] with a manganese salt and a gadolinium salt to give the polymetallic cluster with formula [Mn^{III}₄Gd^{III}₄(OH)₄(C[4])₄(NO₃)₂(DMF)₆(H₂O)₆][OH]₂ (**IV**).^{73, 74} The cluster crystallised as purple blocks and is described as comprising of a near-planar octametalllic core having a square of Gd^{III} ions contained within a square of Mn^{III} ions (Figure 1.13). The Mn^{III} ions are found to be in Jahn-Teller distorted octahedral geometries and an important feature of the cluster is that the Mn^{III}C[4] motif found in **I** is preserved even in this mixed-

metal cluster. Magnetic studies of the complex showed that there was ferromagnetic exchange between the metal centres which resulted in a $S = 22$ spin ground state. The magnetisation vs field data shows that M only increases slowly with increasing H , rather than quickly reaching saturation as expected for an isolated spin state. The data suggests that the population of low-lying levels are only being depopulated at high applied magnetic fields. This result, along with the high magnetic isotropy, suggests that the complex is a suitable candidate for use as a magnetic refrigerant for low-temperature applications.

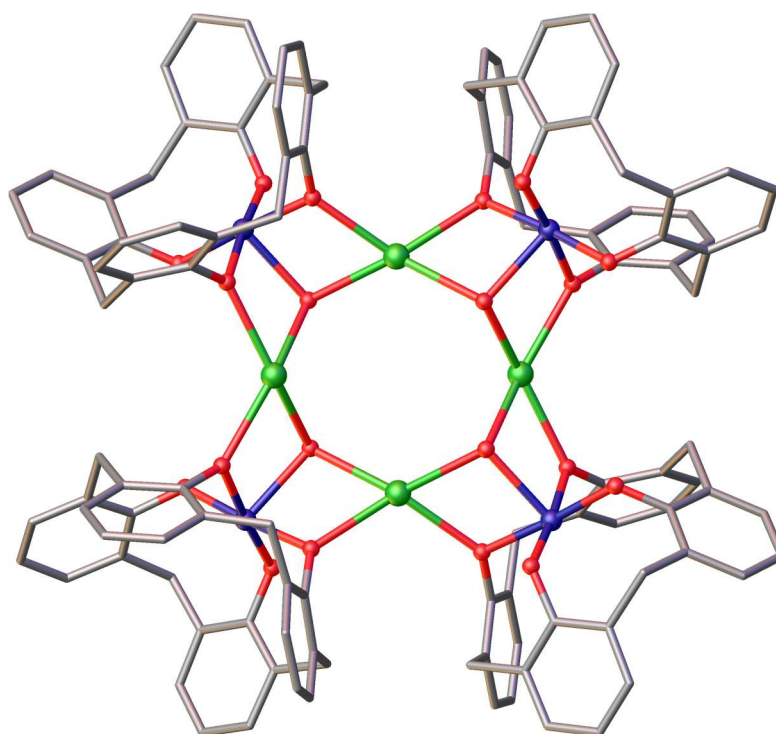


Figure 1.13. Single crystal X-ray structure of **IV** showing the $[\text{Mn}^{\text{III}}_4\text{Gd}^{\text{III}}_4]$ core that is supported by four tetra-anions of C[4] shown in ball and stick representation.⁷³ Colour code: C – grey; O – red; Mn – purple; Gd – green. Hydroxide anions, H atoms and ligated solvent molecules are omitted for clarity.

The group then went onto investigate whether it was possible to replace / interchange the Mn^{II} ions in **I** with other metal ions while maintaining the structural integrity of the complex. From this, the family of calixarene-supported metal clusters was expanded to include the $[\text{Mn}^{\text{III}}_2\text{Mn}^{\text{II}}\text{Ln}^{\text{III}}(\text{TBC}[4])_2(\mu_3\text{-OH})_2(\text{NO}_3)(\text{dmsO})_6]$ (**V**) and $[\text{Mn}^{\text{III}}_2\text{Ln}^{\text{III}}_2(\text{TBC}[4])_2(\mu_3\text{-OH})_2(\text{dmsO})_8]$ (**VI**) complexes shown in Figure 1.14.⁷⁵ In order to isolate this family of clusters fine-tuning of the reaction conditions was required (e.g. metal salt, stoichiometry and solvent).

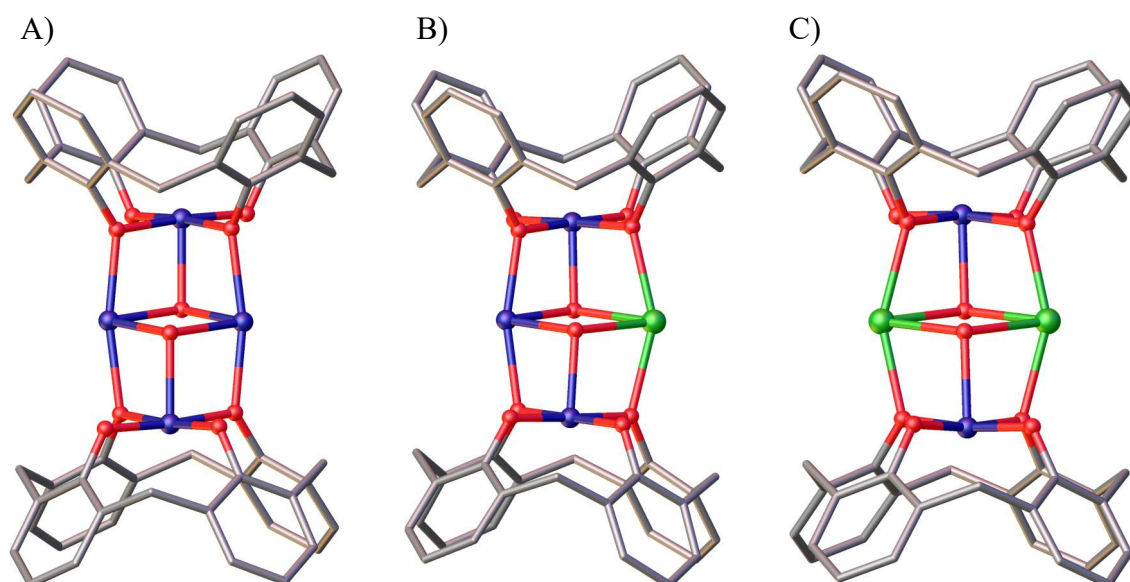


Figure 1.14. Single crystal X-ray structures comparing A) $[\text{Mn}^{\text{III}}_2\text{Mn}^{\text{II}}_2]$ core of **I**, B) $[\text{Mn}^{\text{III}}_2\text{Mn}^{\text{II}}\text{Ln}^{\text{III}}]$ core of **V** and C) $[\text{Mn}^{\text{III}}\text{Mn}^{\text{II}}\text{Ln}^{\text{III}}_2]$ core of **VI** shown in ball and stick representation.⁷⁵ Colour code: C – grey; O – red; Mn – purple; Ln – green. Solvent of crystallisation, ^tBu groups, H atoms and ligated solvent molecules are omitted for clarity.

Inspection of the crystal structures in Figure 1.14 shows that it is possible to replace / interchange either one or both of the Mn^{II} ions in **I** with Ln^{III} cations. Comparing the single crystal X-ray structures of **I** and **V** it can be seen that a larger, more highly coordinated Ln^{III} ion in place of Mn^{II} results in structural changes, albeit small, as it skews the relative orientations of the TBC[4] ligands causing distortion of the co-planarity of the TBC[4] moieties observed in **I** (Figure 1.14B). The co-planarity is then restored after the interchange of the second Mn^{II} ion with another Ln^{III} ion in **VI** (Figure 1.14C). The magnetic properties of these clusters were investigated over the temperature range of 5–300 K. The results from this study are that there is both ferro- and antiferromagnetic interactions observed in the clusters with these interactions becoming weaker as the Mn^{II} ions are replaced. It was found that the $\text{Mn}^{\text{III}}\text{-Mn}^{\text{II}}$ interaction is ferromagnetic and the $\text{Mn}^{\text{II}}\text{-Mn}^{\text{II}}$ interaction is antiferromagnetic. Comparison of the three clusters shows that moving from **I** to **V** to **VI**, two and four relatively strong ferromagnetic interactions ($\text{Mn}^{\text{III}}\text{-Mn}^{\text{II}}$) are replaced with two (**V**) and four (**VI**) very weak antiferromagnetic interactions that are at least an order of magnitude smaller. The antiferromagnetic $\text{Mn}^{\text{II}}\text{-Mn}^{\text{II}}$ interactions have also been replaced with even weaker antiferromagnetic interactions between $\text{Mn}^{\text{II}}\text{-Gd}^{\text{III}}$ and $\text{Gd}^{\text{III}}\text{-Gd}^{\text{III}}$.

Another cluster motif was reported by Taylor and co-workers in which they isolated a dimer of $[\text{Mn}^{\text{III}}\text{Mn}^{\text{II}}]$ clusters through the addition of a co-ligand, phenylphosphinate.⁷⁶ They were able to synthesis this using the same reaction conditions used to form **I** but with the addition of sodium phenylphosphinate to give the cluster with formula $[\text{Mn}^{\text{III}}\text{Mn}^{\text{II}}(\text{TBC}[4])_2(\mu_3\text{-O}_2\text{P}(\text{H})\text{Ph})(\text{DMF})_2(\text{MeOH})_2]_2$ (**VII**). The cluster has been described as an elongated version of **I** as it consists of two $[\text{Mn}^{\text{III}}\text{Mn}^{\text{II}}]$ moieties linked together by two bridging phosphinate ligands in which the two μ_3 -bridging hydroxyl groups of **I** have been replaced by two much larger μ_3 -bridging phosphinates (Figure 1.15). Again, the Mn^{III} ions are bound in the C[4] cavity.

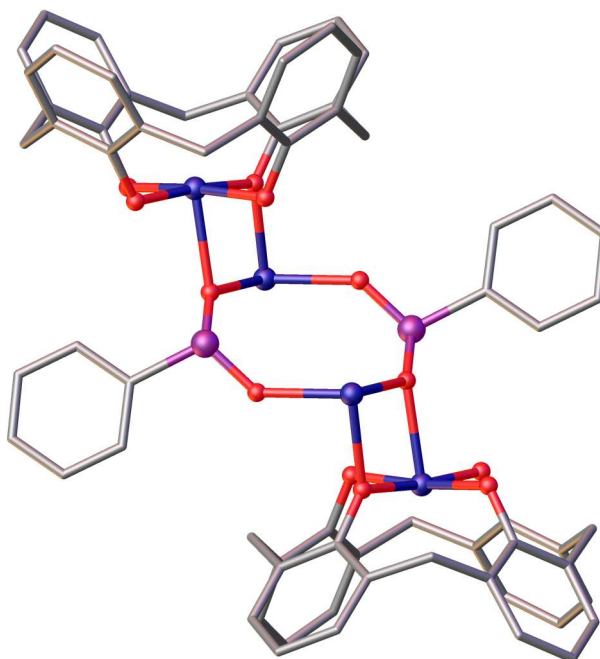


Figure 1.15. Single crystal X-ray structure of **VII** showing the bridging nature of the phenylphosphinate ligands shown in ball and stick representation.⁷⁶ Colour code: C – grey; O – red; Mn – purple; P – pink. H atoms, ^tBu groups and ligated DMF and MeOH molecules are omitted for clarity.

This research group has also investigated the coordination properties of 2,2'-biscalixarene ($\text{H}_8\text{BisTBC}[4]$) under analogous conditions used previously to synthesise the $[\text{Mn}^{\text{III}}_2\text{Mn}^{\text{II}}_2]$ cluster and from this a cluster of formula $[\text{Mn}^{\text{III}}_4\text{Mn}^{\text{II}}_4(\text{BisTBC}[4])_2(\mu_3\text{-OH})_2(\mu\text{-OH})(\mu\text{-Cl})(\text{H}_2\text{O})(\text{MeOH})(\text{DMF})_4] \cdot 2\text{H}_2\text{O} \cdot 12\text{CH}_3\text{CN}$ (**VIII**, Figure 1.16) was obtained.⁷⁷

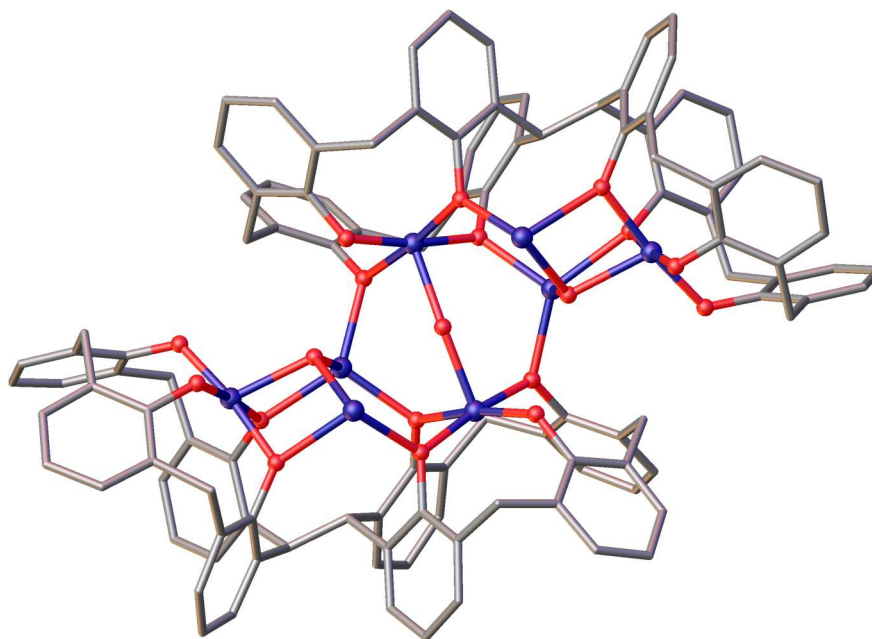


Figure 1.16. Single crystal X-ray structure of **VIII** shown in ball and stick representation.⁷⁷ Colour code: C – grey; O – red; Mn – purple. Water and acetonitrile of crystallisation, ^tBu groups, H atoms and ligated water, DMF and MeOH molecules are omitted for clarity.

The cluster isolated contains a mixed valence $[\text{Mn}^{\text{III}}_4\text{Mn}^{\text{II}}_4]$ core that is similar to the $[\text{Mn}^{\text{III}}_2\text{Mn}^{\text{II}}_2]$ cluster in **I** previously isolated in this group. The four Mn^{III} ions reside within the polyphenolic pocket at the lower-rim of the BisTBC[4] moieties, whereas the Mn^{II} ions reside outside the cavity in the binding pocket of the BisTBC[4]. The magnetic properties of **VIII** were investigated through dc magnetic susceptibility studies in the temperature range of 5-300 K. The results of this are expressed in the form of χT products, where $\chi = M/B$, M is the magnetisation, B is the applied magnetic field and T is the temperature. At 300 K the experimental χT value was lower than the expected χT value. A decrease in temperature resulted in the χT product remaining essentially constant until approximately 150 K, after which the value decreases rapidly. These studies showed that the ground spin-state of **VIII** is a singlet, i.e. ($S = 0$) with several excited spin-states with energies close to that of the ground state.

Another cluster was isolated from the reaction of $\text{H}_8\text{BisTBC}[4]$ with copper(II) nitrate hydrate in a basic medium of DMF/MeOH which was found to be of formula $[\text{Cu}^{\text{II}}_{13}(\text{BisTBC}[4])_2(\text{NO}_3)(\mu\text{-OH})_8(\text{DMF})_7][\text{OH}]\cdot 14\text{CH}_3\text{CN}$ (**IX**).⁷⁷ Structure analysis showed a $\text{Cu}^{\text{II}}_{13}$ cluster supported by two tetra-anions of $\text{H}_8\text{BisTBC}[4]$ moieties. The polyphenolic pockets of the BisTBC[4] units contain Cu^{II} ions and the additional binding

sites are also occupied by Cu^{II} ions. The Cu^{II}₄BisTBC[4] moieties are linked through four additional Cu^{II} ions and is thus described as a tetra-capped square prism. The remaining Cu^{II} ion resides in the centre of the prism and is distorted over several positions, however only one position is shown in Figure 1.17.

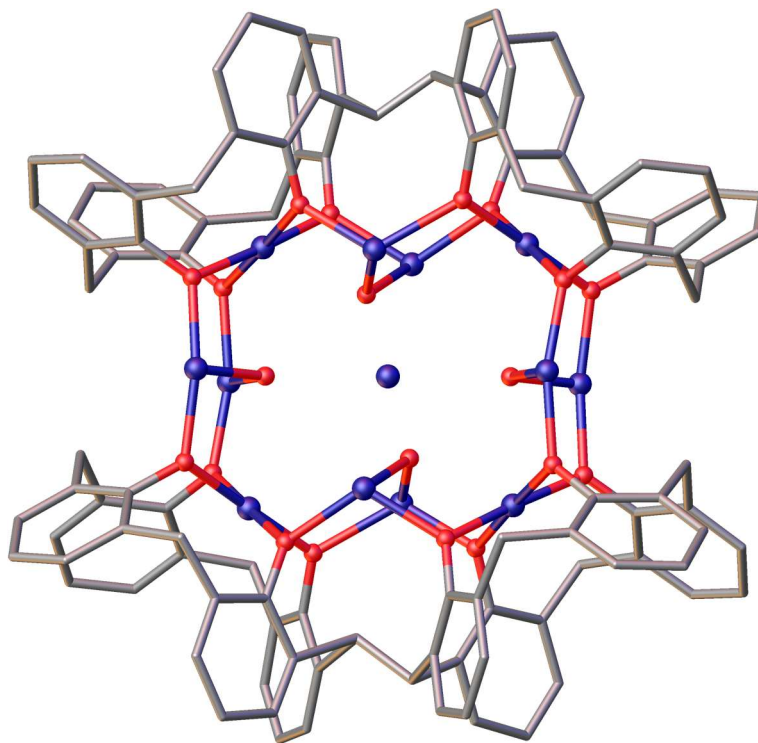


Figure 1.17. Single crystal X-ray structure of **IX** shown in ball and stick representation.⁷⁷ Colour code: C – grey; O – red; Cu – purple. Acetonitrile of crystallisation, hydroxide anion, ^tBu groups, H atoms and ligated nitrate and DMF molecules are omitted for clarity.

Again, the magnetic properties of **IX** were studied and it was found that at 300 K, the χT value is significantly lower than the expected value and this is indicative of strong antiferromagnetic interactions. Upon cooling the sample, the χT value decreases until it plateaus around 25 K and then reaches a minimum at 5 K. The ground spin-state was calculated to be a doubly degenerate $S = 1/2$ state, with the first excited state being a doubly degenerate $S = 1/2$ state lying higher in energy than the ground state.

Reaction of H₈BisTBC[4] with a mixture of manganese(II) chloride and gadolinium(III) chloride in a 1:1 DMF/MeOH mixture in the presence of base afforded single crystals of formula [Mn^{III}₄Mn^{II}₂Gd^{III}₂(BisTBC[4])₂(Cl)₂(μ -3-OH)₄(MeOH)₂(DMF)₈]·5Et₂O·DMF (**X**).⁷⁷ Structure analysis shows that each TBC[4] fragment contains a Mn^{III} ion within the cavity and again additional binding pockets are

created similar to **VIII**, however one of the Mn^{II} ions of **VIII** has been replaced with a Gd^{III} ion (Figure 1.18).

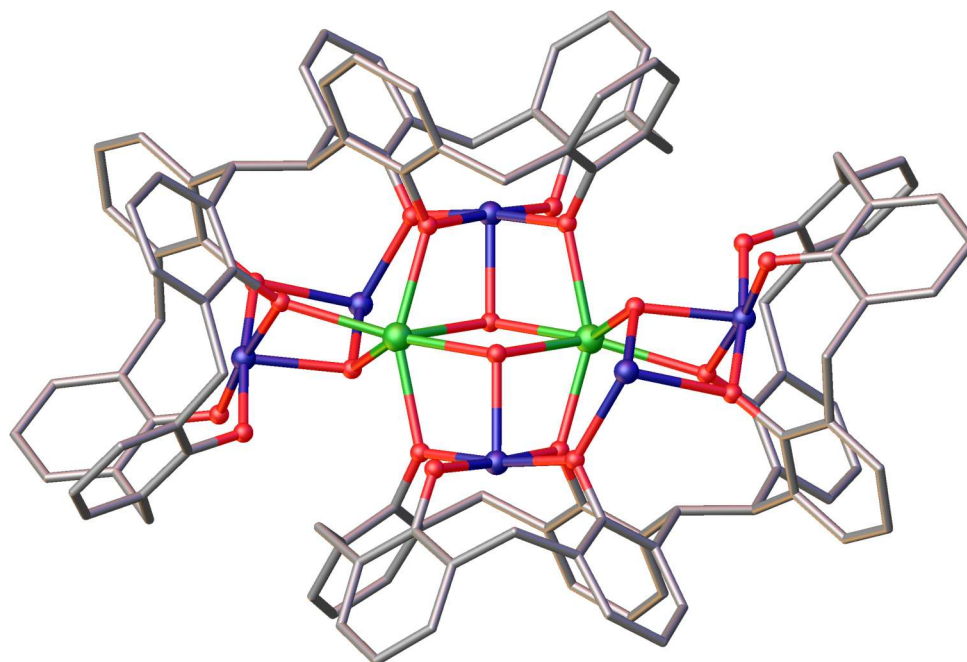


Figure 1.18. Single crystal X-ray structure of **X** shown in ball and stick representation.⁷⁷ Colour code: C – grey; O – red; Mn – purple; Gd – green. Diethyl ether and DMF of crystallisation, $t\text{Bu}$ groups, H atoms and ligated methanol and DMF molecules are omitted for clarity.

The magnetic properties of **X** were investigated and the χT value, at 300 K, was found to be slightly higher than the expected value. As the temperature is decreased the χT product remains constant until 150 K where the value increases reaching a maximum value at 5 K. The ground spin-state was found to be $S = 9$, with numerous excited states close in energy.

Further cluster-forming properties of $\text{H}_8\text{BisTBC}[4]$ were explored by Coletta *et al.*⁷⁸⁻⁸⁰ as well as the coordination properties of alkyl-tethered bis(calix[4]arenes (octane (**XI**), nonane (**XII**) and decane (**XIII**)) again using $3d$ and $4f$ metals. Use of the alkyl-tethered bis(calix[4]arenes showed that the standard $[\text{Mn}^{\text{III}}_2\text{Mn}^{\text{II}}_2]$ clusters formed as well as the $[\text{Mn}^{\text{III}}_4\text{Ln}^{\text{III}}_4]$ (**XIV**) as previously described in this chapter (Figure 1.19).³⁶

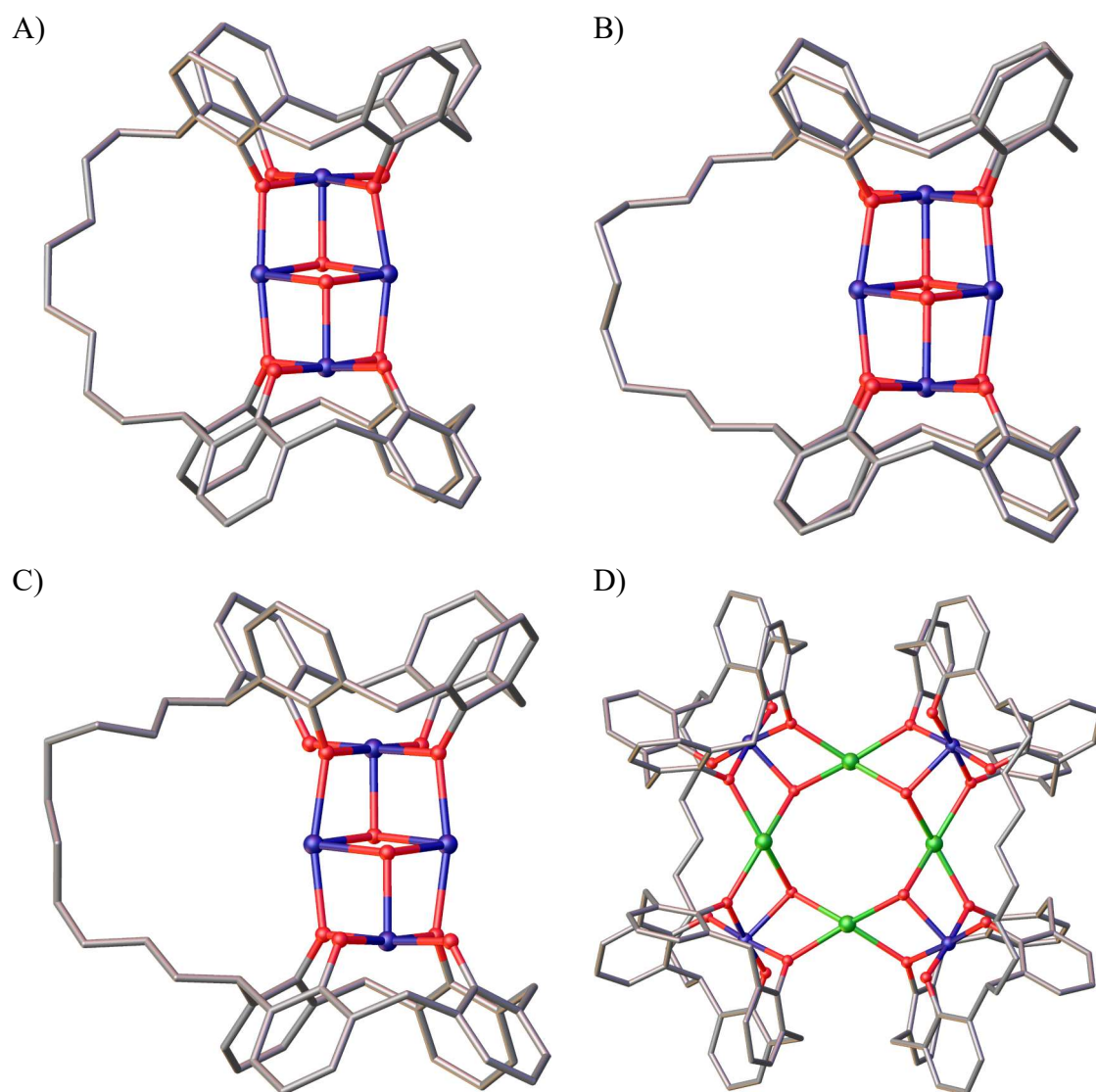


Figure 1.19. Single crystal structures of A) **XI**, B) **XII** and C) **XIII** showing the commonly adopted [Mn^{III}₂Mn^{II}₂] metal core and the single crystal structure of D) **XIV** showing the [Mn^{III}₄Ln^{III}₄] metal core in ball and stick representation. Colour code: C – grey; O – red; Mn – purple and Ln – green. Water, DMF and MeOH of crystallisation, ^tBu groups, H atoms and ligated water and DMF molecules are omitted for clarity.

From the exploratory cluster-forming studies with C[4]s as described so far, it was possible to observe constant structural trends, coordination preferences and common cluster motifs, and to establish the following empirical metal ion binding rules as follows:

1. TM cations are always bound within the polyphenolic pocket of C[4]s.
2. C[4]s will bind TM cations preferentially over Ln cations.
3. Ln^{III} cations are bound within the polyphenolic pockets of C[4]s in the absence of TM cations.

The coordination chemistry of the sulfur-bridged analogues of calixarenes (thiacalixarenes and their sulfinyl and sulfonyl derivatives) is different to that of methylene bridged calixarenes. This is due to the bridging atoms in these frameworks taking part in coordination, thereby producing structures that differ markedly from the clusters formed using methylene-bridged calixarenes. Methylene-bridged calix[4]arenes can coordinate to one metal cation at the lower-rim in an *exo* fashion, whereas the sulfur analogues possess heteroatoms or heteroatom containing groups at the bridge positions that act as additional donor atoms / binding sites resulting in the formation of polymetallic clusters (Figure 1.20).

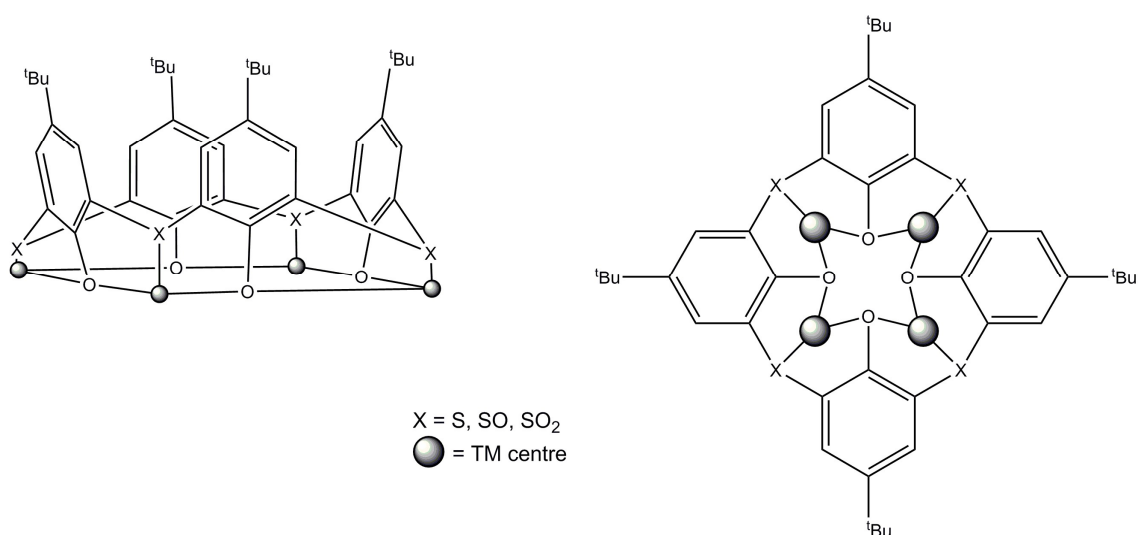


Figure 1.20. A) Metal binding motif and B) Schematic top-view of the metal binding modes of thiacalix[4]arenes and their sulfinyl and sulfonyl derivatives.

Examples of polymetallic clusters formed with thiacalix[4]arene and its sulfinyl derivatives are shown in Figure 1.21, as isolated by Luneau *et al.*⁸¹ Inspection of Figure

1.21 shows metal coordination at the functional groups presented at the bridge positions. Therefore, it was hoped that a similar type of behaviour could be invoked in methylene bridge-substituted C[4]s through the addition of extra donor atoms (e.g. via the introduction of substituents at this position in the C[4] framework).

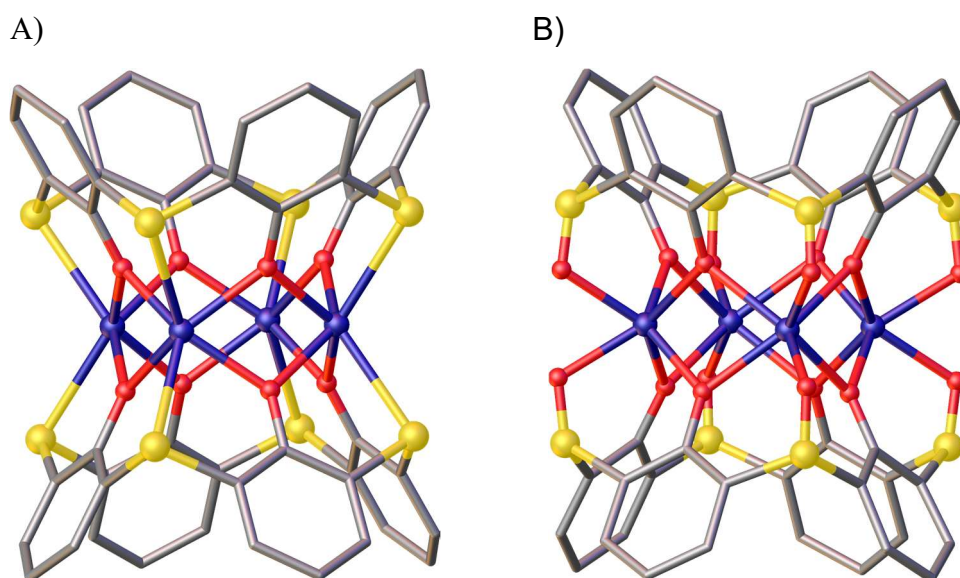


Figure 1.21. Single crystal structures of A) a thiacalix[4]arene-supported Mn_4 cluster showing coordination to the bridge S atoms as well as the lower-rim O atoms⁸¹ and B) a sulfinylcalix[4]arene-supported Mn_4 cluster showing coordination to the O atoms of the sulfinyl bridge groups as well as the lower-rim O atoms in ball and stick representation.⁸¹ Colour code: C – grey; O – red; S – yellow; Mn – purple. Solvent of crystallisation, ^tBu groups, H atoms and ligated solvent molecules have been omitted for clarity.

1.6 Aims

There are relatively few examples of mono-substitution at all four methylene bridge positions of a calix[4]arene. Therefore, the main aims of this thesis were to investigate methylene bridge-substituted C[4]s and their metal cluster formation properties in the hope that the additional functional groups at the bridge positions will introduce new binding sites altering cluster formation. The first aim was to synthesise a known bridge-substituted C[4] and to investigate its coordination chemistry, the goal being to influence the formation of new polymetallic clusters. The second aim was to further derivatise a reported methylene bridge-substituted C[4] to prepare novel compounds, therefore expanding the library of bridge-substituted C[4]s. The third aim involved the study of a pyridyl-substituted C[4] by testing its metal-organic cage formation properties. Finally, the last aim of the project was to investigate the post-synthetic modification of the $[\text{Mn}^{\text{III}}_2\text{Mn}^{\text{II}}_2]$ cluster motif through the addition of chelating co-ligands and to subsequently measure and establish structure activity relationships of the new clusters formed.

1.7 References

1. A. Baeyer, *Chem. Ber.*, 1872, **5**, 280-282.
2. L. H. Baekeland, *J. Ind. Eng. Chem.*, 1909, **1**, 149-161.
3. L. H. Baekeland, *J. Franklin I.*, 1910, **169**, 55-60.
4. A. Zinke and E. Ziegler, *Ber. Dtsch. Chem. Ges.*, 1944, **77**, 264-272.
5. B. T. Hayes and R. F. Hunter, *J. Appl. Chem*, 1958, **8**, 743-748.
6. J. W. Cornforth, P. D. Hart, G. A. Nicholls, R. J. W. Rees and J. A. Stock, *Brit. J. Pharmacol.*, 1955, **10**, 73-86.
7. C. D. Gutsche, *Acc. Chem. Res.*, 1983, **16**, 161-170.
8. C. D. Gutsche and R. Muthukrishnan, *J. Org. Chem.*, 1978, **43**, 4905-4906.
9. C. D. Gutsche, B. Dhawan, K. H. No and R. Muthukrishnan, *J. Am. Chem. Soc.*, 1981, **103**, 3782-3792.
10. C. D. Gutsche, M. Iqbal and D. Stewart, *J. Org. Chem.*, 1986, **51**, 742-745.
11. D. J. Cram and H. Steinberg, *J. Am. Chem. Soc.*, 1951, **73**, 5691-5704.
12. C. D. Gutsche, in *Calixarenes: An Introduction* RSC, 2 edn., 2008.
13. A. Ninagawa and H. Matsuda, *Makromol Chem-Rapid*, 1982, **3**, 65-67.
14. Y. Nakamoto and S. I. Ishida, *Makromol Chem-Rapid*, 1982, **3**, 705-707.
15. D. R. Stewart and C. D. Gutsche, *J. Am. Chem. Soc.*, 1999, **121**, 4136-4146.
16. V. Bohmer, D. Rathay and H. Kammerer, *Org. Prep. Proced. Int.*, 1978, **10**, 113-121.
17. C. D. Gutsche and P. F. Pagoria, *J. Org. Chem.*, 1985, **50**, 5795-5802.
18. M. S. Wong and J. F. Nicoud, *Tetrahedron Lett.*, 1993, **34**, 8237-8240.
19. C. D. Gutsche and K. C. Nam, *J. Am. Chem. Soc.*, 1988, **110**, 6153-6162.
20. C. D. Gutsche, J. A. Levine and P. K. Sujeeth, *J. Org. Chem.*, 1985, **50**, 5802-5806.
21. S. Shinkai, K. Araki, P. D. J. Grootenhuis and D. N. Reinhoudt, *J. Chem. Soc., Perkin Trans. 2*, 1991, 1883-1886.
22. K. Iwamoto, K. Araki and S. Shinkai, *J. Org. Chem.*, 1991, **56**, 4955-4962.
23. I. Bitter, A. Grun, B. Agai and L. Toke, *Tetrahedron*, 1995, **51**, 7835-7840.
24. C. D. Gutsche, B. Dhawan, J. A. Levine, K. H. No and L. J. Bauer, *Tetrahedron*, 1983, **39**, 409-426.
25. M. Iqbal, T. Mangiafico and C. D. Gutsche, *Tetrahedron*, 1987, **43**, 4917-4930.
26. K. A. See, F. R. Fronczek, W. H. Watson, R. P. Kashyap and C. D. Gutsche, *J. Org. Chem.*, 1991, **56**, 7256-7268.

27. C. M. Shu, W. C. Liu, M. C. Ku, F. S. Tang, M. L. Yeh and L. G. Lin, *J. Org. Chem.*, 1994, **59**, 3730-3733.
28. S. Kanamathareddy and C. D. Gutsche, *J. Org. Chem.*, 1995, **60**, 6070-6075.
29. A. Arduini, A. Pochini, S. Reverberi and R. Ungaro, *J. Chem. Soc., Chem. Commun.*, 1984, 981-982.
30. M. Tabatabai, W. Vogt and V. Bohmer, *Tetrahedron Lett.*, 1990, **31**, 3295-3298.
31. K. Agbaria, O. Aleksyuk, S. E. Biali, V. Bohmer, M. Frings and I. Thondorf, *J. Org. Chem.*, 2001, **66**, 2891-2899.
32. K. Agbaria and S. E. Biali, *J. Am. Chem. Soc.*, 2001, **123**, 12495-12503.
33. O. Middel, Z. Greff, N. J. Taylor, W. Verboom, D. N. Reinhoudt and V. Snieckus, *J. Org. Chem.*, 2000, **65**, 667-675.
34. P. A. Scully, T. M. Hamilton and J. L. Bennett, *Org. Lett.*, 2001, **3**, 2741-2744.
35. L. T. Carroll, P. A. Hill, C. Q. Ngo, K. P. Klatt and J. L. Fantini, *Tetrahedron*, 2013, **69**, 5002-5007.
36. M. Coletta, R. McLellan, J.-M. Cols, K. J. Gagnon, S. J. Teat, E. K. Brechin and S. J. Dalgarno, *Supramol. Chem.*, 2016, **28**, 557-566.
37. M. Coletta, R. McLellan, P. Murphy, B. T. Leube, S. Sanz, R. Clowes, K. J. Gagnon, S. J. Teat, A. I. Cooper, M. J. Paterson, E. K. Brechin and S. J. Dalgarno, *Chem. Eur. J.*, 2016, **22**, 8791-8795.
38. G. Gormar, K. Seiffarth, M. Schulz, J. Zimmermann and G. Flamig, *Makromol Chem*, 1990, **191**, 81-87.
39. N. Itzhak and S. E. Biali, *Synthesis-Stuttgart*, 2015, **47**, 1678-1682.
40. B. Klenke, C. Nather and W. Friedrichsen, *Tetrahedron Lett.*, 1998, **39**, 8967-8968.
41. S. Kumar, H. M. Chawla and R. Varadarajan, *Tetrahedron Lett.*, 2002, **43**, 7073-7075.
42. I. Columbus and S. E. Biali, *J. Org. Chem.*, 2008, **73**, 2598-2606.
43. I. Columbus and S. E. Biali, *Org. Lett.*, 2007, **9**, 2927-2929.
44. M. Hofmann, N. Hampel, T. Kanzian and H. Mayr, *Angew. Chem. Int. Ed*, 2004, **43**, 5402-5405.
45. K. Kogan and S. E. Biali, *J. Org. Chem.*, 2009, **74**, 7172-7175.
46. K. Kogan, I. Columbus and S. E. Biali, *J. Org. Chem.*, 2008, **73**, 7327-7335.
47. N. Itzhak, K. Kogan and S. E. Biali, *Eur. J. Org. Chem.*, 2011, 6581-6585.
48. G. Christou, D. Gatteschi, D. N. Hendrickson and R. Sessoli, *MRS Bull.*, 2000, **25**, 66-71.

49. R. A. Layfield, *Organometallics*, 2014, **33**, 1084-1099.
50. L. Sorace, C. Benelli and D. Gatteschi, *Chem. Soc. Rev.*, 2011, **40**, 3092-3104.
51. M. Murrie and D. J. Price, *Annu Rep Prog Chem A*, 2007, **103**, 20-38.
52. A. Bencini, C. Benelli, A. Caneschi, R. L. Carlin, A. Dei and D. Gatteschi, *J. Am. Chem. Soc.*, 1985, **107**, 8128-8136.
53. R. Sessoli, H. L. Tsai, A. R. Schake, S. Y. Wang, J. B. Vincent, K. Folting, D. Gatteschi, G. Christou and D. N. Hendrickson, *J. Am. Chem. Soc.*, 1993, **115**, 1804-1816.
54. R. Sessoli, D. Gatteschi, A. Caneschi and M. A. Novak, *Nature*, 1993, **365**, 141-143.
55. T. Lis, *Acta Crystallogr. B*, 1980, **36**, 2042-2046.
56. A. Caneschi, D. Gatteschi, R. Sessoli, A. L. Barra, L. C. Brunel and M. Guillot, *J. Am. Chem. Soc.*, 1991, **113**, 5873-5874.
57. L. Thomas, F. Lioni, R. Ballou, D. Gatteschi, R. Sessoli and B. Barbara, *Nature*, 1996, **383**, 145-147.
58. Y. I. Spichkin, A. K. Zvezdin, S. P. Gubin, A. S. Mischenko and A. M. Tishin, *J. Phys. D: Appl. Phys.*, 2001, **34**, 1162-1166.
59. M. D. Kuzmin and A. M. Tishin, *J. Phys. D: Appl. Phys.*, 1991, **24**, 2039-2044.
60. V. K. Pecharsky and K. A. Gschneidner, *J. Magn. Magn. Mater.*, 1999, **200**, 44-56.
61. O. Tegus, E. Bruck, K. H. J. Buschow and F. R. de Boer, *Nature*, 2002, **415**, 150-152.
62. C. Delfs, D. Gatteschi, L. Pardi, R. Sessoli, K. Wieghardt and D. Hanke, *Inorg. Chem.*, 1993, **32**, 3099-3103.
63. M. Evangelisti, A. Candini, A. Ghirri, M. Affronte, E. K. Brechin and E. J. L. McInnes, *Appl. Phys. Lett.*, 2005, **87**.
64. M. Manoli, R. D. L. Johnstone, S. Parsons, M. Murrie, M. Affronte, M. Evangelisti and E. K. Brechin, *Angew. Chem. Int. Ed.*, 2007, **46**, 4456-4460.
65. A. J. Petrella and C. L. Raston, *J. Organomet. Chem.*, 2004, **689**, 4125-4136.
66. M. M. Olmstead, G. Sigel, H. Hope, X. J. Xu and P. P. Power, *J. Am. Chem. Soc.*, 1985, **107**, 8087-8091.
67. C. Aronica, G. Chastanet, E. Zueva, S. A. Borshch, J. M. Clemente-Juan and D. Luneau, *J. Am. Chem. Soc.*, 2008, **130**, 2365-2371.
68. G. Karotsis, S. J. Teat, W. Wernsdorfer, S. Piligkos, S. J. Dalgarno and E. K. Brechin, *Angew. Chem. Int. Ed.*, 2009, **48**, 8285-8288.

69. E. K. Brechin, J. Yoo, M. Nakano, J. C. Huffman, D. N. Hendrickson and G. Christou, *Chem. Commun.*, 1999, 783-784.
70. S. M. Taylor, G. Karotsis, R. D. McIntosh, S. Kennedy, S. J. Teat, C. M. Beavers, W. Wernsdorfer, S. Piligkos, S. J. Dalgarno and E. K. Brechin, *Chem. Eur. J.*, 2011, **17**, 7521-7530.
71. G. Karotsis, S. Kennedy, S. J. Dalgarno and E. K. Brechin, *Chem. Commun.*, 2010, **46**, 3884-3886.
72. S. Sanz, R. D. McIntosh, C. M. Beavers, S. J. Teat, M. Evangelisti, E. K. Brechin and S. J. Dalgarno, *Chem. Commun.*, 2012, **48**, 1449-1451.
73. G. Karotsis, M. Evangelisti, S. J. Dalgarno and E. K. Brechin, *Angew. Chem. Int. Ed.*, 2009, **48**, 9928-9931.
74. G. Karotsis, S. Kennedy, S. J. Teat, C. M. Beavers, D. A. Fowler, J. J. Morales, M. Evangelisti, S. J. Dalgarno and E. K. Brechin, *J. Am. Chem. Soc.*, 2010, **132**, 12983-12990.
75. M. A. Palacios, R. McLellan, C. M. Beavers, S. J. Teat, H. Weihe, S. Piligkos, S. J. Dalgarno and E. K. Brechin, *Chem. Eur. J.*, 2015, **21**, 11212-11218.
76. S. M. Taylor, J. M. Frost, R. McLellan, R. D. McIntosh, E. K. Brechin and S. J. Dalgarno, *Crystengcomm*, 2014, **16**, 8098-8101.
77. R. McLellan, M. A. Palacios, C. M. Beavers, S. J. Teat, S. Piligkos, E. K. Brechin and S. J. Dalgarno, *Chem. Eur. J.*, 2015, **21**, 2804-2812.
78. M. Coletta, R. McLellan, A. Waddington, S. Sanz, K. J. Gagnon, S. J. Teat, E. K. Brechin and S. J. Dalgarno, *Chem. Commun.*, 2016, **52**, 14246-14249.
79. M. Coletta, R. McLellan, S. Sanz, K. J. Gagnon, S. J. Teat, E. K. Brechin and S. J. Dalgarno, *Chem. Eur. J.*, 2017, **23**, 14073-14079.
80. M. Coletta, S. Sanz, L. J. McCormick, S. J. Teat, E. K. Brechin and S. J. Dalgarno, *Dalton Trans.*, 2017, **46**, 16807-16811.
81. C. Desroches, G. Pilet, S. A. Borshch, S. Parola and D. Luneau, *Inorg. Chem.*, 2005, **44**, 9112-9120.

Chapter 2

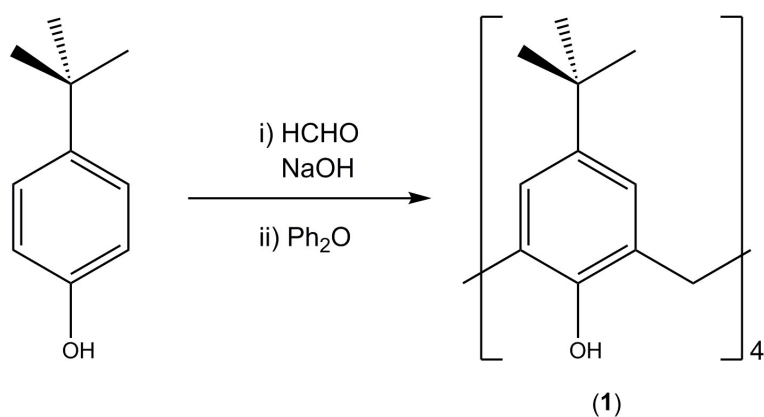
Synthesis of a Methylene Bridge-Substituted Calix[4]arene and its Use in Polynuclear Metal Cluster Formation

2.1 Introduction

The work in this chapter covers the synthesis of a calix[4]arene that has been mono-substituted at the methylene bridge position and its subsequent coordination properties in the hope that the introduction of additional metal binding sites will influence the clusters formed. A search of the literature shows that there are relatively few examples of calix[4]arenes that are mono-substituted at all four methylene bridge positions suggesting that these are difficult compounds to synthesise. However, one suitable candidate that can be readily synthesised with all substituted groups equatorial was found to be 5,11,17,23-tetra-*tert*-butyl-2,8,14,20-tetrakis(2-methylfuranyl)-25,26,27,28-tetramethoxycalix[4]arene (**4**) reported by Biali and co-workers¹ and so this was taken as the starting point for this section of the work. Compound **4** was synthesised following literature procedures by lower-rim alkylation (to afford the tetra-methoxy TBC[4] derivative (**2**)), monobromination at all four bridge positions and subsequent reaction with 2-methylfuran in the presence of 1,2-butylene oxide to afford compound **4** and the coordination properties of 5,11,17,23-tetra-*tert*-butyl-2,8,14,20-tetrakis(2-methylfuranyl)-25,26,27,28-tetrahydroxycalix[4]arene (**H45**) are described below. A general description of the method employed to synthesise *3d* and *4f* clusters is provided, as well as the crystallisation methods used to isolate single crystals that were suitable for X-ray diffraction studies. The crystal structures of any metal clusters obtained from this work are described in detail and these are compared to clusters previously isolated in this research group.

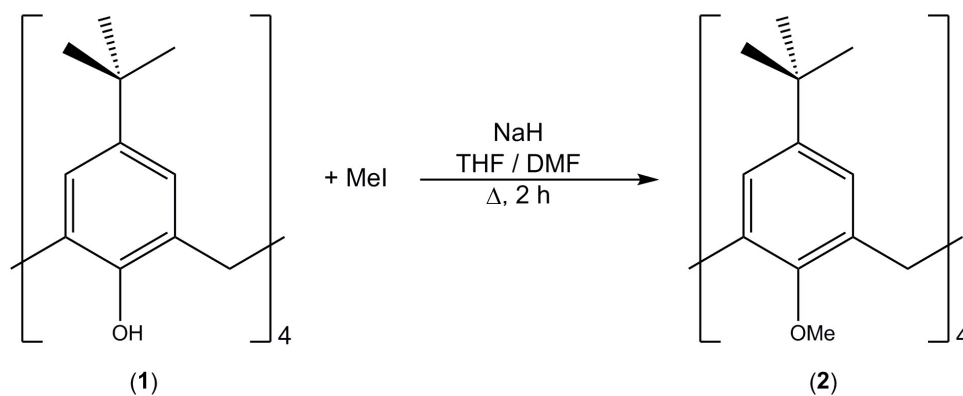
2.2 Furan Derivatisation at the Methylene Bridge of Calix[4]arenes

The synthesis of a calix[4]arene, C[4], that has been mono-substituted at all four methylene bridge positions was carried out according to literature procedures in the work of Gutsche and co-workers.² The first synthetic step involved the preparation of *p*-*tert*-butylcalix[4]arene (H₄TBC[4], **1**) following the modified procedure by Gutsche *et al.* which involved the base-induced condensation reaction between *p*-*tert*-butylphenol and formaldehyde solution (Scheme 2.1).² During the reaction a thick yellow mass forms, which is called the precursor, and this is the product formed from the condensation reaction between the phenol and formaldehyde. This precursor was then suspended in toluene and diphenyl ether, followed by reflux at 260 °C for 4 hours. The solid formed from this step was then filtered and washed with ethyl acetate to afford **1** as a crystalline white solid.



Scheme 2.1. Synthetic scheme for the synthesis of *p*-*tert*-butylcalix[4]arene (**1**).

Due to the acidity of the phenolic hydroxyl protons,³ the lower-rim requires protection in order to restrict hydroxyl reactivity towards other reagents. This was achieved through tetra-alkylation of **1** to yield the corresponding tetra-ether. As described in Chapter 1, the lower-rim of C[4]s can be reacted with haloalkanes of various lengths, but this can drastically change the conformation that the C[4] adopts. The alkylating agent used here was methyl iodide, offering simple methyl protection at the lower-rim. The reaction was carried out by addition of sodium hydride (to deprotonate the lower-rim hydroxyl groups) followed by methyl iodide which acts as an electrophile to afford 5,11,17,23-tetra-*tert*-butyl-25,26,27,28-tetramethoxycalix[4]arene (**2**) as shown in Scheme 2.2.

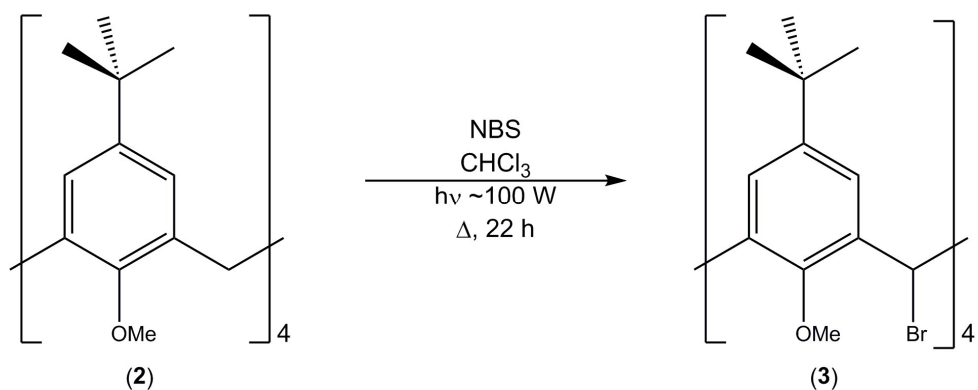


Scheme 2.2. Synthetic scheme for the preparation of 5,11,17,23-tetra-*tert*-butyl-25,26,27,28-tetramethoxycalix[4]arene (**2**).

The ^1H NMR spectrum obtained from this reaction shows loss of the hydroxyl group which appears at 10.35 ppm in the starting material **1**, indicating that the reaction has gone to completion. Interestingly, the ^1H NMR spectrum shows peak broadening which suggests that the calixarene no longer exists in the cone conformation. The consequence of lower-rim alkylation to form **2** means that the hydrogen bonding which is responsible for stabilising the cone conformation is disrupted resulting in rotation through the annulus of the calixarene and therefore rapid interconversion of the four conformers in solution. This ultimately leads to line broadening in the ^1H NMR spectrum. This can be simplified by complexation with a Na^+ ion which reduces the conformational flexibility; this occurs as the lower-rim oxygens bind the Na^+ ions, resulting in the calixarene adopting the cone conformation and leading to much sharper resonances. The ^1H NMR spectrum of **2** was collected in a 3:1 v/v mixture of chloroform- d /acetonitrile- d_3 which had been saturated with sodium iodide. Inspection of the ^1H NMR spectrum shows sharp signals that can easily be assigned to all of the protons in the compound. Comparing the ^1H NMR spectra of **1** and **2** it is possible to see the loss of the hydroxyl group resonance at 10.35 ppm and the introduction of the methoxy group protons at 4.01 ppm confirming the success of the reaction.

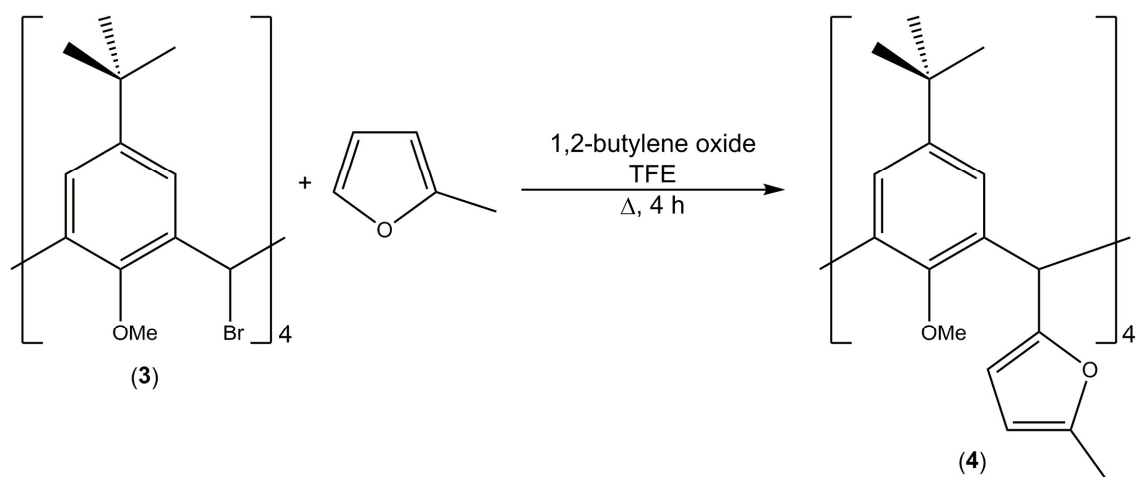
The next step in the synthesis was the photochemical bromination of **2** with *N*-bromosuccinimide (NBS). A slight modification of the literature procedure reported by Biali and co-workers was used here as the authors used carbon tetrachloride as solvent.⁴ Chloroform was used in place of the literature solvent, along with stoichiometric equivalents of NBS to ensure tetra-substitution. The reaction was carried out in the presence of light to facilitate the photochemical reaction, and after subsequent work-up,

5,11,17,23-tetra-*tert*-butyl-2,8,14,20-tetrabromo-25,26,27,28-tetramethoxycalix[4]arene (**3**) was obtained.



Scheme 2.3. Synthetic scheme for the synthesis of 5,11,17,23-tetra-*tert*-butyl-2,8,14,20-tetrabromo-25,26,27,28-tetramethoxycalix[4]arene (**3**).

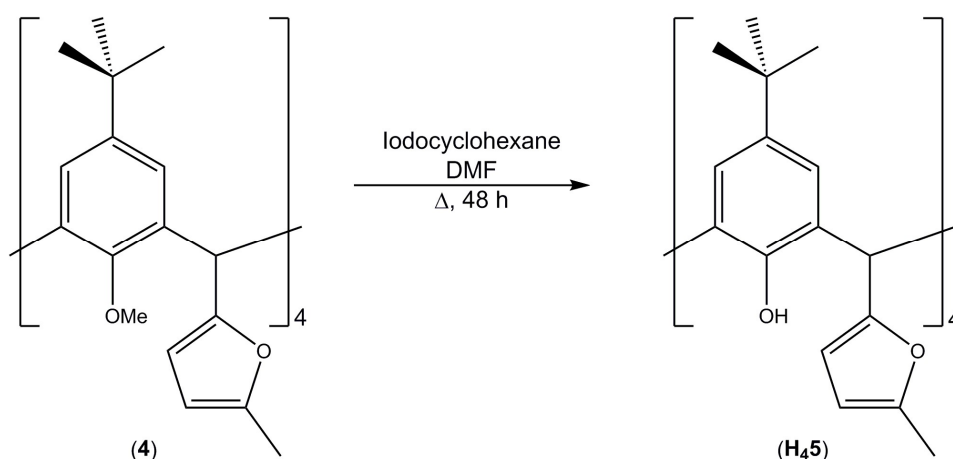
Following the synthesis of compound **3**, this was reacted with 2-methylfuran in trifluoroethanol (TFE) in the presence of 1,2-butylene oxide to yield 5,11,17,23-tetra-*tert*-butyl-2,8,14,20-tetrakis(2-methylfuranyl)-25,26,27,28-tetramethoxycalix[4]arene (**4**). As the reaction reaches reflux, the colour of the solution goes from colourless to pink and then back to colourless once all the solid is in solution. The epoxide is added in this case to act as a HBr scavenger as reported by Sasson *et al.*⁵



Scheme 2.4. Synthetic scheme for the preparation of 5,11,17,23-tetra-*tert*-butyl-2,8,14,20-tetrakis(2-methylfuranyl)-25,26,27,28-tetramethoxycalix[4]arene (**4**).

2.3 Deprotection of the Lower-rim of 4

As lower-rim hydroxyl groups are required for C[4]s to form polymetallic clusters (through coordination and bridging), it is necessary to deprotect compound **4** to restore the phenolic hydroxyl groups. The demethylation step was carried out by heating a DMF solution of **4** in the presence of iodocyclohexane, affording the demethylated derivative (**H45**, Scheme 2.5). In doing so, hydroiodic acid is produced *in-situ* through an elimination reaction. This in turn reacts with the lower-rim methoxy groups to generate iodomethane and restore the lower-rim hydroxyl functionality in the C[4] framework. Iodocyclohexane is the demethylating reagent of choice here, rather than conventional reagents such as boron tribromide or trimethylsilyl iodide, as the methyl groups can be removed under milder reaction conditions with shorter reaction times. Zuo *et al.* investigated demethylation using various iodoalkanes in different solvents, and from this they found that a) iodocyclohexane provided the best yields in the shortest reaction times and b) the reaction is dependent on the basicity of the solvent used as it should be basic enough to induce the elimination reaction of the HI but not strong enough so as to neutralise the HI.⁶ Using these literature reaction conditions for **4**, reaction with a large excess (45 equivalents) of iodocyclohexane at reflux for 48 hours yielded **H45**.



Scheme 2.5. Synthetic scheme for the synthesis of the 5,11,17,23-tetra-*tert*-butyl-2,8,14,20-tetrakis(2-methylfuran-2-yl)-25,26,27,28-tetrahydroxycalix[4]arene (**H45**).

The ¹H NMR spectrum of the compound obtained from this reaction was confirmed to be of the fully deprotected derivative by the loss of the methyl group at 3.89 ppm and the presence of a new peak at 8.94 ppm which is indicative of a phenolic hydroxyl group.

The ^{13}C NMR spectrum also confirms that the target compound was synthesised as the carbon peak of the methoxy group in the methylated furanyl derivative at 61.9 ppm is no longer present. Matrix assisted laser desorption ionisation-time of flight (MALDI-TOF) mass spectrometry and IR analysis were also used to characterise this compound and these also confirm that the target product has been synthesised. Single crystals suitable for X-ray diffraction studies were grown by slow evaporation of a chloroform solution of **H45**. The crystals were found to be in a triclinic cell and structure solution was carried out in the space group *P*-1. Inspection of the structure (Figure 2.1) shows that the protecting methyl groups have been removed, thereby restoring the phenolic hydroxyl groups as expected. It is also interesting to note that the furan moieties remain in the equatorial positions. Biali and co-workers carried out molecular mechanics (MM3) calculations on a C[4] that had been mono-substituted at each of the bridge positions with a methoxy group where the group found that the lowest energy conformation was in fact the cone conformation where all the substituents sit in the equatorial positions.⁴ From this, they concluded that C[4] conformations where the methylene bridge substituents are in the equatorial positions are favoured over the axial positions. After it was confirmed that complete demethylation had occurred, the ligand was in a suitable form to test its potential for metal cluster formation with a view to exploring how the furan moieties affect this process.

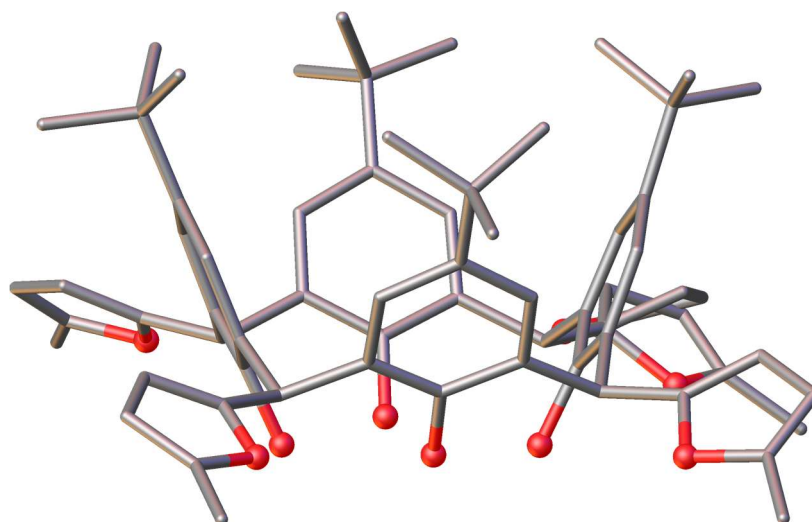


Figure 2.1. Single crystal X-ray structure of **H45** shown in ball and stick representation. Colour code: C – grey, O – red. Methanol and chloroform of crystallisation and H atoms are omitted for clarity.

2.4 Exploration of Metal Cluster Formation with **H45**

Metal complexation with thiacalix[4]arenes affords polymetallic clusters due to the additional functionality at the bridge positions. Although the coordination chemistry of thiacalix[4]arene is necessarily very different to that of methylene-bridged C[4]s, it was thought that this type of behaviour could be invoked in methylene-bridged calix[4]arenes through the addition of various substituents at these positions, offering the potential to control or influence C[4]-supported cluster-forming chemistry in different ways. In order to test this hypothesis, the coordination properties of **H45** were tested through reaction of this ligand with various transition or lanthanide metal salts, or mixtures of both. This was explored by first testing whether the known (and common) $[\text{Mn}^{\text{III}}_2\text{Mn}^{\text{II}}_2]$ butterfly cluster motif would form under standard reaction conditions previously reported by this research group.⁷ The next steps of the investigation involved reaction of **H45** with a mixture of 3*d* and 4*f* metal salts to test whether mixed-metal clusters could in fact be isolated, and also to see if the furans would coordinate a metal ion, potentially a lanthanide, leading to the formation of a new polymetallic cluster. This was investigated through the reaction of the ligand with varying ratios of a transition metal salt and a lanthanide metal salt to test if the stoichiometry played a role in cluster formation.

The general procedure employed to test the coordination properties involved accurately weighing out **H45** and the appropriate metal salts in different equivalents; Mn salts are generally used as the source of TM ions, but Fe and Cu salts can also be used, and in this case Gd, Dy and Tb salts were used as the source of Ln ions. In the case of attempting to form a bimetallic system (using a mixture of 3*d* and 4*f* metals) the anions of the metal salts should be kept the same, e.g. both chloride salts or nitrate salts. This mixture was then dissolved in a 1:1 DMF/MeOH mixture (to aid solubility) and stirred at room temperature for 10 minutes before an excess of triethylamine (Et₃N) was added to ensure full deprotonation of the hydroxyl groups at the lower-rim; in the case of the furanyl derivative, six equivalents of base were added to ensure that all four hydroxyl groups had been deprotonated. The solution was cloudy and contained undissolved ligand before addition of the base, which upon addition rapidly afforded a deep purple solution. The solutions were then stirred at room temperature for two hours before they were filtered to remove any microcrystalline material. The filtered solution was then used in an attempt to grow suitable single crystals for X-ray diffraction studies by either slow evaporation or vapour diffusion of a more volatile solvent into the mother liquor. Vapour diffusions were set up by taking small aliquots of the mother liquor in small vials, and

then transferring these in to larger vials containing counter-solvents such as diethyl ether (Et₂O), acetonitrile (CH₃CN) or petroleum ether (PET). A summary of the cluster-forming reactions attempted is presented in Table 2.1, indicating which experiments were successful from the reaction matrix.

Table 2.1. Summary of cluster-forming reactions attempted with **H45** and transition or lanthanide metal cations, as well as metal ion mixtures. Compound numbers are indicated where single crystals were obtained and studied (*vide infra*).

	Mn ^{II}	Mn ^{II} /Ln ^{III} (1:1)	Mn ^{II} /Ln ^{III} (4:1)	Mn ^{II} /Ln ^{III} (1:4)	Cu ^{II}
H45	✓	✓	✗	✓	✗
Cluster no.	6	7, 8	-	9, 10	-

2.4.1 Reaction of H45 with Mn^{II} ions

Given the frequency with which the [Mn^{III}₂Mn^{II}₂] cluster has been formed in this research group's efforts, this was selected as the first target cluster topology, essentially as a test of cluster-forming capability. Reaction of **H45** with manganese(II) chloride tetrahydrate in a 1:1 DMF/MeOH mixture in the presence of Et₃N as a base afforded a deep purple solution upon stirring at room temperature. Good quality single crystals grew upon vapour diffusion of PET into the mother liquor and diffraction studies showed them to be of the formula [Mn^{III}₂Mn^{II}₂(μ₃-OH)₂(**5**)₂(DMF)₄(MeOH)₂]·3MeOH·Et₂O (**6**). The crystals were found to be in a triclinic cell and structure solution was carried out in the space group *P*-1. The asymmetric unit (ASU) was found to consist of half of the compound formula and upon symmetry expansion revealed that the common [Mn^{III}₂Mn^{II}₂] structural type found previously had formed (Figure 2.2). The cluster is comprised of a [Mn^{III}₂Mn^{II}₂] core in the planar diamond or butterfly-like shape similar to that of the clusters previously formed in the group in which the wing-tip manganese ions (Mn1) are in the oxidation state +3, and the body manganese ions (Mn2) are in the oxidation state +2. The wing-tip manganese ion is bound by the tetra-phenolic pocket upon deprotonation and is in a distorted octahedral geometry in MnO₆ coordination spheres, with the Jahn-Teller axes being defined by O(DMF)-Mn-O(OH) with an angle of O9-Mn1-O12 of 168.22(14)°. A DMF molecule resides within each calixarene cavity

(Mn1-O9, 2.295(4) Å) and the μ_3 -hydroxide bridges Mn^{III} (Mn1-O12, 2.142(4) Å) and Mn^{II} ions (Mn2 and its symmetry equivalent) (Mn2-O12, 2.167(4) Å). The four remaining positions around the Mn1 ion are occupied by the oxygen atoms at the lower-rim of **5** (O1-O4, Mn-O bond length range 1.909(4) – 1.971(4) Å), two of which are also bridging to the Mn2 ions (Mn2-O2, 2.238(4) Å). The two remaining equatorial positions around Mn2 are occupied by a DMF (Mn2-O10, 2.142(4) Å) and methanol molecule (Mn2-O11, 2.152(5) Å).

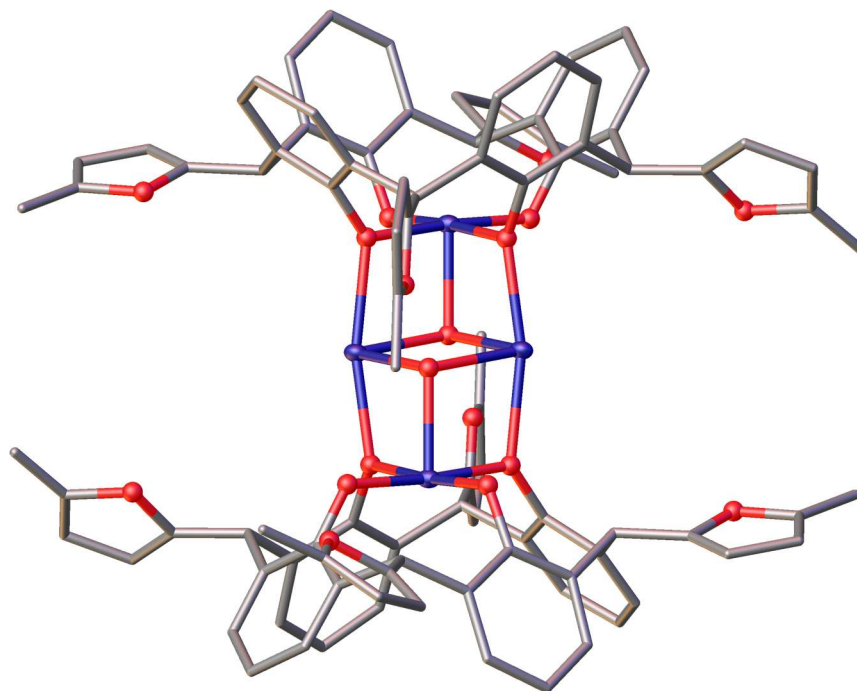


Figure 2.2. Single crystal X-ray structure of **6** showing formation of the mixed-valence $[\text{Mn}^{\text{III}}_2\text{Mn}^{\text{II}}_2]$ core that is supported by two tetra-anions of **H45** shown in ball and stick representation. Colour code: C – grey, O – red, Mn – purple. Methanol and diethyl ether of crystallisation, ^tBu groups, H atoms and ligated methanol and DMF molecules are omitted for clarity.

Inspection of the crystal structure shows that the furan moieties have maintained their equatorial positions on the calixarene framework and that they are far enough away from the core that they do not interfere with the ligated solvent molecules. The metallic core of this cluster varies slightly from the TBC[4]-supported analogue (**I**) as reported by Dalgarno and co-workers,⁸ as it possesses four ligated DMF and two ligated methanol molecules, as opposed to the six ligated DMF molecules on the reported TBC[4] cluster, but otherwise the overall structure is very similar.

2.4.2 Reaction of **H45** with a 1:1 mixture of Mn^{II}:Ln^{III} ions

The next sets of reactions (Table 2.1) attempted to form mixed-metal clusters by using a mixture of metal salts with the first set of crystals formed from the reaction involving a 1:1 ratio of Mn:Gd ions and these were purple in colour, indicating the presence of Mn^{III} ions. These were formed from the reaction of **H45** with manganese(II) chloride tetrahydrate and gadolinium(III) chloride hexahydrate in the presence of Et₃N, followed by slow evaporation of the mother liquor. The crystals were found to be in a triclinic cell and structure solution was carried out in the space group *P*-1. Surprisingly, the crystals were found to be of the formula [Mn^{III}₂Mn^{II}₂(μ₃-OH)₂(**5**)₂(DMF)₆] [Mn^{III}₂Mn^{II}₂(μ₃-OH)₂(**5**)₂(DMF)_{5.5}(H₂O)_{0.5}]₂DMF (**7**) indicating that the Gd^{III} ions are not incorporated in the cluster core. This behaviour is unusual compared to that of the clusters formed from the reaction of 3*d*/4*f* metal salt mixtures with C[4]*s* which gave mixed-metal clusters.⁹ The ASU was found to contain half of the aforementioned formula, and two butterflies were afforded upon symmetry expansion. The metallic core of these butterflies are similar to that of **6** with the exception of ligated solvent. One noticeable difference is that one of the butterflies (A) of **7** (Figure 2.3) possesses six ligated DMF molecules whereas compound **6** possesses four DMF and two MeOH. The second butterfly (B) (Figure 2.3) also differs slightly as, although there are four ligated DMF molecules, the cavities of the symmetry equivalents of **7** are occupied by disordered water (ligated) and DMF (non-ligated). It is also worth noting in butterfly (B) that although the furan groups are still equatorial they have rotated and the oxygen atoms are now pointing up towards the *t*-butyl groups.

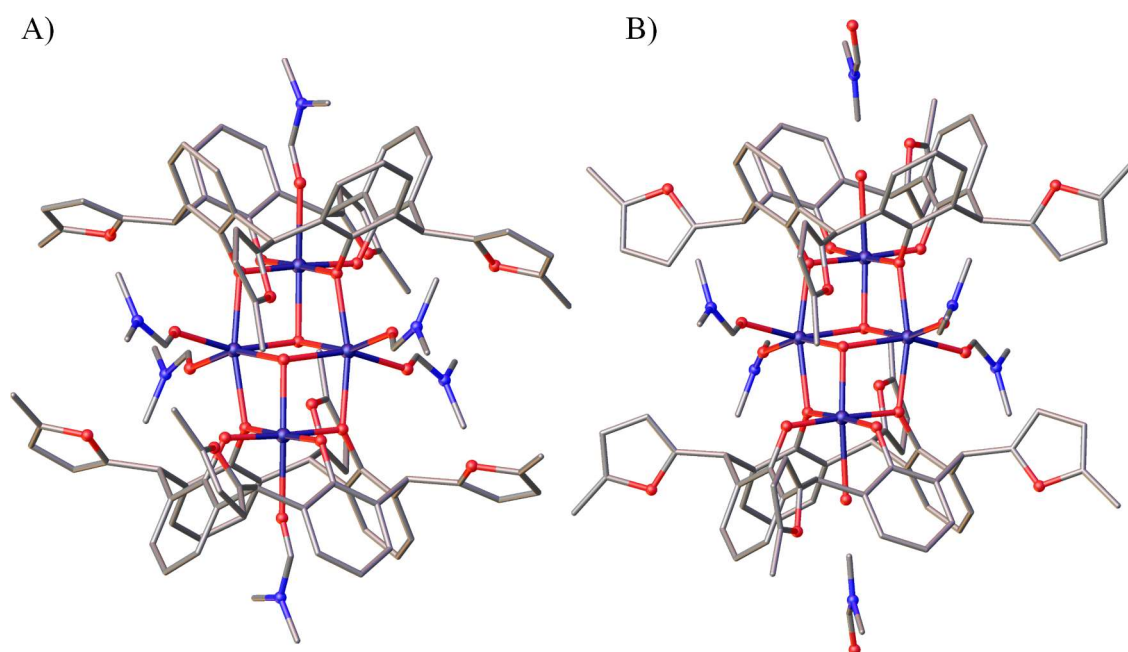


Figure 2.3. Views of sections of the partial single crystal X-ray structure of **7**. A) Butterfly A showing formation of the mixed-valence $[\text{Mn}^{\text{III}}_2\text{Mn}^{\text{II}}_2]$ core with six ligated DMF molecules. B) Butterfly B showing formation of the mixed-valence $[\text{Mn}^{\text{III}}_2\text{Mn}^{\text{II}}_2]$ core which has four peripherally ligated DMF molecules with disordered water (ligated) and DMF (non-ligated) molecules contained within the cavity shown in ball and stick representation. Colour code: C – grey, O – red, Mn – purple, N - blue. DMF of crystallisation, t Bu groups and H atoms are omitted for clarity.

Another set of purple crystals were formed from a similar reaction involving a 1:1 ratio of Mn:Tb ions. These crystals were formed under analogous conditions through the reaction of **H45** with manganese(II) chloride tetrahydrate and terbium(III) chloride hexahydrate in the presence of Et_3N . Again, single crystals suitable for X-ray diffraction studies were formed slow evaporation of the mother liquor. The crystals were found to be in a triclinic cell and structure solution was carried out in the space group $P-1$. Symmetry expansion of the ASU again afforded two butterflies as is the case with compound **7**. However, data quality was poor and so only a partial single crystal structure is shown in Figure 2.4.

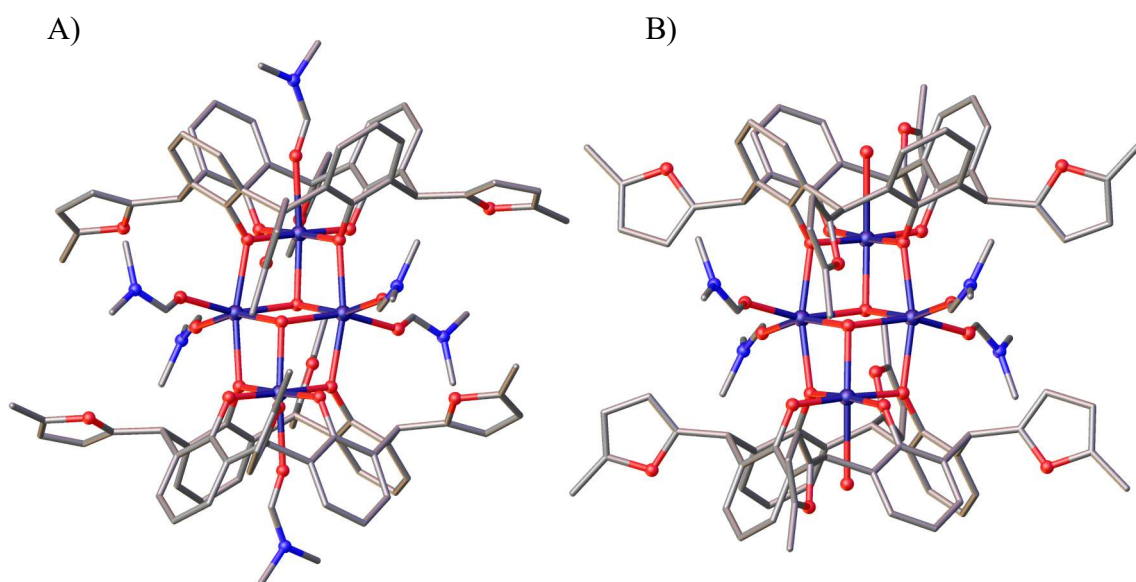


Figure 2.4. Views of sections of the partial single crystal X-ray structure of **8**. A) Butterfly A showing formation of the $[\text{Mn}^{\text{III}}_2\text{Mn}^{\text{II}}_2]$ cluster with six ligated DMF molecules. B) Butterfly B showing formation of the $[\text{Mn}^{\text{III}}_2\text{Mn}^{\text{II}}_2]$ cluster which has four peripherally ligated DMF molecules with disordered water (ligated) and DMF (non-ligated) molecules contained within the cavity shown in ball and stick representation. The non-ligated DMF molecules have been omitted for clarity as the data quality was poor and the solvent could not be modelled. Colour code: C – grey, O – red, Mn – purple, N – blue. DMF of crystallisation, *t*Bu groups and H atoms are omitted for clarity.

Due to the quality of the data, it was not possible to model all of the solvents of crystallisation. One solvent in particular is the non-ligated DMF molecules contained within Butterfly B (Figure 2.4). However, inspection of the crystal structure shows some similarities to compound **7**, as upon symmetry expansion two $[\text{Mn}^{\text{III}}_2\text{Mn}^{\text{II}}_2]$ butterflies were afforded, one of which has six ligated DMF molecules and the other which possesses four peripherally ligated DMF molecules with a disordered DMF (non-ligated) and water (ligated) molecule contained within the C[4] cavity. The exact formula of the crystals could not be determined, however, they may be of a similar formula to that of compound **7** due to the similarities in the ligated solvent employed in cluster formation, as can be seen from Figure 2.4. Again, it is possible to see for butterfly B in Figure 2.4 that, although the furan moieties are in the equatorial position, they have rotated and are now pointing up towards where the *t*-butyl groups are sitting.

2.4.3 Reaction of H45 with a 1:4 mixture of Mn^{II}:Ln^{III} ions

The next sets of reactions (Table 2.1) attempted to form mixed-metal clusters by using a higher ratio of Ln^{III}:Mn^{II} ions. Colourless crystals were formed through reaction of **H45** with manganese(II) chloride tetrahydrate and terbium(III) chloride hexahydrate in a 1:4 ratio of metal ions, respectively. The crystals were found to be in a monoclinic cell and structure solution was carried out in the space group $P2_1/n$, revealing these to be of formula $[\text{Tb}^{\text{III}}_6(\mu_4\text{-O})_2(\mu\text{-HCOO})_2(\mu_4\text{-CO}_3)_2(\mathbf{5})_2(\text{DMF})_8(\text{H}_2\text{O})_2] \cdot 2\text{MeOH} \cdot 2\text{H}_2\text{O}$ (**9**). The ASU was found to contain half of the aforementioned formula, with symmetry expansion giving rise to the cluster shown in Figure 2.5 where the terbium ions are arranged at the vertices of an octahedron as found previously¹⁰ but there is variation in the nature of the anions in and around the cluster core as compared to **III**.

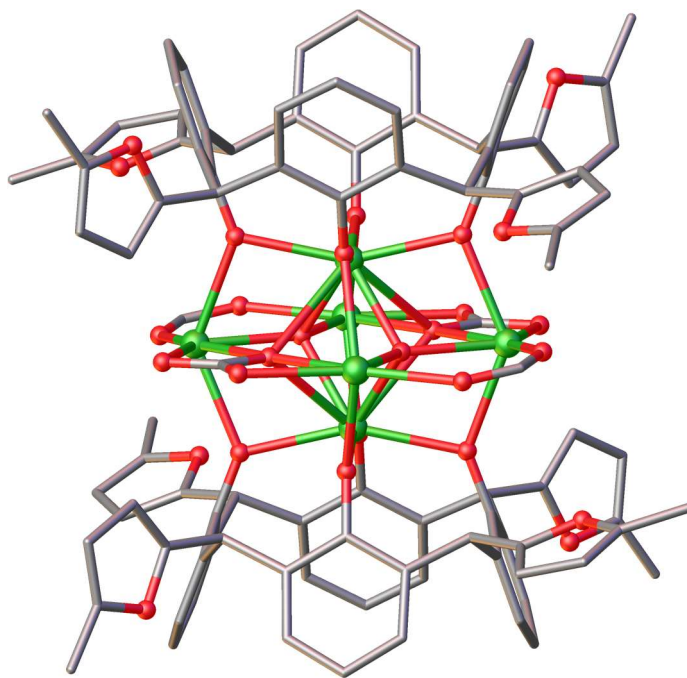


Figure 2.5. Single crystal X-ray structure of **9** showing formation of the $[\text{Tb}^{\text{III}}_6(\mu_4\text{-O})_2(\mu\text{-HCOO})_2(\mu_4\text{-CO}_3)_2]$ core that is supported by two tetra-anions of **H45** shown in ball and stick representation. Colour code: C – grey, O – red, Tb – green. Methanol and water of crystallisation, ^tBu groups, H atoms and ligated DMF and water molecules are omitted for clarity.

The Tb1 ions are in the third oxidation state and these are bound by the lower-rim phenolato pockets (O1-O4, Tb-O bond length range 2.334(3) – 2.355(5) Å). The coordination sphere of Tb1 is completed by a ligated H₂O molecule residing within the

calixarene cavity (Tb1–O13, 2.554(5) Å), a μ_4 -carbonate (Tb1–O15, 2.844(5) Å) which is also bound to Tb2 and Tb3 (Tb2–O15, 2.409(4) Å and Tb3–O15, 2.411(4) Å) and a μ_4 -oxide that bridges Tb1 (and its symmetry equivalent), Tb2 and Tb3 (Tb1–O14, 2.283(4) Å, Tb2–O14, 2.267(5) Å and Tb3–O14, 2.250(4) Å). The μ_4 -carbonate ion is also bound to Tb2 and Tb3 through O16 and O17 respectively (Tb2–O16, 2.415(4) Å and Tb3–O17, 2.423(5) Å). The coordination sphere of Tb2 is completed by two ligated DMF molecules (Tb2–O11, 2.432(6) Å and Tb2–O12, 2.432(5) Å) and a bridging formate anion (Tb2–O19, 2.344(4) Å). The same is true for Tb3 as there are two ligated DMF molecules (Tb3–O9, 2.391(5) Å and Tb3–O10, 2.429(6) Å) and a formate anion (Tb3–O18, 2.353(6) Å) that make up the coordination sphere. Further inspection of the crystal structure shows that the furan moieties are all in the equatorial position, however they are not participating in any coordination chemistry as anticipated, suggesting that these cluster topologies are capable of tolerating the introduction of large groups to the ligand framework without altering the nature of the core itself.

Another set of colourless crystals were formed from the reaction of **H45** with a 1:4 ratio of manganese(II) chloride tetrahydrate and gadolinium(III) chloride hexahydrate. The crystals were found to be in a triclinic cell and structure solution was carried out in the space group *P*-1. The crystals were found to be of the formula $[\text{Gd}^{\text{III}}_6(\mu_4\text{-O})_2(\mu\text{-HCOO})_2(\mu_3\text{-CO}_3)_2(\mathbf{5})_2(\text{DMF})_8(\text{MeOH})_2] [\text{Gd}^{\text{III}}_6(\mu_4\text{-O})_2(\mu\text{-HCOO})_2(\mu_3\text{-CO}_3)_2(\mathbf{5})_2(\text{DMF})_8(\text{MeOH})_2] \cdot 2\text{MeOH}$ (**10**).

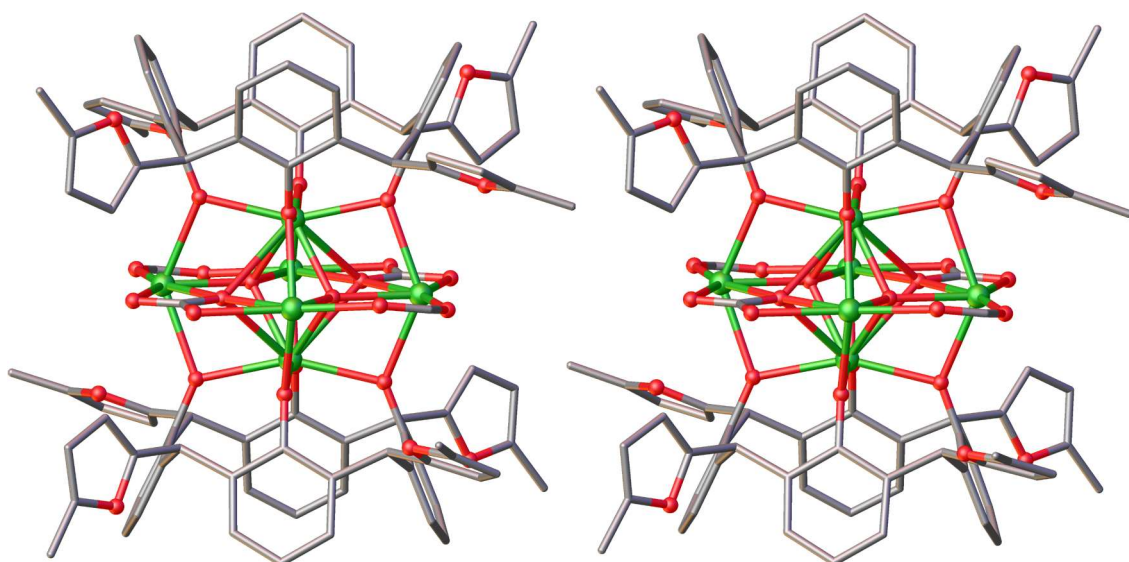


Figure 2.6. Views of sections of the single crystal X-ray structure of **10** shown in ball and stick representation. Two Gd^{III}_6 clusters were afforded upon symmetry expansion, both of which are shown. Colour code: C – grey, O – red, Tb – green. Methanol of crystallisation, *t*Bu groups, H atoms and ligated DMF and methanol molecules are omitted for clarity.

The ASU was found to consist of half of the aforementioned formula which upon symmetry expansion gave two Gd_6 metal clusters. As is the case for compound **9**, the Gd ions are arranged at the vertices of an octahedron and again there is variation of the nature of the anions in and around the metal core. The majority of the anions in compound **10** are the same as in compound **9** with the exception of the solvent molecules contained within the calixarene cavity. Instead of a ligated water molecule as in **9**, compound **10** contains a ligated methanol molecule within the cavity. It was not possible to add the H atoms to the methanol molecules but they have been added to the overall chemical formula for the cluster, $\text{C}_{160}\text{H}_{212}\text{Gd}_6\text{N}_8\text{O}_{40}$. The Gd-O(methanol) bond lengths are 2.569(5) and 2.571(5) Å indicating that these are in fact ligated methanol molecules as the bond lengths of a Gd^{III} to methoxide anion are usually much shorter, around 2.3 Å as reported by Bi *et al.*¹¹ It is possible to see that that the furan moieties are in the equatorial positions, however two furan groups on a single calixarene are pointing up towards where the *t*-butyl groups are positioned with the other two groups pointing down towards the phenolato oxygen atoms. The same can be said for the other Gd_6 metal cluster in the crystal structure of **10**.

2.5 Conclusions

The work presented in this chapter has shown that it is possible to fully demethylate at the lower-rim of a calix[4]arene that has been mono-substituted at all four bridge positions. Compound **4** previously synthesised by Biali and co-workers,⁴ was chosen for this work as it is one of the only calixarene compounds in the literature in which the methylene bridge has been mono-substituted, but importantly one in which all four substituents reside in equatorial positions. Furthermore, **H45** has been successfully used in reactions with various metal salts to synthesise *3d* or *4f* metal clusters. The clusters isolated from this work conform to two known types previously reported by this research group, and the fact that no mixed metal clusters have been isolated suggests that the furan moieties may hinder the formation of *3d-4f* metal clusters. It was hoped that the introduction of additional functional groups, the furan moiety, would lead to a new metal binding site at this position, however none of the clusters isolated in this chapter displayed the desired behaviour. Given this, it was decided that, instead of pursuing this line of investigation, the furan group could be reacted further and alternative functionalities introduced at the methylene bridge positions, thus expanding the chemistry in this region of the C[4] framework. This work is discussed in Chapter 3.

2.6 Experimental

All experiments were carried out in ambient conditions except for the cases where dry solvents were used. The dry solvents were obtained from an MBraun SPS-800 solvent purification system and these reactions were performed under dry, oxygen-free N₂ using standard Schlenk-line techniques. Analytical thin layer chromatography was performed on precoated silica gel plates (Merck, 60 F₂₅₄) and column chromatography was performed using 60 Å silica (Merck, particle size, mesh). ¹H, ¹³C, COSY, HSQC, HMBC, DOSY and VT NMR spectroscopy experiments were carried out on a Bruker Avance^{III} 300 MHz, a Bruker AVIII 400 MHz, a Bruker AVIII 500 MHz and a Bruker AVIII -HD 600 MHz instrument. All chemical shifts are expressed in ppm. MALDI-TOF mass spectra were recorded on a Bruker UltrafleXtreme MALDI-TOF/TOF spectrometer and ESI mass spectra were recorded on a Bruker ESI MicroTOF Focus II spectrometer. IR experiments were performed on a Thermo Scientific Nicolet iS5/iD5 ATR spectrometer. All the single crystals were analysed on a Bruker X8 APEXII diffractometer with a MoK α radiation source, a Bruker D8 diffractometer equipped with a PHOTON 100 detector with a synchrotron radiation source, a Rigaku Oxford Diffraction SuperNova diffractometer with a MoK α radiation source or a Kappa Rigaku Saturn724+ diffractometer with a CuK α radiation source.

Synthesis of 5,11,17,23-tetra-*tert*-butyl-25,26,27,28-tetrahydrocalix[4]arene, **1**.

Compound **1** was synthesised according to the literature procedure as reported by Gutsche *et al.*,² with the quantities being scaled up as appropriate. A mixture of *p-tert*-butylphenol (500 g), 37% formaldehyde solution (300 mL) and NaOH (2.5 g) in water (12 mL) was heated at reflux, under N₂, until the polymer had formed. The water formed from the condensation reaction was removed by means of a Dean-Stark apparatus. Once the polymer was formed, the reaction mixture was cooled to room temperature before toluene (2 L) and diphenyl ether (4 L) was added. The reaction mixture was heated to remove the toluene and then it was heated at 260 °C for 4 h. The mixture was then cooled to room temperature before ethyl acetate (3 L) was added and the solution was stirred for 2 h. The solution was then filtered and the solid was washed with ethyl acetate to afford 312.8 g (58%) of **1** as a white solid.

¹H NMR (300 MHz, CDCl₃) δ ppm: 10.35 (s, 4 H), 7.06 (s, 8 H), 4.27 (d, $J=1.00$ Hz, 4 H) 3.51 (d, $J=1.00$ Hz, 4 H) 1.22 (s, 36 H).

The ^1H NMR spectrum of a fully dissolved CDCl_3 solution of **1** was collected to confirm the purity and the product was used without further analysis.

Synthesis of 5,11,17,23-tetra-*tert*-butyl-25,26,27,28-tetramethoxycalix[4]arene, 2.

Compound **1** (20.0 g, 30 mmol) was suspended in a 10:1 THF:DMF mixture (100:10 mL). NaH (5.0 g) was slowly added to the reaction flask with stirring and then MeI (20 mL) was added using a disposable syringe. The reaction mixture was then heated at reflux for 2 h, after which it was cooled to room temperature before MeOH was added to remove any unreacted NaH. The solvents were then removed under reduced pressure and the resulting solid was collected, washed with water and filtered. The solid was dissolved in CHCl_3 and then the solution was dried using MgSO_4 . After filtering off the MgSO_4 the solvent was removed under reduced pressure. The crude product was recrystallised using hot $\text{CHCl}_3/\text{MeOH}$ to yield 17.6 g (81%) of **2**. The compound was dissolved in a 3:1 mixture of $\text{CDCl}_3/\text{CD}_3\text{CN}$ which had been saturated with NaI in order to lock the calix[4]arene in the cone conformation to obtain a ^1H NMR spectrum with sharp proton signals.

^1H NMR (300 MHz, CDCl_3) δ ppm: 7.07 (s, 8 H), 4.14 (d, $J=12.47$ Hz, 4 H), 4.02 (s, 12 H), 3.31 (d, $J=12.47$ Hz, 4 H), 1.06 (s, 36 H).

The ^1H NMR spectrum of a fully dissolved CDCl_3 solution of **2** was collected to confirm the purity and the product was used without further analysis.

Synthesis of 5,11,17,23-tetra-*tert*-butyl-2,8,14,20-tetrabromo-25,26,27,28-tetramethoxycalix[4]arene, 3.

The tetrabromo TBC[4] derivative was synthesised following the procedure outlined by Biali and co-workers,⁴ however a slight modification to the method was employed to discard of the use of carbon tetrachloride as a solvent system for this reaction. A mixture of **2** (10.0 g, 14.18 mmol) and NBS (10.1 g, 56.74 mmol) was heated at reflux in chloroform (500 mL) for 22 h whilst irradiated with a spotlight (~100 W). After this time the orange/red solution was cooled to room temp and then washed once with $\text{Na}_2\text{SO}_3(\text{aq})$ (100 mL) and twice with water (2 x 100 mL). The organic phase was collected, dried with MgSO_4 and then filtered. The solvent was removed under reduced pressure and the crude was recrystallised from $\text{CHCl}_3/\text{MeOH}$ to yield 7.1 g (49%) of **3**.

^1H NMR (300 MHz, CDCl_3) δ ppm: 7.28 (s, 8 H), 6.72 (s, 4 H), 4.00 (s, 12 H), 1.13 (s, 36 H).

The ^1H NMR spectrum of a fully dissolved CDCl_3 solution of **3** was collected to confirm the purity and the product was used without further analysis.

Synthesis of 5,11,17,23-tetra-*tert*-butyl-2,8,14,20-tetrakis(2-methylfuranyl)-25,26,27,28-tetramethoxycalix[4]arene, 4.

A mixture of **3** (5.0 g, 4.9 mmol), 2-methylfuran (9 mL, 8.19 g, 100 mmol) and 1,2-butylene oxide (40 mL) in TFE (500 mL) was heated at reflux for 4 h. During this time, the solution goes from pink to colourless until a white solid is formed. After cooling to room temperature, the white solid was filtered and then recrystallised from $\text{CHCl}_3/\text{MeOH}$ to yield 1.159 g (23%) of **4**

^1H NMR (300 MHz, CDCl_3) δ ppm: 6.72 (s, 8 H), 6.00 (s, 4 H), 5.95 (d, $J=2.93$ Hz, 4 H), 5.89 (d, $J=2.90$ Hz, 4 H), 3.89 (s, 12 H), 2.28 (s, 12 H), 1.01 (s, 36 H). ^{13}C NMR (75.5 MHz, CDCl_3) δ ppm: 155.3, 154.3, 151.1, 144.6, 134.3, 123.7, 109.1, 105.5, 61.9, 37.8, 34.0, 31.3, 13.6.

Synthesis of 5,11,17,23-tetra-*tert*-butyl-2,8,14,20-tetrakis(2-methylfuranyl)-25,26,27,28-tetrahydroxycalix[4]arene, H45.

Cyclohexyl iodide (9.86 g, 49.91 mmol) was added to a stirred suspension of compound **4** (1.069 g, 1.04 mmol) in DMF (60 mL) and the reaction was heated at reflux for 48 h. The resulting brown solution was cooled to room temperature before being poured into water (100 mL), leading to the precipitation of a brown solid. This solid was collected by filtration and stirred as a suspension in MeOH for 15 min. Subsequent filtration afforded a yellow crude that was recrystallised from $\text{CHCl}_3/\text{MeOH}$ to yield 0.210 g (21%) of pure **H45**.

^1H NMR (300 MHz, CDCl_3) δ ppm: 8.94 (br. s., 4 H), 7.16 (s, 8 H), 6.14 (d, $J=2.57$ Hz, 4 H), 5.94 (d, $J=2.90$ Hz, 4 H), 5.90 (s, 4 H), 2.28 (s, 12 H), 1.11 (s, 36 H). ^{13}C NMR (75.5 MHz, CDCl_3) δ ppm: 152.8, 151.4, 146.2, 143.8, 128.4, 124.0, 109.7, 105.8, 37.3, 34.2, 31.2, 13.6. MS (MALDI-TOF): 991.5, $[\text{M}+\text{Na}]^+$.

Crystal data for H45: $\text{C}_{66}\text{H}_{77}\text{Cl}_3\text{O}_9$, $M = 1120.62$ g/mol, triclinic, space group $P-1$ (no.2), $a = 13.0376(6)$ Å, $b = 13.8967(6)$ Å, $c = 17.1875(7)$ Å, $\alpha = 101.4830(10)^\circ$, $\beta = 98.953(2)^\circ$, $\gamma = 92.116(2)^\circ$, $V = 3007.1(2)$ Å³, $Z = 2$, $T = 100(2)$ K, synchrotron radiation ($\lambda = 0.7288$

Å), 84939 reflections measured ($4.316^\circ \leq 2\theta \leq 52.91^\circ$), 11457 unique ($R_{\text{int}} = 0.0631$, $R_{\text{sigma}} = 0.0380$) which were used in all calculations. The final R_1 was 0.0703 ($I > 2\sigma(I)$) and wR_2 was 0.2016 (all data).

Synthesis of $[\text{Mn}^{\text{III}}_2\text{Mn}^{\text{II}}_2(\mu_3\text{-OH})_2(\text{S})_2(\text{DMF})_4(\text{MeOH})_2] \cdot 3\text{MeOH} \cdot \text{Et}_2\text{O}$, **6.**

$\text{MnCl}_2 \cdot 4\text{H}_2\text{O}$ (40.9 mg, 0.207 mmol) and **H45** (50.0 mg, 0.052 mmol) were dissolved in a 1:1 DMF/MeOH mixture (20 mL). After 10 min of stirring Et_3N (0.045 mL) was added and the resulting deep purple solution was stirred at room temperature for 2 h. The reaction mixture was filtered to remove any microcrystalline material, and purple crystals of **6** grew upon vapour diffusion of petroleum ether into the mother liquor.

Crystal data for 6 (CCDC 1583896): $\text{C}_{149}\text{H}_{196}\text{Mn}_4\text{N}_4\text{O}_{28}$, $M = 2710.85$ g/mol, triclinic, space group $P-1$ (no.2), $a = 13.1012(9)$ Å, $b = 17.0409(11)$ Å, $c = 17.5344(12)$ Å, $\alpha = 72.026(3)^\circ$, $\beta = 86.362(3)^\circ$, $\gamma = 87.172(3)^\circ$, $V = 3714.3(4)$ Å³, $Z = 1$, $T = 100(2)$ K, MoK α radiation ($\lambda = 0.71073$ Å), 57869 reflections measured ($2.444^\circ \leq 2\theta \leq 54.174^\circ$), 15969 unique ($R_{\text{int}} = 0.1222$, $R_{\text{sigma}} = 0.2345$) which were used in all calculations. The final R_1 was 0.0864 ($I > 2\sigma(I)$) and wR_2 was 0.2787 (all data).

Synthesis of $[\text{Mn}^{\text{III}}_2\text{Mn}^{\text{II}}_2(\mu_3\text{-OH})_2(\text{S})_2(\text{DMF})_6] [\text{Mn}^{\text{III}}_2\text{Mn}^{\text{II}}_2(\mu_3\text{-OH})_2(\text{S})_2(\text{DMF})_{5.5}(\text{H}_2\text{O})_{0.5}] \cdot 2\text{DMF}$, **7**

$\text{MnCl}_2 \cdot 4\text{H}_2\text{O}$ (10.1 mg, 0.051 mmol), $\text{GdCl}_3 \cdot 6\text{H}_2\text{O}$ (12.9 mg, 0.049 mmol) and **H45** (50.5 mg, 0.052 mmol) were dissolved in a 1:1 DMF/MeOH mixture (20 mL). After 10 min of stirring Et_3N (0.045 mL) was added and the resulting deep purple solution was stirred at room temperature for 2 h. The reaction mixture was filtered to remove any microcrystalline material, and purple crystals of **7** grew upon slow evaporation of the mother liquor.

Crystal data for 7 (CCDC 1583897): $\text{C}_{148.25}\text{H}_{185.75}\text{Mn}_4\text{N}_{6.75}\text{O}_{25}$, $M = 2682.03$ g/mol, triclinic, space group $P-1$ (no.2), $a = 15.7886(9)$ Å, $b = 23.1399(13)$ Å, $c = 30.3907(17)$ Å, $\alpha = 102.631(3)^\circ$, $\beta = 102.128(3)^\circ$, $\gamma = 98.886(3)^\circ$, $V = 10356.2(10)$ Å³, $Z = 2$, $T = 100(2)$ K, synchrotron radiation ($\lambda = 0.7749$ Å), 111410 reflections measured ($3.224^\circ \leq 2\theta \leq 62.414^\circ$), 51084 unique ($R_{\text{int}} = 0.0495$, $R_{\text{sigma}} = 0.0784$) which were used in all calculations. The final R_1 was 0.0806 ($I > 2\sigma(I)$) and wR_2 was 0.2422 (all data).

Synthesis of **8**.

MnCl₂·4H₂O (10.8 mg, 0.054 mmol), TbCl₃·6H₂O (18.8 mg, 0.050 mmol) and **H45** (49.9 mg, 0.051 mmol) were dissolved in a 1:1 DMF/MeOH mixture (20 mL). After 10 min of stirring Et₃N (0.045 mL) was added and the resulting deep purple solution was stirred at room temperature for 2 h. The reaction mixture was filtered to remove any microcrystalline material, and purple crystals of **8** grew upon slow evaporation of the mother liquor.

The data quality for this set of crystals was poor and so full structure refinement has not been carried out.

Crystal data for 8: Triclinic, space group *P*-1 (no.2), *a* = 14.0077(14) Å, *b* = 20.345(2) Å, *c* = 26.868(3) Å, *α* = 100.898(6)°, *β* = 102.929(6)°, *γ* = 99.743(5)°, *V* = 7147.1(13) Å³, *Z* = 2, *T* = 100(2) K, synchrotron radiation (*λ* = 0.7749 Å).

Synthesis of [Tb^{III}₆(μ₄-O)₂(μ₄-CO₃)₂(μ-HCO₂)₂(**5**)₂(DMF)₈(H₂O)₂]**·2MeOH**·2H₂O, **9**.

MnCl₂·4H₂O (10.1 mg, 0.051 mmol), TbCl₃·6H₂O (76.7 mg, 0.205 mmol) and **H45** (50.6 mg, 0.052 mmol) were dissolved in a 1:1 DMF/MeOH mixture (20 mL). After 10 min of stirring Et₃N (0.045 mL) was added and the resulting deep purple solution was stirred at room temperature for 2 h. The reaction mixture was filtered to remove any microcrystalline material, and colourless crystals of **9** grew upon slow evaporation of the mother liquor.

Crystal data for 9 (CCDC 1583898): C₇₉H₁₀₅N₄O₂₁Tb₃, *M* = 1923.42 g/mol, triclinic, space group *P*2₁/*n* (no.14), *a* = 18.8372(9) Å, *b* = 15.8997(8) Å, *c* = 28.3456(12) Å, *β* = 107.806(2)°, *V* = 8083.0(7) Å³, *Z* = 4, *T* = 100(2) K, MoK α radiation (*λ* = 0.71073 Å), 72883 reflections measured (3.45° ≤ 2 θ ≤ 58.082°), 21054 unique (*R*_{int} = 0.0847, *R*_{sigma} = 0.1167) which were used in all calculations. The final *R*₁ was 0.0527 (*I* > 2 σ (*I*)) and *wR*₂ was 0.1354 (all data).

Synthesis of [Gd^{III}₆(μ₄-O)₂(μ-HCOO)₂(μ₃-CO₃)₂(**5**)₂(DMF)₈(MeOH)₂] [Gd^{III}₆(μ₄-O)₂(μ-HCOO)₂(μ₃-CO₃)₂(**5**)₂(DMF)₈(MeOH)₂]**·2MeOH**, **10**.

MnCl₂·4H₂O (10.1 mg, 0.051 mmol), GdCl₃·6H₂O (53.7 mg, 0.204 mmol) and **H45** (49.8 mg, 0.051 mmol) were dissolved in a 1:1 DMF/MeOH mixture (20 mL). After 10 min of stirring Et₃N (0.045 mL) was added and the resulting deep purple solution was stirred at room temperature for 2 h. The reaction mixture was filtered to remove any

microcrystalline material, and colourless crystals of **10** grew upon slow evaporation of the mother liquor.

Crystal data for 10: $C_{320}H_{420}N_{16}O_{80}Gd_{12}$, $M = 3826.83$ g/mol, triclinic, space group $P-1$ (no.2), $a = 15.9428(8)$ Å, $b = 18.9369(12)$ Å, $c = 28.3365(15)$ Å, $\alpha = 71.945(3)^\circ$, $\beta = 89.603(3)^\circ$, $\gamma = 88.945(3)^\circ$, $V = 8132.4(8)$ Å³, $Z = 1$, $T = 100(2)$ K, MoK α radiation ($\lambda = 0.71073$ Å), 78804 reflections measured ($1.512^\circ \leq 2\theta \leq 57.826^\circ$), 41894 unique ($R_{\text{int}} = 0.0462$, $R_{\text{sigma}} = 0.0992$) which were used in all calculations. The final R_1 was 0.0600 ($I > 2\sigma(I)$) and wR_2 was 0.1800 (all data).

References

1. I. Columbus and S. E. Biali, *Org. Lett.*, 2007, **9**, 2927-2929.
2. C. D. Gutsche, M. Iqbal and D. Stewart, *J. Org. Chem.*, 1986, **51**, 742-745.
3. S. Shinkai, K. Araki, P. D. J. Grootenhuis and D. N. Reinhoudt, *J. Chem. Soc., Perkin Trans. 2*, 1991, 1883-1886.
4. I. Columbus and S. E. Biali, *J. Org. Chem.*, 2008, **73**, 2598-2606.
5. F. de la Vega and Y. Sasson, *J. Chem. Soc., Chem. Commun.*, 1989, 653-654.
6. L. Zuo, S. Y. Yao, W. Wang and W. H. Duan, *Tetrahedron Lett.*, 2008, **49**, 4054-4056.
7. S. M. Taylor, G. Karotsis, R. D. McIntosh, S. Kennedy, S. J. Teat, C. M. Beavers, W. Wernsdorfer, S. Piligkos, S. J. Dalgarno and E. K. Brechin, *Chem. Eur. J.*, 2011, **17**, 7521-7530.
8. G. Karotsis, S. J. Teat, W. Wernsdorfer, S. Piligkos, S. J. Dalgarno and E. K. Brechin, *Angew. Chem. Int. Ed.*, 2009, **48**, 8285-8288.
9. G. Karotsis, M. Evangelisti, S. J. Dalgarno and E. K. Brechin, *Angew. Chem. Int. Ed.*, 2009, **48**, 9928-9931.
10. S. Sanz, R. D. McIntosh, C. M. Beavers, S. J. Teat, M. Evangelisti, E. K. Brechin and S. J. Dalgarno, *Chem. Commun.*, 2012, **48**, 1449-1451.
11. Y. F. Bi, G. C. Xu, W. P. Liao, S. C. Du, R. P. Deng and B. W. Wang, *Sci. China Chem.*, 2012, **55**, 967-972.

Chapter 3

Exploration of Furan Derivatisation at the Methylene Bridge of a Calix[4]arene

3.1. Introduction

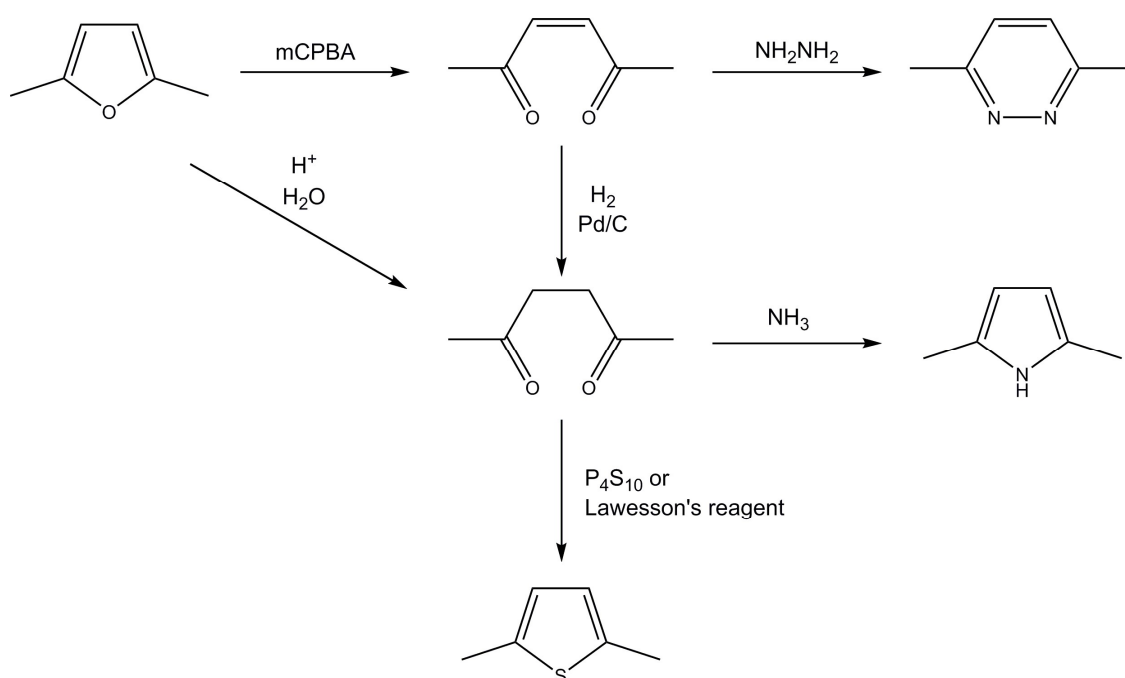
Chapter 3 focusses on the synthesis of a family of new methylene bridge-substituted calix[4]arenes in which **4** was further derivatised to give other heterocyclic compounds through the saturated and unsaturated diketone synthetic intermediates, **11** and **18**, respectively. The ability of **H45** to coordinate to metal centres was outlined in Chapter 2, however, the metal clusters isolated were of known cluster types. Derivatisation of the furan moiety was explored, with the hope of expanding the library of calix[4]arenes that are mono-substituted at the methylene bridge position. The introduction of new groups at this position would hopefully result in new metal binding sites leading to the formation of polymetallic clusters. Furans are synthetically diverse molecules as they can be reacted in numerous ways (examples include electrophilic aromatic substitution, nucleophilic addition, Diels-Alder reactions and the formation of other heterocycles). The application of these reactions to compound **4** allows for the vast expansion of synthetic chemistry at what is a really challenging position on C[4]s. The formation of other heterocyclic compounds using the furan moiety on **4** is described.

3.2. Examples of Derivation of Furan Moiety

Furans are susceptible to ring-opening reactions¹ and this can be achieved in two ways (Scheme 3.1), the first of which is the oxidative ring-opening reaction with a peracid (such as *meta*-chloroperbenzoic acid, *m*CPBA) to yield the unsaturated diketone species.^{2,3} An alternative method of ring-opening is under acidic conditions in which the furan is hydrolysed to give the saturated diketone compound.⁴ Both the saturated and unsaturated diketones can then be further reacted to form other heterocyclic compounds. Pyridazines can be prepared from the unsaturated diketone species through reaction with hydrazine,⁵ whereas thiophenes and substituted pyrroles can be prepared from saturated diketones.⁶ Another compound can be formed from the saturated diketone species and these are

cyclopentenones.⁶ Under basic conditions, an intramolecular aldol reaction occurs in which the diketone species is cyclised to give rise to such compounds. However, due to time constraints the synthesis of the thiophene and cyclopentenone derivatives were not investigated and therefore the scope of the work described in this chapter is based on the pyrrole and pyridazine compounds.¹

The overarching aims of the work presented in this chapter were to try to relate this heterocyclic chemistry to calixarenes by using **4** as a starting material to introduce various heterocyclic groups at the methylene bridge position of a C[4].

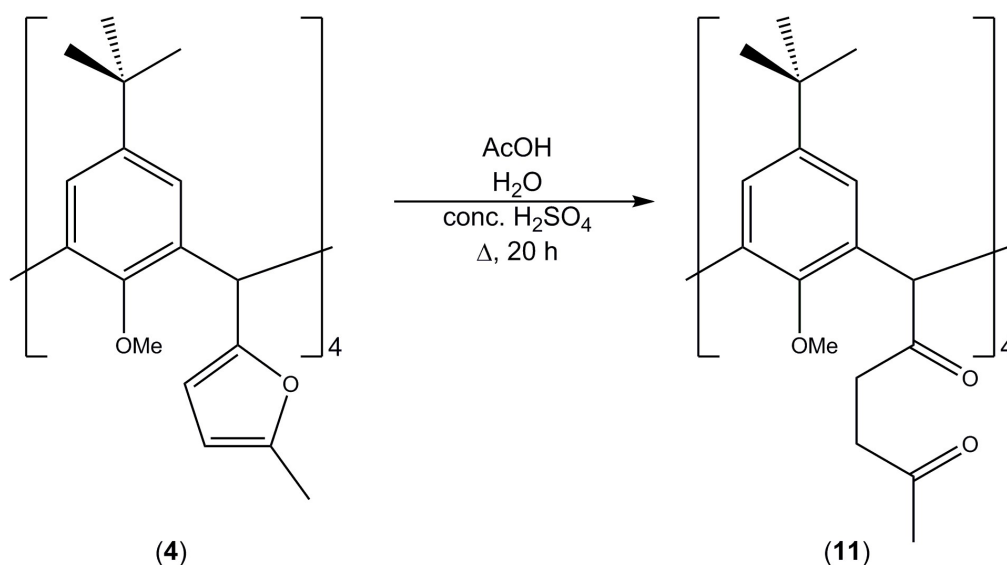


Scheme 3.1. Synthetic scheme for the preparation of various heterocycles using 2,5-dimethylfuran as the starting material.¹

3.3. Hydrolysis of **4** and Subsequent Synthesis of *N*-substituted Pyrrole derivatives

As outlined in the previous reaction scheme (Scheme 3.1), there are various routes to the formation of new heterocyclic compounds. One of these methods was to first hydrolyse compound **4** to afford 5,11,17,23-tetra-*tert*-butyl-2,8,14,20-tetrakis(pentane-1,4-dione)-25,26,27,28-tetramethoxycalix[4]arene (**11**) followed by the Paal-Knorr pyrrole synthesis through reaction with a range of amines differing in nucleophilic character. Compound

11 was synthesised via the acid-catalysed hydrolysis reaction of compound **4** in acetic acid, water and concentrated sulfuric acid (Scheme 3.2) through a modified procedure as reported by Baig *et al.*⁴



Scheme 3.2. Synthetic scheme for the preparation of 5,11,17,23-tetra-*tert*-butyl-2,8,14,20-tetrakis(pentane-1,4-dione)-25,26,27,28-tetramethoxycalix[4]arene (**11**).

Subsequent aqueous work-up and column chromatography in 7:3 CHCl₃/EtOAc gave **11** as a white solid in 48% yield. It is important to highlight the yield for this reaction as the hydrolysis reaction has been carried out four times, once at each bridge position, making the yield for compound **11** comparable to that reported by Baig and co-workers (68%) for the hydrolysis of 2-methyl-5-ethylfuran. Compound **11** was fully characterised, and the ¹H NMR spectrum in Figure 3.1 shows that there are two very distinct triplets that appear at 2.81 and 2.91 ppm which are indicative of the CH₂-CH₂ backbone of the 1,4-diketone species. Both triplets have ³J coupling constants of 6.6 Hz, indicating that the CH₂ groups are indeed coupled, and these distinctive signals serve as an excellent NMR handle to monitor whether a subsequent reaction occurs (*vide infra*).

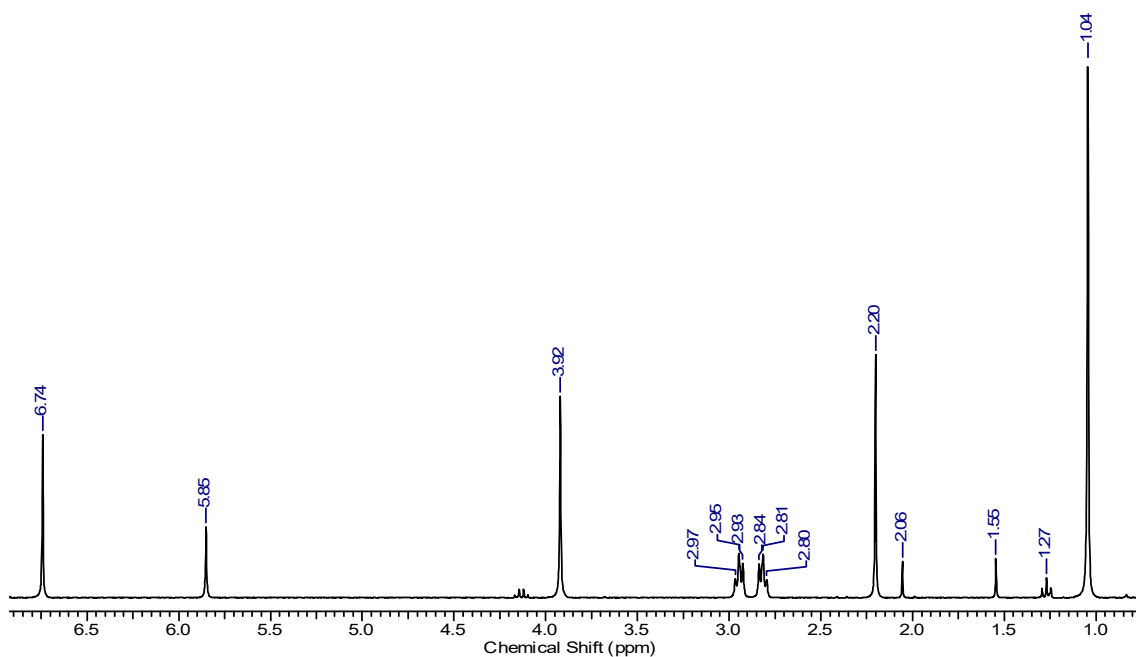


Figure 3.1. ^1H NMR spectrum of compound **11** in chloroform- d showing the indicative triplets of the methylene groups at 2.81 and 2.95 ppm.

The ^{13}C NMR spectrum of compound **11** confirms the successful formation of the target compound, as there are two singlets at 208.76 and 207.37 ppm which are indicative of carbonyl groups. Furthermore, there are two signals in the DEPT spectrum which are inverted, again indicating the presence of CH_2 groups and successful synthesis of compound **11**. Electrospray ionisation mass spectrometry (ESI-MS) and IR spectroscopy were also used as analytical techniques to confirm synthesis, and a carbonyl stretch is clearly observed at 1713.40 cm^{-1} in the latter. Colourless single crystals of compound **11** that were suitable for X-ray diffraction studies were grown from a saturated methanol solution. These were found to be in a monoclinic cell and structure solution was carried out in the space group $P2_1/c$. The ASU contains one full molecule of **11** in a pinched-cone conformation and inspection of the crystal structure (Figure 3.2) shows that the furan moieties have been hydrolysed successfully, affording the 1,4-diketone functionality at all methylene bridge positions. It is interesting to note that the equatorial positions of these substituents has been retained, confirming that this chemistry does not have any impact on their positioning. The C-C bond lengths of the 1,4-diketone backbone range from $1.508(2) - 1.5191(17)\text{ \AA}$ which are indicative of a single bond, providing conclusive evidence that this is the saturated target tetra-1,4-diketone species.

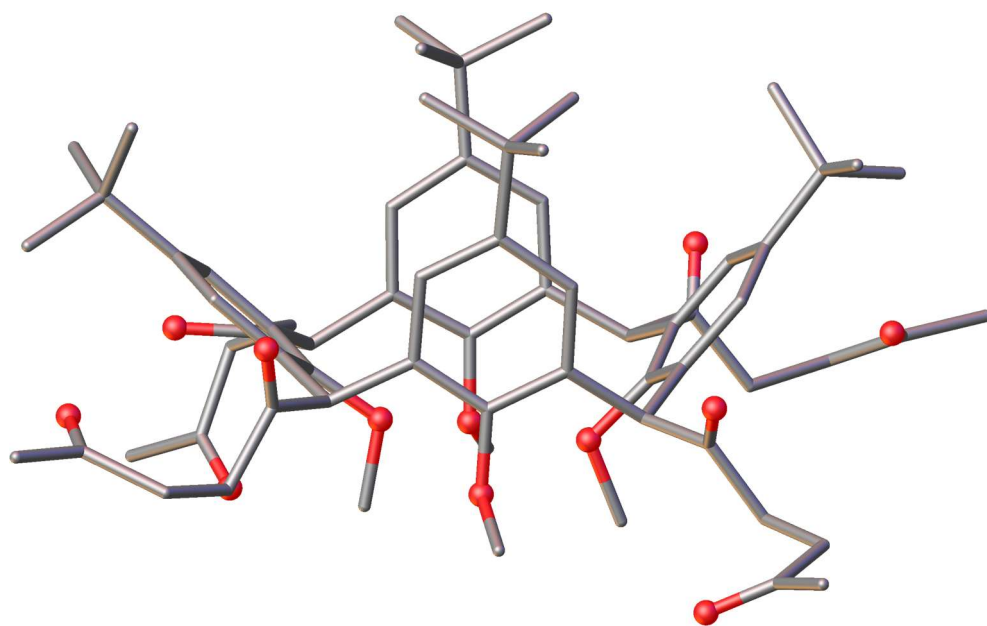


Figure 3.2. Single crystal X-ray structure of **11** showing that the furan groups have been opened giving the 1,4-diketone species at each bridge position shown in ball and stick representation. Colour code: C – grey, O – red. H atoms are omitted for clarity.

Interestingly, a side product (**12**) was formed from the hydrolysis reaction when this was performed over prolonged periods of time. The ^1H NMR spectrum of this side product gave a clear indication that the compound formed was de-symmetrised, as several of the signals that are observed as singlets in the NMR spectrum of compound **11** appear as two distinguishable signals. Integration of the spectrum suggests that one of the lower-rim methoxy protecting groups has been deprotected as the methoxy peaks around 3.8 – 4.2 ppm integrates to nine protons as compared to the twelve protons of the methyl groups on the diketone. Colourless crystals were grown from methanol which were analysed by X-ray diffraction. The crystals were found to be in a monoclinic cell and structure solution was carried out in the space group $P2_1/c$. The ASU contains one full molecule of **12** in a pinched-cone conformation. Inspection of the crystal structure (Figure 3.3) shows that compound **12** is in fact the partially demethylated 1,4-diketone species as assumed from the ^1H NMR spectrum, as it is clear to see that there is one hydroxyl and three methoxy groups at the lower-rim; this is confirmed by integration of the ^1H NMR spectrum.

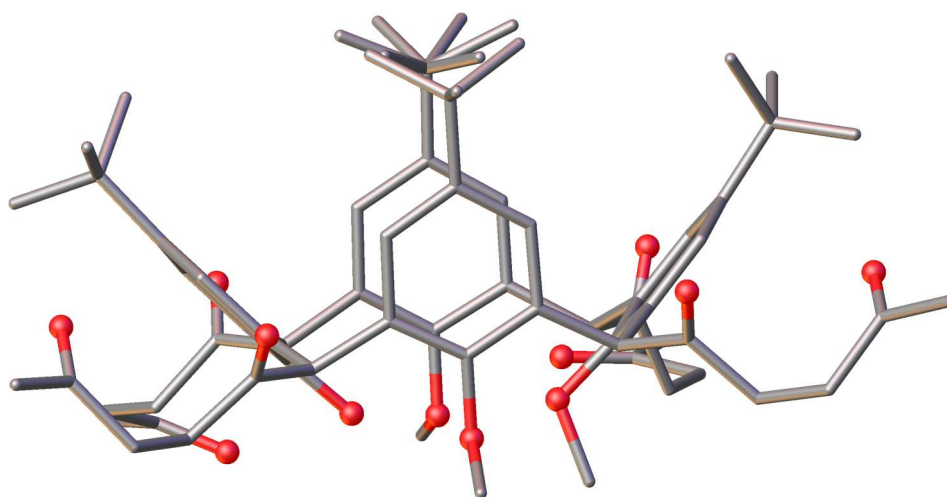


Figure 3.3. Single crystal X-ray structure of **12** showing partial demethylation at the lower-rim of the calix[4]arene shown in ball and stick representation. Colour code: C – grey, O – red. H atoms are omitted for clarity.

Reflux in concentrated H_2SO_4 can result in demethylation and an example of this was reported by Li *et al.* in which they heated a conc. H_2SO_4 solution of 2-bromo-3,5-dimethoxybenzaldehyde where they found it was possible to remove one of the methoxy groups.⁷ Therefore the hydrolysis reaction of **4** was stopped after an overnight reflux to prevent formation of **12**.

After confirmation that compound **11** had been successfully synthesised and with so many commercially available amines, the project progressed onto seeing what could be substituted onto the nitrogen atom of the pyrrole moiety. The use of different amines would allow the introduction of countless groups substituted at the N atom of the pyrrole group affording new, functional host molecules. The properties of these compounds, such as solubility, can be tuned depending on what amine is reacted with the 1,4-diketone. Examples of the amines tested in this section of work are shown in Figure 3.4.

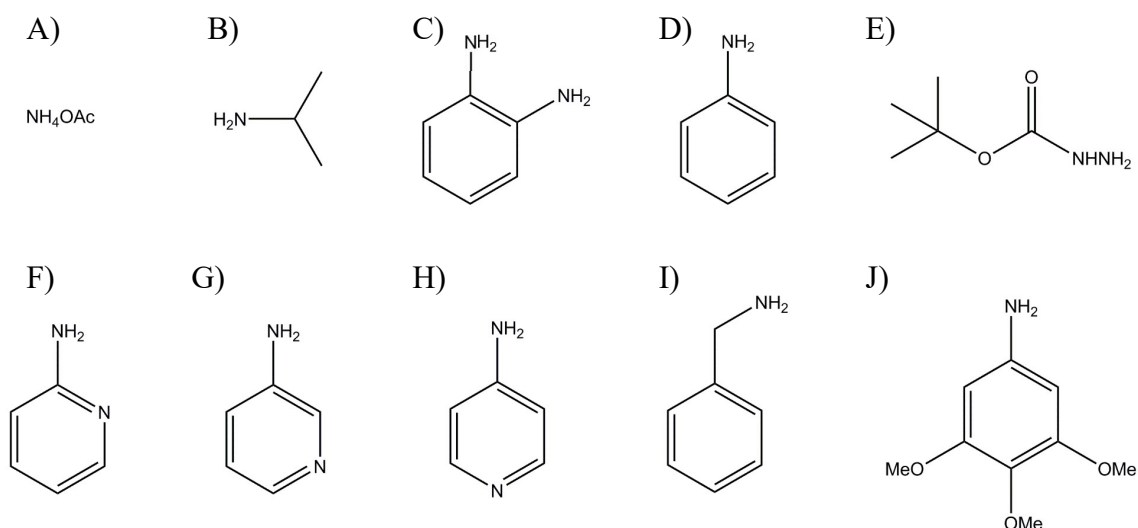


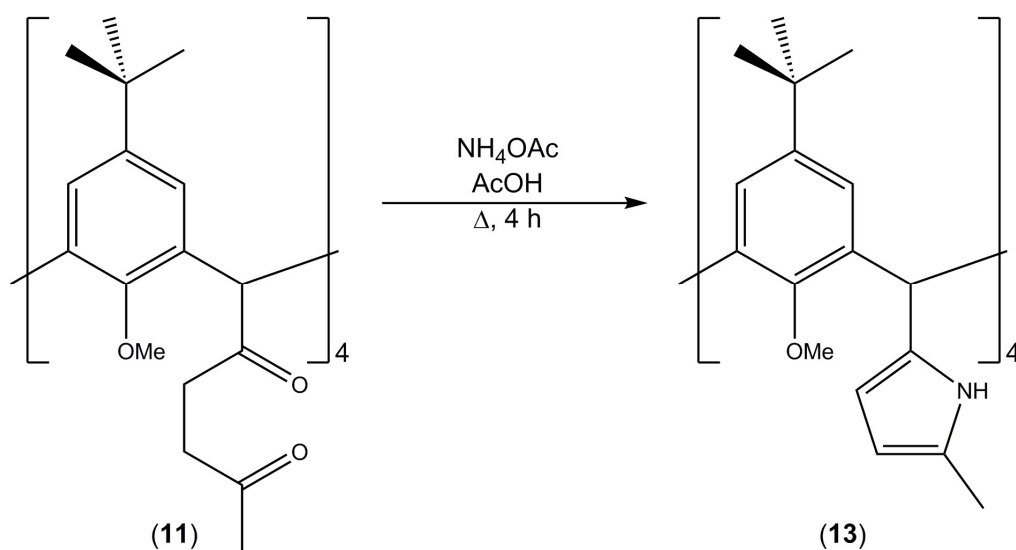
Figure 3.4. Amine reactants investigated for the Paal-Knorr pyrrole synthesis with compound **11**. A) ammonium acetate, B) isopropylamine, C) 1,2-diaminobenzene, D) aniline, E) Boc-hydrazide, F) 2-aminopyridine, G) 3-aminopyridine, H) 4-aminopyridine, I) benzylamine and J) 3,4,5-trimethoxyaniline.

A range of amines were investigated for the Paal-Knorr pyrrole synthesis in this section of work. The reactions involving reactants such as isopropylamine, 1,2-diaminobenzene and benzylamine will not be discussed due to the recovery of starting material indicating that a reaction had not taken place. Therefore, for the purpose of this thesis, only the reactions that gave the target compound and / or promising results will be discussed. Only starting material was recovered from the reactions with 2- and 4-aminopyridine, however, these are discussed in detail in Section 3.2.4 as they are target compounds of high interest due to their potential use in the formation of covalent organic cages.

3.3.1. Synthesis of 5,11,17,23-tetra-*tert*-butyl-2,8,14,20-tetrakis(2-methyl-1*H*-pyrrole)-25,26,27,28-tetramethoxycalix[4]arene (**13**)

The first reaction investigated was the synthesis of the simple pyrrole compound with a H atom substituted on the nitrogen atom. Compound **13** (Scheme 3.3) was successfully synthesised following a modified literature procedure as reported by Orito *et al.*⁶ Reaction of compound **11** with ammonium acetate in acetic acid afforded 69% yield of a brown solid after purification by column chromatography. As the Paal-Knorr pyrrole reaction is carried out four times, once at each bridge position, the yield obtained for

compound **13** equates to an approximate 91% yield per methylene bridge position which is comparable to the yield obtained by Orito and co-workers for the synthesis of 2-benzyl-5-methylpyrrole (99%).



Scheme 3.3. Synthetic scheme for the preparation of 5,11,17,23-tetra-*tert*-butyl-2,8,14,20-tetrakis(2-methyl-1*H*-pyrrole)-25,26,27,28-tetramethoxycalix[4]arene (**13**).

Inspection of the ^1H NMR spectrum immediately suggested that reaction had occurred at all 1,4-diketone functionalities, as the aforementioned triplets in the starting material now appear as a doublet with a chemical shift of 5.82 ppm, with concomitant introduction of a broad singlet at 7.68 ppm which is indicative of the NH moiety. IR spectroscopy was also used to confirm the synthesis of the target product as there was loss of the carbonyl stretch at 1713.40 cm^{-1} and introduction of a new, broad peak at 3458.20 cm^{-1} which indicates an N-H stretch. Pale orange crystals of compound **13** were grown by vapour diffusion of methanol into a saturated DCM solution. The crystals were found to be in a monoclinic cell and structure solution was carried out in the space group $P2_1/c$. The ASU was found to contain one molecule of **13** in a pinched-cone conformation as well as two co-crystallised methanol molecules.

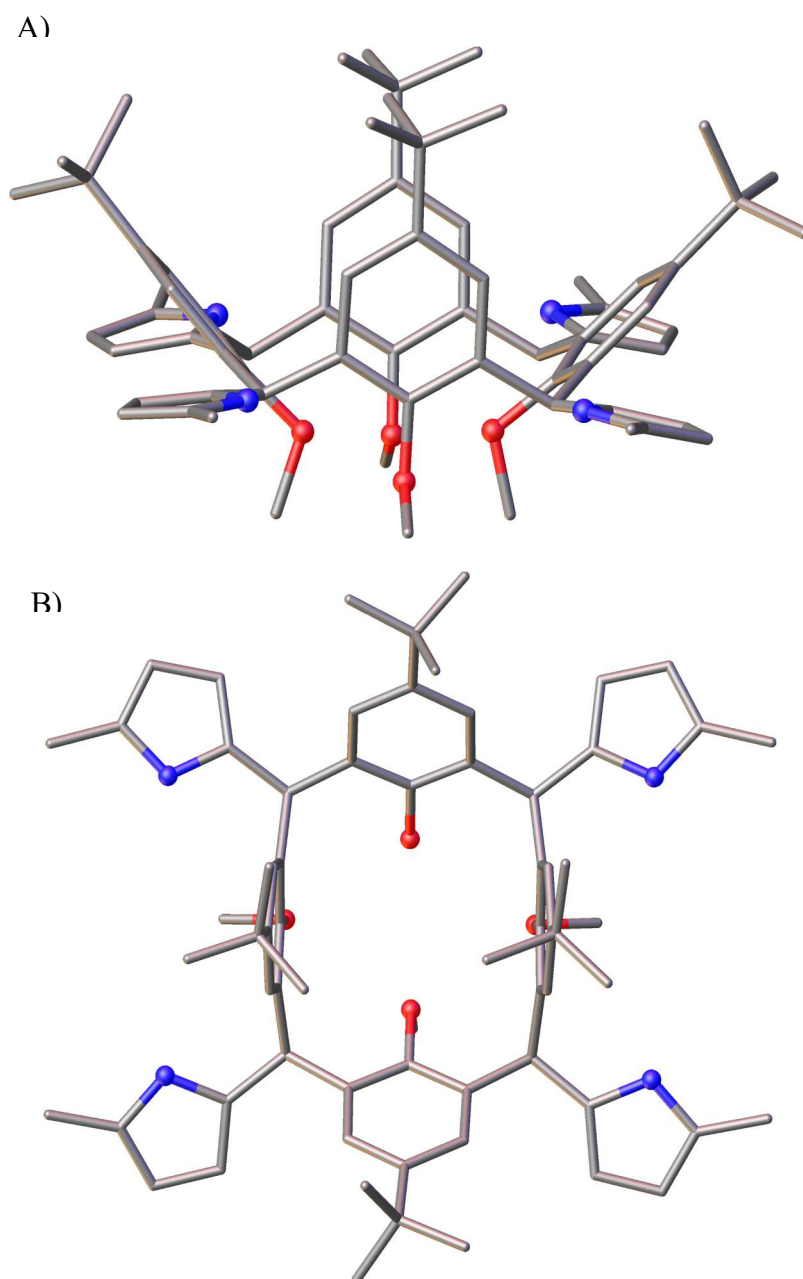
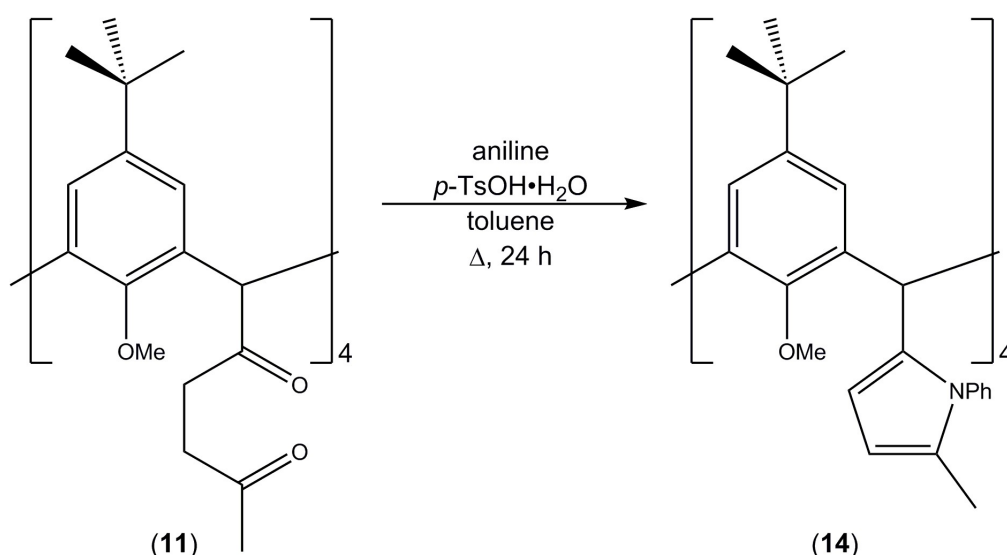


Figure 3.5. Views of the single crystal X-ray structure of **13** shown in ball and stick representation. A) Side-on view showing the C[4] in a pinched-cone conformation and equatorial positioning of the pyrrole moieties. B) View down the C[4] cavity clearly showing the pyrrole moieties. Colour code: C – grey; O – red; N - blue. Acetone of crystallisation and H atoms are omitted for clarity.

Inspection of the crystal structure (Figure 3.5) shows that the reaction has been successful in the ring-closing Paal-Knorr pyrrole synthesis as there are no longer any carbonyl groups and instead there are pyrrole groups with H atoms substituted on the nitrogen atom of the pyrrole.

3.3.2. Synthesis of 5,11,17,23-tetra-*tert*-butyl-2,8,14,20-tetrakis(1-phenyl-2-methyl-1*H*-pyrrole)-25,26,27,28-tetramethoxycalix[4]arene (**14**)

The next reaction tested was with aniline in toluene in the presence of *p*-toluenesulfonic acid monohydrate (*p*-TsOH·H₂O) in order to substitute a phenyl group onto the pyrrole (Scheme 3.4). These reaction conditions are frequently reported in the literature in which hexane-2,5-dione is reacted with an appropriate amine in the presence of *p*-TsOH·H₂O in toluene to yield the relevant pyrrole moiety.⁸⁻¹⁰ After heating at reflux overnight, a sparingly soluble solid (**14**) was formed in a 55% yield. Again, it is important to highlight the percentage yield obtained for these reactions as an overall 55% yield equates to an approximate 86% yield for the reaction at each methylene bridge position.



Scheme 3.4. Synthetic scheme for the preparation of 5,11,17,23-tetra-*tert*-butyl-2,8,14,20-tetrakis(1-phenyl-2-methyl-1*H*-pyrrole)-25,26,27,28-tetramethoxycalix[4]arene (**14**).

Analysis of the ¹H NMR spectrum indicates that a reaction has taken place as the two distinctive triplets of the 1,4-diketone have disappeared and there are several new peaks in the aromatic region. There are broad signals in the aromatic region of the spectrum which may be the protons on the substituted phenyl groups due to hindered rotation around a bond. It would have been interesting to see how the compound behaves at higher temperatures and this could have been achieved by carrying out variable temperature (VT) NMR studies to explore whether the broad peaks would sharpen upon heating. However, this compound is insoluble in common NMR solvents (e.g DMSO, D₂O,

CD₃CO etc), and is only sparingly soluble in CHCl₃ so it was thought unlikely that temperatures higher than 50 °C could be reached (and meaningful studies undertaken). Colourless crystals of **14** grew upon vapour diffusion of PET into a saturated CHCl₃ solution. The crystals were found to be in a monoclinic cell and structure solution was carried out in the space group *P2₁/n*. The ASU was found to contain one half of **14** which upon symmetry expansion afforded the full molecule.

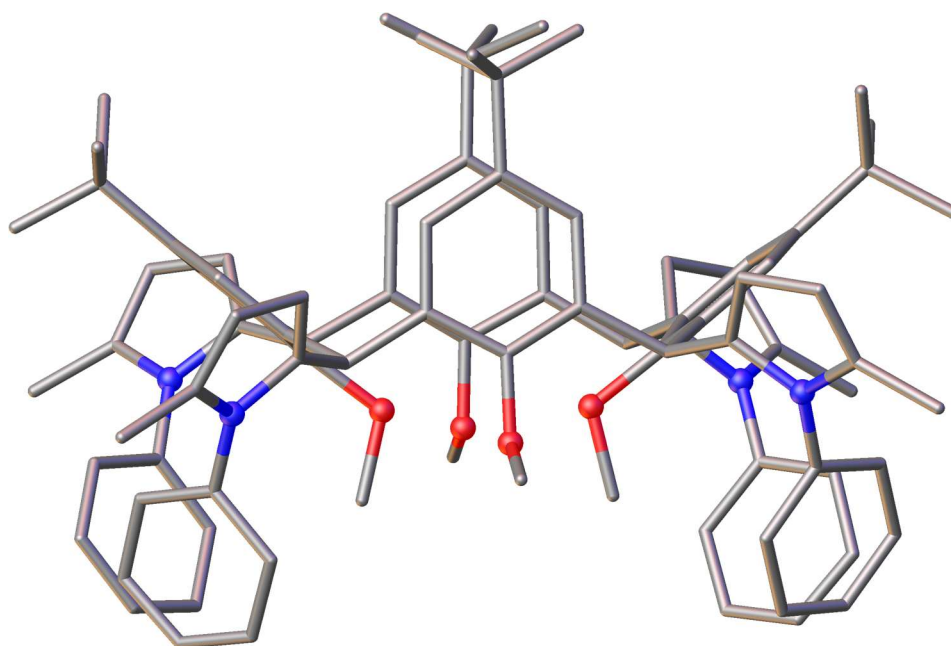
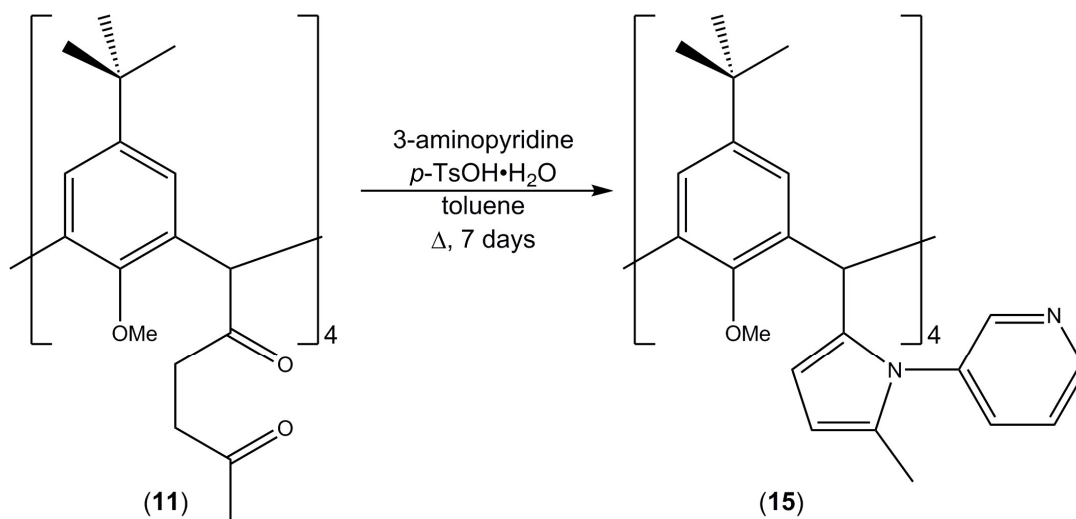


Figure 3.6. Single crystal X-ray structure of **14** showing phenyl substituents on N atom of pyrrole in ball and stick representation. Colour code: C – grey; O – red; N - blue. H atoms are omitted for clarity.

Inspection of Figure 3.6 shows that each 1,4-diketone moiety has been ring-closed to form the pyrrole moiety with a phenyl ring substituent on the N atom in each case. From Figure 3.6, it can also be seen that the bridge substituents have retained their equatorial positions and this may be due to the bulkiness of the groups, therefore preferring to orient in such a way to avoid steric clashes.

3.3.3. Synthesis of 5,11,17,23-tetra-*tert*-butyl-2,8,14,20-tetrakis(3-(2-methyl-1H-pyrrole)pyridine)-25,26,27,28-tetramethoxycalix[4]arene (**15**)

The next amine reaction involved heating to reflux a toluene solution of **11** and 3-aminopyridine with *p*-TsOH·H₂O added as a catalyst (Scheme 3.5). After purification by column chromatography compound **15** was obtained in a 28% yield which equates to a 73% yield for every individual reaction carried out at each of the bridge positions.



Scheme 3.5. Synthetic scheme for the preparation of 5,11,17,23-tetra-*tert*-butyl-2,8,14,20-tetrakis(3-(2-methyl-1H-pyrrole)pyridine)-25,26,27,28-tetramethoxycalix[4]arene (**15**).

The ¹H NMR spectrum of compound **15** was much more complex than was expected but the distinctive triplets of compound **11** had disappeared suggesting that a reaction had taken place. The ¹H NMR spectrum of compound **15** contained broad peaks in the aromatic region and so full integration of the spectrum was carried out over the range of 0 to 9 ppm giving a total of 96 hydrogen atoms which accounts for all the hydrogens in **15**. This gave a good indication that the desired product had formed. The complexity of the spectrum made it difficult to interpret due to multiple signals and broadening around the aromatic region. Inspection of the ¹H NMR spectrum (Figure 3.7) shows that the ^tBu (two singlets at 0.85 and 1.19 ppm), OMe (two singlets at 2.41 and 3.40 ppm) and Ar-H (phenyl, two singlets at 6.38 and 6.67 ppm) protons in the ¹H NMR spectrum are each split into two separate signals, suggesting that the calix[4]arene has been de-symmetrised and could potentially exist in a pinched-cone conformation. It is interesting to see that

there is broadening of peaks, particularly in the aromatic region, and this was thought to be due to hindered rotation around the bond between the bridge and the pyrrole group.

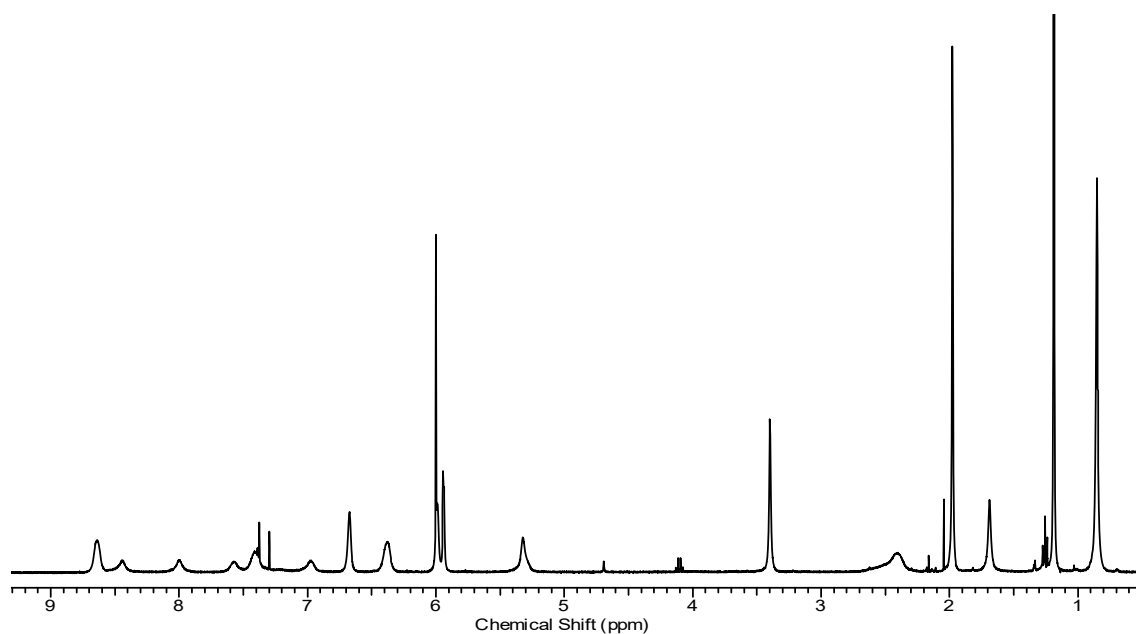


Figure 3.7. ^1H NMR spectrum of compound **15** in tetrachloroethane- d_2 at 25 °C.

Due to the broadness in the aromatic region, and the difficulty in assigning each proton in the structure, the peaks have been tentatively assigned as protons (a) through to (k) for the region (5 to 9 ppm) as shown in Figure 3.8. It was hoped that further NMR analysis would allow for the full assignment of each proton.

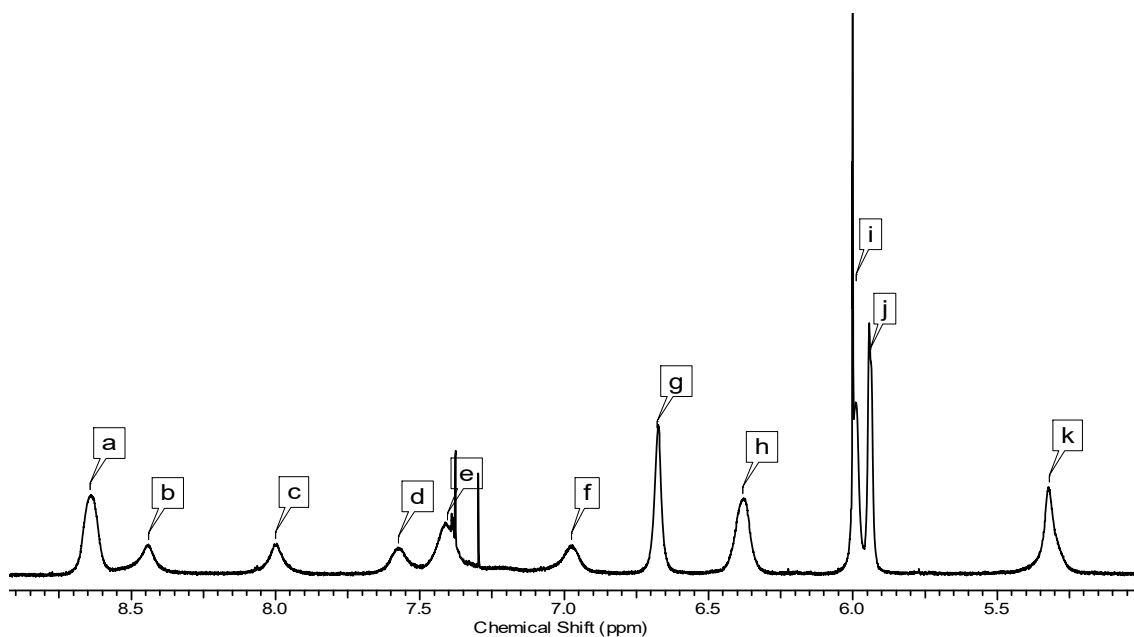


Figure 3.8. ^1H NMR spectrum of compound **15** in tetrachloroethane- d_2 at 25 °C showing the region from 5-9 ppm.

The protons (a) through to (k) from the ^1H NMR spectrum were tentatively assigned as shown in Figure 3.9. A thorough NMR study will now be described with a detailed explanation of how these assignments were made, providing evidence to support these original assignments.

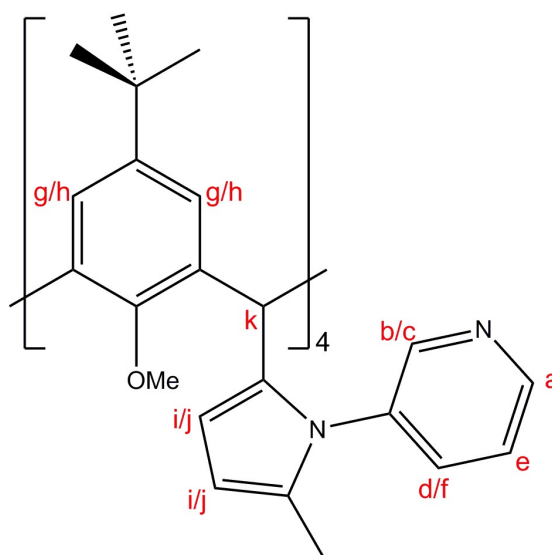


Figure 3.9. Proton assignments made after thorough NMR spectroscopy study.

It is also interesting to note that the ^{13}C NMR spectrum (Figure 3.10) contains broad peaks in the aromatic region and there appear to be multiple signals again for the ^tBu , OMe and Ar-H (phenyl) groups which gives further evidence that the calixarene has been de-symmetrised in some way. This may be due to the C[4] existing in a pinched-cone conformation in solution.

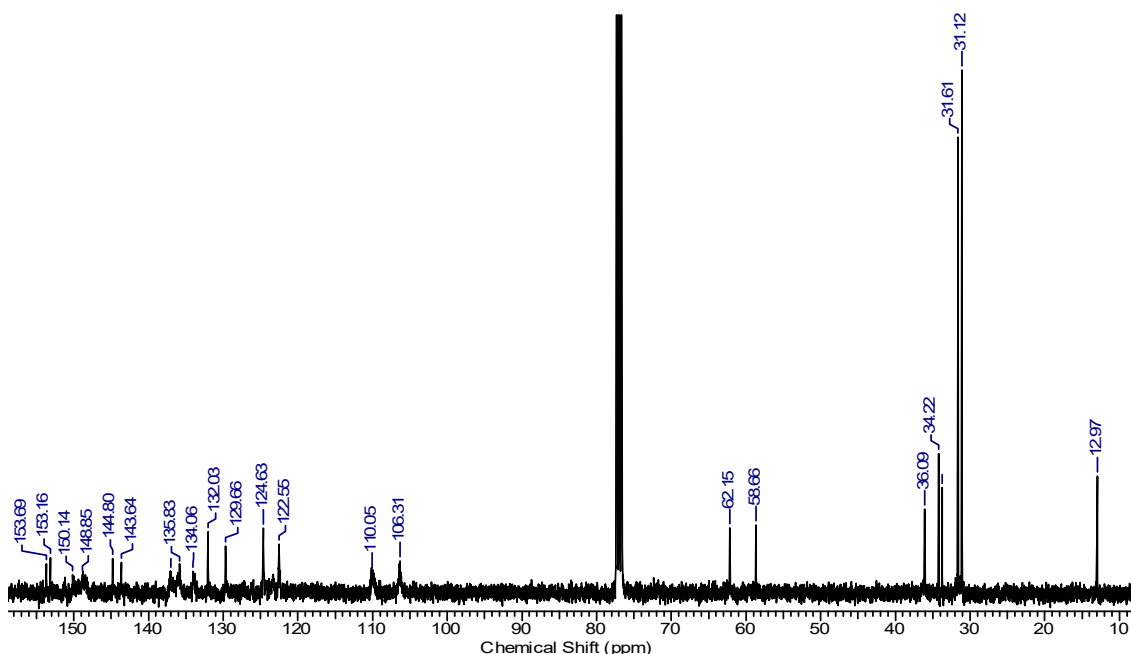


Figure 3.10. ^{13}C NMR spectrum of compound 15.

The DEPT NMR spectrum shows that there are five CH_3 , five CH and no CH_2 environments, suggesting that the CH groups on the pyridine ring have not been picked up in the DEPT spectrum due to their broadness. These are consistent with the expected signals due to two distinguishable ^tBu , OMe and Ar-H (phenyl) environments as found in the ^1H NMR spectrum. The number of CH_3 environments are expected since there is splitting of the ^tBu and OMe groups. The final CH_3 environment corresponds to the methyl group on the pyrrole ring. The CH environments that have been identified are likely to correspond to the bridge protons, the two CH groups of the pyrrole ring and two different CH environments of the phenyl rings. The absence of CH_2 groups in the spectrum also indicates that a reaction has taken place.

Due to these findings, a thorough NMR study of this compound was carried out. The focus of this was to be to attempt a VT study to investigate whether increasing the temperature would thermally induce bond rotation, leading to a much cleaner and simpler NMR spectrum, as well as a 2D NMR study involving experiments such as COSY

(Correlated Spectroscopy), HSQC (Heteronuclear Single Quantum Correlation) and HMBC (Heteronuclear Multiple Bond Correlation). First, a high temperature VT study was attempted due to the solubility of compound **15** in 1,1,2,2-tetrachloroethane- d_2 . This was carried out by increasing the temperature of the sample in 10 °C increments, starting at room temperature (25 °C) and reaching 75 °C, before cooling the sample back to room temperature.

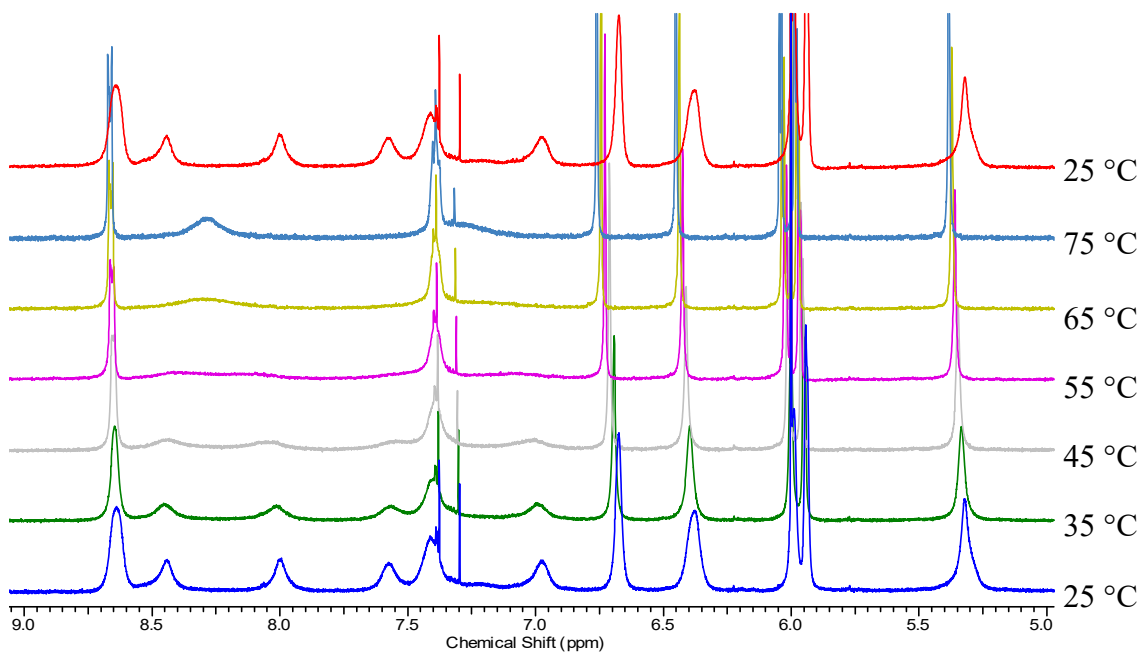


Figure 3.11. High temperature VT NMR spectroscopy study of **15** in tetrachloroethane- d_2 showing the range from 5 – 9 ppm for clarity.

The signals affected most by the higher temperatures are those in the aromatic region and so this is the region that has been focussed on during the VT study. It can clearly be seen in Figure 3.11 that as the temperature is raised the peaks in the NMR spectrum begin to sharpen and become much easier to interpret. It is interesting to note that the process is dynamic as the original ^1H NMR spectrum is obtained after the sample was cooled to room temperature. Upon warming, it is possible to see that the two broad peaks at 8.45 and 8.01 ppm ((b) and (c) protons) have coalesced as the two distinct peaks seen at room temperature have merged into one peak. It would be expected that the peak would become much more distinct and sharper if a temperature higher than 75 °C could be reached, but it was not feasibly possible to reach higher temperatures. The same has also occurred for the two broad peaks at 7.58 and 6.99 ppm ((d) and (f) protons) and again, it is expected that a much sharper signal would be observed if higher temperatures could be

reached. From the VT experiment it is not possible to conclusively assign the protons to the structure. However, the evidence suggests that the peaks corresponding to protons (g) and (h) are the aromatic protons on the calixarene framework, protons (i) and (j) are the protons on the pyrrole moiety and proton (k) is the proton at the bridge position. These assignments have been deduced from both the integrals and splitting pattern of each peak. If compound **15** is indeed in the pinched-cone conformation as hypothesised then two singlets for the protons on the phenyl rings are expected with integrals of four protons each. The two doublets around 6 ppm have been assigned as the protons on the pyrrole group due to the coupling constants of around 3.3 Hz for each peak indicating coupling to one another. Therefore proton (k) has been assigned as the proton on the methylene bridge as it integrates to a total of four protons and has quite a low chemical shift for it to be an aromatic proton. This therefore suggests that protons (a), (b), (c), (d), (e) and (f) are the protons on the pyridine moieties.

A low temperature VT NMR study was also carried out by cooling the sample down to $-60\text{ }^{\circ}\text{C}$ and then collecting ^1H NMR data as the sample temperature was increased in $10\text{ }^{\circ}\text{C}$ increments. The results of this study (Figure 3.12) are inconclusive as the spectra obtained are very complex and difficult to interpret. However, it is interesting to note that the process is dynamic (as is the same with the high temperature VT) as the original ^1H NMR spectrum is obtained once the sample is warmed to room temperature.

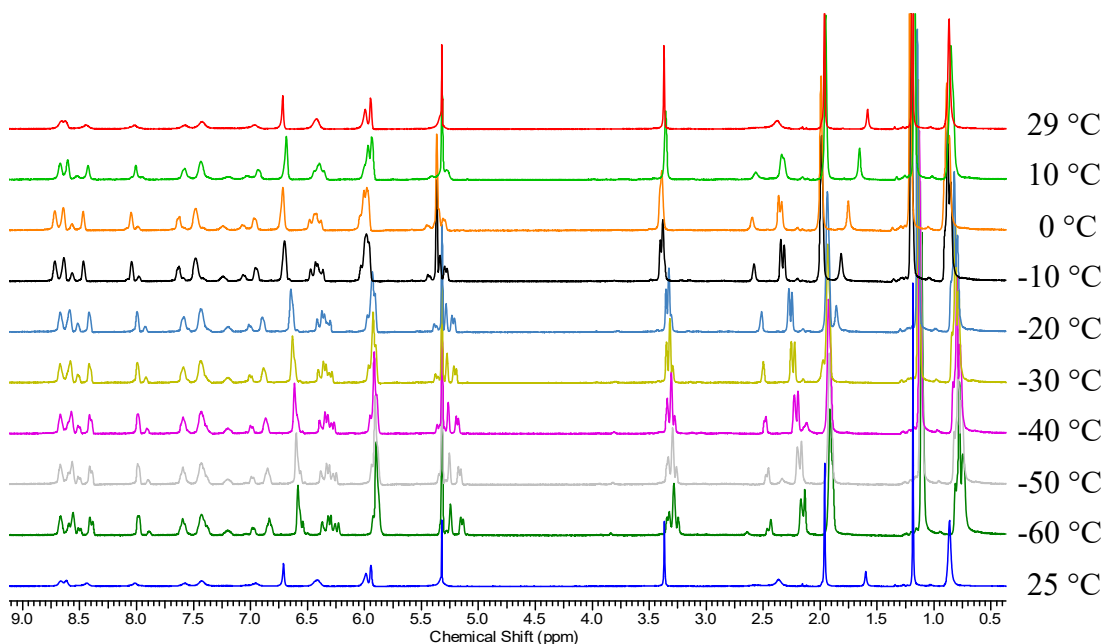


Figure 3.12. Low temperature VT NMR spectroscopy study of **15** in dichloromethane- d_2 .

Inspection of Figure 3.12 shows that cooling to lower temperatures allows several new peaks in the ^1H NMR spectrum of compound **15** to be observed. These new peaks may be due to the low temperatures locking out a number of conformations of **15**, making the spectra much more difficult to interpret. However, it is difficult to see the complexity of the aromatic region at lower temperatures just from Figure 3.12. Figure 3.13 shows the same stacked spectra but enlarged in the 5 to 9 ppm region to show the complexity of the ^1H NMR spectrum at low temperatures.

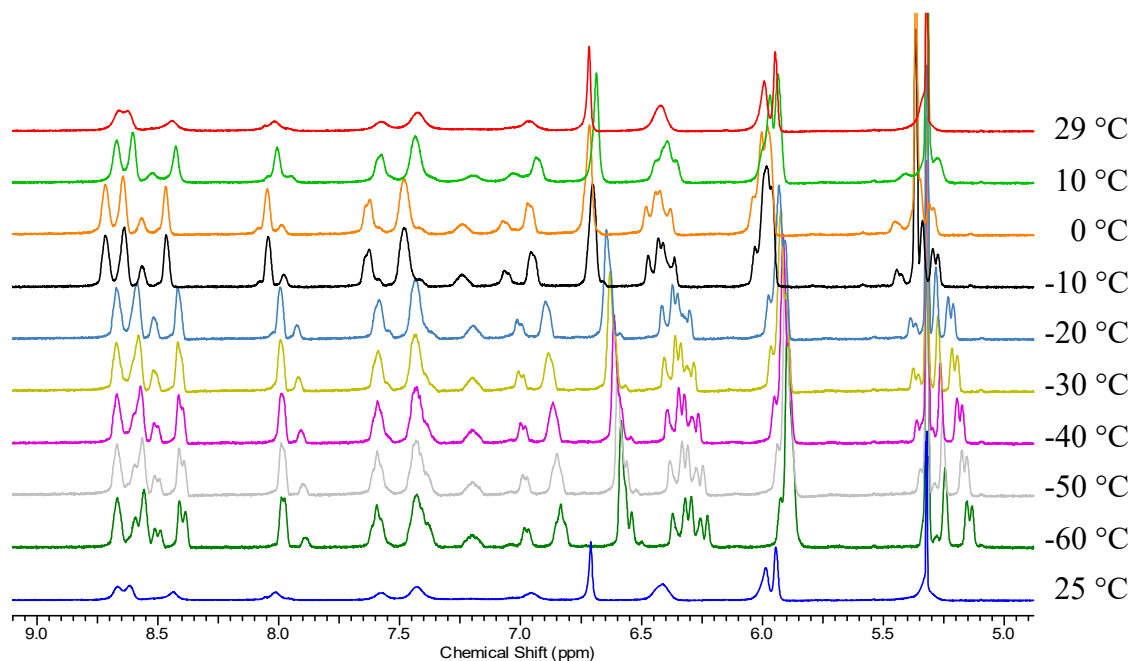


Figure 3.13. Low temperature VT NMR spectroscopy study of **15** in dichloromethane- d_2 showing the region from 5 to 9 ppm for clarity.

A 2D NMR study was also carried out and all of these experiments were carried out at 25 °C, with the exception of an additional high temperature COSY experiment. The first of these was the HSQC experiment, and from this it was possible to identify which peaks in the ^{13}C NMR spectrum correlated to the peaks in the ^1H NMR spectrum, further supporting the assignments made from the ^1H and ^{13}C NMR spectra alone. The peaks at 0.85 and 1.19 ppm of the ^1H NMR spectrum correlate to two CH_3 peaks (31.23 and 31.70 ppm) on the ^{13}C NMR spectrum, which again suggests that these are the *t*-butyl resonances. The peak on the ^1H spectrum at 1.98 ppm correlates to the CH_3 peak at 13.12 ppm on the ^{13}C spectrum and this suggests that these peaks correspond to the methyl group on the pyrrole group due to their relatively low chemical shifts. The peaks at 2.41 and 3.40 ppm correlate to the two CH_3 peaks at 58.75 and 62.23 ppm, respectively, and

these are indicative of the –OMe groups due to their higher chemical shifts as compared to the other CH₃ groups in the compound. The peak at 5.32 ppm on the ¹H NMR spectrum corresponds to the CH group resonating at 36.22 ppm and this is suggestive of the bridge proton as the other CH groups are aromatic which would be expected to have much higher chemical shifts in both the ¹H and ¹³C NMR spectra. The protons at 5.94 and 5.99 ppm correlate to the CH peaks at 106.46 and 110.06 ppm, respectively, and it is suggested that these peaks correspond to the protons on the pyrrole groups due to their chemical shift and coupling constants (3.3 Hz each). The two peaks at 6.38 and 6.67 ppm in the ¹H NMR spectrum correlate to the CH peaks of the ¹³C spectrum at 122.60 and 124.69, respectively, and these are likely to be the aromatic protons on the phenyl rings. The other cross-peaks identified from the HSQC experiment that have not been assigned may be from the pyridine ring as the broad NMR resonances in the ¹H NMR spectrum correlate with the broad resonances in the ¹³C NMR spectrum.

A ¹H-¹⁵N HMBC experiment was carried out to investigate whether correlation peaks would be seen between the N atoms on both the pyrrole and pyridine rings with any of the peaks observed in the ¹H NMR spectrum. The results of this experiment showed two cross-peaks around 165 ppm which correlated to the peaks at 1.98, 5.94 and 5.99 ppm, suggesting that the N atom observed is in close proximity to these proton environments. As these peaks have been tentatively assigned as protons of the methyl group substituent on the pyrrole and the protons on the pyrrole group itself it is suggested that the N atom observed is that of the pyrrole group. Due to the pyridine group being dynamic and only very broad peaks of this group being observed in any NMR spectrum it is plausible that the N atom on the pyridine ring will not be observed in the HMBC experiment.

It is not possible to conclusively assign the protons of the pyridine ring just from the COSY spectrum, however the evidence from this experiment does support the assignments as shown in Figure 3.9. The room temperature COSY experiment shows that protons (b) and (c) exist in their own spin system as they are only coupling to each other and not to any other protons. These protons must be therefore be isolated from the rest of those on the pyridine group. As these resonances have a reasonably high chemical shift (8.45 and 8.01 ppm, respectively), it is suggested that these protons are close in proximity to the N atom (*meta* to the nitrogen atom). It can also be deduced that proton (a) is close to the N atom (*meta*-position) as it also has a high chemical shift of 8.65 ppm and is close to proton (e) as there is a cross-peak indicating coupling between the two protons. Proton (e) has cross-peaks with protons (a), (d) and (f) so therefore the most

contacts so it is likely that proton (e) exists in between the other resonances (*ortho* to the nitrogen atom). Protons (d) and (f) are coupling to one another but they are also coupling to proton (e) suggesting that these are in close proximity.

A high temperature COSY experiment was run at 70 °C which shows that protons (a) and (e) are coupling to one another which had already been deduced from the room temperature experiment. However, due to the broadness of the peaks for protons (d)/(f) the coupling that could be seen at room temperature between (d), (e) and (f) cannot be seen between protons (d)/(f) and (e) at the elevated temperature. It is interesting to note that there is a small cross-peak between protons (j) and (k) which may be due to a 4J coupling between the proton at the bridge position (k) and the proton on the pyrrole ring closest to the methylene bridge (j).

Colourless crystals of this compound were grown upon slow evaporation of **15** in CHCl₃. These were analysed by X-ray diffraction and were found to be the target compound. The crystals were found to be in a monoclinic cell and structure solution was carried out in the space group *P2/c*. The ASU was found to contain one half of **15** which upon symmetry expansion afforded a full molecule of **15** in a pinched-cone conformation as shown in Figure 3.14. The N position on the pyridine ring was disordered over two positions, however these are shown in only one position for clarity. Inspection of the crystal structure shows that each 1,4-diketone group has been ring-closed to afford the pyrrole with the substituted pyridine ring pointing down towards the methoxy groups at the C[4] lower-rim. It can also be seen that the substituents at the methylene bridges have retained their equatorial positions, again suggesting that this chemistry does not impact the positioning of the methylene bridge-substituted groups.

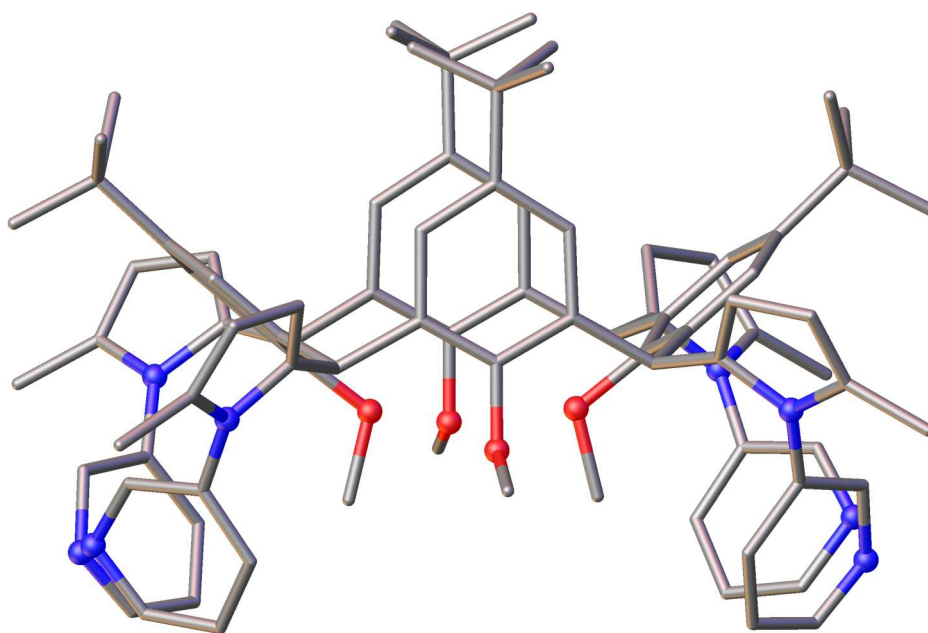


Figure 3.14. Single crystal X-ray structure of **15** showing pyridine substituents on N atom of each pyrrole moiety in ball and stick representation. Colour code: C – grey; O – red; N – blue. H atoms are omitted for clarity.

3.3.4. Reaction of 5,11,17,23-tetra-*tert*-butyl-2,8,14,20-tetrakis(pentane-1,4-dione)-25,26,27,28-tetramethoxycalix[4]arene (**11**) with 2- or 4-aminopyridine

The reactions of either 2- or 4-aminopyridine with compound **11** were attempted under the standard reaction conditions as described before (reflux with appropriate aminopyridine dissolved in toluene in the presence of *p*-TsOH·H₂O). However, these reactions proved to be unsuccessful as only starting material was recovered, indicating that no reaction had taken place and therefore more forcing reaction conditions were required in order to form the desired products. The reactions with 2- and 4-aminopyridine were carried out again in a higher boiling point solvent, mesitylene, in order to investigate whether the elevated reaction temperatures had any effect. Again, only starting materials were recovered from these reactions.

A search of the literature shows that synthesising substituted pyrrole derivatives, albeit not on a calixarene framework, is possible under microwave conditions as outlined by Murugesan and co-workers.¹¹ In the work presented in this paper, Murugesan *et al.* were able to form several substituted pyrrole derivatives using solvent-free conditions in the microwave as they reacted hexane-2,5-dione, the appropriate aniline and *p*-TsOH

bound with silica gel in a microwave oven at 180 °C for 20 minute. A slight modification of this procedure was used in the attempt to form these substituted pyrrole derivatives on calix[4]arenes through the addition of a solvent, either toluene or DMF to aid solubility of the reactants. The first set of reactions attempted were carried out in toluene in the presence of *p*-TsOH·H₂O (instead of the silica bound form) and reacted for 20 mins using either the 2-, 3- or 4-aminopyridine. Only starting material was recovered from these reactions which was clear to see from the ¹H NMR spectra due to the presence of the indicative 1,4-diketone backbone triplets meaning that no reaction had taken place. Toluene is a poor microwave absorbing solvent meaning it took a significant time for the reaction mixture to reach the desired temperature, therefore making the advantage of fast heating and reaction times almost null. It was then decided to try DMF as this is a much better microwave absorbing solvent. After 2 hours of microwave heating, the reaction with 3-aminopyridine looked promising as there was broadening of the NMR spectrum of the crude product obtained from the reaction. Therefore, the same conditions were used for the 2- and 4-aminopyridine reactions in DMF, however, only starting material was recovered from both reactions.

Another reaction method was trialled, and this involved superheating the reaction mixture in a sealed pressure tube. Again, the reaction with 3-aminopyridine was selected as a test in order to establish whether these reaction conditions would form the product formed previously under standard conditions. The reaction was carried out in DMF in the presence of *p*-TsOH·H₂O and heated at 180 °C for 6 hours, after which time a brown solid was obtained after aqueous work-up. This crude solid was found to be starting material, as confirmed by NMR analysis. The reaction was then repeated at 200 °C for 5 hours which, following work-up, was found to have started forming the desired product as the indicative triplets of the starting material had disappeared and there was broadening of the other peaks in the ¹H NMR spectrum. These reaction conditions were then taken forward in the reactions with 2- and 4-aminopyridine. The reaction with 4-aminopyridine was carried out at 200 °C for 6 and 12 hours, and after subsequent work-up of both reactions it was found that only starting material was recovered. The reaction with 2-aminopyridine was also attempted at 200 °C for 6 hours, producing the same outcome.

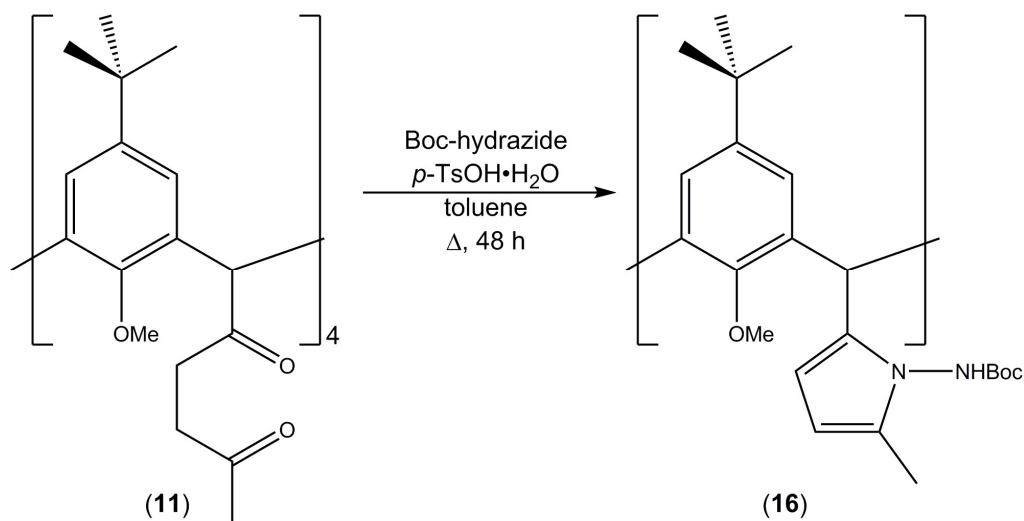
It was thought that the reaction conditions were too acidic and, as such, the 2- and 4-aminopyridines were being protonated and hence not acting as nucleophiles. The pK_a values of 2-, 3- and 4-aminopyridine are 6.86, 5.98 and 9.17,¹² respectively. These values show that 3-aminopyridine is the least basic out of the three isomers and therefore is able to tolerate more acidic reaction conditions, whereas the other two isomers are more basic

and are likely to be protonated in strongly acidic conditions. The pK_a value of *p*-TsOH is -2.8, indicating that this is a strongly acidic compound which is capable of protonating the aminopyridine reactants.¹³ Therefore it was decided to trial the use of pyridinium *p*-toluenesulfonate (PPTS) as a replacement catalyst to investigate the effects this may have on the reaction due to its higher pK_a value of 5.2.¹⁴ An overnight reflux of **11** and 3-aminopyridine in toluene in a catalytic amount of PPTS showed formation of the desired product from the NMR spectrum, and so the reaction was carried out using both 2- and 4-aminopyridine to investigate whether the desired products could be formed using these new reaction conditions. The results from these reactions showed that only starting material was recovered in both cases.

The reaction of hexane-2,5-dione with both 2- and 4-aminopyridine have been observed in the literature and so it is likely that these products on the calix[4]arene framework may be obtained using other reaction conditions. However, there was not sufficient time remaining during the life of this study to explore other conditions using catalysts such as iodine,¹⁵ bismuth nitrate¹⁶ or magnesium iodide etherate.¹⁷ Also, time permitting, it would be interesting to explore these reactions with other catalysts in pressure tubes as this should theoretically reduce the reaction time, thus giving a better indication of whether a reaction will take place in a shorter timeframe.

3.3.5. Synthesis of 5,11,17,23-tetra-*tert*-butyl-2,8,14,20-tetrakis(*tert*-butyl(2-methyl-1H-pyrrole)carbamate)-25,26,27,28-tetramethoxycalix[4]arene (**16**)

Another reaction investigated was the Paal-Knorr pyrrole synthesis using Boc-hydrazide as a method of introducing a protected NH₂ group onto the pyrrole ring. Following deprotection of the Boc group, the NH₂ group was to be further reacted in the attempt to form a cage. The standard reaction conditions of **11** and Boc-hydrazide in toluene in the presence of *p*-TsOH·H₂O gave a yellow crude (Scheme 3.6).

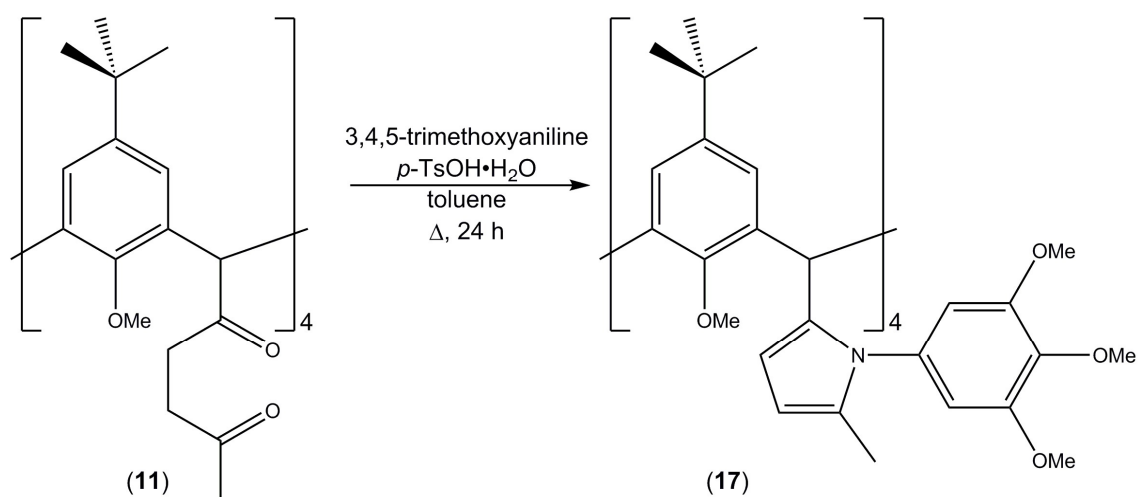


Scheme 3.6. Synthetic scheme for the preparation of 5,11,17,23-tetra-*tert*-butyl-2,8,14,20-tetrakis(*tert*-butyl(2-methyl-1H-pyrrole)carbamate)-25,26,27,28-tetramethoxycalix[4]arene (**16**).

Inspection of the ^1H NMR spectrum of the crude product showed that a reaction had taken place as the triplets indicative of the starting material had disappeared. It was interesting to note that two different ^tBu groups were observed in the spectrum which correlate to the ^tBu groups on the phenyl ring and the Boc protecting group. However, the ^1H NMR spectrum showed impurities and the crude could not be fully purified. Through the use of IR, it would be possible to further investigate whether the desired product was synthesised as there should be a N-H band observed in the IR spectrum. A broad band at 3230 cm^{-1} was observed giving a good indication that the product had formed.

3.3.6. Synthesis of 5,11,17,23-tetra-*tert*-butyl-2,8,14,20-tetrakis(2-methyl-1-(3,4,5-trimethoxyphenyl)-1H-pyrrole)-25,26,27,28-tetramethoxycalix[4]arene (**17**)

One of the final reactions explored with compound **11** was with 3,4,5-trimethoxyaniline in order to incorporate several methoxy groups which could later be deprotected to give new hydroxyl environments capable of metal coordination. This reaction was carried out using the standard conditions of reflux of **11** and 3,4,5-trimethoxyaniline in toluene with the addition of $p\text{-TsOH}\cdot\text{H}_2\text{O}$ as a catalyst in the hope of synthesising 5,11,17,23-tetra-*tert*-butyl-2,8,14,20-tetrakis(2-methyl-1-(3,4,5-trimethoxyphenyl)-1H-pyrrole)-25,26,27,28-tetramethoxycalix[4]arene (**17**, Scheme 3.7).



Scheme 3.7. Synthetic scheme for the preparation of 5,11,17,23-tetra-*tert*-butyl-2,8,14,20-tetrakis(2-methyl-1-(3,4,5-trimethoxyphenyl)-1H-pyrrole)-25,26,27,28-tetramethoxycalix[4]arene (**17**).

Upon aqueous work-up, a yellow/orange crude was afforded which was purified by column chromatography. The ¹H NMR spectrum of what appeared to be the desired product had slight impurities in it so the solid was recrystallised from CHCl₃/MeOH to give a white crystalline solid. However, inspection of the ¹H NMR spectrum of the recrystallised solid showed the same impurities as prior to purification. ESI-MS has confirmed that the product has successfully formed, albeit still with slight impurities as indicated from the ¹H NMR spectrum, as peaks with *m/z* values of 1684.9 and 1708.9 have been identified as M and [M+Na]⁺, respectively. Suitable single crystals for X-ray diffraction analysis were grown from vapour diffusion of PET into a CHCl₃ solution of **17**. The crystals were found to be in a monoclinic cell and structure solution was carried out in the space group *P2*₁/*c*. The ASU was found to contain one full molecule of **17** in the pinched-cone conformation and what appeared to be molecules of solvent. However, the solvent could not be modelled and so a solvent mask was applied to remove the extra electron density.

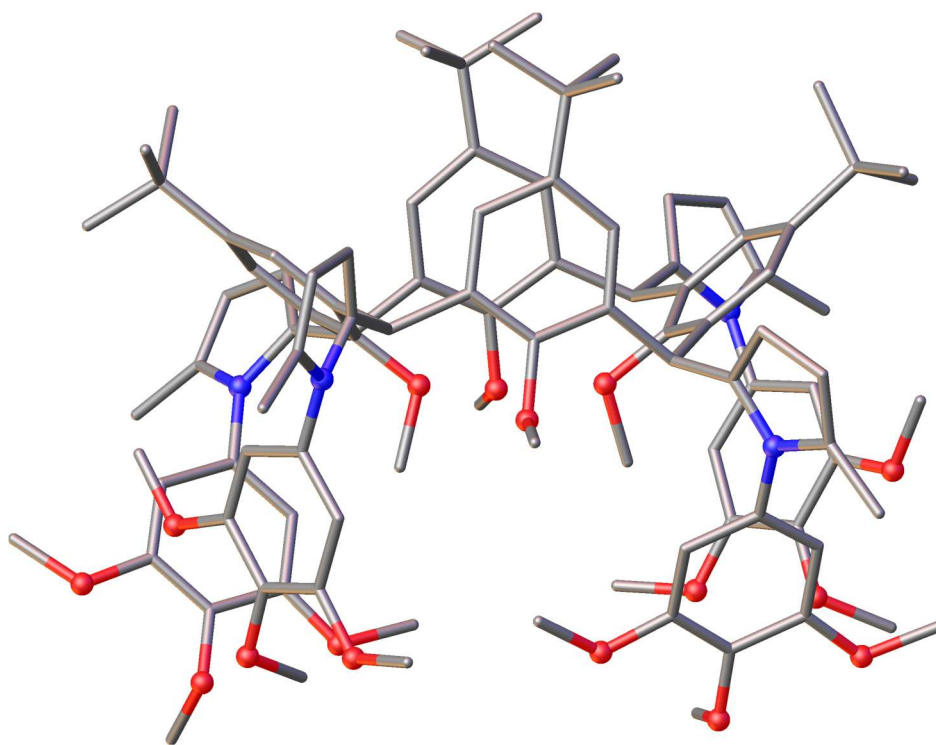


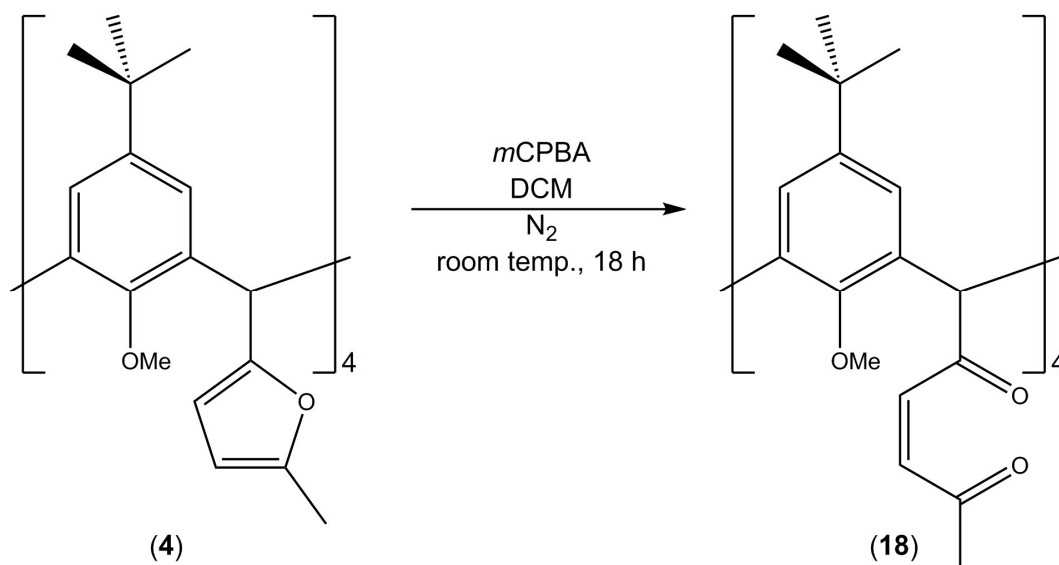
Figure 3.15. Single crystal X-ray structure of **17** shown in ball and stick representation. Colour code: C – grey; O – red; N – blue. H atoms are omitted for clarity.

Inspection of Figure 3.15 shows that the 1,4-diketone groups on the methylene bridge position have been ring-closed to form the pyrrole groups with the substituted trimethoxyphenyl rings pointing down. Again, it is interesting to note that the equatorial positioning of the bridge substituents has been retained. The next synthetic step for this compound would be deprotection of all of the methoxy groups to install a possible sixteen hydroxyl groups. The resultant compound has a significantly increased number of metal-binding sites and the prospect of forming new polymetallic clusters from this compound is of great interest to this research group.

3.4. Oxidation of 4 and Subsequent Synthesis of Pyridazine TBC[4] derivatives

As outlined previously, there are two ways in which a furan moiety can be ring-opened, one of which is the oxidation of the furan group to form the unsaturated 1,4-diketone species. This form of ring-opening will be discussed in this section with the oxidative ring-opening reaction of compound **4** carried out by a room temperature stir with *m*CPBA

in DCM under N₂ (Scheme 3.8) as reported by Lichtenthaler and co-workers.² This produced a pale yellow solid after subsequent aqueous work-up and purification by column chromatography which was found to be 5,11,17,23-tetra-*tert*-butyl-2,8,14,20-tetrakis(pent-2-ene-1,4-dione)-25,26,27,28-tetramethoxycalix[4]arene (**18**) in a 34% yield. This equates to an approximate 76% yield for each bridge position which is lower than the yield obtained by Lichtenthaler *et al.* (90%), however, it is promising to see that this reaction can be applied to C[4]s.



Scheme 3.8. Synthetic scheme for the preparation of 5,11,17,23-tetra-*tert*-butyl-2,8,14,20-tetrakis(pent-2-ene-1,4-dione)-25,26,27,28-tetramethoxycalix[4]arene (**18**).

Colourless crystals of compound **18** were grown from acetonitrile which were analysed by X-ray diffraction. The crystals were found to be in a tetragonal cell and structure solution was carried out in the space group *P4bm*. The ASU was found to consist of two halves of two calix[4]arene units which upon symmetry expansion gave two full calixarenes, one of which is in a cone conformation and the other in a pinched-cone conformation. The calixarene in the cone conformation contains a molecule of acetonitrile in the cavity whereas the calixarene in the pinched-cone conformation does not have any solvent in the cavity.

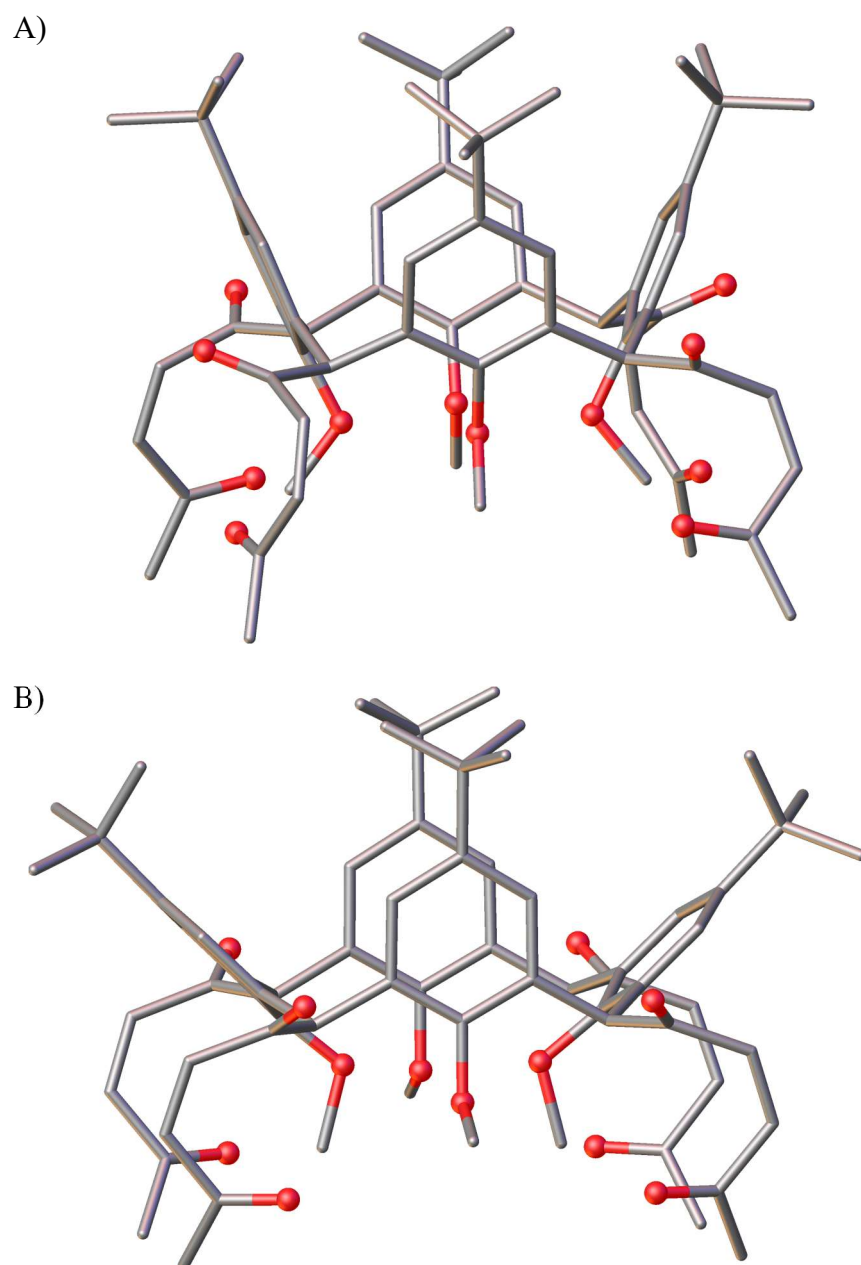
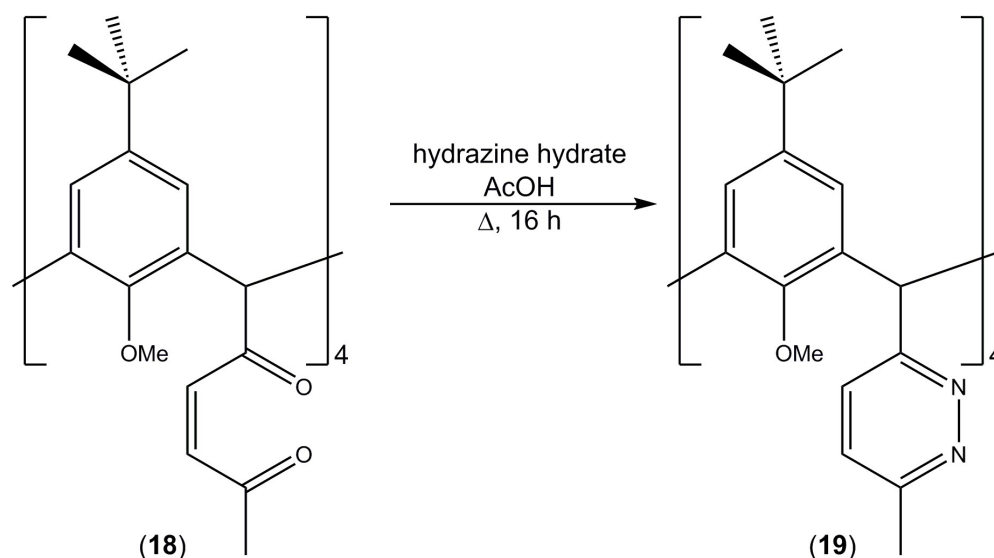


Figure 3.16. Views of the single crystal X-ray structure of **18** shown in ball and stick representation. (A) Cone conformation. (B) Pinched-cone conformation. Colour code: C – grey; O – red. Acetonitrile of crystallisation and H atoms are omitted for clarity.

Inspection of the crystal structure (Figure 3.16) clearly shows that the furan moieties have been ring-opened to afford **18**. The carbon-carbon bond lengths of the backbone are 1.325(6) and 1.318(5) Å for the cone and pinched-cone conformations, respectively, indicating that these are double bonds and hence the unsaturated 1,4-diketone species. It is also clear to see that the equatorial positions of the substituents at the methylene bridge have been retained as expected.

3.4.1. Synthesis of 5,11,17,23-tetra-*tert*-butyl-2,8,14,20-tetrakis(3-methylpyridazine)-25,26,27,28-tetramethoxycalix[4]arene (**19**)

The next reaction explored in this part of the work involved reacting compound **18** with hydrazine hydrate in order to form 5,11,17,23-tetra-*tert*-butyl-2,8,14,20-tetrakis(3-methylpyridazine)-25,26,27,28-tetramethoxycalix[4]arene (**19**). The reaction conditions outlined by Lichtenhaler and co-workers² in which they reacted (Z)-1,6-bis(benzyloxy)hex-3-ene-2,5-dione with hydrazine hydrate in THF to afford 3,6-bis(benzyloxymethyl)pyridazine were not suitable for the reaction of compound **18** under the same conditions as starting material was recovered indicating that no reaction had occurred. Therefore more forcing reaction conditions were required and conditions reported by Ried *et al.*⁵ were employed. The synthesis of **19** was achieved by reflux of compound **18** and hydrazine hydrate in acetic acid which yielded a light brown solid in a 67% yield following an aqueous work-up and column chromatography. This yield equates to an approximate 90% yield per methylene bridge position.



Scheme 3.9. Synthetic scheme for the preparation of 5,11,17,23-tetra-*tert*-butyl-2,8,14,20-tetrakis(3-methylpyridazine)-25,26,27,28-tetramethoxycalix[4]arene (**19**).

Single crystals of **19** were grown upon vapour diffusion of acetonitrile into a solution of the solid in CHCl_3 and the crystal structure of this is shown in Figure 3.17. The crystals were found to be in an orthorhombic cell and structure solution was carried out in the space group *Pnma*. The ASU was found to contain one half of **19** which upon symmetry expansion afforded a full molecule of **19** in the pinched-cone conformation.

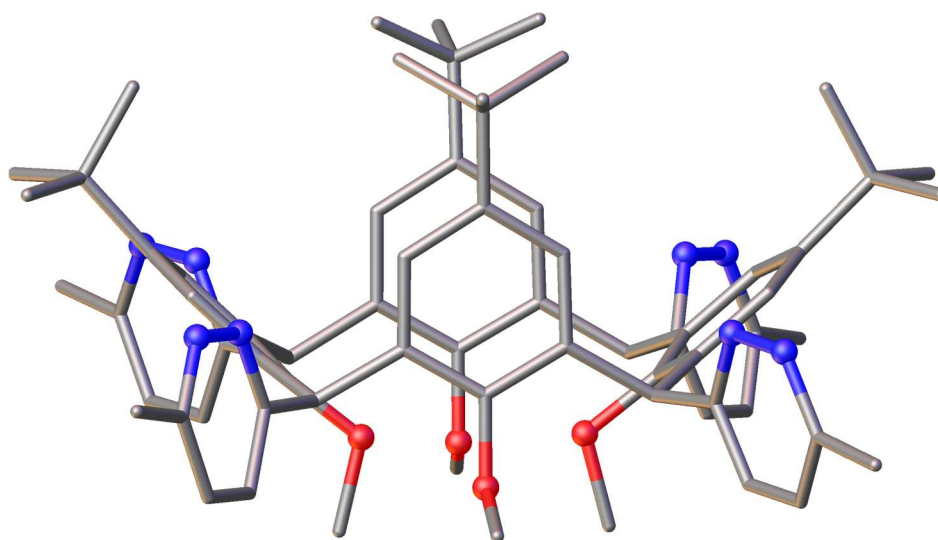


Figure 3.17. Single crystal X-ray structure of **19** shown in ball and stick representation. Colour code: C – grey; O – red; N – blue. H atoms are omitted for clarity.

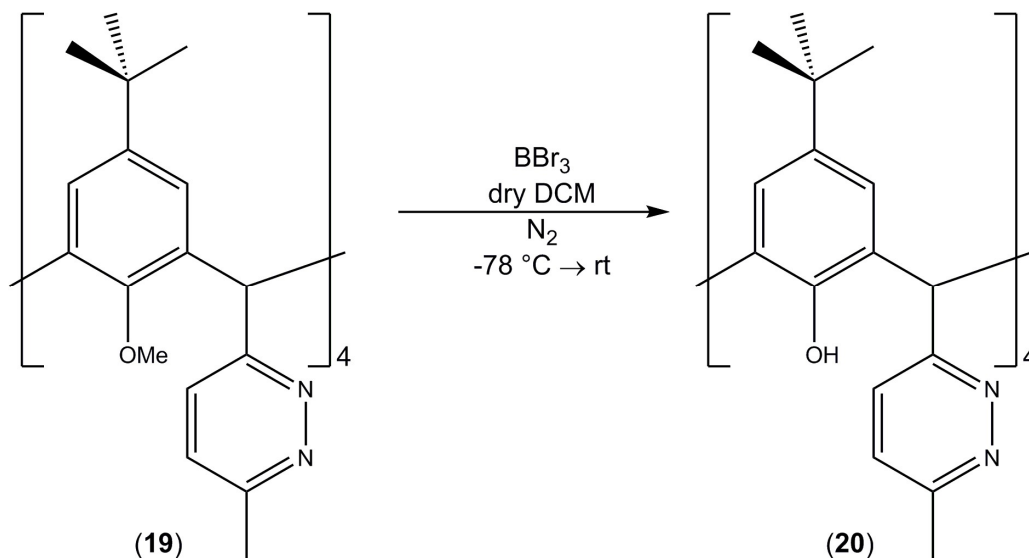
Inspection of Figure 3.17 clearly shows that the diketone groups of compound **18** have reacted with the hydrazine hydrate and formed pyridazine moieties. It can also be seen that the pyridazine substituents remain in the equatorial positions.

3.4.2. Deprotection of 5,11,17,23-tetra-*tert*-butyl-2,8,14,20-tetrakis(3-methylpyridazine)-25,26,27,28-tetramethoxycalix[4]arene (**19**)

The next steps of this work were to be the deprotection of all of the novel methylene bridge-substituted C[4]s synthesised. Due to time issues only the demethylation of compound **19** was investigated as this compound was easy to synthesise in good yields and there were no solubility issues. As explained in Chapter 2, lower-rim hydroxyl groups are required to form polymetallic clusters, and so compound **19** needed to be deprotected before its coordination properties could be investigated. The deprotection step was initially attempted using the standard conditions as outlined in Chapter 2, however this was not a suitable method of demethylation due to the nature of the ^1H NMR spectrum of the solid produced from the reaction. It was unclear if any demethylation had occurred through inspection of the NMR spectrum, and purification of the crude solid by recrystallisation and column chromatography proved to be unsuccessful.

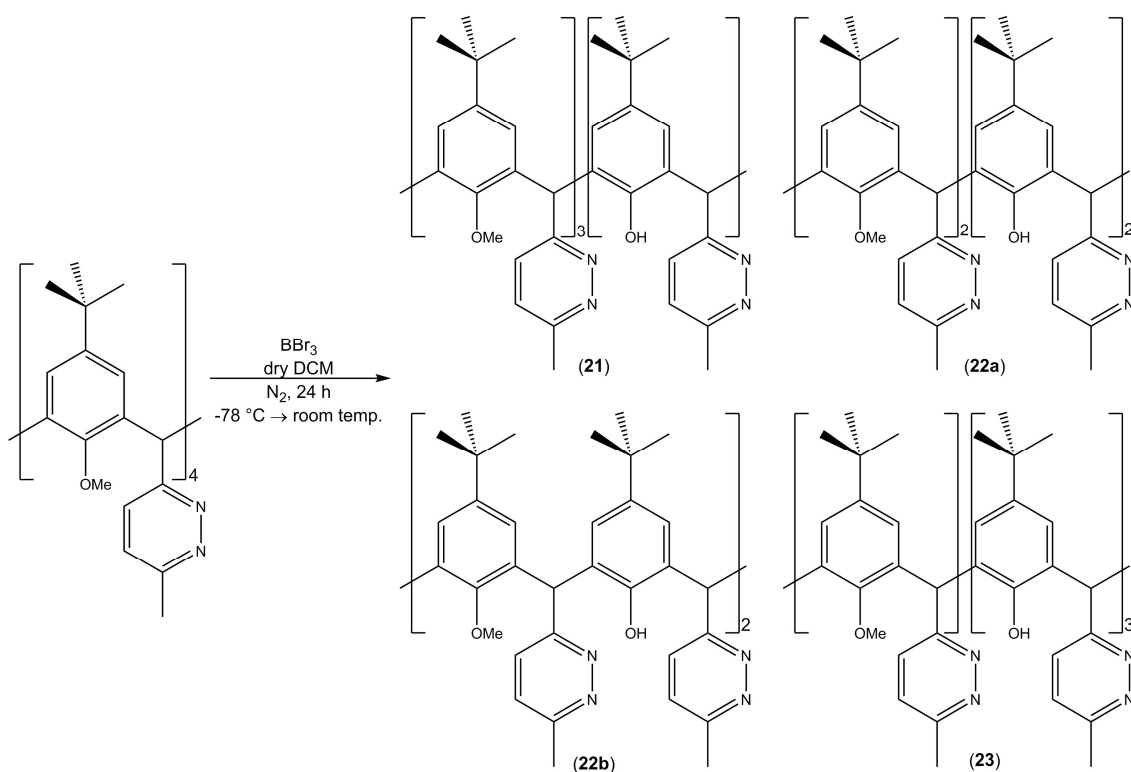
Another method of demethylation by reaction with boron tribromide was investigated and preliminary results from this reaction were promising as evaluated from the ^1H NMR spectrum. Using a modified procedure as reported by Hardman and co-

workers,¹⁸ the reaction was carried out by adding 40 *eq.* of BBr₃ to a solution of compound **19** in dry DCM at -78 °C which was then stirred at this temperature for 1 hour. After this time the reaction mixture was warmed to room temperature and allowed to stir for 24 hours.



Scheme 3.10. Synthetic scheme for the preparation of 5,11,17,23-tetra-*tert*-butyl-2,8,14,20-tetrakis(3-methylpyridazine)-25,26,27,28-tetrahydroxycalix[4]arene (**20**).

Inspection of the NMR spectrum shows that the reaction had not proceeded as planned (Scheme 3.10) as the relative integrals of the methoxy peaks and the methyl peak on the pyridazine group indicated that partial demethylation had occurred. Hardman *et al.* used the same reaction conditions described above to fully demethylate a 2-chloroalkylcalix[4]arene using 6.5 equivalents of BBr₃.¹⁸ This suggests that perhaps the pyridazine substituents on **19** are too bulky, therefore hindering the demethylation step. The spot TLC of the crude in a 9:1 CHCl₃/MeOH eluent system showed multiple spots, suggesting that more than one product has formed from the reaction. The crude may be a mixture of the mono-, di- (vicinal and distal), tri- and tetra-hydroxy products. This in turn suggests that it may be possible to optimise the reaction conditions and / or time in order to isolate selected demethylated products as desired; this would provide a range of benefits depending on how one might exploit the lower-rim binding site. Following column chromatography, it was possible to identify that the mono-, di- and tri-hydroxy derivatives had been isolated from the reaction described as above.



Scheme 3.11. Synthetic scheme showing the possible derivatives formed under the modified reaction conditions as reported by Hardman and co-workers.

The first compound to be discussed is thought to be 5,11,17,23-tetra-*tert*-butyl-2,8,14,20-tetrakis(3-methylpyridazine)-25,26,27-trimethoxy-28-hydroxycalix[4]arene (21). Although the compound appeared to be pure from the spot TLC, the ^1H NMR spectrum showed slight impurities. However, it was possible to postulate what the product may be from the relative integrals of 9 protons for the methoxy groups with the 15 protons for the pyridazine methyl groups. Overlapping signals of impurities around 2.7 ppm may be the cause for the integral observed for the pyridazine methyl groups as 12 protons are expected for these groups. ESI-MS confirmed that it was in fact the mono-hydroxy derivative as m/z peaks were observed at 1059.6 and 1089.6 which correspond to $[\text{M}+\text{H}]^+$ and $[\text{M}+\text{Na}]^+$ values, respectively.

The second compound afforded from the demethylation reaction was thought to be either 5,11,17,23-tetra-*tert*-butyl-2,8,14,20-tetrakis(3-methylpyridazine)-25,26-dimethoxy-27,28-dihydroxycalix[4]arene (22a) or 5,11,17,23-tetra-*tert*-butyl-2,8,14,20-tetrakis(3-methylpyridazine)-25,27-dimethoxy-26,28-dihydroxycalix[4]arene (22b). The spot TLC of this compound suggested that this was only one compound and the ^1H NMR showed only very minor impurities. Again, the product could be postulated from the relative integrals of 6 protons for the methoxy peaks compared with 3:6:3 protons for

the pyridazine methyl peaks suggesting that two methoxy groups had been removed. The splitting pattern of the pyridazine methyl groups suggest that this is the vicinal derivative (**22a**) as a singlet would be expected to be observed for the distal isomer (**22b**) due to symmetry of the molecule. ESI-MS confirmed that the di-hydroxy product had been synthesised as m/z peaks were observed at 1045.6 and 1067.6 which correlate to $[M+H]^+$ and $[M+Na]^+$ values, respectively. However these m/z peaks would be expected for both isomers so further analysis is required (for example X-ray crystallography) in order to conclusively assign this compound as either the vicinal or distal derivative.

The third compound isolated after column chromatography was thought to be 5,11,17,23-tetra-*tert*-butyl-2,8,14,20-tetrakis(3-methylpyridazine)-25-methoxy-26,27,28-trihydroxycalix[4]arene (**23**). Again, the spot TLC of this compound suggested that there was only one product but there were some impurities in the 1H NMR spectrum which might be the reason why the relative integral of 15 protons for the pyridazine methyl groups is higher than expected compared to 3 protons for the methoxy peaks. ESI-MS was used to confirm that this product had in fact been isolated from the reaction as m/z peaks were observed at 1031.6 and 1053.6 which correspond to $[M+H]^+$ and $[M+Na]^+$ values, respectively.

3.5. Conclusions

The results presented here show that the library of methylene bridged-substituted calix[4]arenes has been expanded a great deal. All of these new derivatives have been synthesised using compound **4** as the starting material for these transformations. Compound **4** has been successfully ring-opened to form the saturated 1,4-diketone species, **11**, and the unsaturated 1,4-diketone species, **18**, and from these two compounds a whole raft of other heterocyclic compounds can be synthesised.

Compound **11** can be ring-closed through a Paal-Knorr pyrrole condensation reaction, which gives the option of introducing various substituents on the N atom of the pyrrole moiety. There are a huge number of commercially available primary amines, giving almost limitless possibilities for the generation of new, functional host molecules, the properties of which can be tailored or tuned accordingly. The distinctive triplets in the ^1H NMR spectrum of **11** observed are an excellent NMR handle, giving an immediate indication of whether a reaction has proceeded or not. Compound **16** requires purification before full characterisation can be completed, and once this is pure it can potentially be reacted further in order to investigate organic cage formation. The deprotection of compound **17** will be carried out in the future, along with testing the coordination chemistry of the fully demethylated derivative in the hope of forming new polymetallic clusters.

Compound **18** has been reacted with hydrazine in order to introduce another heterocyclic group onto the methylene bridge position and deprotection studies are underway. Scale-up of the reaction using conditions described in this work are required in order to afford each product in a large enough scale to allow full characterisation. Optimisation of the deprotection step is required to be able to vary the number of methoxy groups removed at certain timeframes during the reaction. Once the fully demethylated compound is obtained, its coordination chemistry can be explored in line with conditions described in Chapter 2. This will provide insight into whether these additional groups at the methylene bridge positions have any effect on the cluster-forming capabilities of these new ligands.

3.6. Experimental

Synthesis of 5,11,17,23-tetra-*tert*-butyl-2,8,14,20-tetrakis(pentane-1,4-dione)-25,26,27,28-tetramethoxycalix[4]arene, **11**.

Compound **4** (0.997 g) in acetic acid (300 mL), water (120 mL) and conc. sulfuric acid (20 mL) was heated at reflux for 20 hours. The green solution was cooled to room temperature and diluted with water (100 mL) before extraction with CHCl₃ (3 x 100 mL). The combined organic phase was washed with water (3 x 100 mL), then dried over MgSO₄ before the solvent was removed under reduced pressure. The crude solid was purified by column chromatography (7:3 CHCl₃/EtOAc) to yield 0.508 g (48%) of **11**.

¹H NMR (300 MHz, CDCl₃): δ ppm 1.04 (s, 36 H) 2.20 (s, 12 H) 2.81 (t, *J*=6.6 Hz, 8 H) 2.95 (t, *J*=6.6 Hz, 8 H) 3.92 (s, 12 H) 5.85 (s, 4 H) 6.74 (s, 8 H). ¹³C NMR (75.5 MHz, CDCl₃): δ ppm 208.8, 207.4, 155.2, 145.9, 131.6, 125.0, 62.5, 51.6, 37.9, 36.7, 34.5, 31.7, 30.3. ESI-MS: 1119.6, [M+Na]⁺.

Crystal data for 11: C₆₈H₈₈O₁₂, *M* = 1008.68 g/mol, monoclinic, space group *P*2₁/*c* (no.14), *a* = 13.0121(5) Å, *b* = 19.7432(8) Å, *c* = 24.1190(10) Å, β = 91.058(2)°, *V* = 6195.1(4) Å³, *Z* = 4, *T* = 173(2) K, synchrotron radiation (λ = 0.7749 Å), 106792 reflections measured (2.906° ≤ 2θ ≤ 76.132°), 26097 unique (*R*_{int} = 0.0993, *R*_{sigma} = 0.0701) which were used in all calculations. The final *R*₁ was 0.0712 (*I* > 2σ(*I*)) and *wR*₂ was 0.2147 (all data).

Synthesis of partially demethylated tetrakis(pentane-1,4-dione) TBC[4], **12**.

This compound was recovered as a side product from the hydrolysis reaction of **4**.

¹H NMR (300 MHz, CDCl₃): δ ppm 0.83 (s, 18 H) 1.26 (s, 9 H) 1.26 (s, 9 H) 2.19 (s, 6 H) 2.20 (s, 6 H) 2.64 - 2.80 (m, 4 H) 2.86 - 2.99 (m, 12 H) 3.82 (s, 6 H) 4.22 (s, 3 H) 5.85 (s, 2 H) 5.86 (s, 2 H) 6.62 (d, *J*=2.20 Hz, 2 H) 6.66 (d, *J*=2.20 Hz, 2 H) 6.92 (s, 2 H) 7.02 (s, 2 H). ¹³C NMR (75.5 MHz, CDCl₃): δ ppm 207.8, 207.6, 206.9, 206.7, 155.1, 152.4, 150.3, 147.2, 145.6, 143.3, 133.9, 128.7, 128.4, 128.1, 126.9, 126.5, 123.3, 122.4, 63.7, 61.8, 51.1, 50.5, 37.6, 37.4, 36.3, 36.2, 34.5, 34.2, 33.9, 31.5, 31.4, 30.9, 29.8. ESI-MS: 1105.6, [M+Na]⁺.

Crystal data for 12: C₆₇H₈₆O₁₂, *M* = 1083.35 g/mol, monoclinic, space group *P*2₁/*c* (no.14), *a* = 10.6655(10) Å, *b* = 29.293(2) Å, *c* = 19.4637(18) Å, β = 93.048(3)°, *V* = 6072.4(9) Å³, *Z* = 4, *T* = 273(2) K, MoKα radiation (λ = 0.71073 Å), 55100 reflections measured (2.514° ≤ 2θ ≤ 41.856°), 6382 unique (*R*_{int} = 0.1257, *R*_{sigma} = 0.0852) which

were used in all calculations. The final R_1 was 0.0901 ($I > 2\sigma(I)$) and wR_2 was 0.2918 (all data).

Synthesis of 5,11,17,23-tetra-*tert*-butyl-2,8,14,20-tetrakis(2-methyl-1*H*-pyrrole)-25,26,27,28-tetramethoxycalix[4]arene, 13.

Compound **11** (0.402 g) and ammonium acetate (1.008 g) in acetic acid (50 mL) was heated at reflux for 4 hours. After this time the reaction mixture was poured into water (~50 mL). This was then extracted with CHCl_3 (3 x 40 mL). The organic phase was then washed once with 1M NaOH solution (40 mL) and twice with water (2 x 40 mL). The combined organic phase was dried over MgSO_4 before removal of the solvent under reduced pressure to yield 0.390 g of crude product. The crude solid was purified by column chromatography (9:1 $\text{CHCl}_3/\text{EtOAc}$) to yield 0.258 g (69%) of **13**.

^1H NMR (400 MHz, CDCl_3): δ ppm 1.01 (s, 36 H), 2.26 (s, 12 H), 3.87 (s, 12 H), 5.82 (d, $J=1.96$ Hz, 8 H), 6.02 (s, 4 H), 6.81 (s, 8 H), 7.68 (br. s, 4 H). ^{13}C NMR (100.6 MHz, CDCl_3): δ ppm 154.9, 145.0, 135.4, 132.1, 126.4, 123.9, 108.4, 105.5, 62.1, 37.2, 34.1, 31.3, 13.1. ESI-MS: 1043.6, $[\text{M}+\text{Na}]^+$.

Crystal data for 13: $\text{C}_{170}\text{H}_{92}\text{N}_4\text{O}_6$, $M = 1085.47$ g/mol, monoclinic, space group $P2_1/c$ (no.14), $a = 16.9164(12)$ Å, $b = 24.2445(17)$ Å, $c = 15.1980(11)$ Å, $\beta = 90.216(3)^\circ$, $V = 6233.1(8)$ Å³, $Z = 4$, $T = 100(2)$ K, synchrotron radiation ($\lambda = 0.7288$ Å), 166057 reflections measured ($2.68^\circ \leq 2\theta \leq 51.054^\circ$), 11603 unique ($R_{\text{int}} = 0.0756$, $R_{\text{sigma}} = 0.0368$) which were used in all calculations. The final R_1 was 0.0625 ($I > 2\sigma(I)$) and wR_2 was 0.1931 (all data).

Synthesis of 5,11,17,23-tetra-*tert*-butyl-2,8,14,20-tetrakis(1-phenyl-2-methyl-1*H*-pyrrole)-25,26,27,28-tetramethoxycalix[4]arene, 14.

Toluene (30 mL), aniline (0.25 mL) and *p*-TsOH· H_2O (0.0050 g) was added to compound **11** (0.200 g) which was then heated at reflux for 24 hours. The cloudy yellow mixture was cooled to room temperature before the solvent was removed under reduced pressure. The yellow solid was dissolved in CHCl_3 and filtered to yield 0.132 g (55%) of **14**.

^1H NMR (400 MHz, CDCl_3): δ ppm 0.89 (s, 18 H), 1.22 (s, 18 H), 1.98 (s, 12 H), 2.49 (s, 6 H), 3.35 (s, 6 H), 5.42 (s, 4 H), 5.93 (d, $J=3.30$ Hz, 4 H), 5.99 (d, $J=3.42$ Hz, 4 H), 6.42 (s, 4 H), 6.68 - 6.75 (m, 4 H), 6.75 (s, 4 H), 7.16 - 7.27 (m, 8 H), 7.32 - 7.37 (m, 4 H), 7.38 - 7.45 (m, 4 H). ^{13}C NMR (100.6 MHz, CDCl_3): δ ppm 153.7, 153.1, 144.2, 143.2,

139.5, 137.4, 134.0, 132.6, 129.1, 128.4, 127.1, 124.6, 122.3, 109.3, 105.6, 62.1, 58.5, 36.1, 34.2, 33.7, 31.7, 31.2, 13.1. ESI-MS: 1347.8, [M+Na]⁺.

Crystal data for 14: C₉₂H₁₀₀N₄O₄, *M* = 1325.75 g/mol, monoclinic, space group *P2/n* (no.13), *a* = 16.383(11) Å, *b* = 11.516(7) Å, *c* = 21.907(15) Å, *β* = 113.553(17)°, *V* = 3789(4) Å³, *Z* = 2, *T* = 100(2) K, synchrotron radiation (*λ* = 0.7288 Å), 3697 reflections measured (2.726° ≤ 2θ ≤ 42.846°), 3697 unique (*R*_{int} = 0.0000, *R*_{sigma} = 0.0454) which were used in all calculations. The final *R*₁ was 0.0772 (*I* > 2σ(*I*)) and *wR*₂ was 0.2095 (all data).

Synthesis of 5,11,17,23-tetra-*tert*-butyl-2,8,14,20-tetrakis(3-(2-methyl-1H-pyrrole)pyridine)-25,26,27,28-tetramethoxycalix[4]arene, 15.

Toluene (50 mL) was added to compound **11** (1.021 g), 3-aminopyridine (0.717 g) and *p*-TsOH·H₂O (0.099 g) which was then heated at reflux for 7 days. The yellow solution was cooled to room temperature before the solvent was removed under reduced pressure. The solid was then dissolved in CHCl₃ (50 mL) before it was washed with water (3 x 50 mL). The organic phase was dried over MgSO₄ before the solvent was removed under reduced pressure. The crude product was purified by column chromatography (9:1 DCM/MeOH) to yield 0.345 g (28%) of **15**.

¹H NMR (400 MHz, C₂D₂Cl₄): δ ppm: 0.85 (br. s, 18 H), 1.19 (s, 18 H), 1.98 (s, 12 H), 2.41 (br. s, 6 H), 3.40 (s, 6 H), 5.32 (br. s, 4 H), 5.94 (br. s, 4 H), 5.99 (br. s, 4 H), 6.38 (br. s, 4 H), 6.67 (br. s, 4 H), 6.98 (br. s, 2 H), 7.39 (br. s, 4 H), 7.57 (br. s, 2 H), 8.00 (br. s, 2 H), 8.44 (br. s, 2 H), 8.64 (br. s, 4 H)

NOTE: NMR solvent peak corresponds with broad singlet at 5.99 ppm and so the whole peak has not been integrated to exclude the solvent peak but the peak integrates to 4 H atoms.

¹H NMR (400 MHz, 75 °C, C₂D₂Cl₄)) δ ppm: 0.91 (s, 18 H), 1.24 (s, 18 H), 2.01 (s, 12 H), 2.53 (s, 6 H), 3.43 (s, 6 H), 5.38 (s, 4 H), 5.98 (d, *J*=3.30 Hz, 4 H), 6.04 (d, *J*=3.34 Hz, 4 H), 6.45 (s, 4 H), 6.76 (s, 4 H), 7.15 - 7.52 (m, 8 H), 8.28 (br. s, 4 H), 8.67 (d, *J*=1.00 Hz, 4 H)

NOTE: The multiplet at 7.15 – 7.52 ppm is actually two different proton environments but they have been integrated together due to overlapping signals – one broad singlet and a multiplet, each with an integral of 4 protons.

¹³C NMR (100.6 MHz, CDCl₃): δ ppm 153.7, 153.3, 151.2, 150.2, 148.8, 144.9, 143.7, 137.1, 136.0, 134.0, 132.1, 129.8, 125.7, 122.6, 110.1, 106.5, 62.2, 58.8, 36.2, 34.4, 33.8, 31.7, 31.2, 13.1. ESI-MS: 1351.8, [M+Na]⁺.

Crystal data for 15: C₈₈H₉₆N₈O₄, *M* = 1329.72 g/mol, monoclinic, space group *P2/c* (no.13), *a* = 16.153(9) Å, *b* = 11.480(6) Å, *c* = 21.506(12) Å, β = 109.163(9)°, *V* = 3767(4) Å³, *Z* = 2, *T* = 100(2) K, synchrotron radiation (λ = 0.7288 Å), 5337 reflections measured (2.738° ≤ 2θ ≤ 47.876°), 5337 unique (*R*_{int} = 0.0000, *R*_{sigma} = 0.0473) which were used in all calculations. The final *R*₁ was 0.1008 (*I* > 2σ(*I*)) and *wR*₂ was 0.2742 (all data).

Synthesis of 5,11,17,23-tetra-*tert*-butyl-2,8,14,20-tetrakis(*tert*-butyl(2-methyl-1H-pyrrole)carbamate)-25,26,27,28-tetramethoxycalix[4]arene, 16.

Compound **11** (0.200 g), Boc-hydrazide (0.199 g) and *p*-TsOH·H₂O (0.078 g) in toluene (100 mL) was heated at reflux for 48 hours. The yellow solution was cooled to room temperature and then the toluene was removed under reduced pressure. The crude solid was dissolved in CHCl₃ (50 mL) and then washed with water (3 x 50 mL). The organic phase was dried over MgSO₄ and then the solvent was removed under reduced pressure to yield 0.194 g of a yellow crude

Synthesis of 5,11,17,23-tetra-*tert*-butyl-2,8,14,20-tetrakis(2-methyl-1-(3,4,5-trimethoxyphenyl)-1H-pyrrole)-25,26,27,28-tetramethoxycalix[4]arene, 17.

Compound **11** (0.445 g), 3,4,5-trimethoxyaniline (0.594 g) and *p*-TsOH·H₂O (0.304 g) in toluene (100 mL) was heated at reflux for 24 hours. The yellow reaction mixture was cooled to room temperature and then the solvent was removed under reduced pressure. The solid was dissolved in CHCl₃ and then washed once with 1M HCl(aq) 100 mL and twice with water (2 x 100 mL). The organic phase was dried over MgSO₄ and then the solvent was removed under reduced pressure to yield a yellow crude. The crude was purified by gradient column chromatography (9:1 CHCl₃/EtOAc → 7:3 CHCl₃/EtOAc) to give an off-white solid which was then recrystallised from CHCl₃/MeOH to yield 0.378 g of **17**.

¹H NMR (400 MHz, CDCl₃) δ ppm: 0.95 (s, 18 H), 1.23 (s, 18 H), 2.04 (d, *J*=0.73 Hz, 12 H), 2.92 (s, 6 H), 3.28 (s, 6 H), 3.42 (s, 12 H), 3.84 (s, 12 H), 3.88 (s, 12 H), 5.66 (s, 4 H), 5.94 (dd, *J*=3.42, 0.73 Hz, 4 H), 6.05 (d, *J*=3.42 Hz, 4 H), 6.09 (d, *J*=1.96 Hz, 4 H), 6.42 (s, 4 H), 6.51 (d, *J*=1.96 Hz, 4 H), 7.00 (s, 4 H). ¹³C NMR (100.6 MHz, CDCl₃) δ ppm: 154.2, 152.9, 152.8, 152.6, 144.7, 143.4, 137.9, 134.4, 133.5, 133.3, 129.2, 124.3,

122.5, 110.3, 107.2, 106.2, 106.0, 62.1, 60.9, 59.4, 56.1, 55.7, 36.1, 34.4, 33.8, 31.8, 31.2, 13.4. ESI-MS: 1684.9, M and 1707.9, [M+Na]⁺.

Crystal data for 17: C₁₀₄H₁₂₄N₄O₁₆, *M* = 1687.07 g/mol, monoclinic, space group *P2₁/c* (no.14), *a* = 24.7454(13) Å, *b* = 21.2032(7) Å, *c* = 19.2492(5) Å, β = 98.714(4)°, *V* = 9983.1(7) Å³, *Z* = 4, *T* = 100.00(10) K, CuK α radiation (λ = 1.54178 Å), 64900 reflections measured (5.516° ≤ 2 θ ≤ 100.862°), 10457 unique (*R*_{int} = 0.1664, *R*_{sigma} = 0.1392) which were used in all calculations. The final *R*₁ was 0.0813 (*I* > 2 σ (*I*)) and *wR*₂ was 0.2232 (all data).

Synthesis of 5,11,17,23-tetra-*tert*-butyl-2,8,14,20-tetrakis(pent-2-ene-1,4-dione)-25,26,27,28-tetramethoxycalix[4]arene, 18.

Compound **4** (1.805 g) and *m*CPBA (2.403 g) in DCM (60 mL) was stirred at room temperature under N₂ for 18 hours. A white precipitate formed overnight which was removed by filtration and washed with DCM. The filtrate was washed once with Na₂SO₃ (aq) (50 mL), once with NaHCO₃ (aq) (50 mL) and once with water (50 mL). The organic phase was collected and dried over MgSO₄ before removal of the solvent under reduced pressure. The crude product was purified by column chromatography (3:2 EtOAc/PET) to yield 0.659 g (34%) of **18**.

¹H NMR (400 MHz, CDCl₃): δ ppm 1.05 (s, 36 H), 2.36 (s, 12 H), 3.86 (s, 12 H), 5.83 (s, 4 H), 6.31 (d, *J* = 11.98 Hz, 4 H), 6.52 (d, *J* = 11.98 Hz, 4 H), 6.82 (s, 8 H). ¹³C NMR (100.6 MHz, CDCl₃): δ ppm 201.5, 199.9, 154.9, 146.0, 139.0, 133.1, 130.8, 125.3, 62.1, 51.2, 34.2, 31.2, 29.6. ESI-MS: 1111.6 [M+Na]⁺.

Crystal data for 18: C₁₄₆H₁₇₅N₅O₂₄, *M* = 2383.90 g/mol, tetragonal, space group *P4bm* (no.100), *a* = 25.0238(7) Å, *b* = 25.0238(7) Å, *c* = 10.8155(6) Å, *V* = 6772.6(5) Å³, *Z* = 2, *T* = 120.01(10) K, MoK α radiation (λ = 0.71073 Å), 77706 reflections measured (5.87° ≤ 2 θ ≤ 59.748°), 8967 unique (*R*_{int} = 0.0857, *R*_{sigma} = 0.0479) which were used in all calculations. The final *R*₁ was 0.0626 (*I* > 2 σ (*I*)) and *wR*₂ was 0.1345 (all data).

Synthesis of 5,11,17,23-tetra-*tert*-butyl-2,8,14,20-tetrakis(3-methylpyridazine)-25,26,27,28-tetramethoxycalix[4]arene, 19.

Compound **18** (0.501 g) and hydrazine hydrate (1.0 mL) in acetic acid (120 mL) was heated at reflux overnight. After this time, water (100 mL) was added to the brown solution and this was then extracted with CHCl₃ (3 x 100 mL). The combined organic

phase was washed with water (3 x 100 mL) before it was dried over MgSO₄. The solvent was removed under reduced pressure and the crude was purified by column chromatography (9:1 CHCl₃/MeOH) to yield 0.329 g (67%) of **19**.

¹H NMR (300 MHz, CD₂Cl₂) δ ppm 0.99 (s, 36 H) 2.69 (s, 12 H) 3.85 (s, 12 H) 6.54 (s, 4 H) 6.78 (s, 8 H) 7.29 (d, *J*=8.80 Hz, 4 H) 7.53 (d, *J*=8.44 Hz, 4 H). ¹³C NMR (75.5 MHz, CDCl₃): δ ppm 162.2, 157.7, 155.2, 145.1, 134.6, 127.0, 126.4, 124.7, 62.1, 34.1, 31.3, 22.0. ESI-MS: 1095.6, [M+Na]⁺.

Crystal data for 19: C₆₈H₈₀N₈O₄, *M* = 1073.40 g/mol, orthorhombic, space group *Pnma* (no.62), *a* = 10.9504(4) Å, *b* = 21.9377(8) Å, *c* = 25.0154(9) Å, *V* = 6009.4(4) Å³, *Z* = 4, *T* = 273.15 K, synchrotron radiation (*λ* = 0.7288 Å), 68008 reflections measured (2.47° ≤ 2θ ≤ 55.014°), 7098 unique (*R*_{int} = 0.0964, *R*_{sigma} = 0.0405) which were used in all calculations. The final *R*₁ was 0.0854 (*I* > 2σ(*I*)) and *wR*₂ was 0.2769 (all data).

Deprotection of compound 19.

Compound **19** (0.162 g) was dissolved in dry DCM (40 mL) under N₂ and this solution was cooled to -78 °C. BBr₃ (0.55 mL) was added with stirring and the reaction mixture was stirred at -78 °C for 1 hour before it was stirred at room temperature for 24 hours. The reaction mixture was quenched with water (~100 mL). The organic phase was then separated and washed with water (3 x 50 mL) before it was dried over MgSO₄ and then evaporated to dryness. The crude solid was then purified by gradient column chromatography (100% CHCl₃ → 9:1 CHCl₃/MeOH (1% increments) → 1:1 CHCl₃/MeOH (10% increments)).

Spot with *R*_f (0.43) in 9:1 CHCl₃/MeOH corresponds to 5,11,17,23-tetra-*tert*-butyl-2,8,14,20-tetrakis(3-methylpyridazine)-25,26,27-trimethoxy-28-hydroxycalix[4]arene, **21**.

Spot with *R*_f (0.30) in 9:1 CHCl₃/MeOH corresponds to 5,11,17,23-tetra-*tert*-butyl-2,8,14,20-tetrakis(3-methylpyridazine)-25,26-dimethoxy-27,28-dihydroxycalix[4]arene, **22a** or 5,11,17,23-tetra-*tert*-butyl-2,8,14,20-tetrakis(3-methylpyridazine)-25,27-dimethoxy-26,28-dihydroxycalix[4]arene, **22b**.

Spot with R_f (0.24) in 9:1 $\text{CHCl}_3/\text{MeOH}$ corresponds to 5,11,17,23-tetra-*tert*-butyl-2,8,14,20-tetrakis(3-methylpyridazine)-25-methoxy-26,27,28-trihydroxycalix[4]arene, **23**.

3.7. References

1. J. Clayden, N. Greeves, S. Warren and P. Wothers, *Organic chemistry*, OUP, 2001.
2. F. W. Lichtenthaler, A. Brust and E. Cuny, *Green Chem.*, 2001, **3**, 201-209.
3. P. W. Jennings and S. B. Gingerich, *J. Org. Chem.*, 1983, **48**, 2606-2608.
4. M. A. Baig, D. V. Banthorpe, G. Carr and D. Whittaker, *J. Chem. Soc., Perkin Trans. 2*, 1989, 1981-1986.
5. W. Ried and K. Wesselborg, *Naturwissenschaften*, 1959, **46**, 142-143.
6. M. Yuguchi, M. Tokuda and K. Orito, *J. Org. Chem.*, 2004, **69**, 908-914.
7. C. M. Li, E. Lobkovsky and J. A. Porco, *J. Am. Chem. Soc.*, 2000, **122**, 10484-10485.
8. S. Varis, M. Ak, C. Tanyeli, I. M. Akhmedov and L. Toppare, *Solid State Sci.*, 2006, **8**, 1477-1483.
9. M. Albrecht and Y. Song, *Synthesis*, 2006, 3037-3042.
10. A. Lutzen and M. Hapke, *Eur. J. Org. Chem.*, 2002, 2292-2297.
11. D. Murugesan, A. Mital, M. Kaiser, D. M. Shackleford, J. Morizzi, K. Katneni, M. Campbell, A. Hudson, S. A. Charman, C. Yeates and I. H. Gilbert, *J. Med. Chem.*, 2013, **56**, 2975-2990.
12. N. A. Caballero, F. J. Melendez, C. Munoz-Cara and A. Nino, *Biophys. Chem.*, 2006, **124**, 155-160.
13. L. H. Chen, J. Z. Dou, Q. L. Ma, N. Li, R. C. Wu, H. Y. Bian, D. J. Yelle, T. Vuorinen, S. Y. Fu, X. J. Pan and J. Y. Zhu, *Sci. Adv.*, 2017, **3**.
14. A. M. Szpilman, D. M. Cereghetti, J. M. Manthorpe, N. R. Wurtz and E. M. Carreira, *Chem. Eur. J.*, 2009, **15**, 7117-7128.
15. B. K. Banik, S. Samajdar and I. Banik, *J. Org. Chem.*, 2004, **69**, 213-216.
16. B. K. Banik, I. Banik, M. Renteria and S. K. Dasgupta, *Tetrahedron Lett.*, 2005, **46**, 2643-2645.
17. X. X. Zhang, G. D. Weng, Y. D. Zhang and P. C. Li, *Tetrahedron*, 2015, **71**, 2595-2602.
18. M. J. Hardman, A. M. Thomas, L. T. Carroll, L. C. Williams, S. Parkin and J. L. Fantini, *Tetrahedron*, 2011, **67**, 7027-7034.

Chapter 4

Metal-Organic Cage Chemistry

4.1 Introduction

The work discussed in Chapter 4 is an investigation into the possibility of using the compounds synthesised in Chapter 3 to form metal-organic cages. The work carried out in this Chapter was undertaken in collaboration with the Lusby group at The University of Edinburgh and focusses on the use of compound **15** as the pyridine moieties on the calixarene framework make it an ideal candidate for such studies. Prior to the discussion of the results, the use of pyridine groups in cage formation will be described in relation to results in the literature, as well as some results in which pyridinecalix[4]arenes have been utilised in metal-organic cage formation.

4.2 Ligand Design for Cage Assembly

The self-assembly of large supramolecular cages using pyridine moieties has been widely reported by Stang and Fujita through the reaction of the ligands shown in Figure 4.1 with metal salts.¹⁻⁶

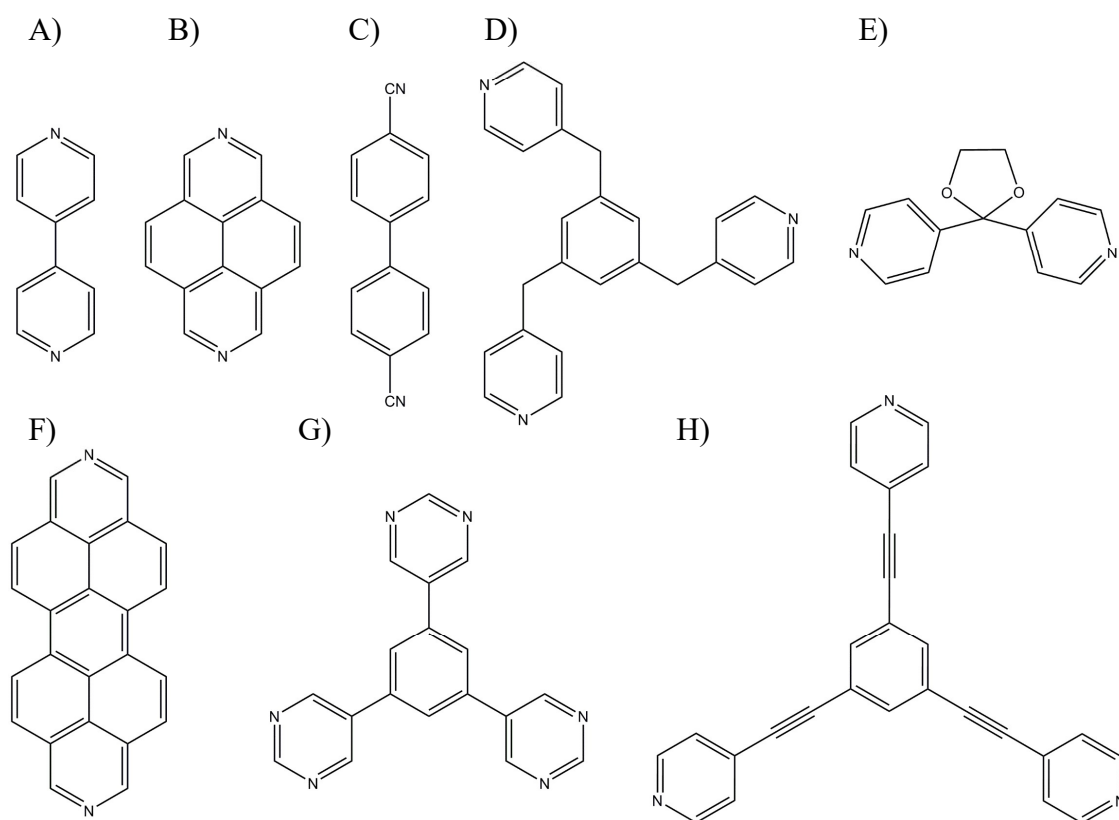


Figure 4.1. Examples of ligands utilised by the Stang and Fujita groups for cage formation. A) 4,4'-bipyridine (L1),¹⁻³ B) 2,7-diazapyrene (L2),² C) 1,4-dicyanobenzene (L3),² D) 1,3,5-tris(4-pyridylmethyl)benzene (L4),⁴ E) 4,4'-bispyridylacetal (L5),⁶ F) 2,9-diazabenzoc[*cd,lm*]perylene (L6),² G) 1,3,5-tris(3,5-pyrimidyl)benzene (L7)⁵ and H) 1,3,5-tris(4-pyridylethynyl)benzene (L8).⁶

Both research groups have investigated the formation of tetranuclear macrocyclic squares prepared from 4,4'-bipyridine (L1, 4,4'-bpy) as well as various other ligands in the presence of palladium or platinum salts.¹⁻⁶ An example of this is shown in Figure 4.2 in which 4,4'-bpy (L1) has been reacted with [Pd(dppp)][OTf]₂ where dppp is 1,3-bis(diphenylphosphino)propane and OTf is a triflate anion.² Inspection of Figure 4.2 shows that the four Pd^{II} centres at the corners of the square are held together by the 4,4'-bpy linkers which make up the edges.

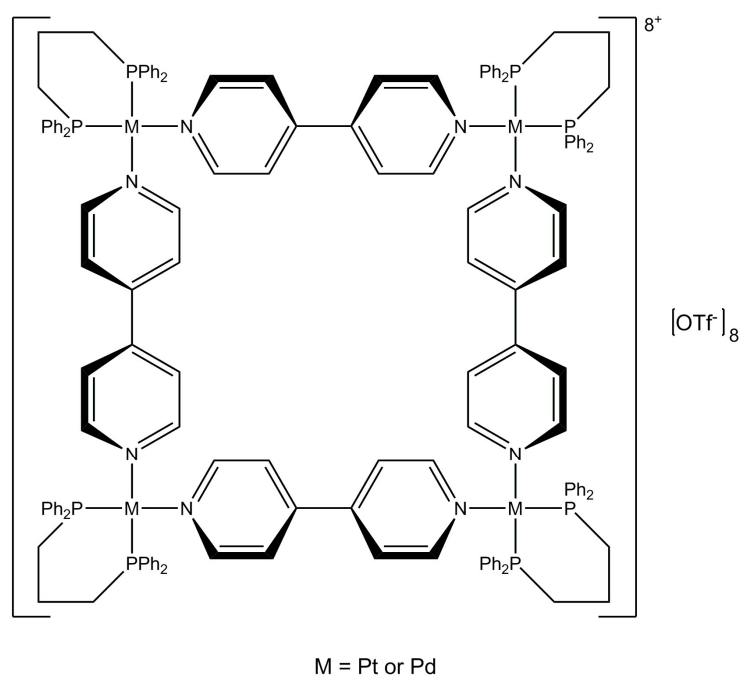


Figure 4.2. Representation of the tetranuclear macrocyclic squares formed by Fujita and Stang.²

The 4,4'-bpy units in the square shown in Figure 4.2 can be replaced with other ligands such as those shown in Figure 4.1. L1, L2, L3 and L6 in Figure 4.1A, B, C and F have been utilised by the groups in the self-assembly of Pt^{II} and Pd^{II} macrocyclic squares as mentioned above, in which the ditopic ligands form the edges of the square with the metal site positioned in the corner, and from these a series of macrocyclic squares were prepared using both Pd^{II} and Pt^{II} salts.²

The self-assembly of a nanoscale cuboctahedra was reported by Stang *et al.* in which they reacted L5 and L8 in Figure 4.1E and H with Pt salts.⁶ The Fujita group formed a hexahedral coordination capsule through the reaction of L7 in Figure 4.1G with a *cis*-protected Pd salt.⁵ They also formed a cage-like complex from L4 in Figure 4.1D in which two ligands bind three separate Pd^{II} ions through each pyridine ring moiety.⁴

The Lusby group at The University of Edinburgh also investigates the self-assembly of molecular cages.⁷⁻¹² In addition to studying the host-guest chemistry of these cages, they also investigate their use for applications such as catalysis and magnetic materials. Examples of ligands used within the group are those containing pyridine moieties and two of these examples will be discussed.

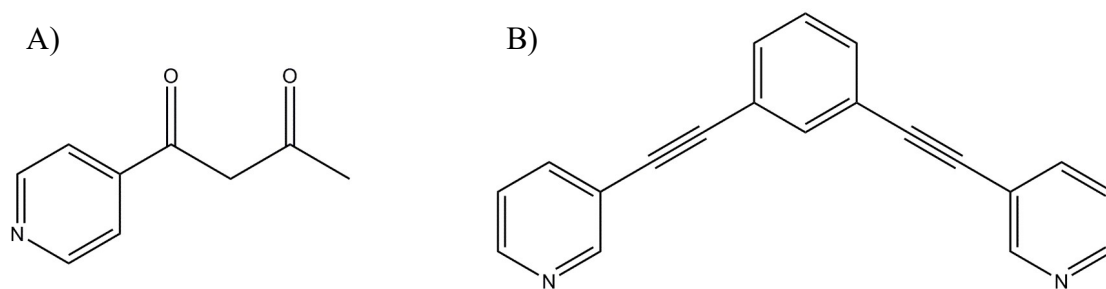


Figure 4.3. Examples of ligands used by the Lusby group in their cage synthesis reactions. A) 1-(4-pyridyl)-butane-1,3-dione (L9)^{7-9, 11} and B) 1,3-bis(3-pyridylethynyl)benzene (L10).^{10, 12}

The reaction of L9 (Figure 4.3A) with a metal results in the formation of a tritopic metalloligand $[M^{III}(L9)_3]$ which features an octahedral geometry metal core that is coordinated by three ligands through the carbonyl groups. This leaves the pyridyl groups available for further metal coordination, which the Lusby group has explored through reaction with other metal salts. Using the tritopic metalloligand they have been able to isolate trigonal bipyramidal cages⁹ and coordination cubes in which the tritopic metalloligands occupy the vertices^{7, 8, 11} as shown in Figure 4.4.

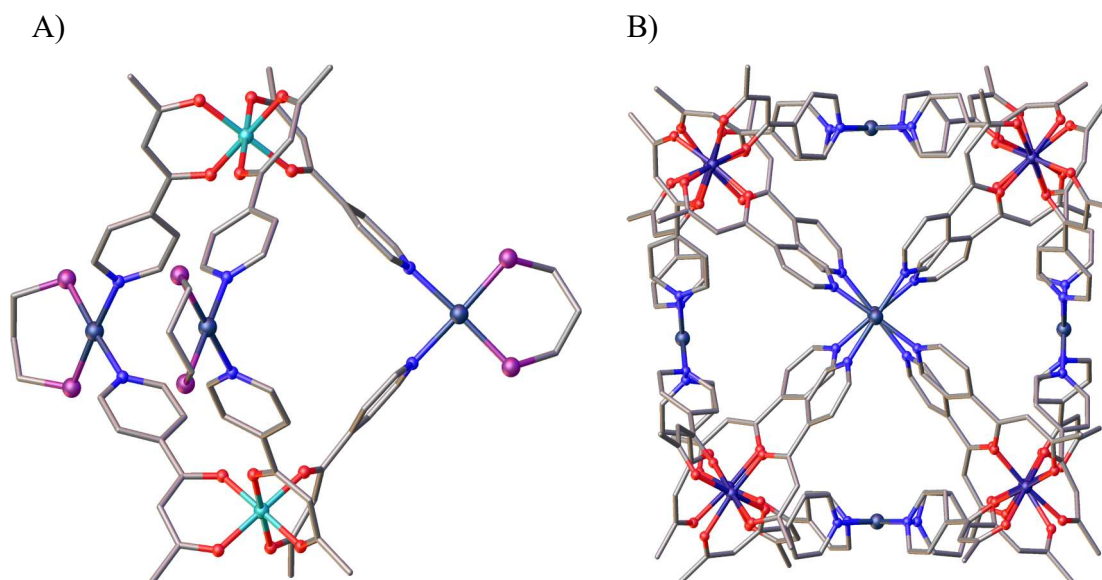


Figure 4.4. Single crystal X-ray structures of A) trigonal bipyramidal cage⁹ and B) coordination cubes¹¹ reported by the Lusby group. Colour code: C – grey; O – red; N – blue; Pd – dark blue; P – light purple; Al – light blue; Fe – dark purple. Solvent of crystallisation, H atoms, counterions and Ph groups are omitted for clarity.

Another cage structure the group has investigated was first reported by Hooley *et al.* in which they use the rigid ditopic ligand (L10, Figure 4.3B) in which two 3-pyridyl groups are connected to a benzene ring through acetylene bonds to form a cage molecule.¹³ From this they have synthesised a Pd₂(L10)₄ cage in which one pyridine group of each ligand is coordinated to one Pd^{II} cation and the other pyridine group of the ligand is coordinated to the other, resulting in the formation of a capsule (Figure 4.5). The Lusby group studied the host-guest chemistry of this cage molecule and found that non-interacting anions in apolar solvents result in maximising favourable interactions between the positively charged cage and charge-neutral guests, leading to increased binding strength.¹⁰

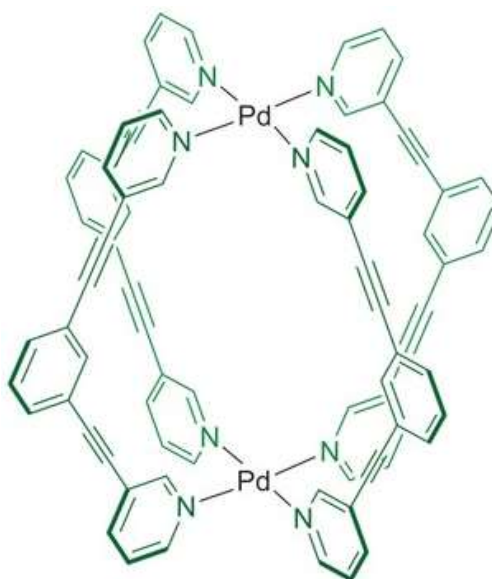


Figure 4.5. Schematic representation of Pd₂(L10)₄ cage reported by the Lusby group.¹⁰ Adapted with permission from D. P. August, G. S. Nichol and P. J. Lusby, *Angew. Chem. Int. Ed.*, 2016, **55**, 15022-15026. Copyright 2016 John Wiley and Sons.

The use of pyridyl calix[4]arenes in the formation of cages has been significantly less well explored. However, in 2001 Zhong *et al.* reported the self-assembly of a molecular capsule with the use of pyridylcalixarenes in which the C[4] is substituted at the upper-rim with pyridine groups.¹⁴ Through this work they managed to isolate molecular cages by taking advantage of pyridyl-Pd^{II} interactions. From their work they found that it is essential to first form a rigid calixarene that will prevent intramolecular binding as this results in the formation of chelates rather than a cage structure.

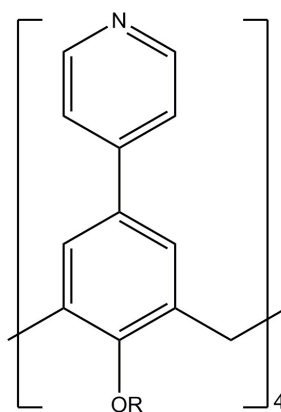


Figure 4.6. Schematic representation of the pyridinecalix[4]arene used in the cage self-assembly reactions by Zhong *et al.*¹⁴

The research group found that a pyridinecalix[4]arene with ethoxyethoxy groups at the lower-rim does not form a cage. They postulated that this is due to the fact that, although the lower-rim groups prevent rotation through the annulus of the C[4], there is still some mobility of the C[4] due to it being in a pinched-cone conformation and there is interconversion between two C_{2v} conformers. They also found that the 1,3-alternate pyridinecalix[4]arene conformer intramolecularly binds a $\text{cis-Pd}^{\text{II}}$ or $\text{trans-Pd}^{\text{II}}$ complex to form chelates. They proposed that intramolecular binding is promoted because the pyridine moieties are proximal. They went on to investigate the introduction of diethyl ether linkages at the lower-rim position as a way of rigidifying the cone conformation with a view to preventing intramolecular binding. They synthesised the pyridinecalix[4]arene bis-crown in which the diethyl ether moieties tether two of the lower-rim oxygen atoms, with the same occurring at the other positions. The introduction of these groups leads to a very rigid cone conformation which prevents the pyridyl groups from being close to one another, and hence there is no intramolecular binding with a metal. Therefore the pyridinecalix[4]arene bis-crown intermolecularly binds with four $\text{cis-Pd}^{\text{II}}$ complexes resulting in the formation of a self-assembled dimeric molecular capsule shown in Figure 4.7.¹⁴ This provides further evidence that in order to form cage structures the ligand itself must be rigid to prevent the possibility of intramolecular binding.

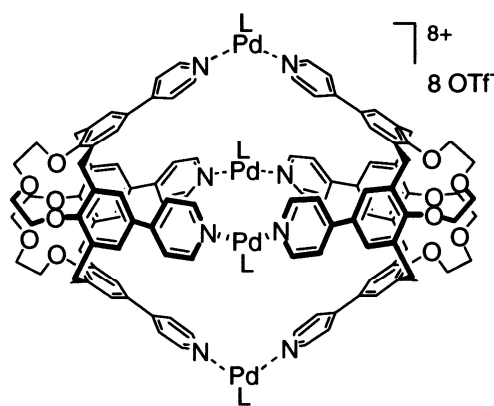


Figure 4.7. Schematic representation of the capsule formed by Zhong *et al.* using a pyridinecalix[4]arene locked in a cone with diethyl ether tethers at the lower-rim.¹⁴ Adapted with permission from Z. L. Zhong, A. Ikeda, M. Ayabe, S. Shinkai, S. Sakamoto and K. Yamaguchi, *J. Org. Chem.*, 2001, **66**, 1002-1008. Copyright 2001 American Chemical Society.

Another example of the self-assembly of macrocycles containing pyridine moieties are the resorcinarenes reported by Dalcanale *et al.*¹⁵ Resorcinarenes are formed from the condensation reaction of resorcinol (1,3-dihydroxybenzene) and an aldehyde. The R groups on the resorcinarene are dependent on the aldehyde used in the condensation reaction (Figure 4.8A). The particular resorcinarene that Dalcanale and co-workers synthesised was one in which the upper-rim has been substituted with pyridine groups shown in Figure 4.8B.

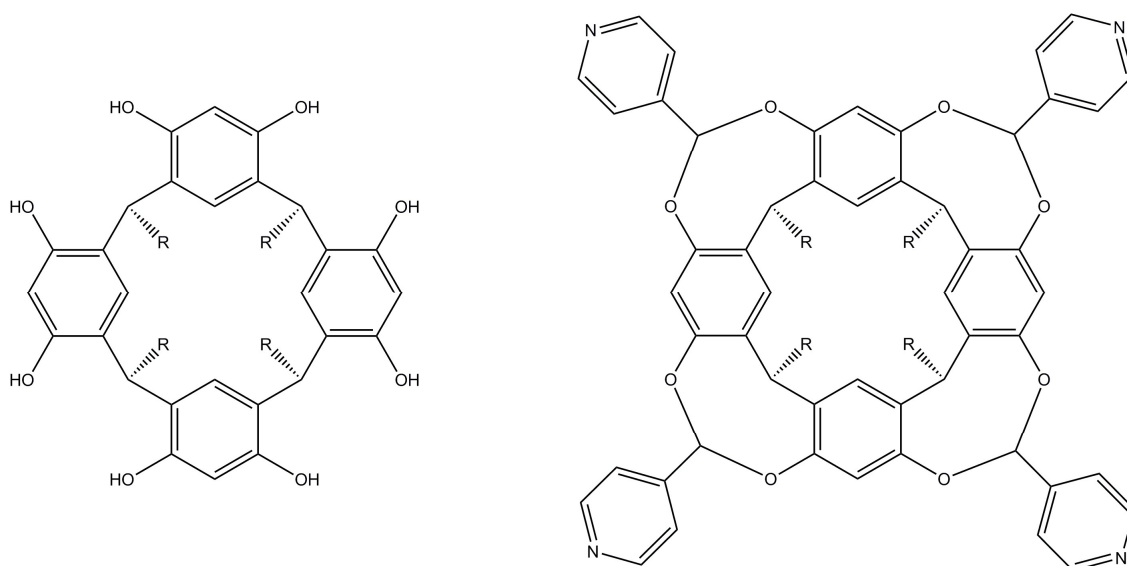


Figure 4.8. Schematic representation of a A) simple resorcinarene and B) pyridyl-substituted resorcinarene.¹⁵

The self-assembled coordination cage produced using the pyridyl-substituted resorcinarene is similar to that of the capsule reported by Zhong and co-workers in that two of the resorcinarenes are connected through four square-planar Pd^{II} or Pt^{II} ions (Figure 4.9). The rigidity of the resorcinarene is also significant here as it allows the ligand to be correctly preorganised for cage self-assembly.

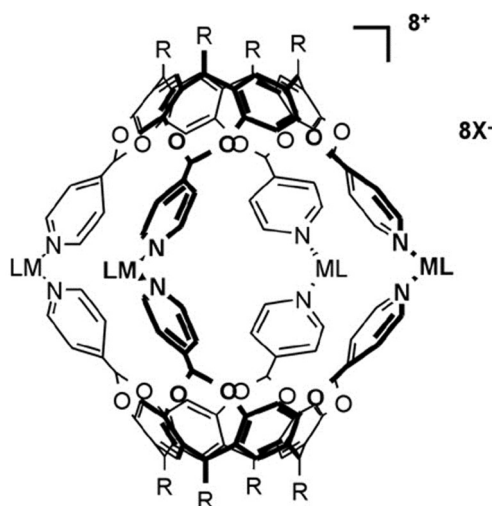


Figure 4.9. Schematic representation of the cage formed by Dalcanale *et al.* using the pyridyl-substituted resorcinarene.¹⁵ Adapted with permission from L. Pirondini, F. Bertolini, B. Cantadori, F. Ugozzoli, C. Massera and E. Dalcanale, *Proc. Natl. Acad. Sci.*, 2002, **99**, 4911-4915. Copyright 2002 National Academy of Sciences, U.S.A.

Therefore, from the literature, it suggests that in order to form a metal-organic cage the ligand needs to be rigid enough to prevent intramolecular binding. The next section of this work involves the reaction of **15** with various metal salts, the aim of which was the formation of a self-assembled metal-organic cage structure.

4.3 Cage Formation using Compound **15**

Before the cage formation investigation was begun a standard ^1H NMR experiment of the ligand in a 6:5 ratio of $\text{CD}_2\text{Cl}_2/\text{CD}_3\text{CN}$ was run. This solvent mixture was chosen as it ensured complete dissolution of reactants due to the solubility of **15** in dichloromethane, and acetonitrile is added to the mixture as it is a coordinating solvent that binds to the vacant sites of the metal salts. This therefore helps to stabilise the intermediate before the ligand binds to the metal centre, and it also helps with self-corrections as these coordination structures are labile in acetonitrile. The ^1H NMR spectrum of **15** in the $\text{CD}_2\text{Cl}_2/\text{CD}_3\text{CN}$ mixture is shown in Figure 4.10.

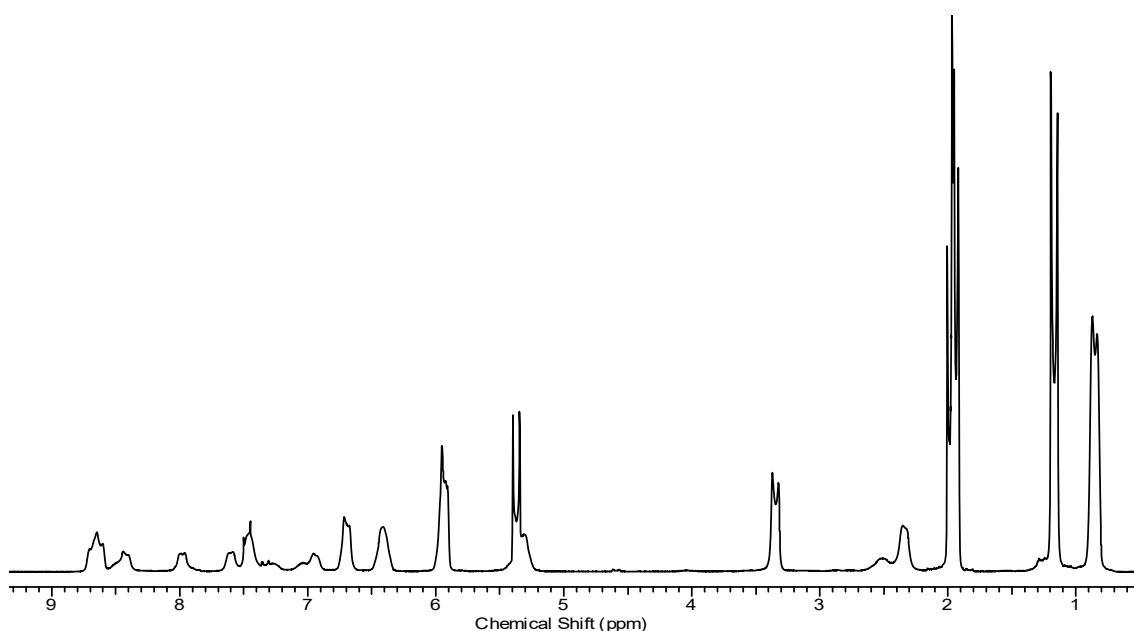


Figure 4.10. ^1H NMR spectrum of **15** in a 6:5 v/v ratio of $\text{CD}_2\text{Cl}_2/\text{CD}_3\text{CN}$.

Diffusion Ordered Spectroscopy (DOSY) is a NMR technique which can be used to determine how many species exist in solution and from the NMR spectrum it is possible to calculate the hydrodynamic radius using the Stokes-Einstein equation shown in equation (1).

$$D = \frac{kT}{6\pi\eta r} \quad (1)$$

In equation (1) D is the diffusion coefficient, k the Boltzmann constant, η the viscosity of the solvent and r the hydrodynamic radius. From this equation and a DOSY NMR experiment it is possible to calculate the radius to give an indication of the size of the species in solution. It is expected that there would be a large difference in the radius of the free ligand compared to that of a potential cage structure.

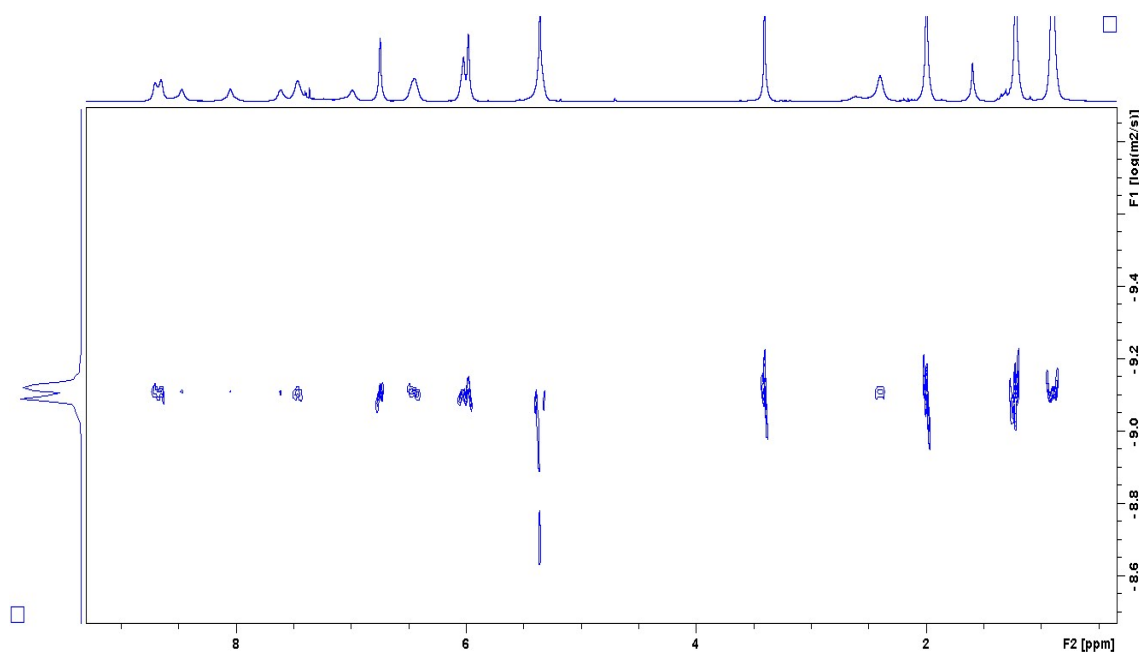


Figure 4.11. DOSY NMR spectrum of **15** in CD_2Cl_2 showing only one species in solution.

Inspection of the DOSY NMR spectrum in Figure 4.11 shows that there is only one species in solution corresponding to the free ligand. Using the diffusion coefficient from the spectrum, a value of 6.6 \AA was obtained for the radius of the free ligand itself in CD_2Cl_2 . This value was then used to compare against the values obtained from the cage self-assembly reactions to determine whether or not a cage might have formed as a larger radius would be expected in the case of cage formation.

In order to form a cage structure, the ligand was reacted with varying stoichiometries of metal salts. The ^1H NMR spectrum was collected for each ratio to investigate how the spectrum changes with the addition of metal salts. Interestingly, the

most promising ratios of metals gave a ^1H NMR spectrum that had sharp peaks unlike the free ligand itself, suggesting that the metal is preventing rotation around the bond from the methylene bridge and the pyrrole moiety as discussed in Chapter 3.

4.3.1 Reaction of **15** with $[\text{Pd}(\text{CH}_3\text{CN})_4][\text{BF}_4]_2$

Reaction of **15** with $[\text{Pd}(\text{CH}_3\text{CN})_4][\text{BF}_4]_2$ in a 1:1, 1:2 and 1:4 ratio was carried out as small-scale NMR reactions. A solution of $[\text{Pd}(\text{CH}_3\text{CN})_4][\text{BF}_4]_2$ in CD_3CN was added to a solution of compound **15** in CD_2Cl_2 and the NMR tube was shaken vigorously before the ^1H NMR spectrum was collected. Figure 4.12 displays the spectra collected for each ratio as a stack to show how each changes with varying stoichiometries of salt.

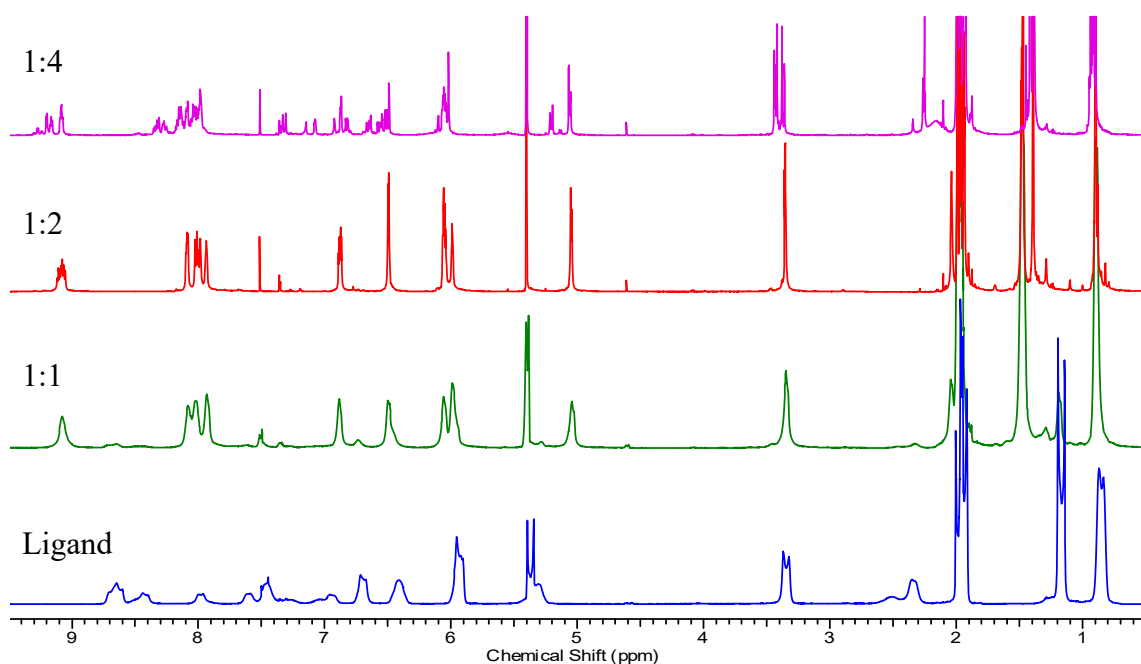


Figure 4.12. Stacked NMR spectra of varying stoichiometries of $[\text{Pd}(\text{CH}_3\text{CN})_4][\text{BF}_4]_2$ showing changes in signals observed.

Inspection of Figure 4.12 shows the significant changes in the ^1H NMR spectrum as varying ratios of Pd^{II} salt are added. The spectrum of the ligand is rather broad, but this can be used as a way of determining whether or not a cage has formed as there is significant sharpening of the resonances upon addition of the metal; this suggests that there has been some form of coordination of the ligand. The ^1H NMR spectrum of the 1:1 ratio remains broad and this suggests that there may be some residual ligand present

in solution. The ^1H NMR spectrum of the 1:2 ratio looked most promising, as this contains the sharpest signals, and suggests that a cage has formed from this ratio of ligand to metal. The ^1H NMR spectrum of the 1:4 reaction appears to be sharp, however there appear to be many more resonances which suggests that another species is being formed with a higher stoichiometry of metal.

Although the results from the small-scale NMR reactions appear to be promising no crystals have been isolated from these reaction mixtures and so it is only possible to postulate that a cage might have formed using a 1:2 ratio of ligand to Pd^{II} salt. DOSY NMR experiments of the solid collected from the 1:2 reaction were carried out in CD_3CN and the hydrodynamic radius was calculated to be 9.3 \AA which is bigger than the free ligand itself (6.6 \AA) giving a good indication that a new species has been formed. The DOSY NMR spectrum (Figure 4.13) also shows that there is only species in solution, which again is a promising result. However, from these results it is not possible to conclusively say if a cage molecule has formed from these self-assembly reactions.

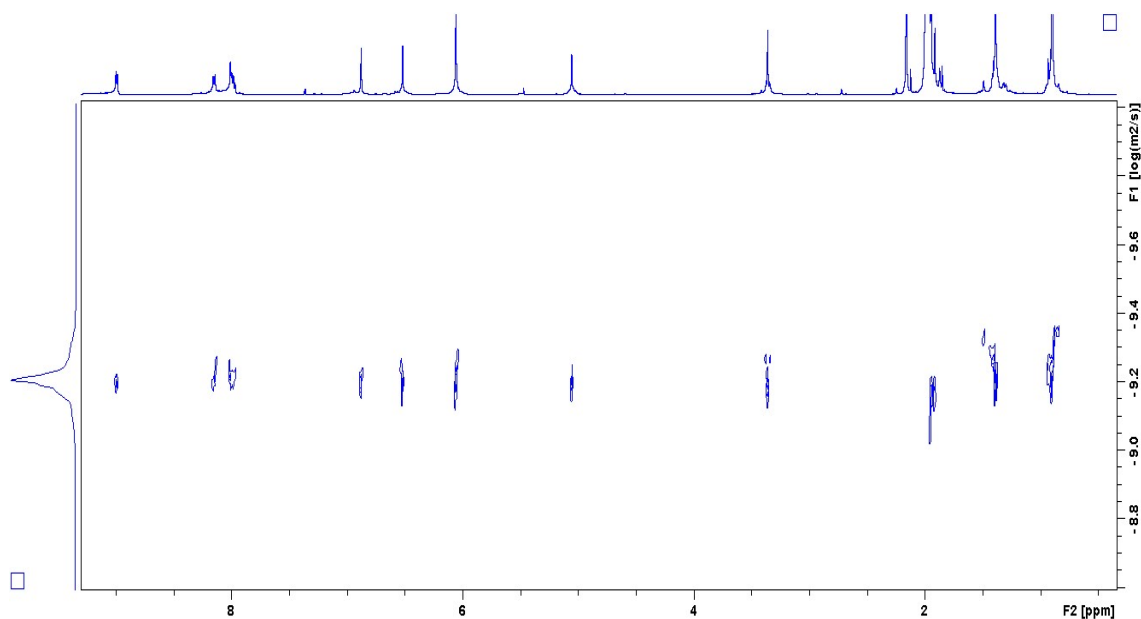


Figure 4.13. DOSY NMR spectrum of **15** with $[\text{Pd}(\text{CH}_3\text{CN})_4][\text{BF}_4]_2$ in a 1:2 ratio showing formation of one species in solution.

4.3.2 Reaction of **15** with ZnBr_2

The conditions as previously described were used for the reactions of **15** with ZnBr_2 as small-scale NMR reactions. Again **15** was dissolved in CD_2Cl_2 and to this a solution of

ZnBr₂ in CD₃CN was added. The NMR tube was vigorously shaken before the ¹H NMR spectrum was collected. The stacked NMR spectra shown in Figure 4.14 shows how each spectrum changes with varying stoichiometries of ZnBr₂.

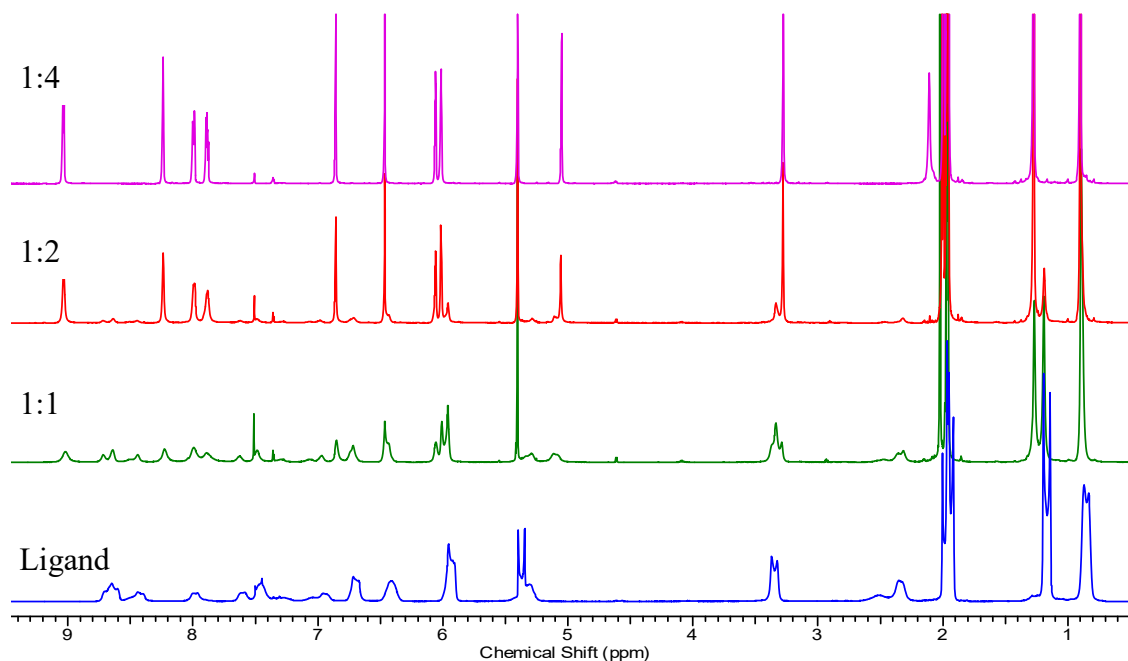


Figure 4.14. Stacked NMR spectra showing the change in ¹H NMR spectrum as the stoichiometries of ZnBr₂ is changed.

Inspection of Figure 4.14 suggests that the ligand to metal ratio that looks the most promising is the 1:4 ratio as the 1:1 NMR spectrum is still quite broad suggesting residual ligand left over in solution. The ¹H NMR spectrum for the 1:2 ratio also suggests that not all of the ligand has been used in coordination, as it appears that there is still some free ligand in solution due to residual ligand peaks in the spectrum. The spectrum of the 1:4 ratio has sharp and distinct peaks.

The DOSY NMR spectrum of the solid collected from the 1:4 reaction was carried out in CD₂Cl₂ (Figure 4.15). The spectrum shows that there is one species in solution and the hydrodynamic radius was calculated to be 9.6 Å. The value obtained is bigger than the value for the free ligand itself (6.6 Å) giving a good indication that something new has formed from the reaction.

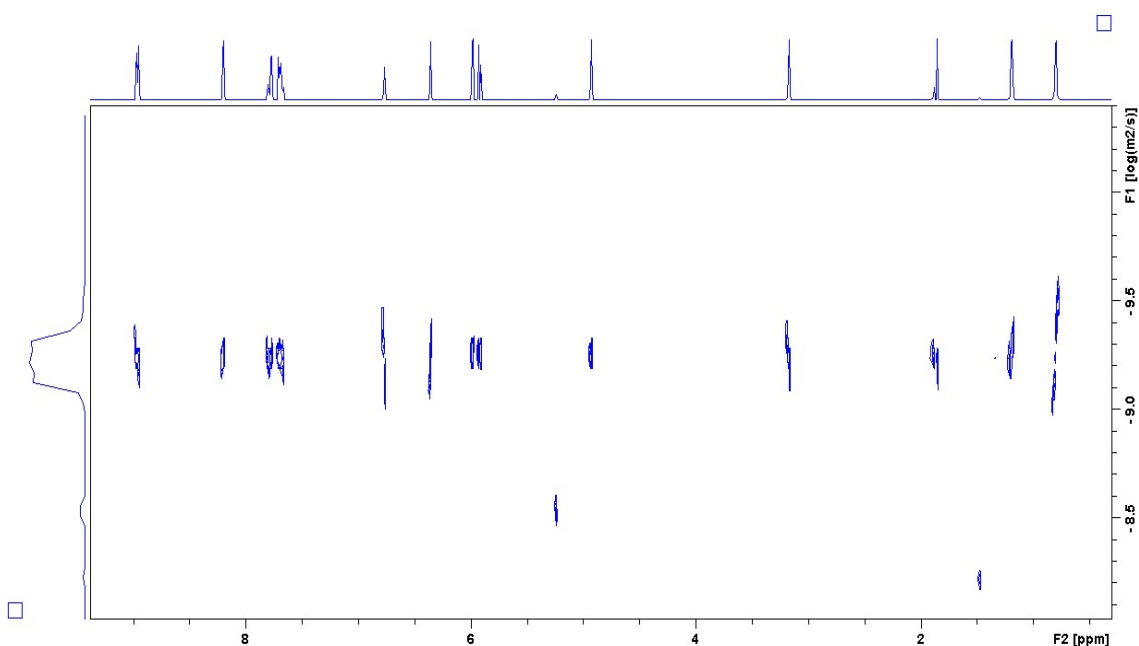


Figure 4.15. DOSY NMR spectrum of **15** with ZnBr_2 in a 1:4 ratio showing formation of one species in solution.

Vapour diffusions of the NMR reactions were set up and suitable single crystals for X-ray diffraction studies grew upon diffusion of Et_2O into the 1:4 reaction mixture. The crystals were found to be in a monoclinic cell and structure solution was carried out in the space group $P2_1/c$. The ASU was found to contain a molecule of **15** which is coordinated to two ZnBr_2 groups and it also contained several disordered Et_2O solvent molecules which were removed by means of a solvent mask. Inspection of the crystal structure shown in Figure 4.16 shows that there is intramolecular binding of two ZnBr_2 units, forming the chelate with formula $[\text{Zn}_2(\mathbf{15})_2\text{Br}_2]$, **24**. The hydrodynamic radius calculated for compound **24** appears to correlate with the obtained crystal structure, as the radius is larger than the radius of the free ligand, however it would be expected to be much larger upon formation of a cage.

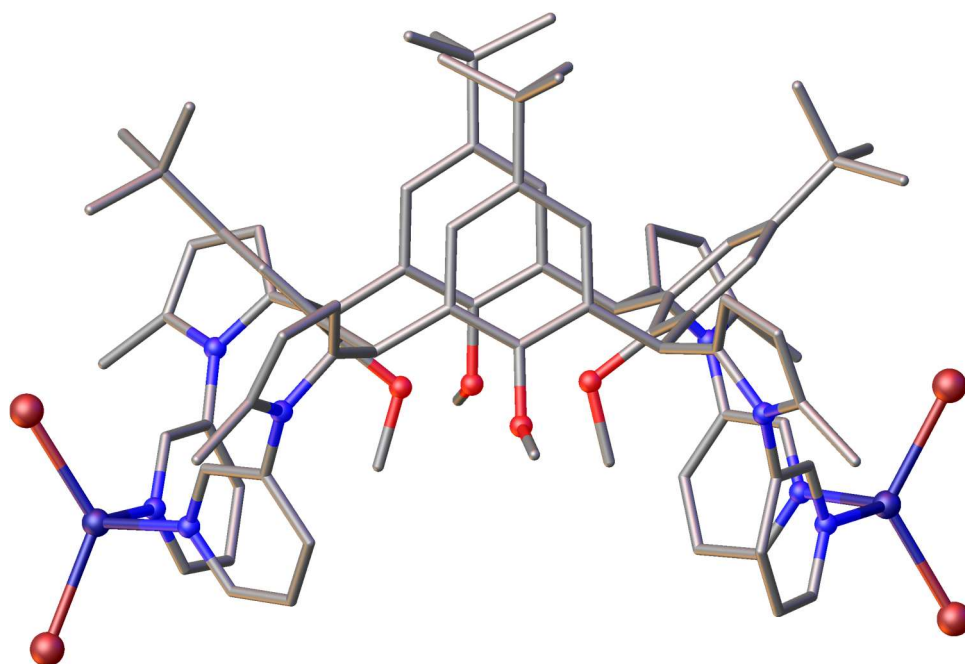


Figure 4.16. Single crystal X-ray structure of **24** showing binding of two ZnBr_2 units in ball and stick representation. Colour code: C – grey; O – red; N – blue; Zn – purple; Br – dark red. H atoms are omitted for clarity.

Figure 4.16 clearly shows that a cage structure has not formed as desired due to the chelation of two pyridine groups to one ZnBr_2 unit. This suggests that there is some flexibility of the ligand which enables intramolecular binding suggesting that **15** is not rigid enough to prevent the pyridine rings coming close to one another leading to chelation. The crystal structure also shows the tetrahedral geometry of the Zn^{II} cations.

4.3.3 Reaction of **15** with CoBr_2

The same conditions were used for the reaction of **15** in CD_2Cl_2 with varying ratios of CoBr_2 in CD_3CN , affording bright blue solutions. As previously described these reactions were carried out on a NMR scale and the NMR tube was shaken vigorously before the ^1H NMR spectrum was collected. Co^{II} is paramagnetic so it was difficult to interpret these spectra. However, blue crystals grew upon vapour diffusion of Et_2O into the mother liquor and suitable single crystals from the 1:2 reaction were analysed by X-ray diffraction. The crystals were found to be in a monoclinic cell and structure solution was carried out in the space group $P2_1/c$ giving rise to the complex with formula $[\text{Co}_2(\mathbf{15})_2\text{Br}_2]$, **25**. The ASU was found to contain a molecule of **15** which is coordinated

to two CoBr₂ groups (Figure 4.17) and again it contained disordered Et₂O molecules which were removed by applying a solvent mask.

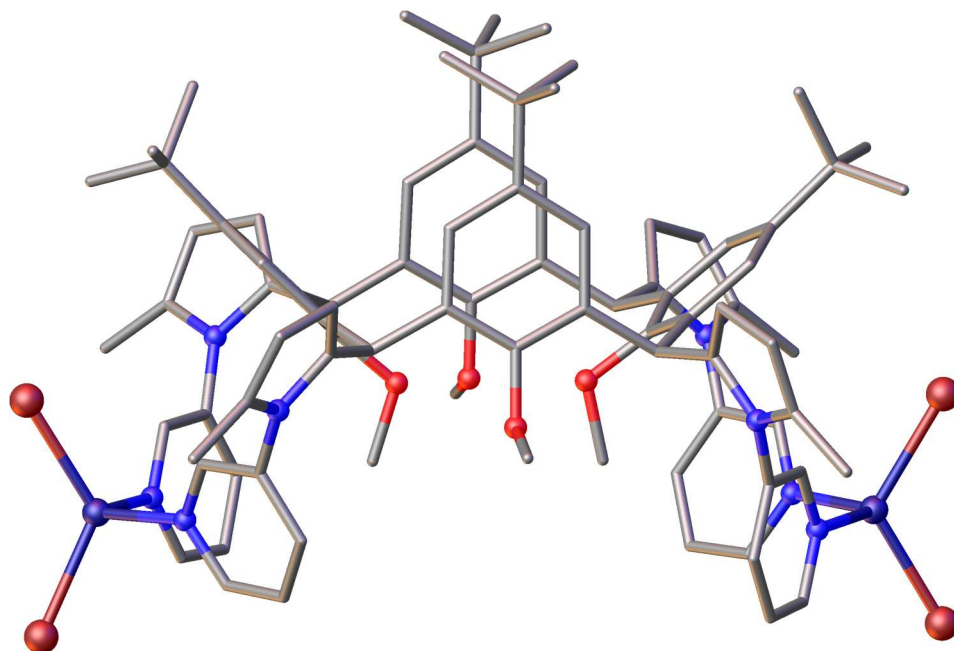


Figure 4.17. Single crystal X-ray structure of **25** showing binding of two CoBr₂ units in ball and stick representation. Colour code: C – grey; O – red; N – blue; Co – purple; Br – dark red. H atoms are omitted for clarity.

Inspection of the crystal structure in Figure 4.17 shows that a cage product has not formed as desired, but instead two sets of pyridine groups of **15** are chelating two CoBr₂ moieties. This again suggests that there is free rotation of these groups and therefore **15** is not rigid enough to prevent intramolecular binding. The crystal structure also shows the Co^{II} ions are in a tetrahedral geometry.

4.3.4 Reaction of **15** [Pd(dppp)][OTf]₂

The reaction of **15** with [Pd(dppp)][OTf]₂ was carried out using the same conditions as described previously in which a solution of [Pd(dppp)][OTf]₂ in CD₃CN was added to a CD₂Cl₂ solution of **15** in a NMR tube. The NMR tube was then shaken vigorously before the ¹H NMR spectrum was collected. Figure 4.18 shows the data collected from each stoichiometry of Pd^{II} used in the form of a stacked spectrum to clearly show how the ¹H NMR spectrum changes with varying ratios of metal salt.

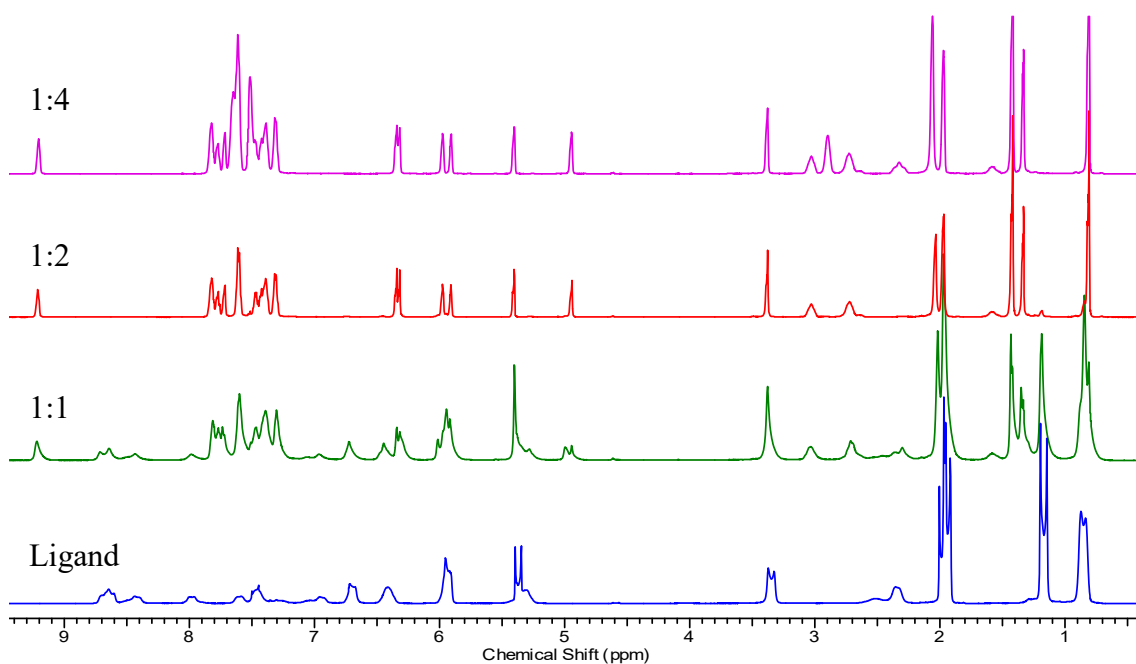


Figure 4.18. Stacked NMR spectra showing the change in ^1H NMR spectrum as the stoichiometries of $[\text{Pd}(\text{dppp})][\text{OTf}]_2$ is changed.

Inspection of Figure 4.18 suggests that there has been some form of complexation as there is significant sharpening of the peaks upon addition of the metal salt. There are still some broad peaks in the 1:1 spectrum which suggests that there may be some residual ligand left in solution. The spectra for the 1:2 and 1:4 ratios appear to be very similar and so vapour diffusions of Et_2O were set up with the mother liquor for both reactions. Pale yellow crystals grew from both crystallisations which were collected and dried. These were then recrystallised through vapour diffusion of Et_2O into DCM solutions of each solid. Pale yellow single crystals grew from the 1:4 ratio which were suitable for analysis by X-ray diffraction. The crystals were found to be in a monoclinic cell and structure solution was carried out in the space group $P2_1/c$ giving rise to the chelate with formula $[\text{Pd}_2(\mathbf{15})_2(\text{dppp})_2]$, **26**. The ASU was found to contain two molecules of **15**, both of which are coordinated to two Pd^{II} ions. However, one of the C[4] units is highly disordered and could not be modelled so only one half of the ASU is shown in Figure 4.19. The ASU also contained several molecules of disordered Et_2O and DCM which were removed by means of a solvent mask.

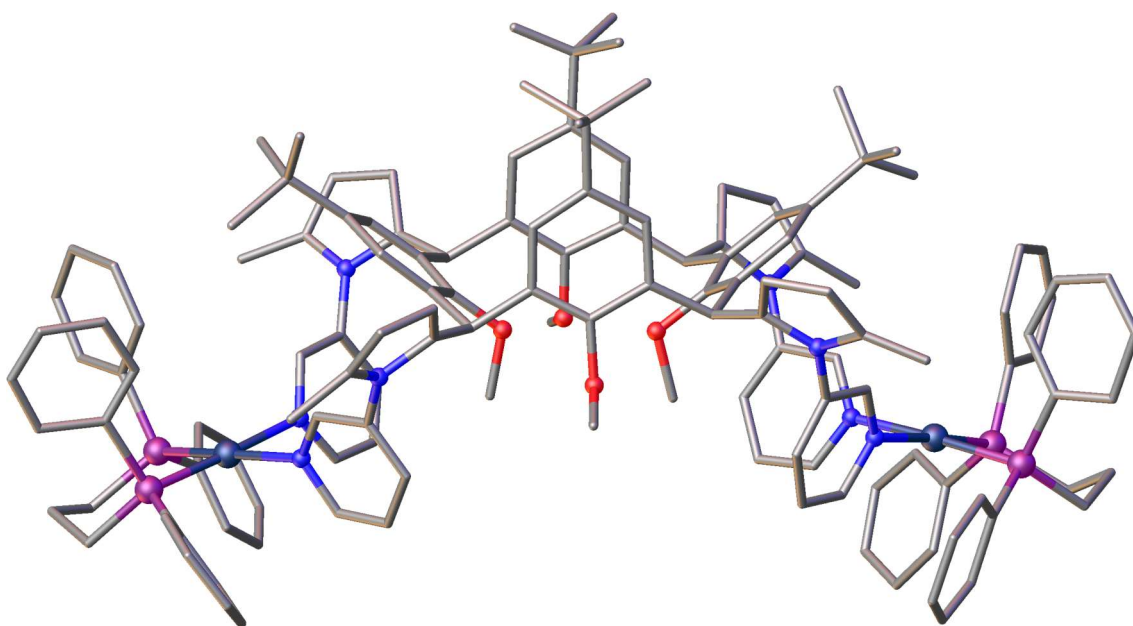


Figure 4.19. Partial single crystal X-ray structure of **26** showing binding of two Pd(dppp)₂ units in ball and stick representation. Colour code: C – grey; O – red; N – blue; Pd – dark blue; P – light purple. H atoms are omitted for clarity.

Inspection of the partial crystal structure (Figure 4.19) shows that two pyridine rings on the same side are coordinated to a Pd^{II} unit and then the same for the other two pyridine rings on the other side. As discussed before, this suggests that there is some flexibility of **15** which leads to the formation of a chelate. The crystal structure also shows the square planar geometry of the Pd^{II} cations.

4.4 Conclusions

The work discussed in this chapter has been carried out in the short timeframe of a few weeks and, as a result, only a small number of metal salts have been trialled in cage formation reactions. The NMR experiments carried out have provided a great insight in predicting whether an assembly has formed as the broadened signals observed in the ^1H NMR spectrum of **15** become sharper and much more distinct upon complexation of a metal. DOSY NMR has been a valuable spectroscopic technique as it has given an indication of the size of systems formed from these reactions as the hydrodynamic radii was calculated using the diffusion coefficient obtained from these NMR experiments. However, the results from X-ray analysis show that compound **15** has not formed a cage when reacted with metal salts as hoped, though three novel metal complexes have formed, which are themselves interesting, giving an indication of how the compounds synthesised in Chapter 3 can be utilised further. The calculated radii match the size of the assemblies formed as much larger radii would be expected in the case of cage formation. The complexes formed (**24** – **26**) indicate that compound **15** is not rigid enough to prevent chelation of two pyridine rings to a metal cation and so future work will focus on the synthesis of a more rigid C[4] in order to synthesise metal-organic cage compounds.

In future it would be interesting to investigate how the isomeric form of **15**, where 4-pyridine rings are attached to the pyrrole moieties, would behave upon reaction with the same metal salts as the nitrogen atoms on the pyridine rings may be held further apart from one another preventing chelation. This in turn will hopefully lead to the formation of a metal-organic cage compound. It would also be interesting in investigating the impact of adding a spacer between the pyrrole and pyridine moieties which again should prevent chelation.

4.5 Experimental

Synthesis of [Zn₂(**15**)₂Br₂], **24**.

In a NMR tube compound **15** (4.3 mg, 0.0032 mmol) was dissolved in CD₂Cl₂ (0.30 mL) and to this was added ZnBr₂ (2.8 mg, 0.0128 mmol) dissolved in CD₃CN (0.25 mL). The NMR tube was shaken vigorously and then the ¹H NMR spectrum was then collected. Colourless crystals grew upon vapour diffusion of Et₂O into the mother liquor.

Crystal data for 24: C₈₈H₉₆Br₄Zn₂N₈O₄, *M* = 1780.10 g/mol, monoclinic, space group *P*2₁/*c* (no.14), *a* = 22.492(9) Å, *b* = 24.205(10) Å, *c* = 21.575(8) Å, β = 92.767(3)°, *V* = 11732(8) Å³, *Z* = 4, *T* = 100.15 K, synchrotron radiation (λ = 0.7288 Å), 77273 reflections measured (3.136° ≤ 2θ ≤ 42.866°), 12314 unique (*R*_{int} = 0.0696, *R*_{sigma} = 0.0509) which were used in all calculations. The final *R*₁ was 0.0478 (*I* > 2σ(*I*)) and *wR*₂ was 0.1470 (all data).

Synthesis of [Co₂(**15**)₂Br₂], **25**.

In a NMR tube compound **15** (4.3 mg, 0.0032 mmol) was dissolved in CD₂Cl₂ (0.30 mL) and to this was added CoBr₂ (1.4 mg, 0.0064 mmol) dissolved in CD₃CN (0.25 mL). The NMR tube was shaken vigorously and then the ¹H NMR spectrum was then collected. Blue crystals grew upon vapour diffusion of Et₂O into the mother liquor.

Crystal data for 25: C₈₈H₉₆Br₄Co₂N₈O₄, *M* = 1767.22 g/mol, monoclinic, space group *P*2₁/*c* (no.14), *a* = 22.4485(8) Å, *b* = 24.1747(9) Å, *c* = 21.4208(8) Å, β = 92.786(2)°, *V* = 11611.0(7) Å³, *Z* = 4, *T* = 100.15 K, synchrotron radiation (λ = 0.7288 Å), 264586 reflections measured (3.726° ≤ 2θ ≤ 46.88°), 15743 unique (*R*_{int} = 0.0572, *R*_{sigma} = 0.0273) which were used in all calculations. The final *R*₁ was 0.0453 (*I* > 2σ(*I*)) and *wR*₂ was 0.1541 (all data).

Synthesis of [Pd₂(dppp)₄(**15**)₂], **26**.

In a NMR tube compound **15** (4.3 mg, 0.0032 mmol) was dissolved in CD₂Cl₂ (0.30 mL) and to this was added [Pd(dppp)₂][OTf]₂ ((10.4 mg, 0.0128 mmol) dissolved in CD₃CN (0.25 mL). The NMR tube was shaken vigorously and then the ¹H NMR spectrum was then collected. Vapour diffusion of Et₂O into the mother liquor was set up and the crystals formed were collected. These were then recrystallised through vapour diffusion of Et₂O into a DCM solution of the crystals.

The data quality for this set of crystals was poor and so full structure refinement has not been completed.

Crystal data for 26: Monoclinic, space group $P2_1/c$ (no.14), $a = 25.6832(10)$ Å, $b = 52.054(2)$ Å, $c = 25.958(1)$ Å, $\beta = 115.748(1)^\circ$, $V = 31258(2)$ Å³, $Z = 4$, $T = 100.15$ K, synchrotron radiation ($\lambda = 0.7288$ Å).

4.6 References

1. P. J. Stang and D. H. Cao, *J. Am. Chem. Soc.*, 1994, **116**, 4981-4982.
2. P. J. Stang, D. H. Cao, S. Saito and A. M. Arif, *J. Am. Chem. Soc.*, 1995, **117**, 6273-6283.
3. M. Fujita, J. Yazaki and K. Ogura, *J. Am. Chem. Soc.*, 1990, **112**, 5645-5647.
4. M. Fujita, S. Nagao and K. Ogura, *J. Am. Chem. Soc.*, 1995, **117**, 1649-1650.
5. N. Takeda, K. Umemoto, K. Yamaguchi and M. Fujita, *Nature*, 1999, **398**, 794-796.
6. B. Olenyuk, J. A. Whiteford, A. Fechtenkotter and P. J. Stang, *Nature*, 1999, **398**, 796-799.
7. S. Sanz, H. M. O'Connor, E. M. Pineda, K. S. Pedersen, G. S. Nichol, O. Monsted, H. Weihe, S. Piligkos, E. J. L. McInnes, P. J. Lusby and E. K. Brechin, *Angew. Chem. Int. Ed.*, 2015, **54**, 6761-6764.
8. H. M. O'Connor, S. Sanz, M. B. Pitak, S. J. Coles, G. S. Nichol, S. Piligkos, P. J. Lusby and E. K. Brechin, *Crystengcomm*, 2016, **18**, 4914-4920.
9. S. Sanz, H. M. O'Connor, V. Marti-Centelles, P. Comar, M. B. Pitak, S. J. Coles, G. Lorusso, E. Palacios, M. Evangelisti, A. Baldansuren, N. F. Chilton, H. Weihe, E. J. L. McInnes, P. J. Lusby, S. Piligkos and E. K. Brechin, *Chem. Sci.*, 2017, **8**, 5526-5535.
10. D. P. August, G. S. Nichol and P. J. Lusby, *Angew. Chem. Int. Ed.*, 2016, **55**, 15022-15026.
11. S. Sanz, H. M. O'Connor, P. Comar, A. Baldansuren, M. B. Pitak, S. J. Coles, H. Weihe, N. F. Chilton, E. J. L. McInnes, P. J. Lusby, S. Piligkos and E. K. Brechin, *Inorg. Chem.*, 2018, **57**, 3500-3506.
12. S. Kai, V. Marti-Centelles, Y. Sakuma, T. Mashiko, T. Kojima, U. Nagashima, M. Tachikawa, P. J. Lusby and S. Hiraoka, *Chem. Eur. J.*, 2018, **24**, 663-671.
13. P. H. Liao, B. W. Langloss, A. M. Johnson, E. R. Knudsen, F. S. Tham, R. R. Julian and R. J. Hooley, *Chem. Commun.*, 2010, **46**, 4932-4934.
14. Z. L. Zhong, A. Ikeda, M. Ayabe, S. Shinkai, S. Sakamoto and K. Yamaguchi, *J. Org. Chem.*, 2001, **66**, 1002-1008.
15. L. Pirondini, F. Bertolini, B. Cantadori, F. Ugozzoli, C. Massera and E. Dalcanale, *Proc. Natl. Acad. Sci.*, 2002, **99**, 4911-4915.

Chapter 5

The Effects of Co-Ligands on the Magnetic Properties of a Mn₄ Cluster

5.1 Introduction

Chapter 5 covers the investigation of the effects of co-ligands on a [Mn^{III}₂Mn^{II}₂] cluster core. As previously described in Chapter 1, the introduction of co-ligands can have a huge impact on the cluster core obtained. For example, Taylor *et al.* isolated a metal cluster with formula [Mn^{III}Mn^{II}(TBC[4])₂(μ₃-O₂P(H)Ph)(DMF)₂(MeOH)₂]₂ (**VII**) that was described as two [Mn^{III}Mn^{II}] moieties held together by two bridging phenylphosphinate ligands (Figure 1.23).¹ The work carried out in this chapter differs slightly as Taylor and co-workers used a one-pot synthesis approach to afford **VII**, whereas the work described here was carried out through post-synthetic modification of the [Mn^{III}₂Mn^{II}₂] cluster periphery. This was undertaken first by synthesising the standard [Mn^{III}₂Mn^{II}₂] cluster, **I**, followed by the introduction of various co-ligands with the aim of displacing ligated solvent molecules around the periphery of the cluster core. The crystal structures of metal clusters obtained in this study are described below.

5.2 Examples of Mn₄ Clusters as Building Blocks for Extended Systems

The post-synthetic modification of Mn₄ clusters with chelating co-ligands is scarce in the literature. However, there are some examples where a Mn₄ cluster with chelating ligands is formed through reaction of [Mn₃O(O₂CR)₆(py)₃] where R = Me, Et or Ph and py = pyridine. Reaction of this Mn₃ cluster with chelating ligands gave tetranuclear Mn complexes in which the py ligands have been displaced by the chelates. For example, reaction of [Mn₃O(O₂CMe)₆(py)₃] with 2,2'-bipyridine (2,2'-bpy), resulted in the formation of cluster with formula [Mn₄O₂(O₂CMe)₆(2,2'-bpy)₂] (Figure 5.1A);² the chelating ligands are attached to the wing-tip Mn ions in this case. Grillo *et al.* reported the reaction with 1,2-bis(2,2'-bipyridine-6-yl)ethane (L11) which gave a cluster of formula [Mn₄O₂(O₂CMe)₆(L11)₂] (Figure 5.1B) in which two [Mn₂O(O₂CMe)₂(L11)]⁺

units are held together by a μ_3 -bridging oxide. There is coordination of one molecule of L11 on each half of the cluster at both the body and wing-tip Mn ions.³ In the same paper, the research group reacted $[\text{Mn}_3\text{O}(\text{O}_2\text{CEt})_6(\text{py})_3][\text{ClO}_4]$ with 1,2-bis(5'-methyl-[2,2'-bipyridine]-5-yl)ethane (L12) to give the cluster with formula $[\text{Mn}_8\text{O}_4(\text{O}_2\text{CEt})_{14}(\text{L12})_2][\text{ClO}_4]_2$ (Figure 5.1C) in which two Mn_4 units are linked through the L12 ligands.³

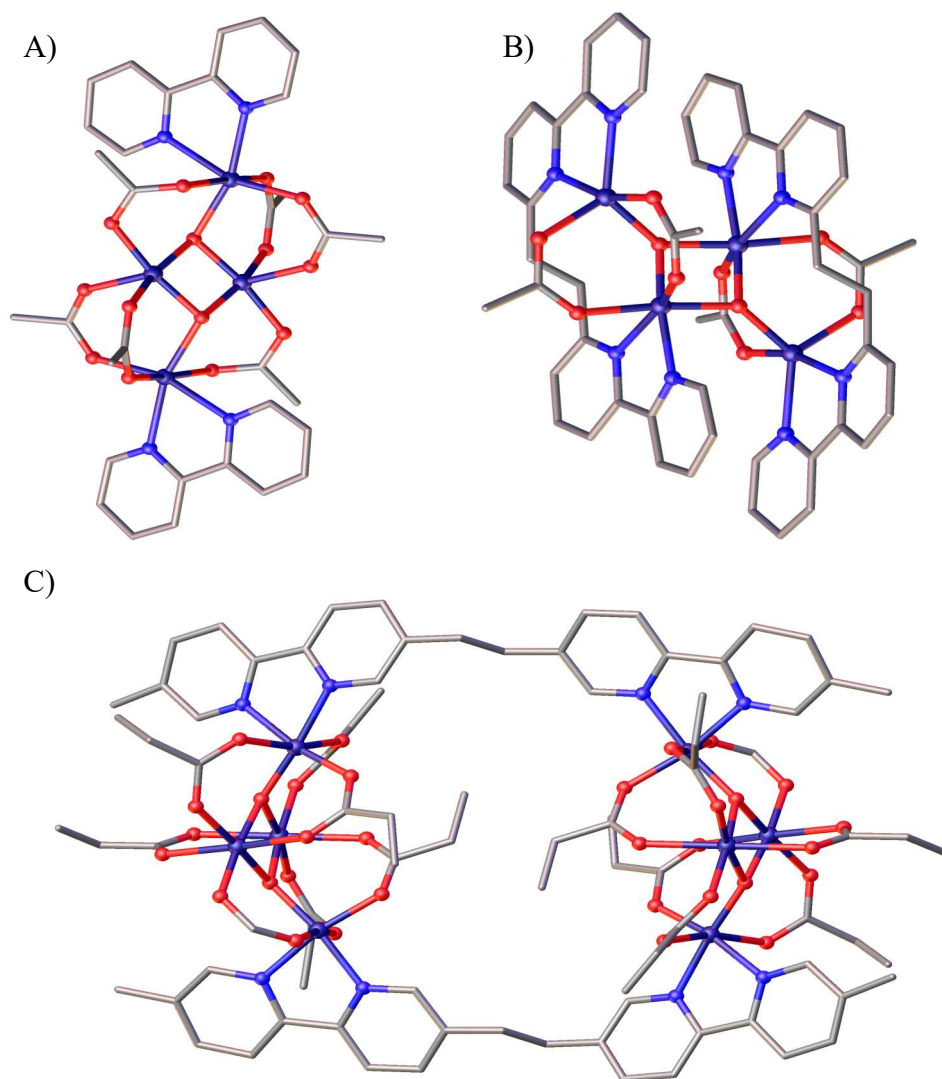


Figure 5.1. Single crystal X-ray structures of A) $[\text{Mn}_4\text{O}_2(\text{O}_2\text{CMe})_6(2,2'\text{-bpy})_2]_2$,² B) $[\text{Mn}_4\text{O}_2(\text{O}_2\text{CMe})_6(\text{L11})_2]_3$ and C) $[\text{Mn}_8\text{O}_4(\text{O}_2\text{CEt})_{14}(\text{L12})_2][\text{ClO}_4]_2$ ³ shown in ball and stick representation. Colour code: C – grey; O – red; Mn – purple; N – blue. Solvent of crystallisation, H atoms and anions are omitted for clarity.

Christou *et al.* also reported the covalent linkage of a Mn_4 cluster into a dimer and a one-dimensional coordination polymer (1-D CP) through the reaction of $[\text{Mn}_4\text{O}_2(\text{O}_2\text{CPh})_6(\text{dbm})_2]$ (where dbmH is dibenzoylmethane) with *trans*-1,2-bis(4-

pyridyl)ethane (bpe) or 4,4'-bipyridine (4,4'-bpy), respectively.⁴ The central Mn anions in the Mn₄ cluster are only five-coordinate and therefore have a vacant site available to bind other ligands. The group postulated that the same chemistry can be applied to the cluster with formula [Mn₄O₂(O₂CPh)₆(EtOAc)₂(dbm)₂] as the ethyl acetate ligands are poorly coordinating groups, however they have only reported products formed from [Mn₄O₂(O₂CPh)₆(dbm)₂]. Following reaction of [Mn₄O₂(O₂CPh)₆(dbm)₂] with bpe in CH₂Cl₂, deep red/brown crystals grew upon layering with Et₂O and these were found to be of formula [Mn₄O₂(O₂CPh)₆(dbm)₂(bpe)]₂·2CH₂Cl₂·2CH₃CN (Figure 5.2). The crystal structure shows that the two Mn₄ units are in the butterfly-like arrangement with two bpe ligands attached *syn* to the two central Mn ions. Also, both bpe ligands are attached to another Mn₄ cluster and are therefore bridging two Mn₄ units to form the dimeric complex.

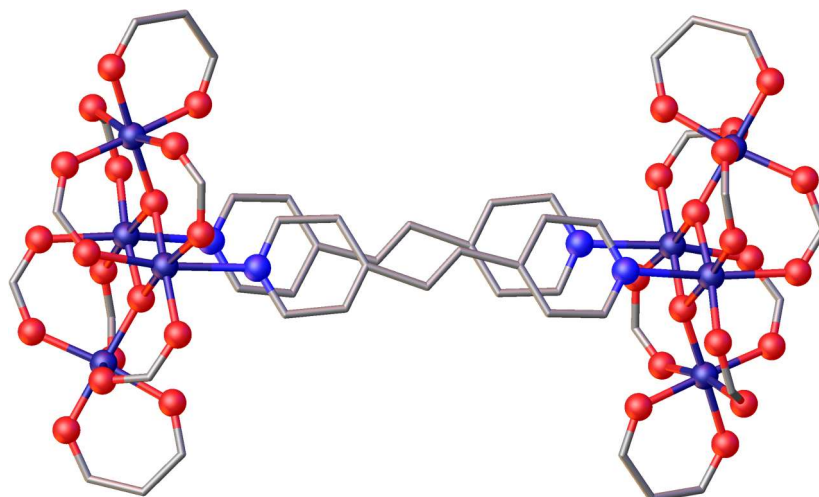


Figure 5.2. Molecular structure of [Mn₄O₂(O₂CPh)₆(dbm)₂(bpe)]₂·2CH₂Cl₂·2CH₃CN shown in ball and stick representation. Colour code: C – grey; O – red; Mn – purple; N – blue. Dichloromethane and acetonitrile of crystallisation, H atoms and Ph groups are omitted for clarity.

Alternatively, if [Mn₄O₂(O₂CPh)₆(dbm)₂] is reacted with 4,4'-bipyridine then a 1-D CP is formed with formula [Mn₄O₂(O₂CPh)₆(dbm)₂(4,4'-bpy)]_n (Figure 5.3). This was isolated as a red/brown crystalline product in which the bipyridine ligands are arranged *anti*, hence linking the Mn₄ units into a polymer.

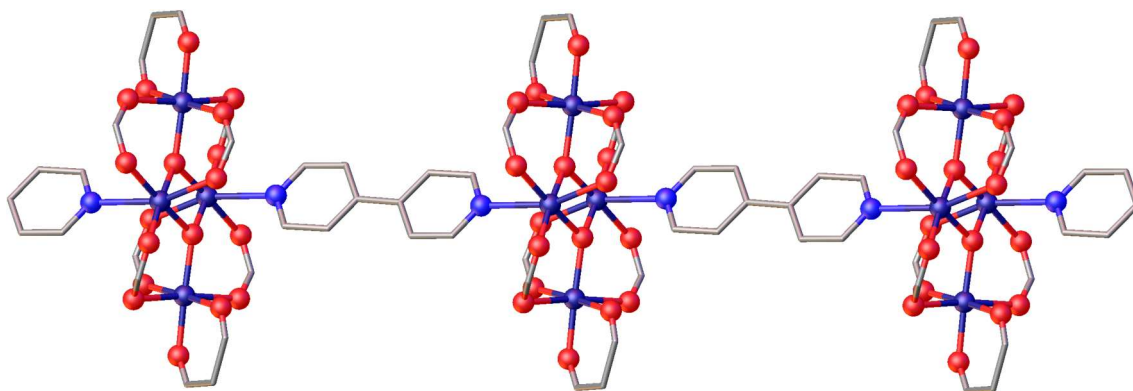


Figure 5.3. Extended view of three repeating units of the chain $[\text{Mn}_4\text{O}_2(\text{O}_2\text{CPh})_6(\text{dbm})_2(4,4'\text{-bpy})]_n$ shown in ball and stick representation. Colour code: C – grey; O – red; Mn – purple; N – blue. H atoms and Ph groups are omitted for clarity.

Another example of ligand substitution was reported by Lecren *et al.* in which they reacted carboxylate ligands with the Mn_4 cluster $[\text{Mn}^{\text{III}}_2\text{Mn}^{\text{II}}_2(\text{hmp})_6(\text{CH}_3\text{CN})_2(\text{H}_2\text{O})_4]^{4+}$ where hmp = 2-hydroxymethylpyridine.⁵ The arrangement of the Mn ions are different to that of compound **I** as the body and wing-tip ions are in the +3 and +2 oxidation states, respectively. The ligated solvent molecules on the Mn^{II} ions are labile and can be exchanged with other ligands resulting in the formation of extended systems. Reaction with simple ligands such as acetate, trichloroacetate and benzoate results in the substitution of two CH_3CN and two water molecules for two moieties of each carboxylate ligand where these chelate the Mn^{II} ions. The cluster with formula $[\text{Mn}^{\text{III}}_2\text{Mn}^{\text{II}}_2(\text{hmp})_6(\text{CH}_3\text{COO})_2(\text{H}_2\text{O})_2][\text{ClO}_4]_2 \cdot 2\text{H}_2\text{O}$ is shown in Figure 5.4.

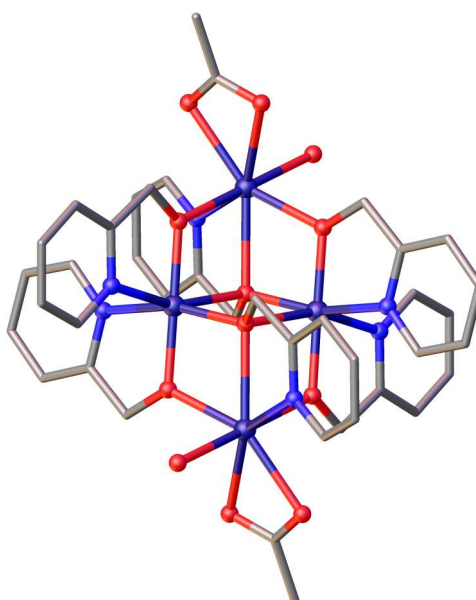


Figure 5.4. Single crystal X-ray structure of $[\text{Mn}^{\text{III}}_2\text{Mn}^{\text{II}}_2(\text{hmp})_6(\text{CH}_3\text{COO})_2(\text{H}_2\text{O})_2][\text{ClO}_4]_2 \cdot 2\text{H}_2\text{O}$ shown in ball and stick representation. Colour code: C – grey; O – red; Mn – purple; N – blue. Water of crystallisation, H atoms and anions are omitted for clarity.

The research group also managed to form 1-D CPs through bridging carboxylate ligands. One example resulted from the reaction of $[\text{Mn}^{\text{III}}_2\text{Mn}^{\text{II}}_2(\text{hmp})_6(\text{CH}_3\text{CN})_2(\text{H}_2\text{O})_4]^{4+}$ with chloroacetate ligands, and the Mn^{II} ions of neighbouring $[\text{Mn}^{\text{III}}_2\text{Mn}^{\text{II}}_2]$ clusters are linked by two bridging chloroacetate moieties in a *syn-syn* mode (Figure 5.5). It was hoped that similar chemistry could be applied to the $[\text{Mn}^{\text{III}}_2\text{Mn}^{\text{II}}_2]$ cluster, compound **I**, isolated by this research through substitution of the ligated DMF molecules on the Mn^{II} ions with chelating ligands in a similar manner with a view to tuning the magnetic properties through alteration of the coordination sphere.

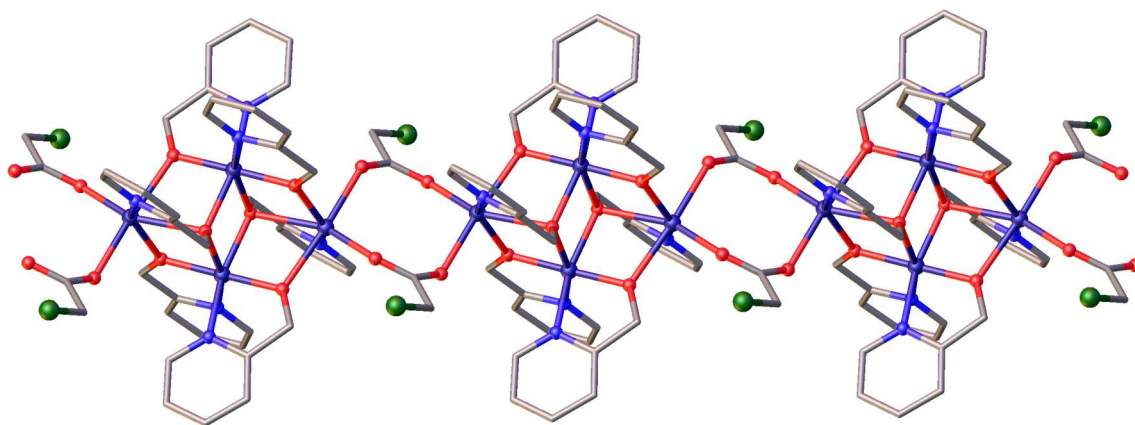


Figure 5.5. Extended view of three repeating units of the 1-D CP $([\text{Mn}_4(\text{hmp})_6(\text{ClCH}_2\text{COO})_2][\text{ClO}_4]_2 \cdot 1.2\text{H}_2\text{O})_n$ shown in ball and stick representation. Colour code: C – grey; O – red; Mn – purple; N – blue; Cl – green. Water of crystallisation, H atoms and anions are omitted for clarity.

There are examples in literature where the ligand periphery on the $[\text{Mn}^{\text{III}}_2\text{Mn}^{\text{II}}_2]$ cluster formed with C[4] has been substituted with chelating ligands, as reported by Aldoshin *et al.*^{6, 7} Using a one-pot method in which they reacted $\text{Mn}(\text{OAc})_2$, C[4] and pyridine in MeOH in a microwave reactor, the research group were able to isolate black crystals which were found to be of formula $[\text{Mn}^{\text{III}}_2\text{Mn}^{\text{II}}_2(\text{C}[4])_2(\mu_3\text{-OH})_2(\text{MeOH})_4(\text{py})_2]$. The structure of the cluster formed is similar to that of compound **I** in which the $[\text{Mn}^{\text{III}}_2\text{Mn}^{\text{II}}_2]$ core is housed within two tetra-anions of $\text{H}_4\text{C}[4]$ with the exception of ligated solvent molecules. Instead of the six ligated DMF molecules in **I** the cluster isolated by Aldoshin and co-workers contains four ligated methanol molecules and two pyridine ligands. Two of these methanol molecules reside within the cavities of the C[4]s and the remaining equatorial positions around the Mn^{II} ions are occupied by a methanol and pyridine.⁶ This result shows that the $[\text{Mn}^{\text{III}}_2\text{Mn}^{\text{II}}_2]$ clusters formed with C[4]s can be modified through the addition of external co-ligands.

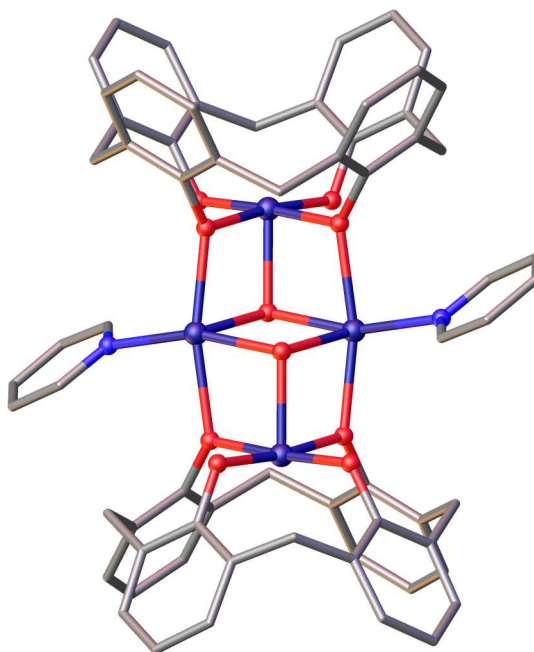


Figure 5.6. Single crystal X-ray structure of $[\text{Mn}^{\text{III}}_2\text{Mn}^{\text{II}}_2(\text{C}[4])_2(\mu_3\text{-OH})_2(\text{MeOH})_4(\text{py})_2]$ in ball and stick representation.⁶ Colour code: C – grey; O – red; Mn – purple; N – blue. H atoms and ligated methanol molecules have been omitted for clarity.

Another example isolated by the same research group was the $[\text{Mn}^{\text{III}}_2\text{Mn}^{\text{II}}_2]$ cluster with chelating 2,2'-bpy ligands. The reaction was carried out in the same way as before but with the addition of 2,2'-bpy instead of pyridine. Again, black crystals formed which were suitable for X-ray diffraction studies and these were found to be of formula $[\text{Mn}^{\text{III}}_2\text{Mn}^{\text{II}}_2(\text{C}[4])_2(\mu_3\text{-OH})_2(\text{MeOH})_2(2,2'\text{-bpy})_2]$ (Figure 5.7). These were found to be comprised of the same metal core as before in which the $[\text{Mn}^{\text{III}}_2\text{Mn}^{\text{II}}_2]$ cluster is capped by two C[4] moieties. However, the ligand periphery is different as the methanol and pyridine moieties located at the equatorial positions of the Mn^{II} ions have been substituted by the bidentate ligand, 2,2'-bpy.⁷ Again, this results indicates that the $[\text{Mn}^{\text{III}}_2\text{Mn}^{\text{II}}_2]$ cluster can be modified through the addition of other ligands.

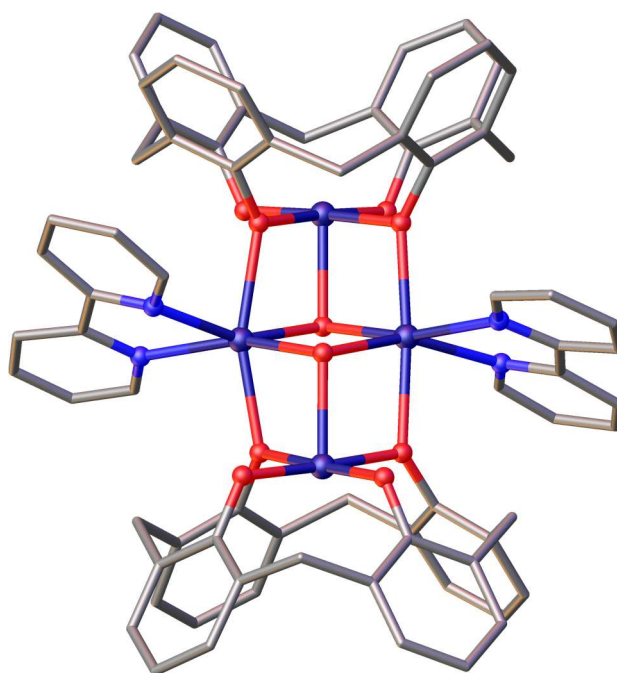


Figure 5.7. Single crystal X-ray structure of $[\text{Mn}^{\text{III}}_2\text{Mn}^{\text{II}}_2(\text{C}[4])_2(\mu_3\text{-OH})_2(\text{MeOH})_2(2,2'\text{-bpy})_2]$ synthesised by Aldoshin *et al* in ball and stick representation.⁷ Colour code: C – grey; O – red; Mn – purple; N – blue. H atoms and ligated methanol molecules have been omitted for clarity.

The clusters formed by Aldoshin *et al.* have been isolated using a one-pot synthesis. However, the aim for the work presented in this chapter was to post-synthetically modify compound **I** through the addition of chelating co-ligands using a similar procedure reported by Christou and co-workers.⁴

5.3 $[\text{Mn}^{\text{III}}_2\text{Mn}^{\text{II}}_2]$ Cluster Formation using $\text{H}_4\text{TBC}[4]$ (**1**)

Compound **I** previously prepared in this research group was synthesised by literature procedure for use in this study.⁸ This cluster was synthesised through the reaction of **1** with manganese(II) chloride tetrahydrate in a 1:1 DMF/MeOH solution in the presence of Et_3N to afford deep purple crystals of **I**. The purple crystals were found to be **I** by confirming the unit cell of a single crystal as well as powder X-ray diffraction studies of the bulk material. The unit cell of these crystals matched that of the literature reported by Karotsis *et al.*, confirming that **I** had successfully been synthesised.⁹ Also, the powder pattern obtained from this experiment was compared to that of a computed pattern generated from the single crystal X-ray structure of **I** (Figure 5.8). This also confirmed

that **I** had been synthesised as there is strong correlation between the calculated and experimental patterns.

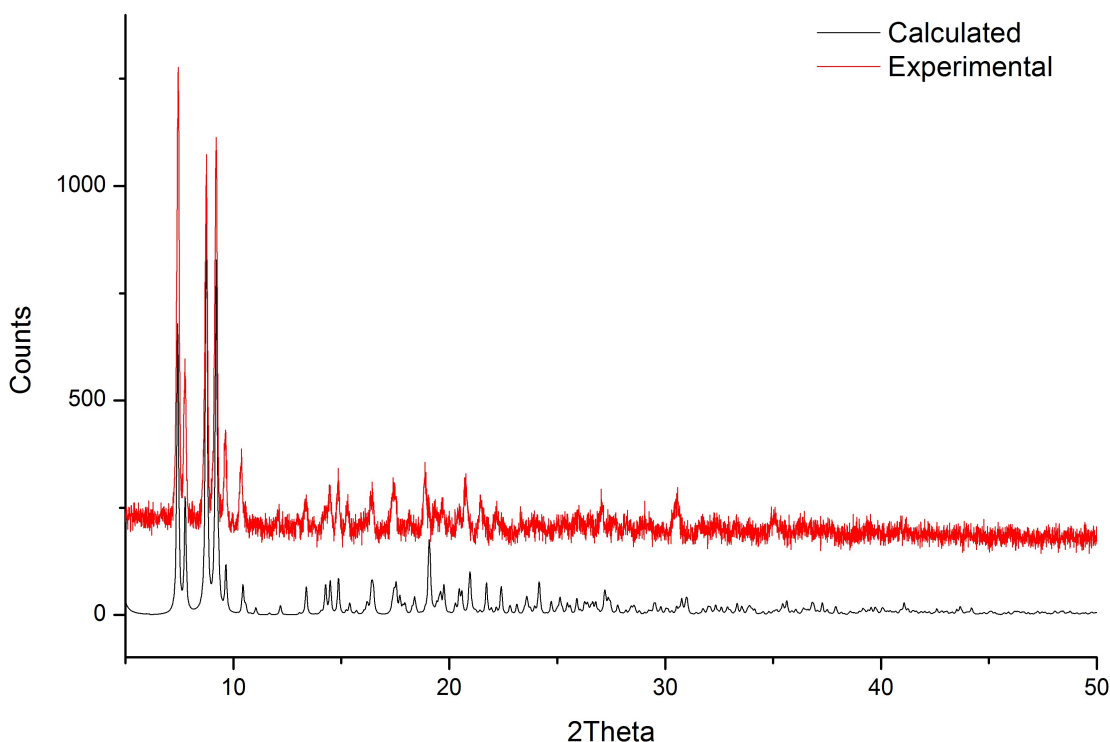


Figure 5.8. Overlay of experimental (red) and calculated (black, from single crystal structure) in powder pattern of compound **I**.

Following confirmation that the $[\text{Mn}^{\text{III}}_2\text{Mn}^{\text{II}}_2]$ cluster had formed, a stock acetone solution of **I** was prepared in order to first test small-scale reactions with varying stoichiometries of co-ligands; this was undertaken in order to determine whether single crystals would grow and what ratios gave the best quality crystals for diffraction studies. Once these stoichiometries had been determined the reactions were to be scaled up in order to compare their powder patterns against those of the calculated powder pattern in each case prior to carrying out magnetic measurements.

5.4 Structural Alteration of the $[\text{Mn}^{\text{III}}_2\text{Mn}^{\text{II}}_2]$ Cluster Motif through the Addition of Chelating Co-Ligands

Small-scale reactions of the $[\text{Mn}^{\text{III}}_2\text{Mn}^{\text{II}}_2]$ cluster with the co-ligands were attempted in order to investigate whether or not the co-ligands would displace the ligated solvent molecules around the periphery of the cluster core. This was achieved by adding small aliquots of the co-ligands in varying stoichiometries (2, 4, 6, 8 and 10 *eq.* relative to 1 *eq.* of **I**) to an acetone solution of **I**. Single crystals suitable for X-ray diffraction studies were isolated from some reactions involving various co-ligands and these are summarised in Table 5.1.

Table 5.1. Summary of cluster-forming reactions attempted with **I** and various co-ligands where bpy – bipyridine, Phen – phenanthroline, MePhen – methylphenanthroline, TetraMePhen – tetramethylphenanthroline, BPhen – bathophenanthroline and Neo – neocuproine.

	H₄TBC[4], 1	Cluster no.
2,2'-bpy	x	-
4,4'-bpy	x	-
1,10-Phen	✓	27
2-MePhen	✓	28
3-MePhen	✓	29
TetraMePhen	x	-
BPhen	x	-
Neo	x	-

5.4.1 Reaction of **I** with 1,10-Phenanthroline (1,10-Phen)

Single crystals suitable for X-ray diffraction studies were isolated from a 1:4 reaction of **I** with 1,10-Phen in acetone, followed by slow evaporation. The crystals were found to be in a triclinic cell and structure solution was carried out in the space group *P*-1. The

deep purple crystals were found to be of the formula $[\text{Mn}^{\text{III}}_2\text{Mn}^{\text{II}}_2(\text{TBC}[4])_2(\mu_3\text{-OH})_2(1,10\text{-Phen})_2((\text{CH}_3)_2\text{CO})_2]\cdot(\text{CH}_3)_2\text{CO}$ (**27**). The ASU contained half of the aforementioned formula and upon symmetry expansion afforded the $[\text{Mn}^{\text{III}}_2\text{Mn}^{\text{II}}_2]$ core in which the peripherally ligated solvent molecules have been displaced by 2 molecules of 1,10-Phen (Figure 5.9). The structure contained several disordered molecules of acetone which could not be modelled so a solvent mask was applied.

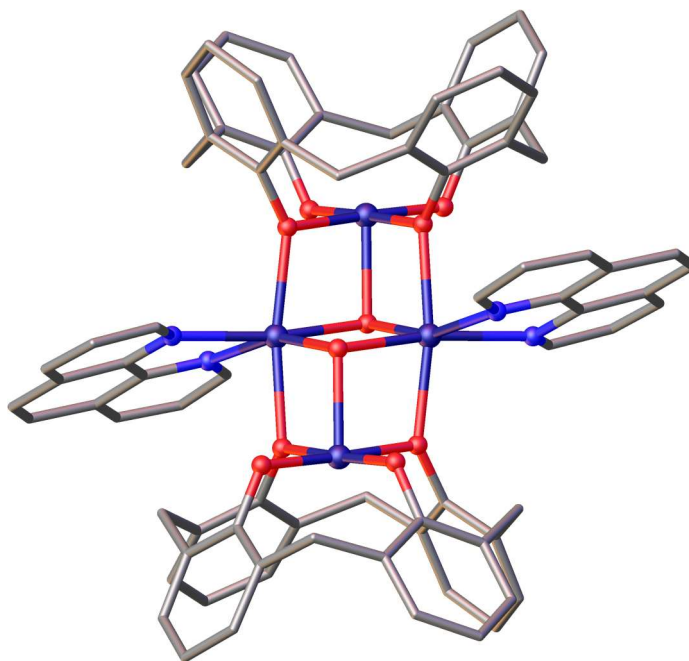


Figure 5.9. Single crystal X-ray structure of **27** showing the introduction of 1,10-Phen chelating ligands in ball and stick representation. Colour code: C – grey; O – red; Mn – purple; N – blue. H atoms, ^tBu groups and ligated acetone molecules are omitted for clarity.

Inspection of the single crystal X-ray structure in Figure 5.9 confirms that the standard $[\text{Mn}^{\text{III}}_2\text{Mn}^{\text{II}}_2]$ butterfly core has been retained. However, the peripherally ligated solvent molecules of **I** have been replaced by two molecules of 1,10-Phen. There is another difference in ligated solvent compared to **I**, as the ligated solvent molecules within the C[4] cavities are acetone as opposed to DMF molecules.

5.4.2 Reaction of I with 2-Methylphenanthroline (2-MePhen)

Reaction of **I** with 2-MePhen in a 1:8 ratio in acetone afforded a deep purple solution and single crystals were isolated upon slow evaporation of the mother liquor. These were found to be in a triclinic cell and structure solution was carried out in the space group *P*-1. The purple crystals were found to be of the formula $[\text{Mn}^{\text{III}}_2\text{Mn}^{\text{II}}_2(\text{TBC}[4])_2(\mu_3\text{-OH})_2(2\text{-MePhen})_2((\text{CH}_3)_2\text{CO})_2]$ (**28**) with the ASU containing half of the aforementioned formula. Upon symmetry expansion a $[\text{Mn}^{\text{III}}_2\text{Mn}^{\text{II}}_2]$ metal core was obtained (Figure 5.10) and it was clear to see that 2-MePhen had displaced any peripherally ligated solvent molecules. Again, disordered acetone was observed in the crystal structure which could not be modelled and so these were removed by means of a solvent mask.

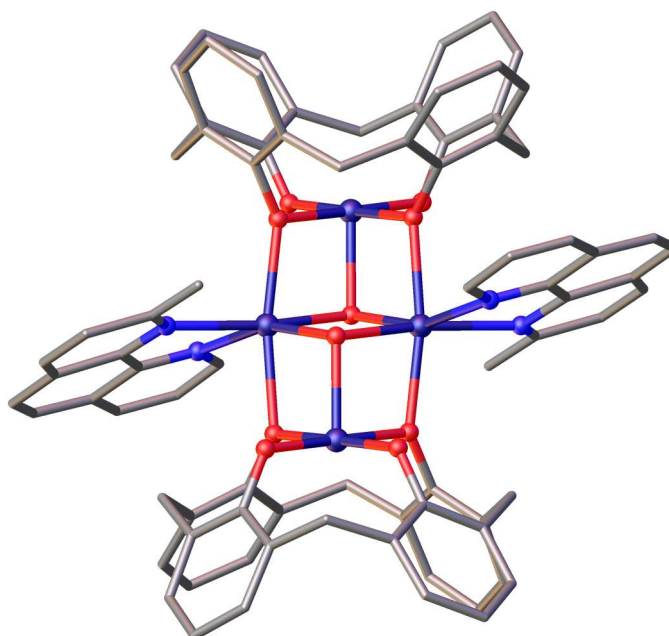


Figure 5.10. Single crystal X-ray structure of **28** showing the introduction of 2-MePhen molecules in ball and stick representation. Colour code: C – grey; O – red; Mn – purple; N – blue. H atoms, ^tBu groups and ligated acetone molecules are omitted for clarity.

Inspection of Figure 5.10 shows that the $[\text{Mn}^{\text{III}}_2\text{Mn}^{\text{II}}_2]$ core has not been affected by the addition of 2-MePhen as the butterfly-like shape of the cluster has been retained. However, it is possible to see that the ligated DMF molecules have been displaced by two molecules of 2-MePhen. Another difference is that the ligated DMF molecule contained within the cavities of **I** have been replaced with acetone in **28**.

5.4.3 Reaction of I with 3-Methylphenanthroline (3-MePhen)

Reaction of **I** with 3-MePhen in a 1:8 ratio in acetone afforded a deep purple solution and single crystals were isolated upon slow evaporation of the mother liquor. These were found to be in a monoclinic cell and structure solution was carried out in the space group $P2_1/c$. The crystals were found to be of the formula $[\text{Mn}^{\text{III}}_2\text{Mn}^{\text{II}}_2(\text{TBC}[4])_2(\mu_3\text{-OH})_2(3\text{-MePhen})_2((\text{CH}_3)_2\text{CO})_2]$ (**29**) and the ASU contained half of the aforementioned formula. Symmetry expansion afforded a $[\text{Mn}^{\text{III}}_2\text{Mn}^{\text{II}}_2]$ core in which the peripherally ligated solvent molecules have been replaced with two molecules of 3-MePhen (Figure 5.11). The structure contained several disordered acetone molecules that could not be modelled so a solvent mask was applied to remove the diffuse electron density.

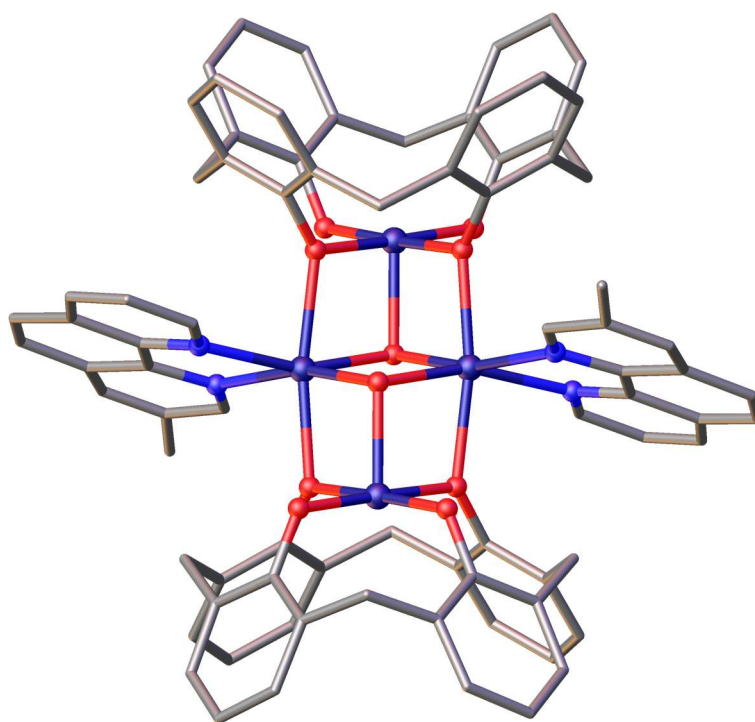


Figure 5.11. Single crystal X-ray structure of **29** showing the introduction of 3-MePhen molecules in ball and stick representation. Colour code: C – grey; O – red; Mn – purple; N – blue. H atoms, ^tBu groups and ligated acetone molecules are omitted for clarity. The methyl groups of 3-MePhen were disordered over two positions so only one of these positions is shown.

Figure 5.11 clearly shows that the $[\text{Mn}^{\text{III}}_2\text{Mn}^{\text{II}}_2]$ butterfly-like core has been retained. It is possible to see that the peripherally ligated DMF molecules of **I** have been replaced by the chelating co-ligand 3-MePhen in **29**. As with clusters **27** and **28**, the DMF contained

within the cavity of **I** has been replaced with acetone molecules. The methyl groups of the 3-MePhen moieties were disordered over two positions and only one of these positions has been shown in Figure 5.11 for clarity.

5.5 Structural Comparison of Chelating Systems 27 – 29

The structural differences between compounds **I** and **27 – 29** were investigated by measuring the angles between mean planes in the clusters. The mean plane created by the central Mn-O-Mn diamond was taken as a reference (red/brown plane, Figure 5.12). The angle between the plane of the ligand (blue plane, Figure 5.12) and the reference was then measured to compare how the addition of the chelate affects the angle.

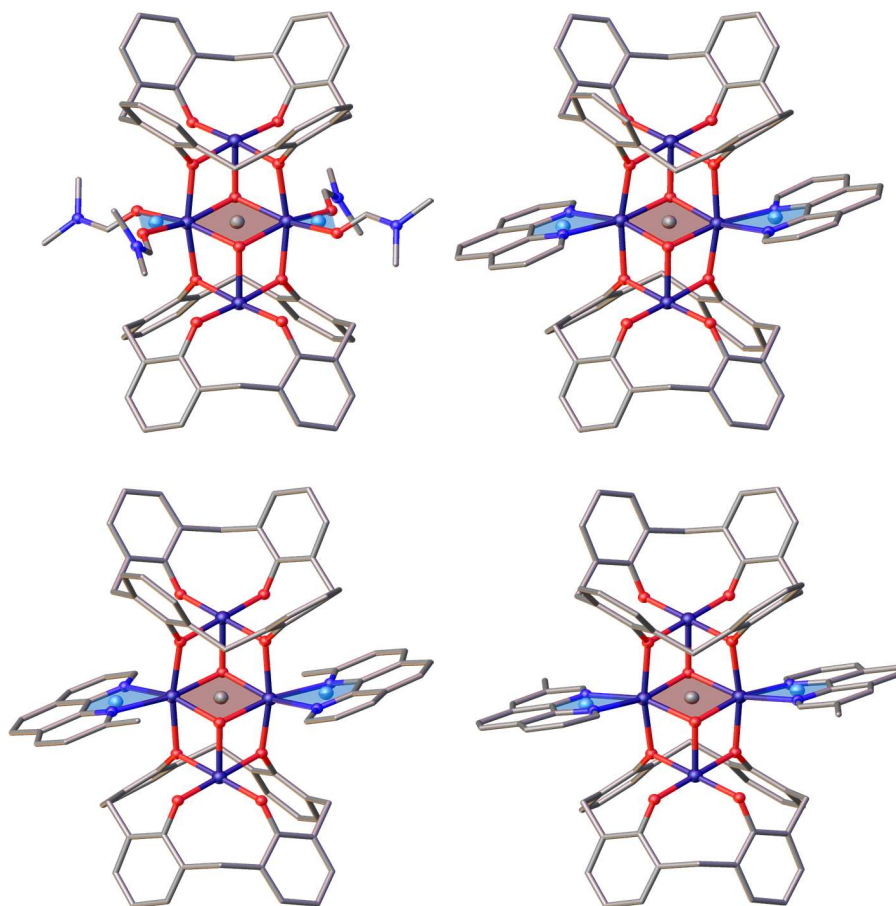


Figure 5.12. Single crystal structures of A) compound **I**, B) **27**, C) **28** and D) **29** showing the mean plane created by the Mn-O-Mn diamond (red/brown) and the mean plane of the chelating ligand (light blue). Colour code: C – grey; O – red; Mn – purple; N – dark blue. Solvent of crystallisation, ^tBu groups, H atoms and ligated solvent molecules are omitted for clarity.

Table 5.2. Summary of angles measured between mean planes of compound **I** and compounds **27** – **29**.

Compound	I	27	28	29
Ligand	2 x DMF	1,10-Phen	2-MePhen	3-MePhen
Plane to Plane Angle	21.85(14)°	24.33(7)°	25.5(3)°	27.2(2)°
Plane to Plane Twist Angle	21.81(14) °	20.87(8)°	21.0(3)°	26.5(2)°
Plane to Plane Fold Angle	1.29(10) °	12.78(4)°	14.68(19)°	6.22(13)°

From the summary of angles in Table 5.2 it is possible to see that there are changes in the angles as the chelating co-ligand is altered and these variations might be due to the properties of the ligand that have displaced the solvent molecules. By altering the cluster periphery of compound **I** it is hoped that there will be a change in the magnetic properties of the compounds synthesised in this study.

5.6 Powder X-ray Diffraction Studies of Co-Ligand Appended [Mn^{III}₂Mn^{II}₂] clusters

The magnetic measurements of compounds **27**, **28** and **29** were to be carried out at the University of Edinburgh. However, before this was possible, the clusters formed in the screening process were to be scaled up using the same reaction conditions as the small-scale tests. Again, a deep purple solid formed upon slow evaporation of the mother liquor which was collected by gravity filtration. Powder X-ray diffraction studies were carried out on the solids isolated from these reactions which were then compared with calculated patterns obtained from the single crystal X-ray structures to confirm that the clusters had formed.

5.6.1 Powder X-ray Diffraction Studies of 27

The 1:4 reaction of compound **I** with 1,10-phen resulted in the formation of a deep purple solid. The powder pattern of this solid was collected through 1 and 8 hour scans. Inspection of the overlay of the powder patterns in Figure 5.13 shows that there are some similarities between the calculated and 1 hour scan patterns, suggesting that the cluster (**27**) has formed. However, there does not appear to be any correlation between the calculated and 8 hour scan patterns, suggesting that the crystals are not stable in air for prolonged periods of time and are de-solvating upon removal from the mother liquor.

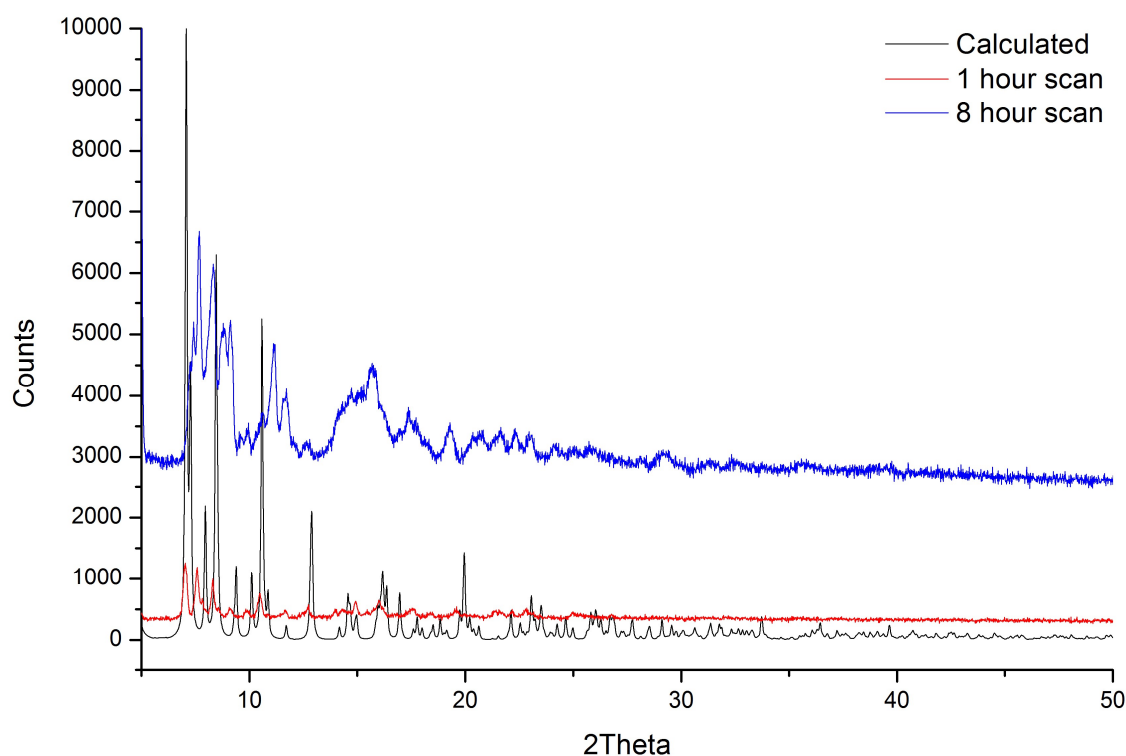


Figure 5.13. Overlay of calculated (black, from single crystal structure) and experimental (red – 1 hour scan and blue – 8 hour scan) in powder pattern of **27**.

5.6.2 Powder X-ray Diffraction Studies of 28

Reaction of a 1:8 ratio of **I** and 2-MePhen in acetone afforded a deep purple solid which was analysed by powder X-ray diffraction studies. The powder pattern was collected through 1 and 8 hour scans and these patterns can be compared with the calculated pattern in the overlay shown in Figure 5.14. There is no real correlation of the calculated pattern

with either the 1 or 8 hour scan, suggesting that **28** had not formed, or the sample had already been out of solution too long before the powder experiments were run and that it had potentially de-solvated.

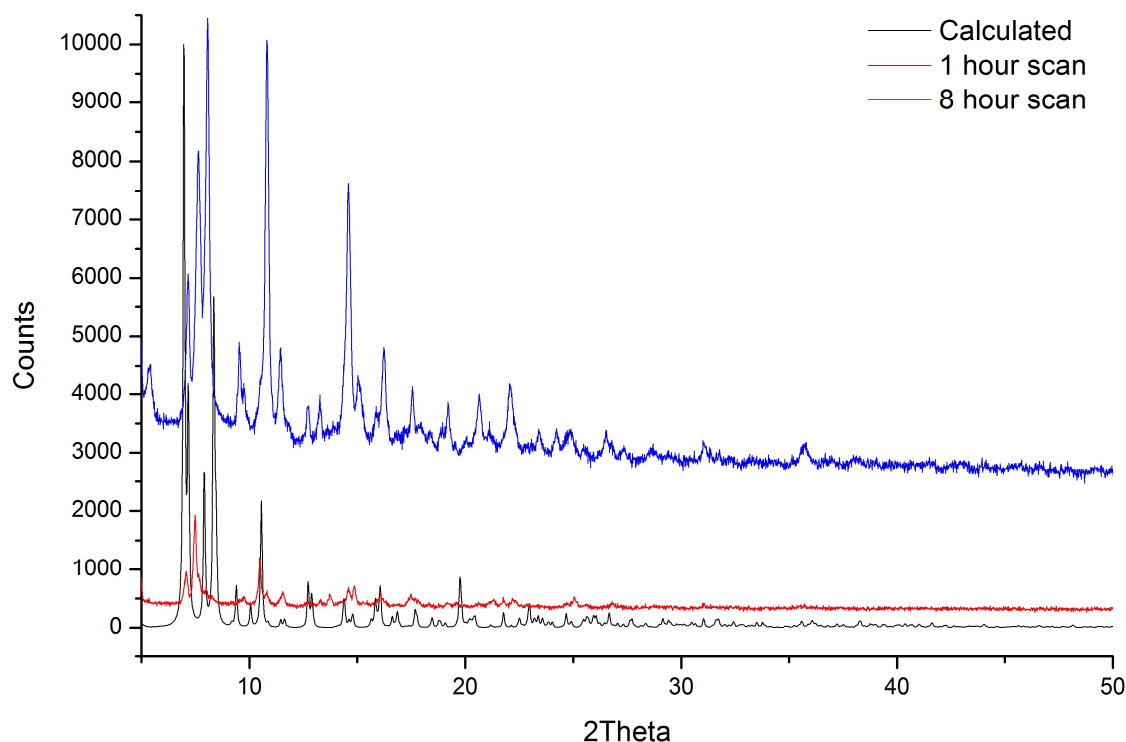


Figure 5.14. Overlay of calculated (black, from single crystal structure) and experimental (red – 1 hour scan and blue – 8 hour scan) in powder pattern of **28**.

5.6.3 Powder X-ray Diffraction Studies of **29**

A deep purple solid was obtained from the 1:8 reaction of compound **I** with 3-MePhen which was collected by filtration and studied using powder X-ray diffraction. As before, both 1 and 8 hour scans were performed. Inspection of the overlay of powder patterns in Figure 5.15 shows that there is some correlation between the calculated and 1 hour pattern suggesting that **29** has formed. However, the pattern has changed dramatically between performing the 1 and 8 hour scan indicating that the cluster may have de-solvated upon removal from the mother liquor and is therefore not stable in air for prolonged periods of time.

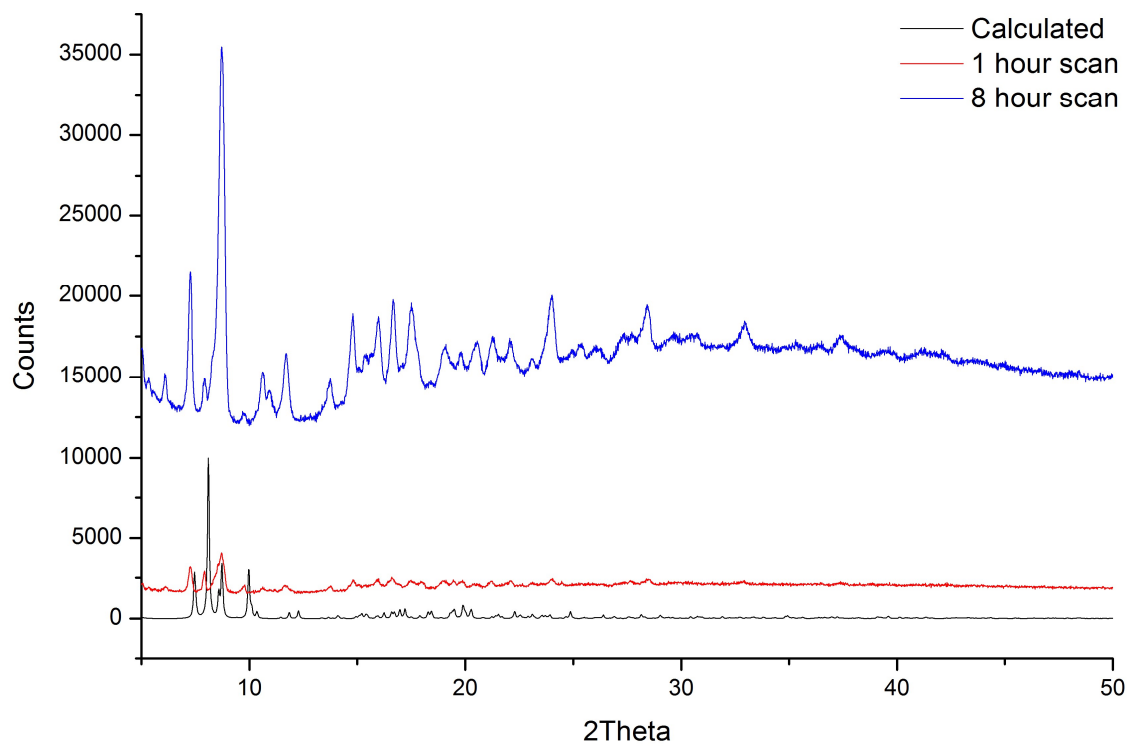


Figure 5.15. Overlay of calculated (black, from single crystal structure) and experimental (red – 1 hour scan and blue – 8 hour scan) in powder pattern of **29**.

5.7 Conclusions

The work presented in this chapter shows that it is possible to post-synthetically modify **I**, the result being a new family of structurally modified $[\text{Mn}^{\text{III}}_2\text{Mn}^{\text{II}}_2]$ clusters. The single crystal X-ray structures of **27** – **29** have shown ligand substitution as the chelating co-ligands, 1,10-Phen, 2-MePhen and 3-MePhen, have displaced the ligated DMF molecules at the cluster periphery. A structural comparison of the clusters isolated in this study was carried out and it was found that the angle between the mean plane of the Mn-O-Mn central diamond and the mean plane of the ligand is changing and it was hoped that these small changes in the coordination sphere would result in different magnetic properties. The reactions were scaled up to compare the bulk powder X-ray diffraction patterns with those calculated from the single crystal X-ray structures. The results from these show that the clusters are unstable in the air for prolonged periods of time and are potentially de-solvating upon removal from the mother liquor. Repetition of these reactions is required, in which the clusters are left in solution, and only filtered immediately prior to studying their magnetic properties to prevent de-solvation. Due to time constraints, the magnetic properties of **27** – **29** were not studied, however, these properties will be tested in the future to investigate whether it is possible for them to be used as SMMs or MRs.

5.6 Experimental

Synthesis of $[\text{Mn}^{\text{III}}_2\text{Mn}^{\text{II}}_2(\mu_3\text{-OH})_2(\text{TBC}[4])_2(\text{DMF})_6]$, **I**.

$\text{MnCl}_2 \cdot 4\text{H}_2\text{O}$ (1 g, 5.05 mmol) and compound **1** (1 g, 1.54 mmol) were dissolved in a 1:1 DMF/MeOH mixture (100:100 mL). After 10 min of stirring Et_3N (1.4 mL) was added and the resulting deep purple solution was stirred at room temp. for 2 h. The reaction mixture was filtered to remove any microcrystalline material, and purple crystals of **I** grew upon slow evaporation of the mother liquor. The crystals were analysed by both single crystal and powder X-ray diffraction and they were confirmed to be **I**.

Synthesis of $[\text{Mn}^{\text{III}}_2\text{Mn}^{\text{II}}_2(\text{TBC}[4])_2(\mu_3\text{-OH})_2(1,10\text{-Phen})_2((\text{CH}_3\text{CO})_2)] \cdot (\text{CH}_3)_2\text{CO}$, **27**.

1,10-Phenanthroline (0.8 mg) was added to a 5 mL aliquot of a stock solution of **I** in acetone (0.120 mmol/L). Dark purple crystals of **27** grew upon slow evaporation of the mother liquor.

Crystal data for 27: $\text{C}_{124}\text{H}_{144}\text{Mn}_4\text{N}_4\text{O}_{14}$, $M = 2134.18$ g/mol, triclinic, space group $P-1$ (no.2), $a = 12.3299(5)$ Å, $b = 12.4922(5)$ Å, $c = 19.1012(8)$ Å, $\alpha = 89.407(2)^\circ$, $\beta = 80.244(2)^\circ$, $\gamma = 89.417(2)^\circ$, $V = 2899.3(2)$ Å³, $Z = 1$, $T = 100(2)$ K, synchrotron radiation ($\lambda = 0.7749$ Å), 43707 reflections measured ($3.654^\circ \leq 2\theta \leq 70.326^\circ$), 19818 unique ($R_{\text{int}} = 0.0382$, $R_{\text{sigma}} = 0.0565$) which were used in all calculations. The final R_1 was 0.0628 ($I > 2\sigma(I)$) and wR_2 was 0.2002 (all data).

Synthesis of $[\text{Mn}^{\text{III}}_2\text{Mn}^{\text{II}}_2(\text{TBC}[4])_2(\mu_3\text{-OH})_2(2\text{-MePhen})_2((\text{CH}_3\text{CO})_2)]$, **28**.

2-Methylphenanthroline (2.4 mg) was added to a 5 mL aliquot of a stock solution of **I** in acetone (0.301 mmol/L). Dark purple crystals of **28** grew upon slow evaporation of the mother liquor.

Crystal data for 28: $\text{C}_{120}\text{H}_{136}\text{Mn}_4\text{N}_4\text{O}_{12}$, $M = 2046.08$ g/mol, triclinic, space group $P-1$ (no.2), $a = 12.4868(6)$ Å, $b = 12.6771(6)$ Å, $c = 19.0641(9)$ Å, $\alpha = 90.715(2)^\circ$, $\beta = 99.308(2)^\circ$, $\gamma = 90.485(2)^\circ$, $V = 2977.6(2)$ Å³, $Z = 1$, $T = 100(2)$ K, synchrotron radiation ($\lambda = 0.7749$ Å), 11737 reflections measured ($4.672^\circ \leq 2\theta \leq 65.280^\circ$), 6651 unique ($R_{\text{int}} = 0.0461$, $R_{\text{sigma}} = 0.0850$) which were used in all calculations. The final R_1 was 0.1068 ($I > 2\sigma(I)$) and wR_2 was 0.2786 (all data).

Synthesis of $[\text{Mn}^{\text{III}}_2\text{Mn}^{\text{II}}_2(\text{TBC}[4])_2(\mu_3\text{-OH})_2(3\text{-MePhen})_2((\text{CH}_3\text{CO})_2]$, **29.**

3-Methylphenanthroline (2.4 mg) was added to a 5 mL aliquot of a stock solution of **I** in acetone (0.301 mmol/L). Dark purple crystals of **29** grew upon slow evaporation of the mother liquor.

Crystal data for 29: $\text{C}_{120}\text{H}_{134}\text{Mn}_4\text{N}_4\text{O}_{12}$, $M = 2196.16$ g/mol, monoclinic, space group $P-1$ (no.2), $a = 19.8652(9)$ Å, $b = 12.3177(6)$ Å, $c = 24.8515(11)$ Å, $\beta = 109.119(2)^\circ$, $V = 5745.6(5)$ Å³, $Z = 2$, $T = 100(2)$ K, synchrotron radiation ($\lambda = 0.7749$ Å), 74919 reflections measured ($2.366^\circ \leq 2\theta \leq 64.988^\circ$), 15988 unique ($R_{\text{int}} = 0.0522$, $R_{\text{sigma}} = 0.0386$) which were used in all calculations. The final R_1 was 0.1063 ($I > 2\sigma(I)$) and wR_2 was 0.2852 (all data).

5.7 References

1. S. M. Taylor, R. D. McIntosh, C. M. Beavers, S. J. Teat, S. Piligkos, S. J. Dalgarno and E. K. Brechin, *Chem. Commun.*, 2011, **47**, 1440-1442.
2. J. B. Vincent, C. Christmas, H. R. Chang, Q. Y. Li, P. D. W. Boyd, J. C. Huffman, D. N. Hendrickson and G. Christou, *J. Am. Chem. Soc.*, 1989, **111**, 2086-2097.
3. V. A. Grillo, M. J. Knapp, J. C. Bollinger, D. N. Hendrickson and G. Christou, *Angew. Chem. Int. Ed.*, 1996, **35**, 1818-1820.
4. S. Wang, H. L. Tsai, K. Folting, J. D. Martin, D. N. Hendrickson and G. Christou, *J. Chem. Soc., Chem. Commun.*, 1994, 671-673.
5. L. Lecren, O. Roubeau, Y. G. Li, X. F. Le Goff, H. Miyasaka, F. Richard, W. Wernsdorfer, C. Coulon and R. Clerac, *Dalton Trans.*, 2008, 755-766.
6. S. M. Aldoshin, I. S. Antipin, V. I. Ovcharenko, S. E. Solov'eva, A. S. Bogomyakov, D. V. Korchagin, G. V. Shilov, E. A. Yur'eva, F. B. Mushenok, K. V. Bozhenko and A. N. Utenyshev, *Russ. Chem. Bull.*, 2013, **62**, 536-542.
7. S. M. Aldoshin, I. S. Antipin, S. E. Solov'eva, N. A. Sanina, D. V. Korchagin, G. V. Shilov, F. B. Mushenok, A. N. Utenyshev and K. V. Bozhenko, *J. Mol. Struct.*, 2015, **1081**, 217-223.
8. S. M. Taylor, G. Karotsis, R. D. McIntosh, S. Kennedy, S. J. Teat, C. M. Beavers, W. Wernsdorfer, S. Piligkos, S. J. Dalgarno and E. K. Brechin, *Chem. Eur. J.*, 2011, **17**, 7521-7530.
9. G. Karotsis, S. J. Teat, W. Wernsdorfer, S. Piligkos, S. J. Dalgarno and E. K. Brechin, *Angew. Chem. Int. Ed.*, 2009, **48**, 8285-8288.

Chapter 6

Conclusions

Calixarene chemistry has developed a great deal since von Baeyer first synthesised the resin-like material in 1872.¹ Since then many efforts have gone into the characterisation of this compound, and it is with thanks to these researchers that there are now standard reaction procedures to allow for the optimised synthesis of calixarenes with varying ring size in relatively high yields.^{2,3} One prominent researcher in the field that has made important contributions is Gutsche,⁴ and through his study of these molecules scientists around the world have a much deeper understanding of the reaction between phenols and formaldehyde. Along with this, Gutsche also made another huge impact by inventing the now very common systematic nomenclature of such molecules. Gutsche's contribution to calixarene chemistry has given other researchers the opportunity to further study the properties and structures of these fascinating molecules through the use of many analytical techniques such as NMR and IR spectroscopies, and single crystal X-ray diffraction, all of which have provided key knowledge surrounding their structure, composition and conformational behaviour. This has led to the growing interest in the study of these macrocycles and they have played a prominent role in the development of supramolecular chemistry as a whole.

Modification of the calix[*n*]arene scaffold is of particular interest to researchers as it provides the opportunity to tune the framework through the introduction of targeted structural features of interest. This renders them a versatile macrocycle type with numerous applications in fields such as complexing agents, enzyme mimics and optoelectronics. Calix[*n*]arenes can be synthetically modified at the upper- and lower-rim positions as well as at the methylene bridge. As discussed in this thesis, far less work has been carried out at the methylene bridge position, however Biali and co-workers have pioneered this area of functionalisation. Much of the work discussed in this thesis has used the tetra-brominated calix[4]arene as a starting material to explore the synthesis of other methylene bridge-substituted calix[4]arenes, seeking to expand this chemistry which is at an embryonic stage.

The work presented in Chapter 2 describes the synthesis and characterisation of a calix[4]arene that has been mono-substituted at the methylene bridge position with 2-methylfuran groups (**4**), and its subsequent demethylation of this to afford **H45**. The

cluster-forming properties of **H45** were investigated through reaction with various metal salts in line with standard protocols developed in this research group. It was hoped that additional metal binding sites would be created through the introduction of functional groups at the methylene bridge leading to the formation of mixed-metal clusters. However, none of the clusters isolated from this work display the desired behaviour, and instead the *3d* and *4f* clusters formed from the reactions conform to two known cluster types that have been previously reported by this research group. This suggests that the furan groups may hinder the formation of *3d-4f* metal clusters, as only homo-metallic species were isolated.

Another viable route to mixed-metal cluster synthesis is to introduce other functional groups at the methylene bridge position which will partake in coordination of metal ions. This was achieved through further derivatisation of compound **4** and this work is discussed in Chapter 3. Furans are extremely versatile compounds allowing for synthetic modification, and as such several new compounds can be obtained through simple reactions of these groups. It was hoped that analogous chemistry could be applied to the furan-substituted C[4], and that a plethora of new compounds could be synthesised. The results from this work have clearly demonstrated this to be the case. Simple hydrolysis or oxidation reactions of compound **4** afford the saturated or unsaturated diketones, respectively, and from these a whole new array of bridge-substituted C[4]s can be synthesised. The saturated diketone is a useful synthetic intermediate for the preparation of C[4]s with all four bridges being mono-functionalised, as it can be reacted with an almost limitless number of amines to afford pyrrole-substituted C[4]s. The library of methylene bridge-substituted C[4]s has been significantly expanded in the course of this study, and future work within this research group will build on this contribution and greatly expand this library of new supramolecular building blocks. Future work will also focus on the deprotection of all of the compounds synthesised in Chapter 3, particularly compounds **17** and **19**. Once deprotected, their cluster-forming properties will be investigated using standard reaction conditions, and hopefully the new functional groups introduced at the bridge positions will lead to the isolation of mixed-metal clusters that are of interest from a molecular magnetism perspective.

Work in this project then progressed onto studying how the compounds synthesised in Chapter 3 can be utilised in coordination chemistry, employing the expertise of the Lusby group at The University of Edinburgh. The potential metal-organic cage forming ability of **15** was investigated. Cage-formation using ligands containing pyridine moieties is well known in the literature and this is the reason that **15** was selected

for this study. The result of this work has led to the formation of three new coordination compounds which demonstrate the versatility of compound **15** prior to deprotection at the lower-rim, and all have been characterised by NMR and X-ray diffraction studies. Exploring these reactions in the solution phase was extremely beneficial as the ^1H NMR spectrum sharpened upon complexation of a metal. In addition, DOSY NMR provided insight into the size of the compounds formed from these reactions, and these results show strong correlation between the hydrodynamic radius and the complexes characterised in the solid state. However, metal-organic cages were not formed from these reactions, suggesting that the C[4] is not rigid enough to prevent intramolecular binding which leads to chelation products. Future work in this area will focus primarily on the synthesis of the 4-pyridine analogue of **15**, as well as introducing spacers between the pyrrole and pyridine group which will hopefully prevent chelation due to the increased rigidity of the compound (and increased spacing of the pyridine moieties).

The magnetic properties of clusters isolated using methylene-bridged C[4]s is of interest to this group for their use as SMMs or MRs. One way of altering the properties is through ligand substitution at the metal core of the $[\text{Mn}^{\text{III}}_2\text{Mn}^{\text{II}}_2]$ cluster previously isolated by this research group. Compound **I** was therefore reacted with various chelating co-ligands in the hope of displacing ligated solvent molecules. Three new clusters were synthesised in this study, and single crystal and powder X-ray diffraction studies were carried out in each case. The structures of these clusters showed that the ligated solvent had been successfully replaced by 1,10-phenanthroline, 2-methylphenanthroline and 3-methylphenanthroline molecules. The powder patterns of these clusters showed some correlation between the calculated and experimental pattern obtained after a 1 hour scan, however subsequent 8 hour scans suggest that these species / crystals are sensitive to solvent loss upon removal from the mother liquor. The magnetic properties of these new clusters were not studied due to equipment issues and related time constraints, however these measurements will be carried out in the near future. To prevent solvent loss, the clusters will be filtered immediately prior to measurement of their magnetic properties, hopefully circumventing the issue of de-solvation.

From the results discussed in this thesis it is evident that the study of calixarenes is still a growing area of supramolecular chemistry and, until now, relatively little attention has been paid to the synthesis of calixarenes that are mono-substituted at all methylene bridge positions. The work presented has significantly expanded the library of methylene bridge-substituted calix[4]arenes. This study is only a small fraction of the potential number of molecules that can be synthesised, but the results presented provided

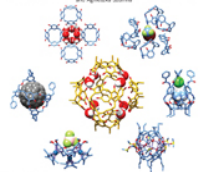
great insight into the possibilities for this new area of calixarene chemistry. The reactions proceed with ease, often with high yields at each position within the molecule (e.g. four reactions on each molecule giving an overall yield of 60%, reflecting very high yield per position), and this groundwork will facilitate further investigation into many research avenues and potential applications for these fascinating new molecules.

References

1. A. Baeyer, *Chem. Ber.*, 1872, **5**, 280-282.
2. C. D. Gutsche and R. Muthukrishnan, *J. Org. Chem.*, 1978, **43**, 4905-4906.
3. C. D. Gutsche, M. Iqbal and D. Stewart, *J. Org. Chem.*, 1986, **51**, 742-745.
4. C. D. Gutsche, *Acc. Chem. Res.*, 1983, **16**, 161-170.

Appendix

Publication adapted with permission from A. Fong, L. McCormick, S. J. Teat, E. K. Brechin and S. J. Dalgarno, *Supramol. Chem.*, 2018, **30**, 504-509. Copyright 2018 Taylor and Francis.



Exploratory studies into 3d/4f cluster formation with fully bridge-substituted calix[4]arenes

Angela Fong, Laura McCormick, Simon J. Teat, Euan K. Brechin & Scott J. Dalgarno

To cite this article: Angela Fong, Laura McCormick, Simon J. Teat, Euan K. Brechin & Scott J. Dalgarno (2018) Exploratory studies into 3d/4f cluster formation with fully bridge-substituted calix[4]arenes, *Supramolecular Chemistry*, 30:5-6, 504-509, DOI: [10.1080/10610278.2018.1430894](https://doi.org/10.1080/10610278.2018.1430894)

To link to this article: <https://doi.org/10.1080/10610278.2018.1430894>

View supplementary material

Published online: 01 Feb 2018.

Submit your article to this journal

Article views: 67

View related articles

View Crossmark data



Exploratory studies into 3d/4f cluster formation with fully bridge-substituted calix[4]arenes*

Angela Fong^a, Laura McCormick^c, Simon J. Teat^c, Euan K. Brechin^b and Scott J. Dalgarno^a

^aInstitute of Chemical Sciences, Heriot-Watt University, Edinburgh, UK; ^bEaStCHEM School of Chemistry, The University of Edinburgh, Edinburgh, UK; ^cLawrence Berkeley National Laboratory, Berkeley, CA, USA

ABSTRACT

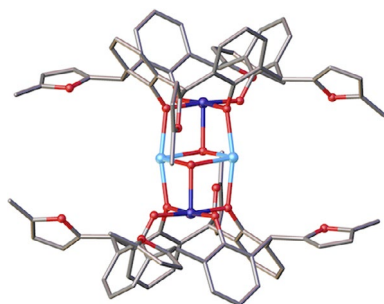
Calix[4]arenes are extremely versatile ligands that are capable of supporting the formation of a wide variety of polymetallic clusters of paramagnetic metal ions. One can exert influence over cluster formation through alteration of the calix[4]arene framework and subsequent 'expansion' of the lower-rim polyphenolic binding site. The present contribution investigates cluster formation with calix[4]arenes substituted at all four methylene bridge positions with furan moieties. Two known cluster types have been isolated with this ligand, the structures of which lend insight into factors that may ultimately preclude the formation of mixed-metal species.

ARTICLE HISTORY

Received 4 November 2017
Accepted 15 January 2018

KEYWORDS


Calixarenes; coordination chemistry; clusters; synthesis; crystallography




1. Introduction

The ability to influence the formation of paramagnetic metal ion clusters from multi-component systems is a challenging synthetic goal that holds great potential when considering the possibility to control or fine tune physical properties such as molecular magnetism (1–5). We have found that methylene-bridged calix[4]arenes (cyclic tetraphenols, collectively termed C[4]s hereafter, Figure 1(A)), are remarkably versatile ligands for cluster synthesis under ambient conditions, affording a wide range of structural topologies as a result (6–12). This is primarily due to their possessing a tetraphenolic pocket that readily binds 3d or 4f metal ions when deprotonated with a suitable base. These phenolato groups bridge to neighbouring ions within a cluster (for example

see Figure 1(B)) and impart a degree of directionality in the assembly process; this can also be considered as structural capping behaviour (*vide infra*). C[4]-supported clusters can also be synthesised under solvothermal (13, 14) or air-sensitive conditions (15–17), but discussion of this expansive chemistry is far beyond the scope of this contribution; in these cases the resulting structures differ markedly from those reported herein. Thia-, sulfonyl- and sulfinyl-bridged C[4]s have also been used in cluster-forming chemistry, but lower-rim coordination chemistry is drastically different to that of the methylene-bridged analogues, leading to vastly different structure types and physical properties. Again, this is far outwith the scope of this manuscript, but the reader is directed to recent reviews on the subject (18–20).

CONTACT Scott J. Dalgarno  s.j.dalgarno@hw.ac.uk

*Dedicated to Professor Jerry L. Atwood on the occasion of his 75th birthday

 Supplemental data for this article can be accessed <https://doi.org/10.1080/10610278.2018.1430894>

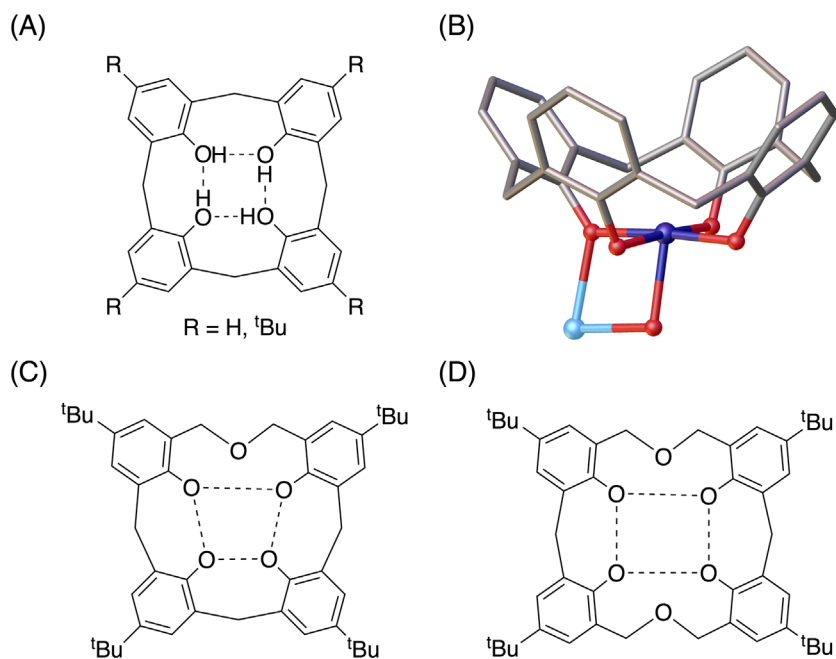


Figure 1. (Colour online) (A) Schematic of calix[4]arene ($R = H$) and p - t Bu-calix[4]arene ($R = t$ Bu), collectively termed C[4]s. Concerted hydrogen bonding interactions at the tetraphenolic lower-rim are shown as dashed lines between OH groups. (B) Section of the single crystal X-ray structure of a C[4]-supported $\{Mn^{III}_2Mn^{II}_2(OH)_2\}$ cluster showing wing-tip Mn^{III} binding in the tetraphenolato pocket, as well as phenolato and hydroxide bridging to a body Mn^{II} ion (7, 11). (C) Schematic of dihomooxalix[4]arene showing the distortion to the lower-rim tetraphenolato binding pocket through introduction of one ethereal bridge, the result of which is a trapezoidal binding pocket. (D) Schematic of tetrahomodioxalix[4]arene showing a rectangular binding pocket that results from 'expansion' through the introduction of distal ethereal bridges. Color code: C – grey, O – red, Mn^{III} – dark blue, Mn^{II} – pale blue. H atoms omitted in (B) for clarity.

With respect to methylene-bridged C[4]s, the first result of our exploratory investigations into C[4]-supported cluster formation was a series of $[Mn^{III}_2Mn^{II}_2(\mu_3-OH)_2(C[4])_2]$ SMMs (**1**) that possess a common structural butterfly-like $\{Mn^{III}_2Mn^{II}_2(\mu_3-OH)_2\}$ core, half of which is shown in Figure 1(B) (7, 11). The oxidation state distribution is rare (21), is the reverse of that found in the majority of structural analogues in the literature (22, 23), and is driven by the C[4] tetraphenolic pocket which preferentially binds the wing-tip manganese ions in the 3+ oxidation state. The C[4]s bridge to the body ions (in the 2+ oxidation state) and $[Mn^{III}(C[4])]^-$ moieties in the structure can be considered as capping units; these structure capping moieties, the nature of which depends on the metal ions present, are found in every C[4]-supported cluster we have reported to date. With the content of this contribution in mind, a second cluster that is worthy of mention is a $[Ln^{III}_6(\mu_3-O)_2(\mu-OH)_{3.32}(\mu-Cl)_{0.68}(HCOO)_2(C[4])_2]$ species (**2**) in which the lanthanide ions are arranged at the vertices of an octahedron (12). In this case a Ln^{III} ion is bound by the tetraphenolic pocket upon deprotonation, sitting just outside the basal plane of the oxygen atoms, affording a $[Ln^{III}(C[4])]^-$ structural capping moiety as a result. Liao and co-workers reported the solvothermal synthesis of a cluster of formula $[Ln^{III}_6(\mu_4-O)_2(\mu-CH_3O)_2(\mu-HCOO)_2(NO_3)_2(C[4])_2]$ (**3**) (14), the core of which is similar to that of **2**, showing that

this is a versatile cluster topology for C[4]. Reactions containing both 3d and 4f ions give several different heterometallic clusters depending on the stoichiometries and metal salts employed (6, 8, 10, 24), an interesting example of which is the ability to systematically interchange the body ions in the $[Mn^{III}_2Mn^{II}_2(\mu_3-OH)_2(C[4])_2]$ butterfly for Ln^{III} ; this affords either $[Mn^{III}_2Ln^{III}Mn^{II}(\mu_3-OH)_2(C[4])_2]$ or $[Mn^{III}_2Ln^{III}_2(\mu_3-OH)_2(C[4])_2]$ clusters as a result. Our exploratory cluster-forming studies with C[4]s have provided empirical metal ion binding rules as follows: (1) C[4]s will bind Mn^{III} preferentially over TM^{II} and Fe^{III} ions; (2) C[4]s will bind Fe^{III} preferentially over TM^{II} ions; (3) C[4]s will bind $TM^{II/III}$ preferentially over Ln ions; (4) C[4]s will bind Ln^{III} in the absence of TM ions. Every structure isolated to date contains either $[TM^{III}(C[4])]^-$, $[TM^{II}(C[4])]^{2-}$ or $[Ln^{III}(C[4])]^-$ capping moieties, and these act to cap polyhedral structures in a consistent manner.

In addition to carrying out such exploratory work with C[4], we have also reported on aspects of binding site alteration and the subsequent effect this has on cluster formation/composition (25–27). Our first effort in this regard was to employ oxalixarenes to systematically vary the size of the tetraphenolato pocket (26, 27). The introduction of one or two ethereal bridges between neighbouring aromatic rings 'expands' the C[4] framework, giving trapezoidal (Figure 1(c)) or rectangular (Figure 1(d)) binding

pockets respectively. The use of these oxacalixarenes in cluster formation gave markedly different results, an excellent example of which is the isolation of a Ln_5 cluster that can be considered an analogue of the aforementioned Ln_6 species. In this case one of the equatorial ions from the octahedron has been omitted due to the targeted 'expansion' of the lower-rim binding pocket; this Ln^{III} ion omission coincides directly with the position of the ethereal bridge. We also recently tethered C[4]s with alkyl chains of varying length through synthetic modification at one methylene bridge position (25). In doing so we found cluster formation with these bis-C[4]s to be challenging, except in cases where the tether was long enough to allow the constituent C[4]s to form previously reported cluster topologies (e.g. 1).

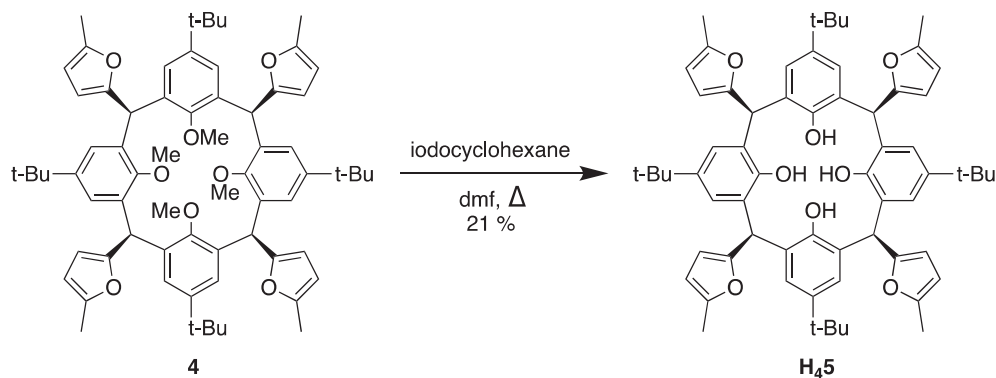
Here we present initial results from a new investigation that aims to explore the limits of cluster formation with C[4]s substituted at all methylene bridge positions. A search of the literature shows that there are relatively few fully substituted C[4]s that can be readily synthesised with all substituted groups equatorial, but one candidate that represented a viable starting point for this work is 5,11,17,23-tetra-tert-butyl-2,8,14,20-tetra(2-methylfuran-yl)-25,26,27,28-tetramethoxycalix[4]arene (**4**, Scheme 1) (28). Compound **4** is synthesised from C[4] in three steps: lower-rim alkylation to afford the tetra-methoxy derivative, monobromination at all four methylene bridge positions and subsequent reaction with 2-methylfuran in the presence of butylene oxide. This affords a C[4] with all furan groups equatorial as shown in Scheme 1.

2. Results and discussion

The use of compound **4** in cluster formation (via our typically employed ambient reaction conditions) first required de-protection of lower-rim methoxy groups to afford the required tetraphenolic C[4] pocket for metal ion binding/bridging. This was achieved using iodocyclohexane, giving

5,11,17,23-tetra-tert-butyl-2,8,14,20-tetra(2-methylfuran-yl)-25,26,27,28-tetrahydroxycalix[4]arene, **H₄5**, in 21% yield following purification. Given the frequency with which we have isolated $[\text{Mn}^{\text{III}}_2\text{Mn}^{\text{II}}_2(\mu_3\text{-OH})_2(\text{C}[4])_2]$ clusters, we selected this as our first target cluster topology. Reaction of **H₄5** with manganese(II) chloride tetrahydrate in a 1:1 dmf/MeOH mixture (to aid solubility), and in the presence of Et_3N as a base, rapidly afforded a deep purple solution upon stirring at room temperature. Good quality purple single crystals grew readily following vapour diffusion of petroleum ether into the mother liquor, and subsequent diffraction studies found them to be of formula $[\text{Mn}^{\text{III}}_2\text{Mn}^{\text{II}}_2(\mu_3\text{-OH})_2(\mathbf{5})_2(\text{dmf})_4(\text{MeOH})_2] \cdot 3\text{MeOH} \cdot \text{Et}_2\text{O}$ (**6**). Crystals of **6** were in a triclinic cell and structure solution was carried out in the space group *P*-1. The asymmetric unit (ASU) was found to contain half of the compound formula and, as expected, symmetry expansion revealed formation of the common butterfly cluster topology as shown in Figure 2. Inspection of Figure 2(A) shows that the furans substituted at the methylene bridge positions are all equatorial as expected, and that they are sufficiently far from the cluster core to prevent interference with solvent ligation at the body Mn^{II} ions (ligated solvent is shown in Figure S1). Bond lengths and angles relating to the cluster are similar to those of the C[4]-supported analogue, **1** (7, 11). The positioning of the furan groups around the cluster periphery is naturally dictated by the coordination chemistry, and as can be seen in Figure 2(B), the two equivalents of **5** are arranged in an offset manner due to the cluster core topology.

With the orientation/positioning of the furan groups in mind, we expanded our investigation to include the formation of 3*d*-4*f* clusters to establish whether: (1) it would be possible to isolate mixed-metal clusters, (2) different stoichiometries would lead to 3*d*/4*f* metal ion interchange akin to C[4]-supported cluster chemistry, and (3) the furans would play a role in cluster formation, potentially coordinating to Ln^{III} ions. We investigated this by exploring three



Scheme 1. Deprotection of the lower-rim of **4** to give 5,11,17,23-tetra-tert-butyl-2,8,14,20-tetra(2-methylfuran-yl)-25,26,27,28-tetrahydroxycalix[4]arene, **H₄5**.

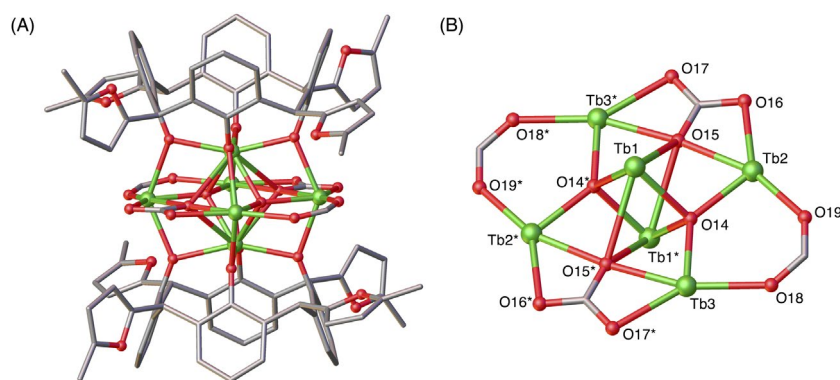


Figure 3. (Colour online) Views of the single crystal X-ray structure of **8**. (a) Side-on view showing formation of the $[\text{Tb}^{\text{III}}_6(\mu_4\text{-O})_2(\mu\text{-HCOO})_2(\mu_4\text{-CO}_3)_2]$ core that is supported by two tetra-anions of $\text{H}_4\mathbf{5}$. (b) View of the central core with selected atoms labelled according to discussion. Color code: C – grey, O – red, Tb^{III} – green. Solvent of crystallisation, H atoms and ligated solvent molecules are omitted for clarity.

ratios of Mn:Ln (Dy/Tb/Gd) ion present in the reaction mixture, these being 4:1, 1:1 and 1:4.

The first set of single crystals that were isolated were purple, and these arose from the reaction involving a 1:1 ratio of Mn:Tb ions. The crystals were found to be in a triclinic cell and structure solution was carried out in the space group $P\bar{1}$. Somewhat surprisingly, the crystals were found to be of formula $[\text{Mn}^{\text{III}}_2\text{Mn}^{\text{II}}_2(\mu_3\text{-OH})_2(\mathbf{5})_2(\text{dmf})_6]$ $[\text{Mn}^{\text{III}}_2\text{Mn}^{\text{II}}_2(\mu_3\text{-OH})_2(\mathbf{5})_2(\text{dmf})_{5.5}(\text{H}_2\text{O})_{0.5}]\cdot 2\text{dmf}$, **7**, indicating that 4f ions were not involved in cluster formation; this is atypical for C[4]-supported clusters formed in the presence of such ion mixtures. The ASU was found to contain half of the aforementioned formula, and symmetry expansion afforded two butterflies (Figure S2) that are closely related to the structure of **6**. Upon inspection, one noticeable difference upon moving to **7** is that one of the butterflies possesses six ligated dmf molecules, as opposed to four dmf and two MeOH in **6**. The second butterfly is also different as, although it also possesses four peripherally ligated dmf molecules, the cavities of symmetry equivalents of **5** are occupied by disordered water (ligated) and dmf

(non-ligated). As in the case of **6**, the cluster cores found in **7** are closely related to their respective C[4]-supported cluster analogue (**1**).

The only other set of crystals that were obtained from the current set of experiments were colourless, arising from the reaction involving a 1:4 ratio of Mn:Tb ions. The crystals were in a monoclinic cell, and structure solution in space group $P2_1/n$ revealed these to be of formula $[\text{Tb}^{\text{III}}_6(\mu_4\text{-O})_2(\mu\text{-HCOO})_2(\mu_4\text{-CO}_3)_2(\mathbf{5})_2(\text{dmf})_8(\text{H}_2\text{O})_8]\cdot 2\text{MeOH}\cdot 2\text{H}_2\text{O}$ (**8**). The asymmetric unit was found to contain half of the aforementioned formula, with symmetry expansion giving rise to the cluster shown in Figure 3. Inspection of the structure shows that this overall cluster topology conforms to the previously reported lanthanide octahedra discussed in the introductory section, but in this case there is yet another variation in the nature of anions in and around the cluster core. Figure 3(B) shows the central core with tetra-anions of $\text{H}_4\mathbf{5}$ omitted for clarity. As can be seen, the inner part of the core contains two μ_4 -oxides that bridge Tb1, its symmetry equivalent (s.e., Tb1*), Tb2 and Tb3. This is a common feature to all three Ln^{III} octahedra (**3**, **12**), as

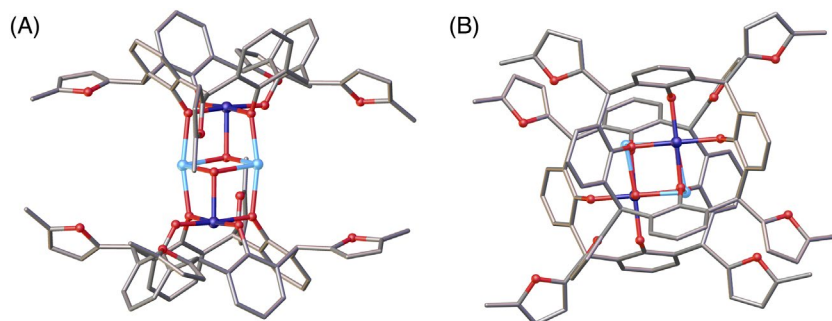


Figure 2. (Colour online) Views of the single crystal X-ray structure of **6**. (A) Side-on view showing formation of the expected mixed-valence $[\text{Mn}^{\text{III}}_2\text{Mn}^{\text{II}}_2(\mu_3\text{-OH})_2]$ core that is supported by two tetra-anions of $\text{H}_4\mathbf{5}$. (B) View down the cavity of **5** clearly showing Mn^{III} ion binding in the tetraphenolato pocket and the orientation of furan groups on the methylene bridge positions. Color code: C – grey, O – red, Mn^{III} – dark blue, Mn^{II} – pale blue. Solvent of crystallisation, H atoms and ligated solvent molecules are omitted for clarity.

is the presence of two peripheral bridging formate anions (e.g. see Figure 3(B), O18/O19 and s.e. O18*/O19*). The main difference observed upon moving from either **2** or **3** to **8** is the introduction of the μ_4 -CO₃²⁻ (O15/O16/O17 and O15*/O16*/O17*) anions in place of μ -OH⁻/ μ -Cl⁻ and μ -CH₃O⁻/terminal NO₃⁻ respectively. We propose that the bridging formate and carbonate anions originate from decomposition of dmf; this is commonplace for such reactions involving C[4] as a cluster support. As is the case in **2**, each of the four Tb^{III} ions in the central plane of the cluster possesses two ligated dmf molecules that, together, can be seen to define the vertices of a near-perfect square prism (Figure S3). These eight ligated dmf molecules are positioned between the furan moieties at the calixarene bridge positions, further indicating that these cluster topologies are capable of withstanding the introduction of relatively large moieties to the supporting ligand framework.

The magnetic properties of clusters **6–8** were not investigated, as all are very closely related to previously published topologies and can be expected to be very similar.

3. Conclusions

To conclude, we have shown that a C[4] substituted at all methylene bridge positions can be de-protected at the lower-rim and successfully used in the synthesis of *3d* or *4f* clusters. The three species isolated conform to two known types reported for analogous C[4]-supported cluster chemistry, and the fact that *3d–4f* clusters were not isolable suggests that the presence of furan moieties at the C[4] bridge positions hinders mixed-metal cluster formation. This may be due to the increased coordination number/presence of additional ligands around the cluster periphery, but further investigation is required in order to confirm this hypothesis. This will be the subject of future work in the area of fully bridge-substituted C[4]-supported cluster chemistry and results will be reported in due course, including magnetic properties of clusters isolated if these are found to deviate from existing topologies.

4. Experimental

Compound **4** was synthesised according to literature procedures and purity was confirmed by ¹H NMR prior to use (28). **Synthesis of 5,11,17,23-tetra-tert-butyl-2,8,14,20-tetra(2-methylfuran-yl)-25,26,27,28-tetrahydroxycalix[4]arene, H₄5**: Cyclohexyl iodide (9.86 g, 46.91 mmol) was added to a stirred suspension of compound **4** (1.069 g, 1.04 mmol) in dmf (60 mL) and the reaction was heated at reflux for 48 h. The resulting brown solution was cooled to RT before being poured into water (100 mL), leading to the precipitation of a brown solid. This solid was collected by filtration and stirred as a suspension

in MeOH for 15 min. Subsequent filtration afforded a yellow crude that was recrystallised from CHCl₃/MeOH to yield 0.210 g (21%) of pure **H₄5**. ¹H NMR (300 MHz, CDCl₃) δ ppm: 8.94 (br. s., 4 H) 7.16 (s, 8 H) 6.14 (d, *J* = 2.57 Hz, 4 H) 5.94 (d, *J* = 2.90 Hz, 4 H) 5.90 (s, 4 H) 2.28 (s, 12 H) 1.11 (s, 36 H). ¹³C NMR (75.5 MHz, CDCl₃) δ ppm 152.75, 151.44, 146.19, 143.80, 128.39, 124.01, 109.74, 105.76, 37.31, 34.18, 31.20, 13.61. MS (MALDI-TOF): 991.5, [M + Na]⁺.

Synthesis of [Mn^{III}₂Mn^{II}₂(μ_3 -OH)₂(5)₂(dmf)₄(MeOH)₂].3 MeOH.Et₂O, **6**: MnCl₂·4H₂O (40.9 mg, 0.207 mmol) and **H₄5** (50.0 mg, 0.052 mmol) were dissolved in a 1:1 dmf/MeOH mixture (20 mL). After 10 min of stirring Et₃N (0.045 mL) was added and the resulting deep purple solution was stirred at RT for 2 h. The reaction mixture was filtered to remove any microcrystalline material, and purple crystals of **6** grew upon vapour diffusion of petroleum ether into the mother liquor. These were found to be sensitive towards solvent loss upon removal of the mother liquor, and sample homogeneity was assessed by multiple unit cell determinations. **Crystal data for 6 (CCDC 1583896)**: C₁₄₉H₁₉₆Mn₄N₄O₂₈, *M* = 2710.85 g/mol, triclinic, space group *P*-1 (no. 2), *a* = 13.1012(9) Å, *b* = 17.0409(11) Å, *c* = 17.5344(12) Å, α = 72.026(3)°, β = 86.362(3)°, γ = 87.172(3)°, *V* = 37 14.3(4) Å³, *Z* = 1, *T* = 100(2) K, MoK α radiation (λ = 0.71073 Å), 57869 reflections measured (2.444° ≤ 2 θ ≤ 54.174°), 15969 unique (*R*_{int} = 0.1222, *R*_{sigma} = 0.2345) which were used in all calculations. The final *R*₁ was 0.0864 (*I* > 2 σ (*I*)) and *wR*₂ was 0.2787 (all data). Single crystals that were isostructural to **6** were obtained when 4:1 ratios of Mn:Ln ions were used. This was confirmed through comparison of unit cell parameters.

Synthesis of [Mn^{III}₂Mn^{II}₂(μ_3 -OH)₂(5)₂(dmf)₆][Mn^{III}₂Mn^{II}₂(μ_3 -OH)₂(5)₂(dmf)_{5.5}(H₂O)_{0.5}].2dmf, **7**: MnCl₂·4H₂O (10.1 mg, 0.051 mmol), TbCl₃·6H₂O (1 eq., 19.2 mg, 0.051 mmol) and **H₄5** (50.6 mg, 0.052 mmol) were dissolved in a 1:1 dmf/MeOH mixture (20 mL). After 10 min of stirring Et₃N (0.045 mL) was added and the resulting purple solution was stirred at RT for 2 h. The reaction mixture was filtered to remove any microcrystalline material, and purple crystals of **7** grew upon slow evaporation diffusion of petroleum ether into the mother liquor. These were found to be sensitive towards solvent loss upon removal of the mother liquor, and sample homogeneity was assessed by multiple unit cell determinations. **Crystal data for 7 (CCDC 1583897)**: C_{148.25}H_{185.75}Mn₄N_{6.75}O₂₅, *M* = 2682.03 g/mol, triclinic, space group *P*-1 (no. 2), *a* = 15.7886(9) Å, *b* = 23.1399(13) Å, *c* = 30.3907(17) Å, α = 102.631(3)°, β = 102.128(3)°, γ = 98.886(3)°, *V* = 10356.2(10) Å³, *Z* = 2, *T* = 100(2) K, μ (synchrotron) = 0.361 mm⁻¹, 111410 reflections measured (3.224° ≤ 2 θ ≤ 62.414°), 51084 unique (*R*_{int} = 0.0495, *R*_{sigma} = 0.0784) which were used in all calculations. The final *R*₁ was 0.0806 (*I* > 2 σ (*I*)) and *wR*₂ was 0.2422 (all data).

Synthesis of $[\text{Tb}^{\text{III}}(\mu_4\text{-O})_2(\mu_4\text{-CO}_3)_2(\mu\text{-HCO}_2)_2(\text{5})_2(\text{dmf})_8(\text{H}_2\text{O})_2] \cdot 2\text{MeOH} \cdot 2\text{H}_2\text{O}$, **8:** $\text{MnCl}_2 \cdot 4\text{H}_2\text{O}$ (10.1 mg, 0.051 mmol), $\text{TbCl}_3 \cdot 6\text{H}_2\text{O}$ (4 eq., 76.7 mg, 0.205 mmol) and **H₄5** (50.6 mg, 0.052 mmol) were dissolved in a 1:1 dmf/MeOH mixture (20 mL). After 10 min of stirring Et_3N (0.045 mL) was added and the resulting purple solution was stirred at RT for 2 h. The reaction mixture was filtered to remove any microcrystalline material, and colourless crystals of **8** grew upon slow evaporation of the mother liquor. These were found to be sensitive towards solvent loss upon removal of the mother liquor, and sample homogeneity was assessed by multiple unit cell determinations. **Crystal data for **8** (CCDC 1583898):** $\text{C}_{79}\text{H}_{105}\text{N}_4\text{O}_{21}\text{Tb}_3$, $M = 1923.42$ g/mol, monoclinic, space group $P2_1/n$ (no. 14), $a = 18.8372(9)$ Å, $b = 15.8997(8)$ Å, $c = 28.3456(12)$ Å, $\beta = 107.806(2)^\circ$, $V = 8083.0(7)$ Å³, $Z = 4$, $T = 100(2)$ K, MoK α radiation ($\lambda = 0.71073$ Å), 72883 reflections measured ($3.45^\circ \leq 2\theta \leq 58.082^\circ$), 21054 unique ($R_{\text{int}} = 0.0847$, $R_{\text{sigma}} = 0.1167$) which were used in all calculations. The final R_1 was 0.0527 ($I > 2\sigma(I)$) and wR_2 was 0.1354 (all data).

Author contributions

A.F., E.K.B. and S.J.D. authors conceived and designed the experiments; A.F. performed the experiments; A.F., L.J.M. and S.J.T. acquired data; A.F. and S.D. analyzed the data; A.F., E.K.B. and S.J.D. wrote the paper.

Disclosure statement

The authors declare no conflicts of interest.

Funding

We thank the EPSRC for financial support (DTP studentship for AF). The Advanced Light Source is supported by the Director, Office of Science, Office of Basic Energy Sciences, of the US Department of Energy under [grant number DE-AC02-05CH11231].

References

- Thiele, S.; Balestro, F.; Ballou, R.; Klyatskaya, S.; Ruben, M.; Wernsdorfer, W. *Science* **2014**, *344*, 1135–1138.
- Rebilly, J.N.; Mallah, T. Synthesis of single-molecule magnets using metallocyanates. In *Single-Molecule Magnets and Related Phenomena*; Winpenny, R., Ed.; Springer-Verlag: Berlin, Heidelberg, **2006**; Vol. 122, pp. 103–131.
- Gatteschi, D.; Sessoli, R.; Villain, J. *Mol. Nanomagn.* **2006**, *1*–395.
- Aromi, G.; Brechin, E.K. Synthesis of 3d Metallic Single-Molecule Magnets. In *Single-Molecule Magnets and Related Phenomena*; Winpenny, R., Ed.; Springer-Verlag: Berlin, Heidelberg, **2006**; Vol. 122, pp. 1–67.
- Wernsdorfer, W.; Sessoli, R. *Science* **1999**, *284*, 133–135.
- Karotsis, G.; Evangelisti, M.; Dalgarno, S.J.; Brechin, E.K. *Angew. Chem. Int. Ed.* **2009**, *48*, 9928–9931.
- Karotsis, G.; Teat, S.J.; Wernsdorfer, W.; Piligkos, S.; Dalgarno, S.J.; Brechin, E.K. *Angew. Chem. Int. Ed.* **2009**, *48*, 8285–8288.
- Karotsis, G.; Kennedy, S.; Dalgarno, S.J.; Brechin, E.K. *Chem. Commun.* **2010**, *46*, 3884–3886.
- Karotsis, G.; Kennedy, S.; Teat, S.J.; Beavers, C.M.; Fowler, D.A.; Morales, J.J.; Evangelisti, M.; Dalgarno, S.J.; Brechin, E.K. *J. Am. Chem. Soc.* **2010**, *132*, 12983–12990.
- Sanz, S.; Ferreira, K.; McIntosh, R.D.; Dalgarno, S.J.; Brechin, E.K. *Chem. Commun.* **2011**, *47*, 9042–9044.
- Taylor, S.M.; Karotsis, G.; McIntosh, R.D.; Kennedy, S.; Teat, S.J.; Beavers, C.M.; Wernsdorfer, W.; Piligkos, S.; Dalgarno, S.J.; Brechin, E.K. *Chem. Eur. J.* **2011**, *17*, 7521–7530.
- Sanz, S.; McIntosh, R.D.; Beavers, C.M.; Teat, S.J.; Evangelisti, M.; Brechin, E.K.; Dalgarno, S.J. *Chem. Commun.* **2012**, *48*, 1449–1451.
- Aronica, C.; Chastanet, G.; Zueva, E.; Borshch, S.A.; Clemente-Juan, J.M.; Luneau, D. *J. Am. Chem. Soc.* **2008**, *130*, 2365–2371.
- Bi, Y.F.; Xu, G.C.; Liao, W.P.; Du, S.C.; Deng, R.P.; Wang, B.W. *Sci. China Chem.* **2012**, *55*, 967–972.
- Furphy, B.M.; Harrowfield, J.M.; Ogden, M.I.; Skelton, B.W.; White, A.H.; Wilner, F.R. *J. Chem. Soc. Dalton Trans.* **1989**, 2217–2221.
- Homden, D.M.; Redshaw, C. *Chem. Rev.* **2008**, *108*, 5086–5130.
- Redshaw, C. *Dalton Trans.* **2016**, *45*, 9018–9030.
- Su, K.Z.; Jiang, F.L.; Qian, J.J.; Chen, L.; Pang, J.D.; Bawaked, S.M.; Mokhtar, M.; A-Thabaiti, S.A.; Hong, M.C. *Inorg. Chem.* **2015**, *54*, 3183–3188.
- Bi, Y.F.; Du, S.C.; Liao, W.P. *Coord. Chem. Rev.* **2014**, *276*, 61–72.
- Mislin, G.; Graf, E.; Hosseini, M.W.; Bilyk, A.; Hall, A.K.; Harrowfield, J.M.; Skelton, B.W.; White, A.H. *Chem. Commun.* **1999**, 373–374.
- Wittick, L.M.; Jones, L.F.; Jensen, P.; Moubaraki, B.; Spiccia, L.; Berry, K.J.; Murray, K.S. *Dalton Trans.* **2006**, 1534–1543.
- Yoo, J.; Brechin, E.K.; Yamaguchi, A.; Nakano, M.; Huffman, J.C.; Maniero, A.L.; Brunel, L.C.; Awaga, K.; Ishimoto, H.; Christou, G.; Hendrickson, D.N. *Inorg. Chem.* **2000**, *39*, 3615–3623.
- Brechin, E.K.; Yoo, J.; Nakano, M.; Huffman, J.C.; Hendrickson, D.N.; Christou, G. *Chem. Commun.* **1999**, 783–784.
- Palacios, M.A.; McLellan, R.; Beavers, C.M.; Teat, S.J.; Weihe, H.; Piligkos, S.; Dalgarno, S.J.; Brechin, E.K. *Chem. Eur. J.* **2015**, *21*, 11212–11218.
- Coletta, M.; McLellan, R.; Cols, J.-M.; Gagnon, K.J.; Teat, S.J.; Brechin, E.K.; Dalgarno, S. *J. Supramol. Chem.* **2016**, *28*, 557–566.
- Fairbairn, R.E.; McLellan, R.; McIntosh, R.D.; Palacios, M.A.; Brechin, E.K.; Dalgarno, S.J. *Dalton Trans.* **2014**, *43*, 5292–5298.
- Fairbairn, R.E.; McLellan, R.; McIntosh, R.D.; Taylor, S.M.; Brechin, E.K.; Dalgarno, S.J. *Chem. Commun.* **2012**, *48*, 8493–8495.
- Columbus, I.; Biali, S.E. *J. Org. Chem.* **2008**, *73*, 2598–2606.